

Energy Absorption Capability of Damage Affected Composite Structures

by Michael Ribeaux, MEng (Hons)

Thesis submitted to The University of Nottingham for the degree of Doctor of Philosophy, October 2003

Contents

Abstract.....	iv
Acknowledgements	vi
Glossary	vii
Nomenclature.....	ix
1.0 Introduction.....	1
2.0 Literature Review	6
2.1 Damage	6
Impact damage.....	6
Holes.....	13
Ways of improving damage tolerance	16
2.2 Energy Absorption	19
2.2.1 Failure Modes	20
Splaying	22
Fragmentation.....	24
Buckling.....	24
2.2.2 Constituent materials	25
Matrix material	25
Fibre material.....	27
Fibre content.....	28
Fibre Architecture.....	29
2.2.3 Geometric properties	30
Cross sectional shape.....	30
Dimensional Effects	32
Trigger mechanism.....	33
2.2.4 Testing conditions.....	36
Test speed (Quasi-static / Impact)	36
Off-axis testing	39
Crush platen condition.....	39
2.3 Conclusions.....	41

3	Experimental Methods	42
3.1	Experimental Objectives	42
3.2	Materials	44
3.3	Specimen Manufacture	44
3.4	Damage Characterisation	48
3.4.1	Holes	49
3.4.2	Delaminations	50
3.4.3	Impact Damage	51
3.4.4	Interlaminar Toughening via Interleaves	52
3.5	Test Methods	52
3.5.1	Quasi-Static Tube Crush	53
3.5.2	Dynamic Tube Crush	54
3.5.3	Determination of Ultimate Compressive Stress	56
3.5.4	Friction Testing	56
3.5.5	Determination of Fibre Volume Fraction	58
3.5.6	Microscopy	59
3.5.7	Environmental Scanning Electron Microscope (ESEM)	59
4	Results	60
4.1	Tube Crush Test Results	61
4.1.1	Rate Effects	61
4.1.1.1	Circular Tubes	62
4.1.1.2	Square Tubes	63
4.1.2	Damage - Holes	65
4.1.2.1	Hole Size	71
4.1.2.2	Hole Position – Axially	77
4.1.2.3	Multiple Holes	82
4.1.3	Damage – Delaminations	85
4.1.4	Damage - Impact Damage	87
4.1.4.1	Damage Levels	90
4.1.4.2	Damage Position – Axially	95
4.1.5	Interlaminar Toughening via Interleaves	99

4.1.5.1	No Damage – Rate Effects	100
4.1.5.2	Damage Levels with Interleaf.....	101
4.2	Ultimate Compressive Stress (UCS).....	106
4.3	Friction	107
4.4	Optical Microscopy.....	110
4.5	Environmental Scanning Electron Microscopy (ESEM)	112
4.6	Fibre Volume Fraction	115
5	Discussion	116
5.1	Rate Effects	116
5.2	Geometric Effects	118
5.3	Damage	119
5.3.1	Holes.....	119
5.3.2	Simulated Delaminations.....	120
5.3.3	Impact Damage	122
5.4	Interleaves	123
6	Conclusions.....	126
7	Publications	131
8	References.....	132
9	Appendix 1 – Load vs Displacement Results	140
10	Appendix 2 – Micrographs	176

Abstract

The aim of this project is to consider the effect of damage on the energy absorption potential of continuous filament random mat (CoFRM) E-glass / polyester composite tubes. Composite materials have been shown to absorb significantly higher specific energy levels than metals under axial crushing conditions. This property can be exploited in automotive crashworthiness applications. Replacing steel crash structures with composites can lead to significant weight reductions. However, damage in composite structures can be difficult to assess and may not be visible by casual inspection. There is a concern that damage may accumulate in the crash structures, as a result of in-service wear and tear or due to operator negligence. It is important to understand how much accidental damage the crash structures can sustain before they are no longer able to fulfil their requirements. Two wall thicknesses of circular and square tube geometries were tested, with over 650 samples crushed either quasi-statically at 5mm/min or dynamically at 5m/s. Damage was induced in three ways: drilled holes, delamination in the form of Melinex® inserts moulded into the samples, and out-of-plane impact damage of various energy levels.

Cylindrical samples made from this low cost composite are able to absorb up to 87 kJ/kg when tested quasi-statically. Dynamic testing was carried out as it provides a better representation of the loading conditions the parts will see in operation. Dynamically tested samples absorbed less energy than the quasi-statically tested samples (up to 18%). This was due to the viscoelastic nature of the matrix causing a greater degree of fragmentation at the higher test speed, leaving the load bearing fibres less well constrained and therefore reducing their load bearing capability.

Square section tubes absorb less energy (up to 31%) than a circular section of the same cross sectional area and fibre volume fraction. This is due to geometric stress raisers at the corners causing intralaminar failure. This splitting at the corners leaves the fronds less constrained and allows them to splay at a lower load.

A threshold level was found for each type of damage. Below the threshold level the damage zone had no effect on the progressive failure mode or the specific energy absorption (SEA). Above the threshold level unstable compressive failure occurs in

the form of a crack initiating at the damage zone and then propagating around the tube. In this situation a portion of the tube breaks off uncrushed and therefore reduces the energy absorption capability of the structure.

For this material tested, relatively small hole sizes (5mm) and relatively low impact energy levels (1.5J – 3J) can cause unstable failure to occur at quasi-static test speeds. However, it has been shown that the damage tolerance of the material increases (to 10mm and 3J – 9J) at higher test rates (5m/s).

Having observed the failure modes and damage tolerance of the tubes under various testing parameters it was important to look at ways of improving the damage tolerance of the samples. Moulding a thermoplastic interleaf into the sample to increase the interlaminar fracture toughness increases the damage tolerance of the tubes. Increasing the wall thickness and adding an interleaf increases the damage tolerance by up to a factor of 9. However, the increased damage tolerance of samples with interleaf was offset by a reduction in SEA by up to 48% due to a reduction in coefficient of friction in the crush zone from 0.36 to 0.22.

The ultimate compressive stress (UCS) increases at dynamic test speeds and the mean crush load observed decreases. Therefore the crushing stress of the dynamically tested samples is a far lower percentage of the UCS of the material than under quasi-static loading. A greater stress concentration is therefore required to cause unstable failure at higher rates. Improved damage tolerance is also seen by increasing the wall thickness of the sample, testing square rather than circular section samples, and moulding interleaves into the samples. In all of these cases the changes that lead to improved damage tolerance lead to a reduction in the crush load of samples as a percentage of the ultimate crush load.

Understanding the work in this thesis will enable the design of damage tolerant composite crash structures for the automotive industry. Such a part will, even with the inclusion of accidental damage, be able to absorb the energy required in the event of a collision.

Acknowledgements

The author would like to thank the following:

Dr. N. A. Warrior for his supervision throughout the period of this research.

The Automotive Composites Consortium (ACC) of the United States Council for Automotive Research (USCAR) and the University of Nottingham who provided the financial support for this programme.

R. A. Jeryan and A. G. Caliskan of Ford Motor Company and other members of the Energy Management Working Group of the ACC for their technical contributions.

The Engineering and Physical Sciences Research Council (EPSRC) for use of a Kodak HS4540 high speed camera loaned from their engineering instrument pool.

School of Mechanical, Materials, Manufacturing Engineering and Management for the use of all their facilities.

Members of the University of Nottingham Composite Group, in particular Thomas Turner, Richard Fernie, Kristofer Bottome, Daniel Bailey and Lee Harper for their assistance.

Technical staff at the University of Nottingham, especially Paul Johns, Dave Smith, Roger Smith and Geoff Tomlinson for their help and support.

Family and friends for their ongoing support and encouragement throughout my study at the University of Nottingham.

Glossary

ACC	Automotive Composites Consortium
ASTM	American Society for Testing and Materials
Binder	A substance which provides cohesion between fibres within a reinforcement
BS	British Standard
CAI	Compression After Impact
CoFRM	Continuous Filament Random Mat
CSM	Chopped Strand Mat
Cure	Polymerisation of a resin - changing from liquid to solid
DCB	Double Cantilever Beam
E-glass	Electrical glass, the type of glass most commonly used for fibre reinforcement
ESEM	Environmental Scanning Electron Microscope
FRP	Fibre Reinforced Plastic
Filament	A single fibre
GRP	Glass Reinforced Plastics
IFW	Instrumented Falling Weight

Isotropic	Having properties which do not vary with direction within the material
Preform	An arrangement of dry fibres in the shape of a mould cavity
Reinforcement	Fibres used to provide strength in a composite
RTM	Resin Transfer Moulding
SEA	Specific Energy Absorption
Size	The surface treatment applied to glass fibres during manufacture which protects the surface during processing and provides a chemical link with the resin
SRIM	Structural Reaction Injection Moulding
Thermoplastic	A polymeric material which is softened by the application of heat and hardened by cooling in a reversible process
Thermoset	A polymeric material which is hardened by an irreversible chemical reaction
Tow	An assembly of filaments
UD	Unidirectional
Warp	The direction along the roll of a commercial reinforcement material
Weft	The direction across the roll of a commercial reinforcement material
Wet-out	Contact between fibre surface and matrix after polymerisation

Nomenclature

		S.I. Units
a	Acceleration	ms^{-2}
A	Cross-sectional area	m^2
D	Diameter	m
E	Elastic Modulus	Pa
E_s	Specific energy absorption	kJ/kg
F	Force	N
g	Acceleration due to gravity	ms^{-2}
L	Length	m
m	Mass	kg
OD	Outside diameter	m
P_{\max}	Maximum crush force during stable crushing	N
t	Tube wall thickness	m
V	Speed	ms^{-1}
V_f	Fibre volume fraction	-
W	Width	m
ε	Strain	-
ρ	Density	kgm^{-3}
σ	Stress	Pa

1.0 Introduction

Composites are a mixture of two or more materials where the composite exhibits greater properties than the sum of the individual parts. Modern composite materials are made up using high modulus fibres in a brittle matrix. The fibres, which are the main load bearing part of the composite, can be laid up in many ways. By weaving the fibres with higher percentages in certain directions it can give the composite greater directional reinforcement. This is useful for applications where the direction of the applied force is known. A 45° braid angle will give the composite greater torsional stiffness by again orientating the fibres in line with the load path. Continuous filament random mat (CoFRM) and chopped strand mat (CSM) are also used as they provide a certain amount of in-plane isotropy. CoFRM E-glass fibres were used in this project due to their ease of use and relative cheapness.

Composites have a major advantage over other materials because of their high specific strengths (4 times that of steel or aluminium for a glass reinforced plastic). However, their main disadvantage is their cost. The raw materials are expensive, as are the manufacturing costs for complicated shapes or certain materials. These are generally found to be low volume production operations, but ongoing research into reducing the manufacturing cost of composites will make them more accessible for use in high volume production. Also, manufacturing techniques, such as automated preform manufacture, as well as part integration are making composites more viable. The evolution of this technology has brought unprecedented opportunities in terms of shape evolution and local tailoring of reinforcement with orientation and local architecture changing from one area to the next. As a result, designs can be optimised for complex applications such as combined structural integrity and crashworthiness.

As well as improved energy absorption composites offer mass reduction (by up to half over steel or aluminium for a glass reinforced plastic crash structure), allowing reduced fuel consumption and improved vehicle performance. This has promoted their increasing use in automotive design. The ability of a structure to absorb impact energy and survive is called crashworthiness. Increasing public demand and legislation make crashworthiness an essential requirement in vehicle design and

manufacture, from cars and trucks to ships and helicopters. In automotive applications primary energy absorbers, such as bumpers, are designed to absorb the energy from small impacts seen in circumstances such as parking accidents. At higher velocities the energy is absorbed in impact crumple zones, with the aim of preserving the passenger cell integrity and limiting the forces seen by the occupant.

Extensive research into energy absorbing properties of composite tubes has shown that, under appropriate conditions and with the correct design, composite materials can absorb more energy per unit mass than an equivalent metallic structure. The way they absorb the energy with a constant crush load is in line with the ideal deceleration curve. A constant load and therefore constant deceleration is seen as ideal because the crash energy is absorbed for a minimum deceleration level experienced by the occupant. Metals fail by plastic buckling, which causes oscillations of the crush load (see Figure 1). This means that higher deceleration levels are experienced by the occupant for the same level of energy dissipation. Also due to the nature of their failure mode composites are able to crush for a greater proportion of their length before the compaction of the material causes the sustained load to rise sharply. Therefore, their importance in the design of modern crashworthy components is growing considerably.

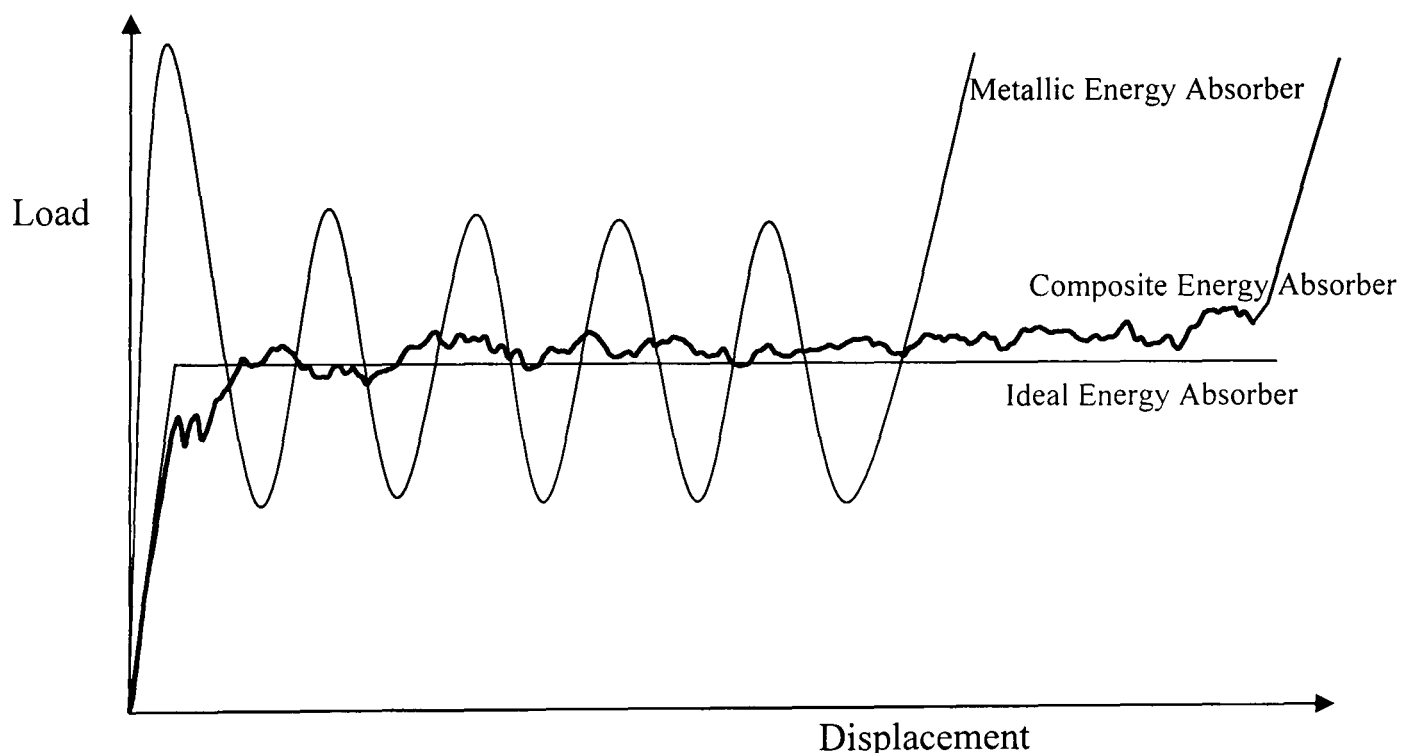


Figure 1: Idealised Load-Displacement Graph of Different Energy Absorbers

Theory

The CoFRM E-glass/polyester tubes tested in this project are positioned between two parallel crush platens. The top crush platen then places the sample under axial compression. Without a trigger the samples would fail by compressive shear (see Figure 10). The 45° bevel provides a stress concentration by reducing the cross sectional area of the tube at the crush platen. As the sample crushes the length of the chamfer, the load steadily increases until a steady state load is achieved and a progressive splaying mode is observed (see Figure 2 and section 2.2.1).

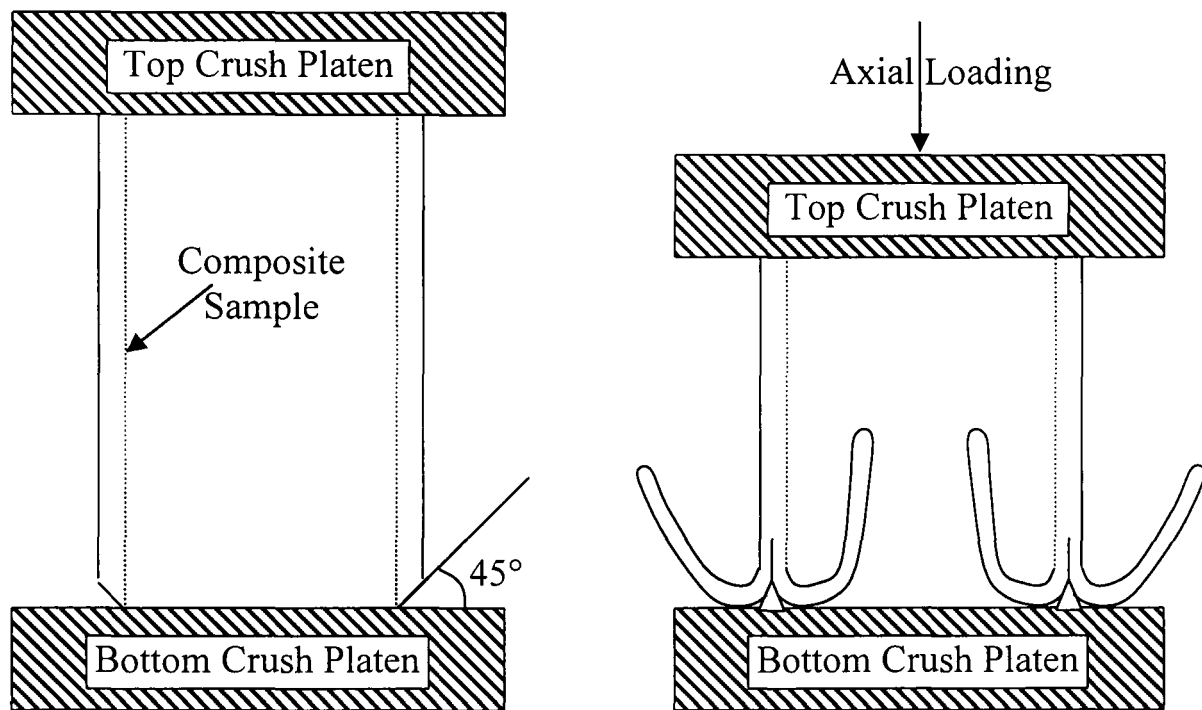


Figure 2: Schematic of Progressive Splaying Development

This is the same for both quasi-static and dynamic tests. The wave velocity in the samples is calculated as 2582m/s from Equation 1 (longitudinal wave velocity through a material), using values of $E=10\text{GPa}$ and $\rho=1500\text{kg/m}^3$. The dynamic samples are crushed with an initial velocity of 5m/s. As the stress wave propagation is 500 times this value samples can be considered to be under a uniform stress state as are the quasi-statically tested samples.

$$C = \sqrt{\frac{E}{\rho}} \quad (1)$$

At the steady state crushing stress the sample will either continue to crush progressively, or fail by fast fracture. The crushing stresses for the tubes studied here are such that fast fracture will only occur in the presence of a stress raiser. A zone of delamination, which will divide the tube wall into 2 or 3 thinner sections (depending on the number of delaminations), can cause local buckling. Holes or areas of impact damage will cause a stress concentration, which can also lead to fast fracture (see Figure 3).

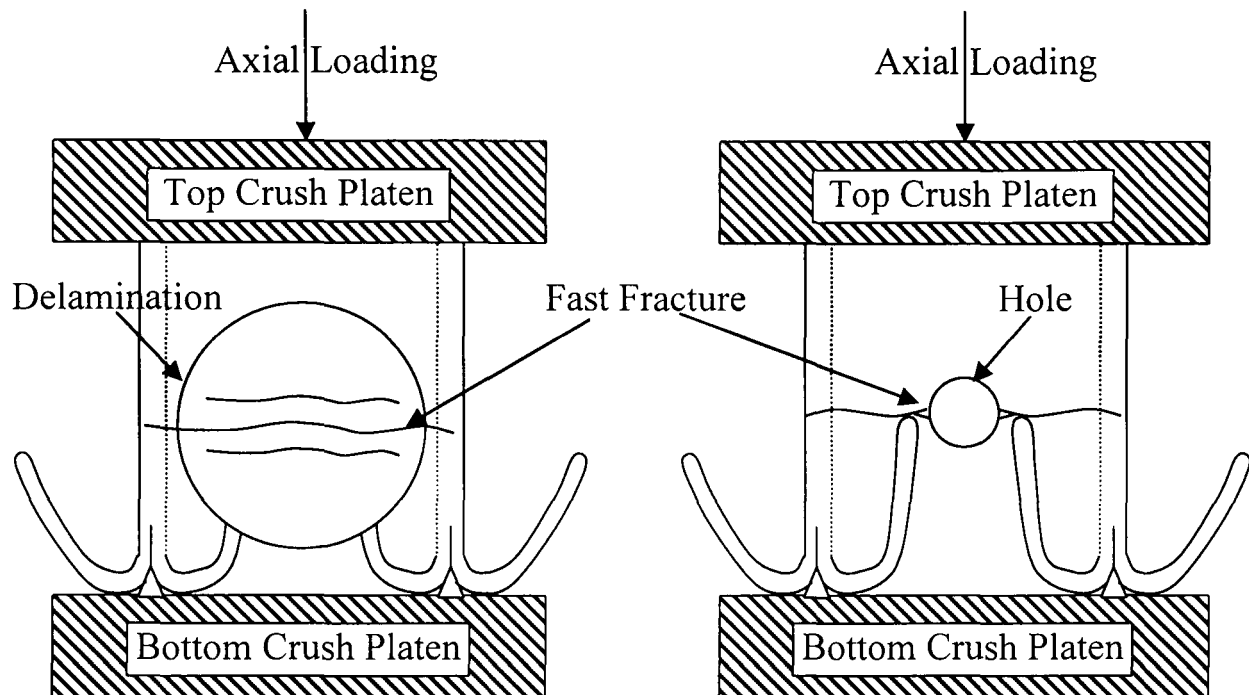


Figure 3: Schematic of Fast Fracture Development

Fast fracture occurs if the stress in the sample exceeds the ultimate compressive stress or the local buckling stress. A threshold damage level or hole size exists where the stress in the material is just below that required for fast fracture. As the crush front progresses, the centre wall crack splits the wall of the tube and acts as a stress raiser, which cause fast fracture to occur in the vicinity of the crush zone.

Application

The tubes tested in this study are laboratory scale parts. In an automotive application the composite part would be designed to absorb the energy of the car in the event of a frontal impact. They would be manufactured into the front end of the vehicle and subjected to axial compression. The final part would have to be designed to absorb 160kJ of energy, which is equivalent to the energy from a 1000kg car in a 40mph crash (as required in the EuroNCAP crash test [1]). The frontal impact is offset so the

energy would have to be absorbed in a single crash structure. The crush load it would have to sustain would be 320kN assuming a 0.5m length of crush. This load level can be achieved by tailoring the dimensions and geometry of the energy absorber. An estimation of the size of energy absorber required based on experiments done in this thesis would give a circular section tube, manufactured from CoFRM E-glass and polyester, with outer diameter of approximately 150mm and an 8mm wall thickness. These values also assume that the composite energy absorber is the only part of the vehicle absorbing energy, which will not be the case, so values stated here would be for a worst case scenario.

A structure with a higher specific energy absorption (SEA) level will have a lower mass than a structure with a lower SEA level to absorb the same amount of energy. As reducing the mass is beneficial in terms of being able to improve vehicle performance higher SEA levels are therefore desirable.

Vehicles are designed with energy absorbing structures constrained so as to deform in a manner that will absorb the maximum amount of energy. However, during the vehicle life, non-service damage may accumulate in the structure. This damage may be caused by low speed crashes, debris thrown up off the road, or user negligence (such as jacking away from approved points or a tool being dropped during a service), and may not be visible by casual inspection. Unstable modes of failure can result in a catastrophic collapse of the structure resulting in a considerable reduction in strength and stiffness making it unable to perform its primary function, absorbing energy. The presence of damage can cause an unstable mode of failure. It is therefore important to understand the effects of damage on the properties of composite structures.

This work sets out to provide an understanding of the effects of a range of non-service type defects on the mode of failure and consequent energy absorption characteristics of tubes manufactured from glass reinforced polymer composites. Non-service defects are described as defects caused accidentally during the everyday running of the vehicle, but are not induced by the use of the composite energy absorber for its primary function, absorbing energy in a crash. The quasi-static and dynamic crushing effects are also observed as are ways of improving the damage tolerance of the parts investigated.

2.0 Literature Review

This section will look at how damage affects composite structures as well as ways of improving the damage tolerance of a composite part. It will also observe how the constituent materials of a composite, fabrication conditions, geometry and test conditions affect the energy absorption capability of a composite structure.

2.1 Damage

Impact damage

In this section we are looking at the effects of an out of plane impact on a composite structure. Low velocity impacts are observed up to 30m/s. High velocity ballistic impacts tend to be above 100m/s. There are four major modes of failure in low-velocity impact as illustrated in Figure 4. Matrix damage is the first type of failure induced by transverse low-velocity impact, and usually takes the form of matrix cracking, but also debonding between fibre and matrix. The second, delamination, is a crack, which runs in the resin-rich area between each ply of fibres. Delamination caused by transverse impact only occurs after a threshold energy level has been reached. Fibre failure mode generally occurs much later in the fracture process than matrix cracking and delamination. It occurs under the impactor due to locally high stresses and indentation effects, and on the non-impacted face due to high bending stress. Perforation is a macroscopic mode of failure and occurs when the fibre failure reaches a critical extent enabling the impactor to completely penetrate the material [2-4]. Perforation in laminates subjected to impact loading has been identified as the most important damage stage, as far as material response is concerned. However, perforation alone causes only a small portion of mechanical properties degradation, with delamination being identified as the other primary damage mode in impacted composite laminates [5]. With high velocity impacts the tup can completely penetrate the structure without creating a large zone of delamination. For a constant energy situation a low velocity impact with a heavy object induces an overall target response, whereas a high velocity impact by a light projectile induces a localised mode of target deformation resulting in energy being dissipated over a small region immediate to the point of impact [6].

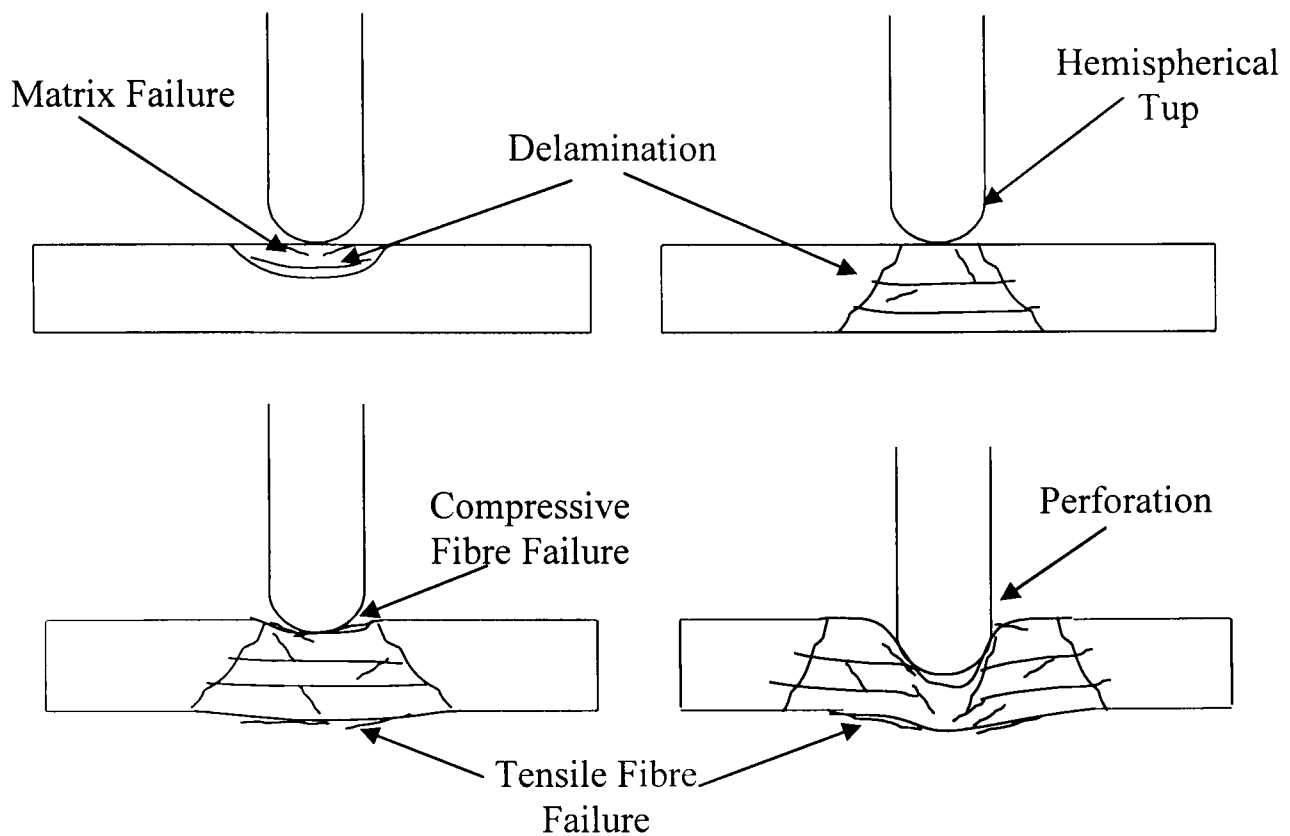


Figure 4: Modes of Failure in Low Velocity Impact

Cantwell and Morton [6] reviewed research papers and found that, of these four failure modes, those that involve fracture of the matrix or interphase region result in low fracture energies whereas failures involving fibre fracture result in significantly greater energy dissipation.

It has been shown that an impact that may not produce any visible damage can create a damage area in the order of 50% of the damage area for a fully penetrated specimen. Dear and Brown [7] showed this through C-scan imaging of the damage zone after damaging sheet moulding compound (SMC) laminates. The onset of visible surface damage does not appear until the load displacement trace reaches its peak (see Figure 5), at which point through thickness damage starts to occur.

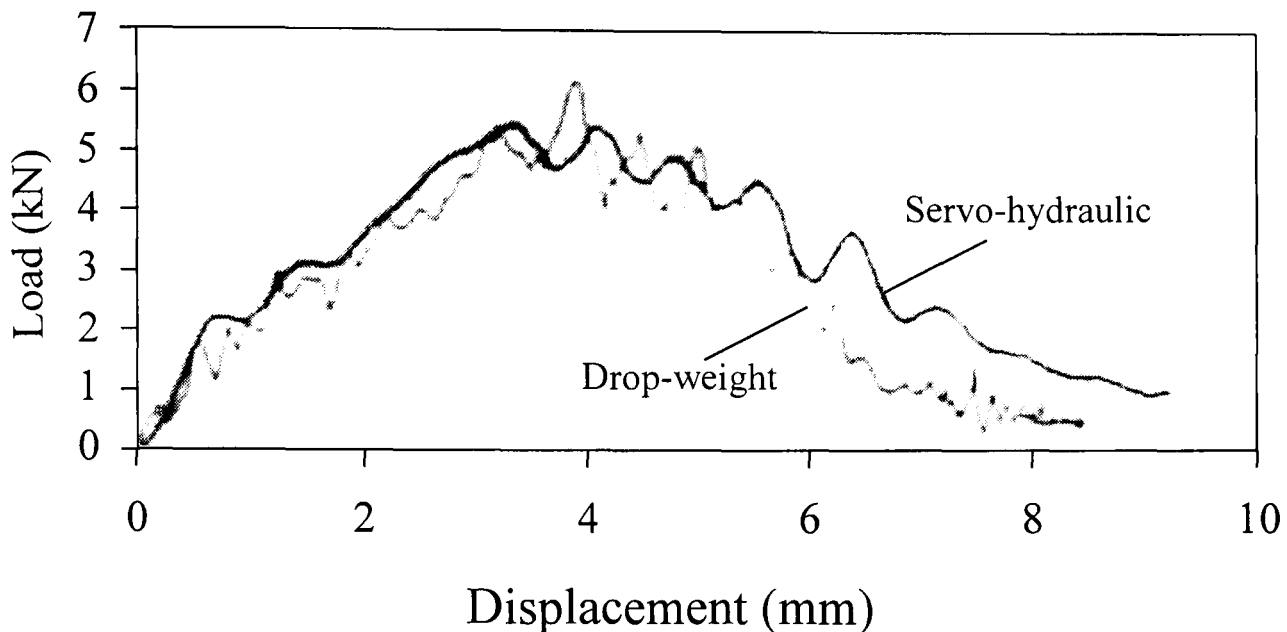


Figure 5: Load displacement graph for a drop-weight impact at 4.4m/s compared with servo-hydraulic impact at 1m/s

It is important to identify what effect impact damage has on the residual compressive strength of the composite laminate as the structural integrity of the structure can be compromised by the impact. There has been much work on this in the form of compression after impact (CAI) testing (Boeing standard BSS 7260) on samples cut from flat plaques. All sources show a reduction in compressive strength as impact energy is increased [8, 9]. CAI testing by Rigas and Petrie [10] on polyester/S2 glass laminates of thickness 0.5", 0.625" and 0.75" impacted at 300 ft-lb (407J), 550 ft-lb (746J) and 800 ft-lb (1085J) showed that compressive strengths were reduced by up to 50% after impact. Further reductions in post impact performance were minimal even at the highest energy level.

Cantwell and Morton [6] suggest that the strain energy absorbing capacity of the fibres is one of the most important parameters in determining the impact resistance of a composite structure. Work by Corum *et al.* [11] supports this, finding that a glass fibre composite was less susceptible to damage than a carbon fibre laminate resulting in a smaller damage area for a given impact. However, the degradation of material compressive strength due to the impact was greater for the glass than the carbon. Different types of reinforcement can be incorporated in a matrix material to form hybrid fibre composites. Adding low-modulus fibre reinforcements, such as glass, aramid and ultra high molecular weight polyethylene (UHMWPE), to brittle carbon

fibres can greatly improve the energy absorption capability from an out of plane impact. Peijs [12] found that this type of hybridisation could improve CAI strength by 140%.

Work by Found *et al.* states that materials with higher flexural stiffness give better resistance to cracking when impacted [9]. This suggests the opposite of all the previous findings, where carbon fibre composites were found to be less damage tolerant than glass fibre composites. This work was done on purely glass fibre samples and may not be generally applicable to all types of composite.

Mahfuz *et al.* [13] also found degradation in compressive performance of graphite laminates with increased impact energy levels. Matrix toughening is another method found to increase the damage tolerance of composites. Testing was on laminates impregnated with three different toughened thermoset resins, two epoxy and one cyanate ester. They found that the undamaged epoxy samples exhibited a greater compressive strength, due to good adhesion to the sizing of the graphite fibre. However, the CAI results show a greater damage tolerance of the cyanate laminates as the energy of the impact appears to get dissipated effectively from the impact location. This suggests that improved damage tolerance is often coupled with reduced virgin properties. Bibo and Hogg [14] found similar trends with preforms produced by a textile process, which did not perform as well as unidirectional prepreg tapes, showing increased compression after impact performance. Their greater economic viability may also lead to their greater usage in future aerospace applications.

It was found experimentally that the damage threshold for an impacted laminate is strongly dependent on the thickness. With increasing laminate thickness, the damage threshold moves to higher impact energies. Thus if we look at the size of the damage zone then thick laminates are less susceptible to impact energy than thin ones [15].

Low velocity impact tests carried out on carbon-epoxy laminates of different thickness suggested that the force at the point of delamination initiation, the maximum force and related energy, and penetration energy all increase to the power of approximately 1.5 with increasing plate thickness [16]. Therefore, by increasing the wall thickness of a structure it is possible to increase its damage tolerance.

Studying the contact between a rigid sphere and a laminate, some researchers including Tan and Sun [17] demonstrated that the elastic Hertzian contact law could be successfully applied. Here, the radius R of the contact zone is yielded by:

$$R \propto \sqrt[3]{F_i} \quad (2)$$

where F_i is the applied load. From equilibrium considerations, it follows that the average shear stress τ along the specimen thickness at the boundary of the contact zone is:

$$\tau = \frac{F_i}{2\pi R t} \quad (3)$$

where t is the laminate thickness. Assuming that the shear stress is responsible for delamination initiation, from Equations (2) and (3) F_i is calculated as:

$$F_i \propto (\tau \cdot t)^{1.5} \quad (4)$$

This compares well with the power law quoted above.

Sample thickness is not the only factor that increases the damage tolerance of a sample. Papanicolaou *et al.* [15] suggest that impact damage is more sensitive to the change of stacking sequence than of target thickness. Impact damage is less likely when there are low modulus layers on the outside such as $\pm 45^\circ$ layers of Kevlar® or glass fibres. Although this suggestion is contradicted by de Freitas and Reis [18]. They found the delamination area due to impact loading to be a function of the absorbed energy and relatively independent of stacking sequences used, but suggested it is highly dependent on the number of interfaces

It has been shown that a delamination threshold load (DTL) for low velocity impact loading on composite laminates can be found [19]. This is the impact load level at which delamination occurs in laminated composites. The DTL can be identified on load-time history curves for impact events. The DTL has been shown to vary with the laminate thickness to the 3/2 power as predicted by other investigators.

During the scaling of impact damage from test specimens to larger structures it has been shown that delamination increases with specimen size more than would be expected if stresses controlled the delamination extent, as would be predicted by fracture mechanics [20]. To see this consider a generic expression for energy release rate is given by:

$$G_I = \sigma^2 \pi a f(a/w) / Q \quad (5)$$

where G_I is the energy release rate for delamination, σ is the applied stress, a is delamination size, $f(a/w)$ is a finite width geometry factor, and Q is an appropriate material stiffness constant. Noting that applied stress is proportional to impact velocity in the present experiments, it can be seen that the impact velocity required to produce a delamination size that is a given fraction of the specimen size should decrease with increasing specimen size. Specifically, the velocity to cause this relative delamination should decrease with the square root of specimen size. This was observed experimentally with, for a constant damage area, velocities decreased from 24.4m/s to 18.3m/s to 12.2m/s as test specimen dimensions were doubled and then doubled again. Fibre breakage does not show this effect, and appears to depend only on the applied stresses or strains, independent of specimen size.

Pre-existing micro-cracks induced by thermal stresses can reduce the impact resistance of composites [3]. Micro-cracks could also be formed due to shrinkage of the resin, suggesting that epoxy matrix composites, which shrink by approximately 2% will be more damage tolerant than polyester matrix composites which have typical shrinkage levels of 7-9%. This idea is supported by work by Sjogren and Berglund [21] who state that the properties of polyester-based composites were usually inferior to those of vinylester composites as a consequence of pre-existing debonds and subcritical cracks resulting from microlevel curing stresses. However, other factors are also influential, such as the failure strain and ultimate tensile strength of the matrix.

Sjogren *et al.* [22] impacted carbon/epoxy plaques with either 16 or 48 plies. Post impact, the tensile modulus of the 16 ply samples was seen to decrease by up to 80%

in the most damaged region of the laminate, but only a 6% decrease was seen in the thicker laminates. In the region of the plaques where the impact had caused mainly delamination, only a moderate decrease in tensile modulus was observed, affirming that the effect on elastic tensile modulus by delaminations is rather small.

All the work described so far on CAI is for test samples from flat plaques. Short *et al.* [23] found that the post impact compressive strength for a curved laminate was similar to that for a flat plate. This suggests that similar trends will be observed in the compression of tubular samples after impact. This is confirmed by the limited literature on the subject, where it was seen that there is a reduction in the SEA of composite tubes after impact damage has been caused [24, 25].

With tubes subjected to an impact the wall thickness greatly affects the amount and even the type of damage caused to the specimen. For tubes with a 1mm wall thickness, cracks developed at the lateral sides with respect to the impact point due to large elastic deformation of the thin walls. In contrast the thicker specimens, being stiffer, developed cracks and delaminations in the vicinity of the impact area [26], as was observed in the plaque samples.

As with plaque samples the extent of the effect of damage was dependent on the constituent materials and fibre architectures. Karbhari [24] tested carbon / epoxy, glass and carbon hybrid / epoxy and glass / epoxy tubular samples. The largest impact related damage area was seen in the all carbon fibre specimens, with the damage area decreasing with an increase in the number of layers of braid used. The glass fibre triaxially braided tubes showed overall better response to impact than the glass biaxially braided tubes. Increasing the tow size of the axial tows in the triaxially braided tubes resulted in better overall performance due to the greater stabilizing effect of the larger size tows. Many researchers have stated how it is possible to decrease the damage caused by a given impact by using lower modulus fibres or using a toughened matrix. However, the best damage tolerance for a given impact is often in samples which require the smallest damage area to affect the properties of the composite. Thus damage area is not always a good representation of damage tolerance. Improvements in damage tolerance are often coupled with a reduction in properties of the composite.

Holes

For many structures it is necessary to drill holes for various purposes. One important requirement is bolt holes. Bolted joints are used to transfer loads within a structure. The strength of a bolted joint may be, to a considerable extent, influenced by the quality and accuracy of the machined holes. If it were possible to machine holes without defects, weight reduction and increased fatigue life would be possible. However, machining defects, such as delamination, chip-out of fibres / matrix, and degradation of the matrix due to overheating can reduce the strength of the composite (see Figure 6).

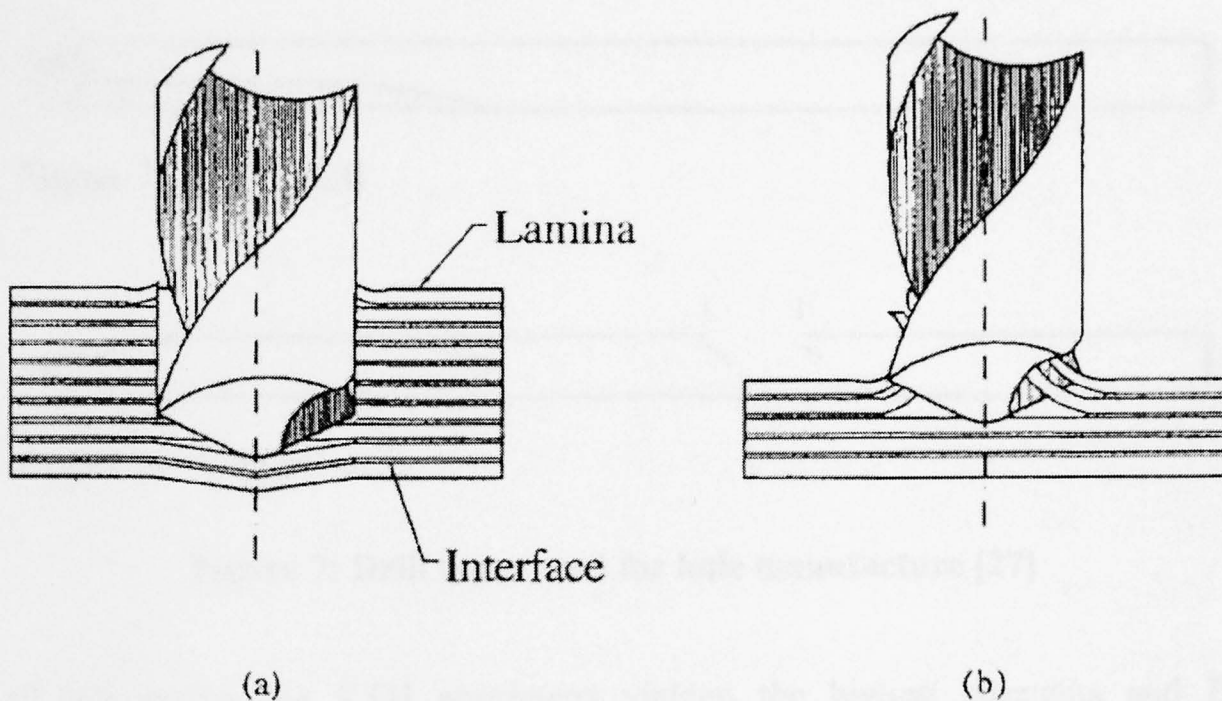


Figure 6: Delamination at exit (a) and at the entrance (b) side of the drilled hole [27]

Testing by Persson *et al.* [27] was done using three methods of hole manufacture. KTH, a new method developed at Kungl Tekniska Högskolan, produced defect-free holes in the specimens, by machining the laminate both axially and radially by rotating the cutting tool about its own axis as well as eccentrically about a principal axis while feeding the tool through the laminate. Around the holes made using a polycrystalline diamond-tipped (PCD) drill, the defects extended from the edge of the hole to a depth in the laminate nearly equal to one hole radius. Using a cemented carbide drill with a sharp tip angle (Dagger drill) produced defects that extended from

the edge of the hole to a depth in the laminate of nearly a quarter of the hole radius. All drill types used are shown in Figure 7.

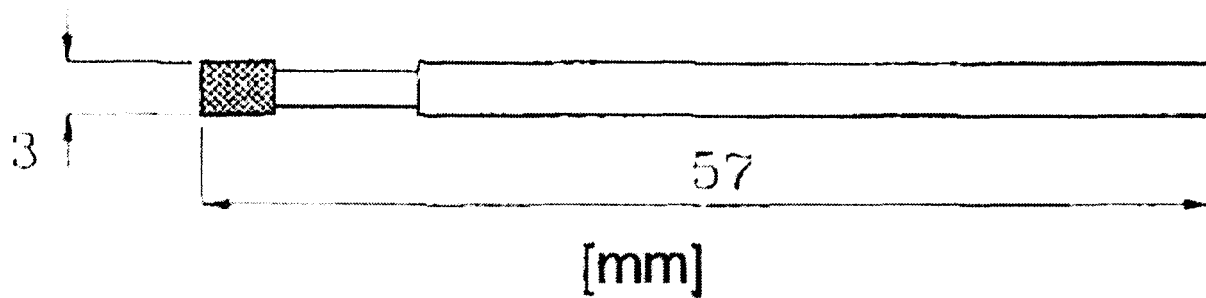


Figure 6 Diamond grain-coated mandrel used for hole generation using the KTH method

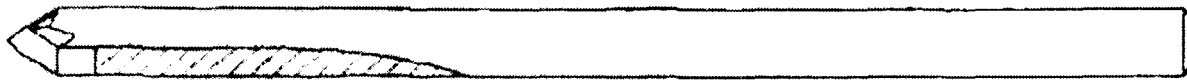


Figure 7 PCD drill

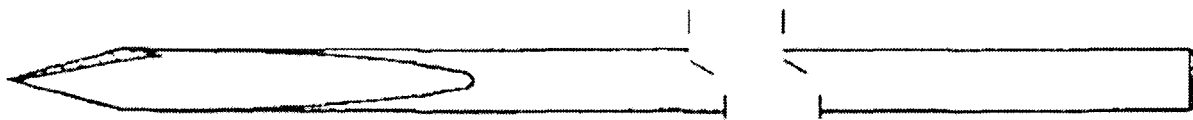


Figure 8 Dagger drill

Figure 7: Drill types used for hole manufacture [27]

In all the testing the KTH specimens yielded the highest strengths and PCD specimens the lowest. When new drills machined the holes the specimens exhibited significantly higher strengths than when used drills were employed. This emphasises the importance of hole manufacture as two identically sized holes may not cause the same reduction in strength of a composite. It is important to maintain the sharpness of a drill bit or replace it regularly throughout a test programme.

The inclusion of a 5mm diameter hole was used by Cowley and Beaumont [28] in centre notched tensile samples. The materials tested were Hercules IM8 carbon fibre in an amorphous poly(ether sulphone) (PES) matrix, and a toughened thermosetting polymer of cyanate esters, reinforced with IM8 fibres. Both materials used $[90^{\circ}/0^{\circ}]_s$ and $[90_2/0_2]_s$ orientations. Damage was seen to grow by splits in the 0° plies extending from the notch tip, transverse ply cracks in the 90° plies and a delamination

zone at the $0^\circ/90^\circ$ interface extending from the 0° split. The rate of split growth was seen to be 50% lower in the PES samples than the cyanate ones due to the difference in toughness of the two matrices, as was seen for impact damaged samples.

Caprino, Falzon and Herszberg [29, 30] modelled the effect of impact damage on CAI strength. They chose to model the damage zone as an equivalent implanted hole and found it was possible to show good correlations between experimental tests and theoretical predictions for CAI strength. This makes it important to compare the response of a material to an impact and the inclusion of a hole of an equivalent size.

Clarke and Pavier [31] also tried to simulate an impact damage zone in the form of a delamination caused by a PTFE insert and by cutting some of the 0° fibres to reduce the strength of the part prior to curing. By calibrating the size of the delamination and number of cut plies against some damaged CFRP samples it was possible to simplify a zone of damage and provide a means of predicting its effect.

Hamada *et al.* [32] designed FRP energy absorbers, which were bolted to a steel column. The work investigates the effect of bolt diameter and number of bolts on the energy absorption properties of the bolted pipe. It was found that progressive crushing occurs when applied stresses on bolt joining regions do not exceed the material strength. Although this work describes the attachment of the composite to a steel column as a bolted joint, the bolt through the hole is merely acting as a bar, without being held in place by a nut. This therefore doesn't realistically simulate the condition that would attach a composite energy absorber to a steel column.

In this section the importance of the drilling mechanism of the hole has been highlighted. The drill bit used to manufacture the holes must therefore be regularly replaced to minimise the impact of a hole on the SEA of a tube. It has also been shown that it might be possible to relate a particular hole size to a particular impact energy level, which would facilitate predicting the effect of the damage.

Ways of improving damage tolerance

There are many variables that affect the material properties of a composite structure. It is shown later how by selecting these variables carefully it is possible to improve the energy absorption of a structure. In the same way, by tailoring the composite, it is possible to increase the damage tolerance of a part.

Various approaches have been employed to improve the damage tolerance or penetration resistance of composite materials. These include control of matrix modifications, fibre-matrix interfacial adhesion, lamination design, introduction of through-the-thickness reinforcements, insertion of interlaminar “interleaf” layers, fibre hybridisation and utilisation of high-strain fibres [33]. The inclusion of interleaves during manufacture can reduce the damage area [34], but reduces slightly the compressive strength of the undamaged laminates tested. Interleaving techniques decrease the area of damage due to impact and increase the CAI of the composite by up to 100% [35, 36]. The role of the interleaves is to alter the failure mode by allowing the transverse and delamination cracks to be arrested upon reaching the interleaved strips and have been shown to greatly improve the interlaminar fracture toughness [37].

Testing with a number of interleaf materials was carried out by Duarte *et al.* [38]. Polyethylene interleaves were successfully used to increase impact resistance, shown by a decrease in damage area. However, this was accompanied by a reduction in compression strength attributed to a lack of lateral support for the fibres. For structural components the compression strength may be improved using a higher shear modulus interleaf material such as polyetherimide film, which produced reductions in damage area and significant improvements in compression after impact strength. This is supported by Walker *et al.* who found that interleaving and short fibre interlaminar reinforcement techniques improved the impact resistance of $[0^\circ/90^\circ]_5$ carbon fibre/epoxy laminates [39].

Kim [35] reviews methods to improve impact performance of CFRPs. By adding materials to toughen thermosets or using high performance thermoplastics it is possible to improve the impact resistance of the composite. These can improve the

CAI properties of the composite by up to 90%. Kim *et al.* [40] found that the residual mechanical properties for composites with rubber-modified matrices are better than those with unmodified matrices.

Using fibre stitching through the thickness of laminates is another way of enhancing the interlaminar fracture resistance and hence impact performance. Composites reinforced this way were found to be much more damage tolerant than those that were unstitched, better than laminates with a toughened matrix and equal to a tough thermoplastic matrix (APC-2). This corresponded to a compression strength of a 3mm laminate after a 45J impact of 270MPa compared to 150MPa for the unstitched laminate [8].

However, Bibo *et al.* [41] have shown that the use of high tenacity aramid stitching yarn does not necessarily translate to improved post impact compression strength over fabrics produced with a conventional polyester stitching yarn despite a measurable reduction in damage area caused by equivalent impacts. Suh *et al.* [42] showed that selective stitching with Kevlar® 29 can improve the failure strength of stiffened AS-4k fabric / 3501-6 epoxy composite panels after impacts. Hosur *et al.* [43] found that stitching of the laminate improved the damage resistance as the stitching helped in containing the damage within the grid location. However, preform stitching can damage the fibre tows and lead to localised resin pooling at the stitch location.

Cantwell *et al.* [44] used high strain carbon fibres to improve the impact performance of CFRP epoxy laminates. Increasing the strain to failure of a composite improves its ability to absorb elastic strain energy in flexure resulting in superior impact resistance. Damage size was significantly less than that observed in CFRP reinforced with standard carbon fibres. After a 6J impact the residual tensile strength was 100% greater than the standard composite, and 30% greater in compression.

The incipient energy (elastic strain energy stored before inelastic deformation occurs owing to damage initiation) required for damage initiation can be increased by improving the fibre/matrix interfacial bond strength. One way this can be achieved is by changing the fibre surface treatment. This would lead to a reduced level of damage for a given input energy if successful. However, due to increased notch

sensitivity of the laminate arising from the brittle interface, the effect on residual strength in tension is detrimental [45]. Hirai *et al.* also investigated the effect of temperature on damage tolerance [46] and found reduced impact damage resistance and damage tolerance of the laminates at elevated temperatures. This was attributed to the poor mechanical properties of the matrix at high temperatures reducing the incipient damage load, increasing the extent of major damage for a given impact energy level. The tensile strength of epoxy resin decreases by about 80% whereas the failure strain increased 11 times when the temperature is changed from -50°C to 80°C.

A study by Kessler and White [47] into the healing of delamination damage in woven E-glass/epoxy composites found that it was possible to repeat DCB tests after healing and achieve up to 67% of the virgin fracture toughness by injecting a catalysed dicyclopentadiene (DCPD) monomer into the delamination. Another healing system was tested where capsules of catalyst for the monomer were embedded in the original matrix of the composite. These capsules would be ruptured in the delaminated area, allowing the catalysing of the monomer once it is injected into the delamination zone. Healing by this method only achieved only 19% of the original fracture toughness.

In this section we have seen a number of ways to improve the damage tolerance of a composite. Introducing an interleaf was seen to reduce the area of damage caused by an impact and increase the CAI strength. However, this was at the expense of a reduction in compressive strength. Toughened thermosets and tough thermoplastics were also seen to improve impact performance, as was the use of high strain fibres. Stitching the preform was also seen to improve damage tolerance, but not in all sample tested.

2.2 Energy Absorption

An ideal energy absorber will decelerate the passenger cell at a constant rate. Metallic crash structures and some composites, such as those with aramid fibres, undergo extensive plastic deformation after the onset of yielding and crush by buckling when subjected to axial compression (see Figure 8).



Figure 8: Buckling Failure Mode of Aluminium Tube [48]

Thermosetting polymers are brittle, as are both carbon and glass fibre, which means that they generally observe little plastic deformation. This means that they tend to deform in a different manner to metals in order to absorb energy. During crushing, the load on the specimen over the crush length affects the amount of energy absorbed as the SEA is calculated from the area under the load-displacement graph.

A typical load – displacement graph for the progressive crushing of composite tubes has a rising section, where there is a transition between the crushing mode associated with the chamfer region and the establishing of the progressive crush mode. A steady state crushing load is then achieved, during which there are small amplitude fluctuations due to stable crack propagation, and then a sharp rise at a displacement where debris is being crushed between the crush platens (see Figure 1).

Many parameters affect the specific energy absorption of composite materials. This is highlighted in Figure 9.

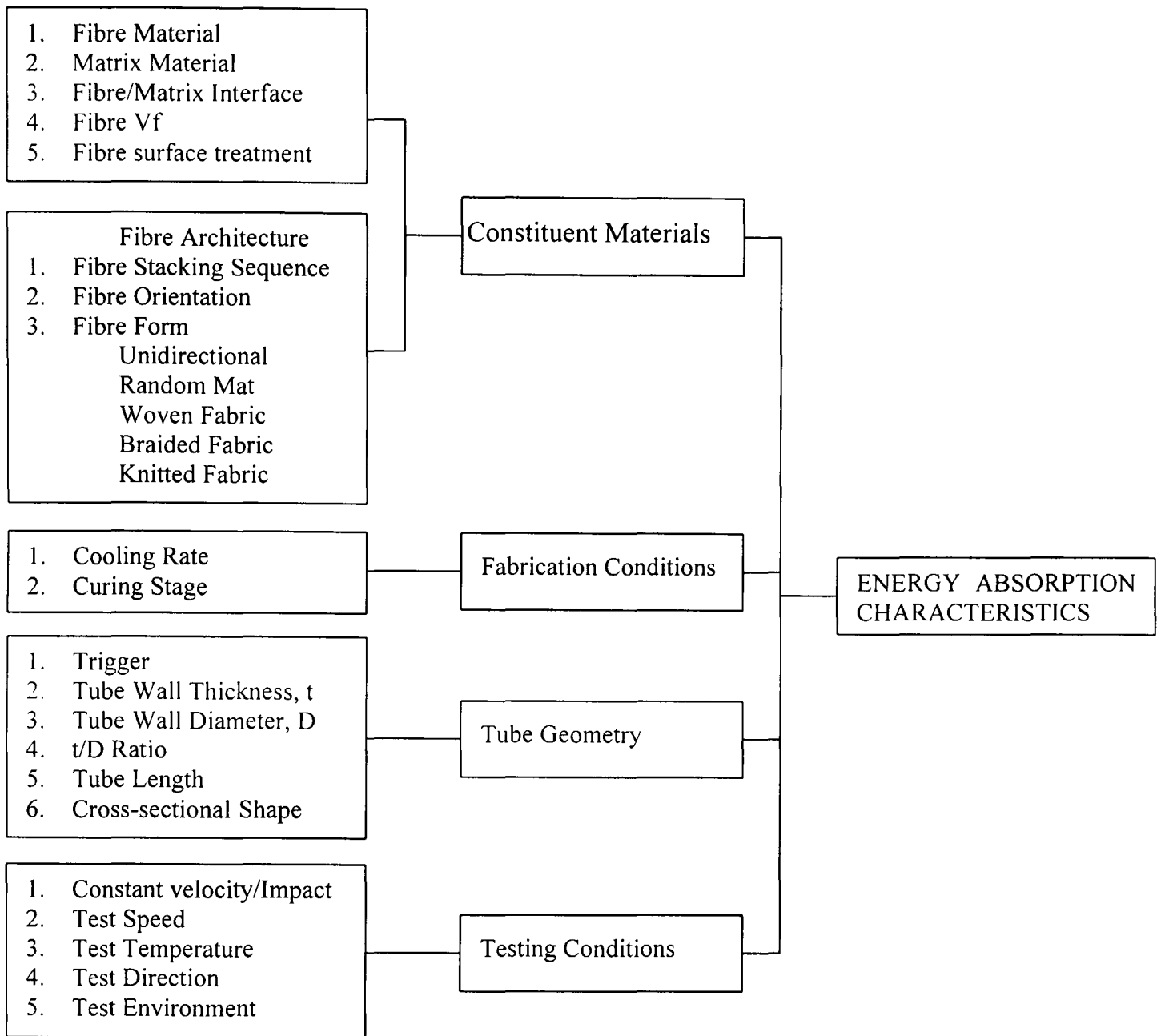
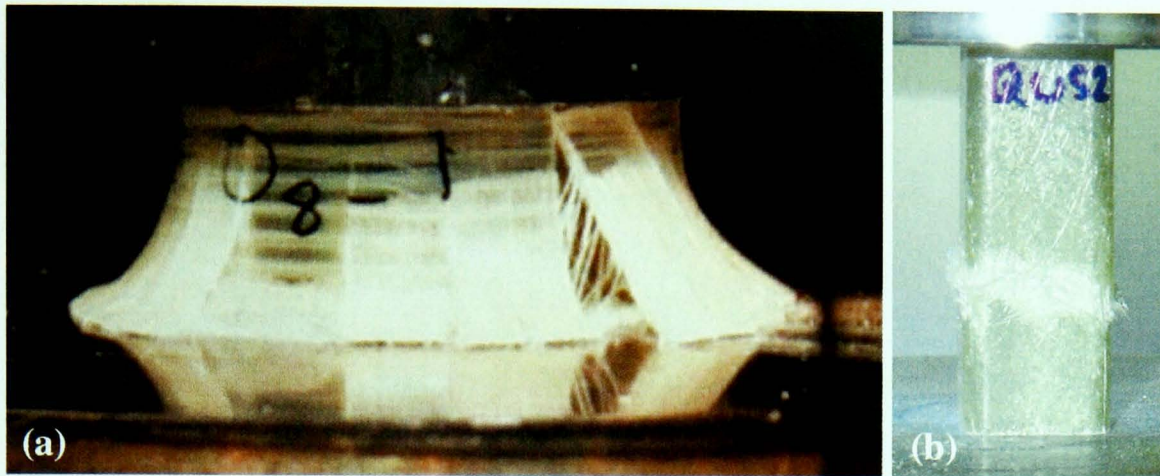


Figure 9: Parameters Affecting Specific Energy Absorption [49, 50]

2.2.1 Failure Modes

Composite tubes can fail by a number of modes due to axial compression, either catastrophically or progressively [51, 52]. Under axial compressive force tubes can fail catastrophically by compressive shear or axial splitting of the tube wall (see Figure 10). Composite components made from brittle materials like glass and carbon fibres, and epoxy and polyester matrix materials are more susceptible to this type of failure. Catastrophic failure modes absorb less energy than if they had crushed by a progressive failure mode, making them of little interest for use in crashworthy structures. Composites made with ductile fibres (e.g. aramid) can fail by buckling,

which provides the same problems as with metallic tubes with the load taken oscillating with large amplitude.



**Figure 10: Unstable Failure of Composite Tubes under Axial Compression
(a) Axial Splitting, (b) Compressive Shear**

Farley [53] describes the crush efficiency of energy absorbing structures. Metals can only crush to 50% of their original length due to the folding mode before bottoming out and the load increases sharply. Wierzbicki and Abramowicz [54] state that generally a metal tube will have a crushing distance equal to about 67% of the original height of the member. Jones [55] describes stroke efficiency as crush length before bottoming out (point at which the load taken increases rapidly) divided by original length. He quotes typical stroke efficiency values for steel tubes of 75%. Typical SEA values for metallic energy absorbers are 45kJ/kg for steel and 60kJ/kg for aluminium [56]. Snowdon and Hull [57] state a value for the SEA of steel tubes of about 20-25kJ/kg, which failed by multiple hinge formation involving significant plastic deformation.

With composite materials it is possible to crush the energy absorber further than metals before the debris trapped inside the tube becomes compacted and reduces the effective crushable length of the tube. For CoFRM / polyester tubes the stroke efficiency was calculated at over 80% [48]. SEA values for composite materials have been achieved as high as 227kJ/kg [58] for carbon fibre [$\pm 15^\circ$]/PEEK while cheap SMC (Sheet Moulding Compound) can achieve 50-70kJ/kg [50] (see Figure 11 for reported SEA values).

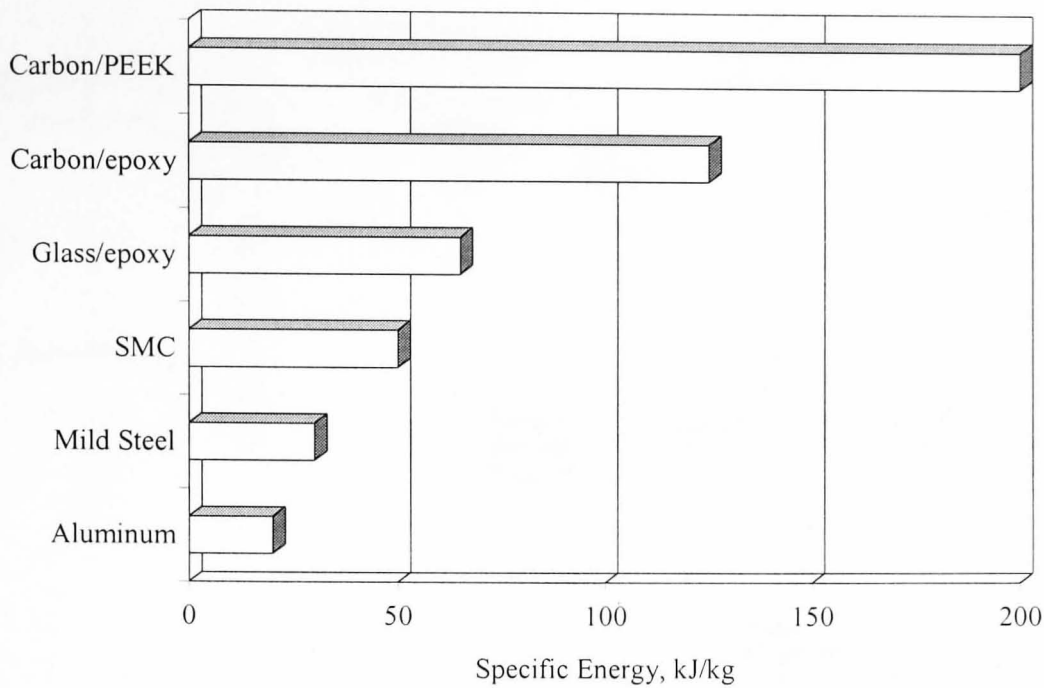


Figure 11: Typical Specific Energies of Different Materials [50].

Crashworthy composite structures are designed to absorb energy in a controlled manner. This is achieved by progressive crushing. Crush is initiated at a stress concentrator, such as a chamfer. Microfracture then initiates in the chamfered region leading eventually to the generation of a stable crush zone. The energy absorbed in this way is greater than the energy absorbed in catastrophic failure modes. The form of the crush zone is dependent on many factors including fibre arrangement, tube geometry and test conditions. Based on the crush zone morphology, they can be grouped into splaying (see Figure 12) or fragmentation modes (see Figure 13). As well as these, progressive folding modes, similar to those experienced by metals, occur in the more ductile fibre composite tubes.

Splaying

The main feature of the splaying crush mode is the annular wedge of tightly compacted and highly fragmented debris that is forced axially through the tube wall. The wedge is formed during crushing of the trigger and subsequently deflects delaminated strips from the wall radially inward and outward in the form of a continuous frond (see Figure 12 from Fairfull and Hull [59]). The splaying mode is usually observed in structures containing a relatively high percentage of axial fibres [60].

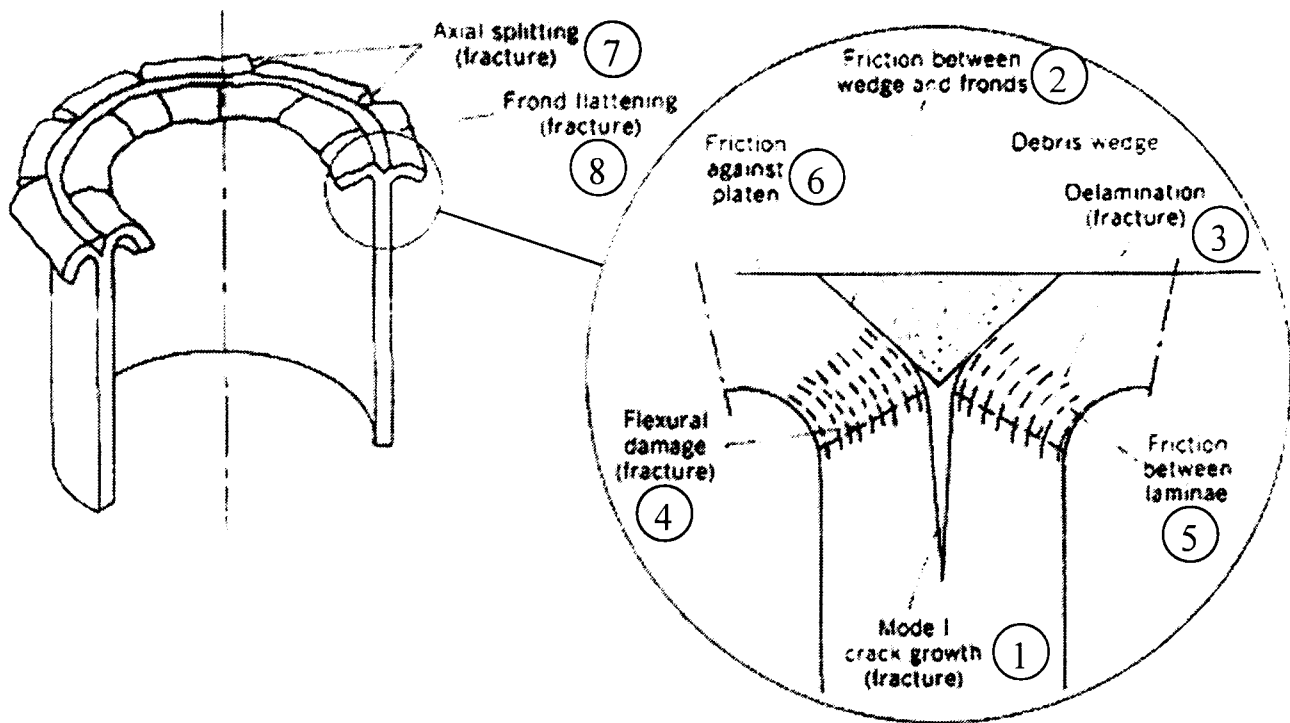


Figure 12: Schematic of the Splaying Crush Mode [59]

Eight factors contribute to the energy dissipation [59].

1. Propagation of mode I opening crack at the apex of the debris wedge.
2. Frictional resistance to penetration of the debris wedge between the internal and external fronds.
3. Extensive delamination in the fronds, where they are deflected through a small radius of curvature by the wedge.
4. Flexural damage at the delamination limits in the form of multiple transverse cracking through the individual plies of the fronds.
5. Frictional resistance to sliding between adjacent plies as they pass through the deflection arc of the crush zone.
6. Frictional resistance to internal and external fronds sliding across the crush platen. With cylindrical tube, there is no relative movement between the debris wedge and the crush platen, since after its initial formation the wedge has been shown to remain essentially unchanged [61].
7. Propagation of the axial splits between fronds. The spacing of the splits and hence number of fronds is governed primarily by the initial external curvature of the tube.
8. Multiple longitudinal cracking through the individual plies of the fronds facilitating their transverse flattening.

Five of these are fracture mechanisms (1, 3, 4, 7 and 8), resulting in the creation of new surfaces, and three are friction processes resulting in energy absorption. Berry [62] and Keal [63], found that the fracture mechanisms account for approximately one-third of the overall energy absorption. Fairfull suggests that the frictional effects account for approximately one-half of the total energy absorption.

Farley [53, 64-66] reported that the principal energy absorbing mechanism for splaying is matrix crack growth and that the central wall crack length is usually at least one order of magnitude greater than that of the fragmentation mode (see centre wall crack lengths in Figure 13 and Figure 14).

Fragmentation

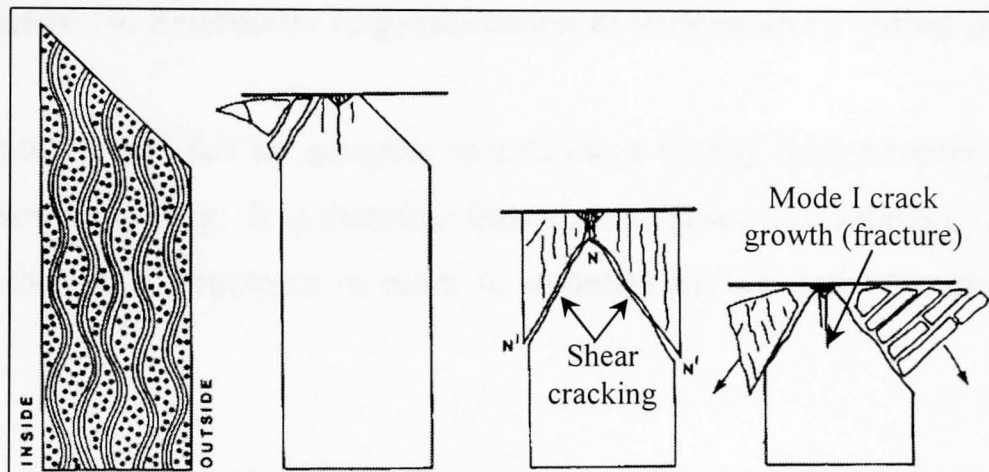


Figure 13: Schematic of the Fragmentation Crush Mode [60]

In fragmentation the tube wall fragments due to shear cracking and fragments are forced to the inside and outside of the tube before complete separation from the tube wall (see Figure 13).

Buckling

During progressive folding the load-displacement curve can be divided into three sections. In the first region the load increases rapidly and reaches a maximum load before dropping rapidly because of load relaxation associated with the initiation of a folded region at one end of the tube. The fold is initiated by shell buckling. In the second region the load oscillates about an average load as successive folds are

formed. The second stage is complete once the tube is fully folded and leads to a rapid increase in load in stage three (see Figure 1 and Figure 14).

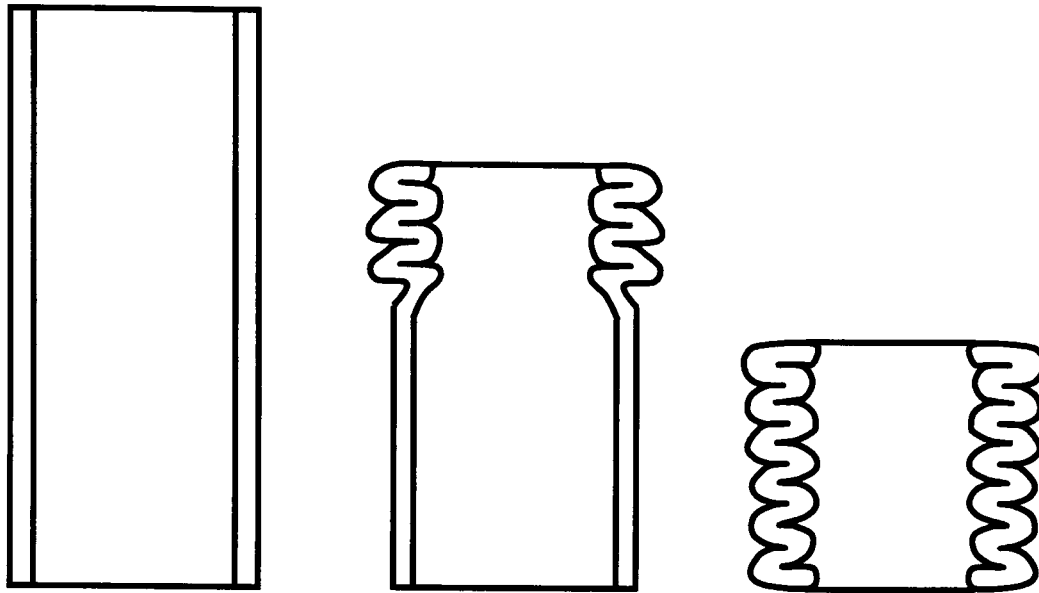


Figure 14: Schematic Representation of Progressive Folding [60].

Composite tubes that fail by splaying absorb more energy than samples that fail by fragmentation or folding. It is therefore important to promote a splaying failure mode for composite crash structures in order to optimise the amount of energy they can absorb.

2.2.2 Constituent materials

Matrix material

Ramakrishna and Hamada [49, 50] state that the SEA order for thermoset resins is phenolic < polyester < vinylester < epoxy when used as the matrix material in composite crash structures. Thermoplastics have order Polyetheretherketone (PEEK) > Polyetherimide (PEI) > Polyimide (PI) > Polyarylsulphone (PAS) [50]. Satoh *et al.* [67] provided SEA values for carbon/PEEK of 194kJ/kg, carbon/PEI of 155kJ/kg, carbon/PI of 131kJ/kg and carbon/PAS of 128kJ/kg. These results for expensive (up to £67/kg), high temperature thermoplastics compare with values for equivalent carbon/epoxy tubes of 110kJ/kg and glass/unsaturated polyester tubes of 80 kJ/kg [60].

Turner [68] at the University of Nottingham fabricated tubes from CoFRM E-glass and found that epoxy resin provided the greatest SEA, then vinylester and finally unsaturated polyester (see Figure 15). By blending vinylester and polyester it was possible to change the SEA in proportion to the mix ratio. The cylindrical tubes tested in the work by Turner had outer diameter of 88.9mm, wall thickness of 4mm and fibre volume fraction of 23%.

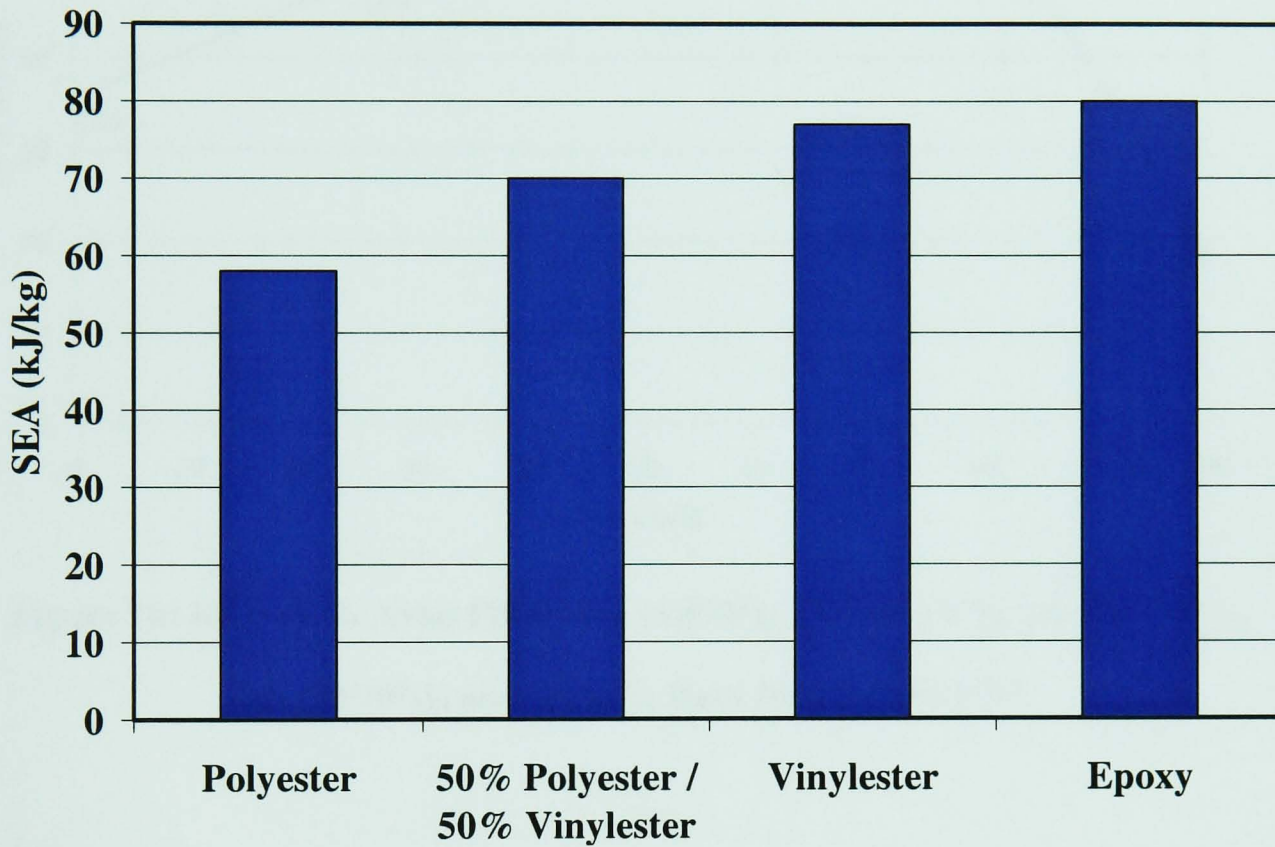


Figure 15: Effect of Resin Type on SEA of CoFRM E-Glass Composite Tubes [68]

Hamada *et al.* [69] compared carbon fibre tubes with thermoplastic (PEEK) and thermoset (epoxy) matrices. With 0° fibres the epoxy tubes failed by extensive cracking parallel to the fibres (as shown in Figure 10 (a)). The PEEK tubes crushed by splaying with an SEA of 180kJ/kg. Measurements showed that the G_{Ic} of carbon/PEEK (1560 to 2400Jm⁻²) was over 10 times the corresponding value for the epoxy based material (120 to 180Jm⁻²). The PEEK matrix therefore provides much higher resistance to crack growth between the fibres so the tube does not fail unstably before the onset of progressive crush. It is important to have some type of hoop constraint to prevent axial splitting. This may be in the form of a high fracture toughness matrix, such as PEEK, or by orientating some fibres in the hoop direction. At £67 per kilogram the former may be prohibitively expensive, whereas the latter

may require the removal of some axial fibres to enable their inclusion and therefore reduce the load bearing capacity of the composite. By optimising the percentage of axial fibres it is possible to ensure stable crush and maximise SEA (see Figure 16).

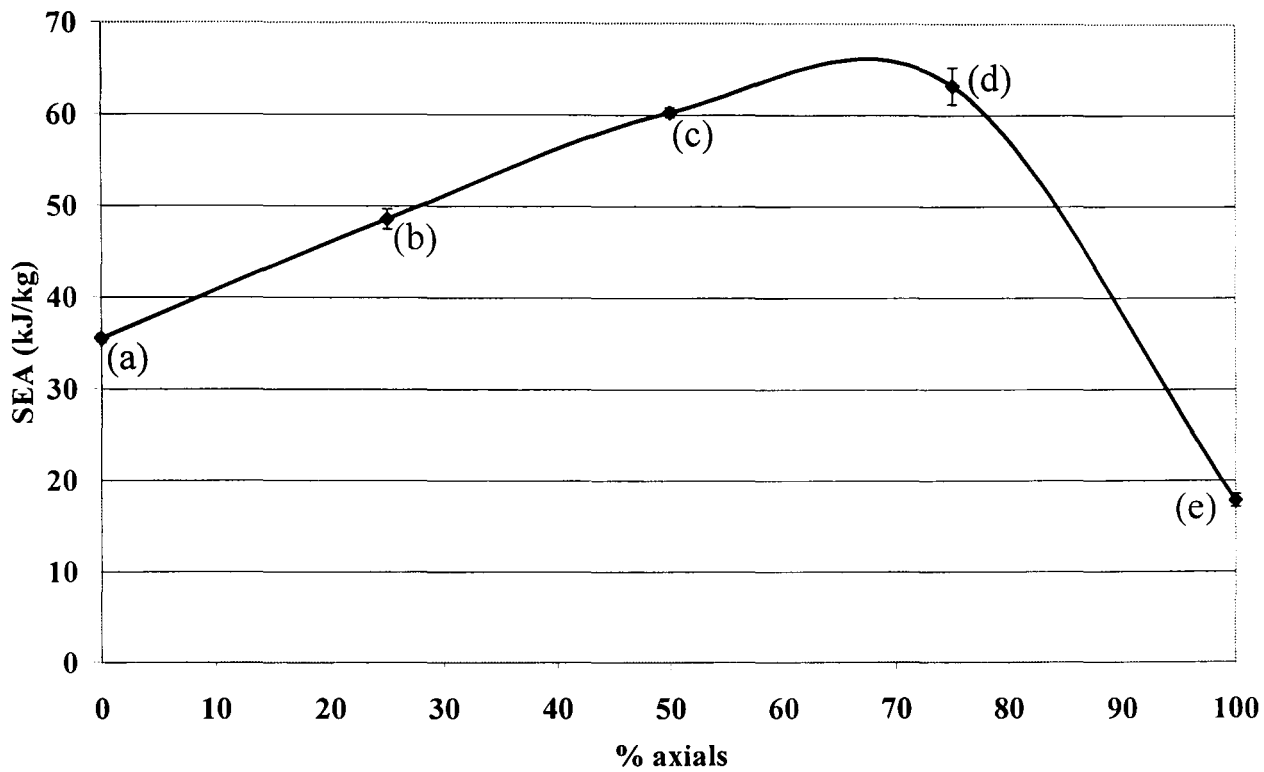


Figure 16: SEA vs % Axial Fibres for (a) $[90^\circ]_8$, (b) $[90^\circ_3/0^\circ]_S$, (c) $[90^\circ_2/0^\circ_2]_S$, (d) $[90^\circ/0^\circ_3]_S$ and (e) $[0^\circ]_8$ Data from Curtis [70]

Fibre material

The main fibres being used include in research and industry for composite structures are carbon, graphite, glass, aramid and hybrids of these. Thornton and Edwards [71], Schmeuser and Wickliffe [72], Farley [65, 73, 74] and Hull [60, 75] observed that carbon and glass fibre reinforced thermoset composite tubes crush progressively by splaying and fragmentation modes. Aramid fibres in a thermosetting matrix, however fail by progressive folding like metallic parts. This can be attributed to the lower strain to failure of the carbon and glass fibres at about 1% and 4% respectively, compared to 8% for aramid fibres. The carbon fibre reinforced tubes have higher specific energy absorption potential due to higher modulus and strength, and lower density of the carbon fibres compared to glass fibres. Aramid fibre reinforced tubes are generally shown to have even lower SEA values.

Karbhari [76-78] found that it was possible to improve the SEA through hybridisation. By replacing the glass or Kevlar® axials with carbon in triaxially braided glass or Kevlar®/vinylester tubes it was possible to significantly increase crush performance while retaining post-crush integrity. This is to be expected as carbon fibre composites generally have higher SEA values than glass or Kevlar® of the same architecture. The results also show increased performance in all samples with the triaxial braid over the biaxial ones. The work by Peijs [12] took carbon samples and made hybrids by increasing the amount of glass and Kevlar® and improved CAI by 140%. This work by Karbhari shows that the overall crush performance due to such hybridisation is reduced. This emphasises that it may be necessary to find a balance between energy absorption and damage tolerance.

Fibre content

Snowdon and Hull [57] found that an increase in fibre volume fraction in sheet moulding compound (SMC) from 13% - 18% gave an increase in specific energy from 38.7kJ/kg to 53.5kJ/kg. Increasing the volume fraction further to 25% only gave a further smaller increase to 56kJ/kg

Tao *et al.* [79] varied the fibre volume fraction in glass fibre / epoxy tubes from 10% - 60% and saw an increase in SEA up to saturation at 50%. Another study by Tao *et al.* [80] using unidirectional E-glass fibre rods found the specific energy absorption to increase with fibre content. These rods (7mm OD) also showed increases in SEA with fibre diameter, matrix yield strength and crush rate.

Farley [81] reported in his work with carbon fibre / epoxy samples with volume fractions between 40-70% that the SEA decreased with increasing volume fraction. This was attributed to reduced interlaminar shear strength of the composite with increased fibre content.

Work in this section shows how increasing the fibre volume fraction, where the fibres are the main load bearing part of the composite, increases the SEA. However above a critical level, which seems to be determined by the type of fibre and matrix involved, the SEA can decrease due to reduced ILSS as suggested by Farley [81].

Fibre Architecture

The architecture of the fibre in the composite material can come in many forms. This enables composites to be tailor made for the application and stresses that the part is likely to see in use. It is possible to vary the stacking sequence and orientation of the fibres, although it is necessary to keep the laminate balanced. Fibre is produced woven or knitted in the required orientation, such as unidirectional or $\pm\theta^\circ$. The fibre can also be braided or come in a random form with fibres either as a continuous filament or chopped strands.

Quek *et al.* [82] found that under quasi-static crush conditions the crush load for CSM glass fibre tubes oscillated less about the steady state crush load than braided tubes, which exhibited a more distinct periodicity (see Figure 17).

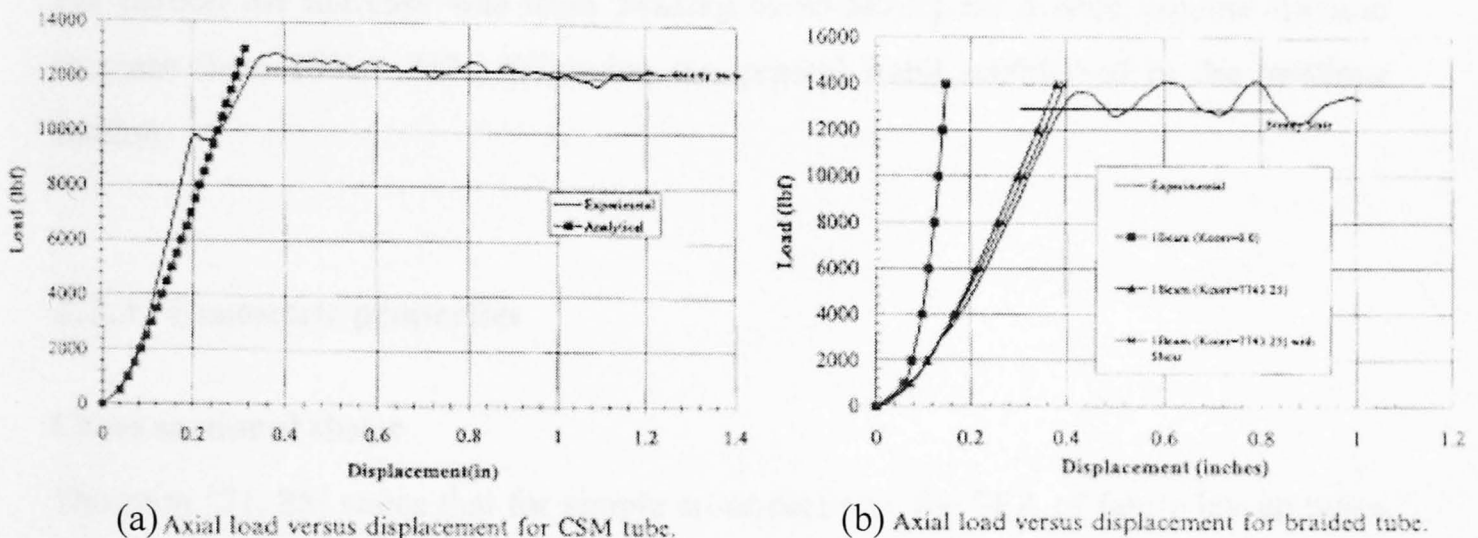


Figure 17: Graphs Showing Crush Response of (a) Axially Loaded CSM Tube, and (b) Axially Loaded Braided Tube

This response suggests that braided tubes are more likely to fail by a buckling failure mode. If it were then possible to promote splaying by adding more axial fibres (as suggested by Hull [60]) then it may be possible to increase the SEA further.

Hamada and Ramakrishna [83] found that by changing the angle of the carbon fibres from 0° to $\pm 15^\circ$ it was possible to increase the SEA of the carbon/PEEK tubes from 194kJ/kg to 225kJ/kg. Increasing the proportion of axial fibres within a composite will generally increase the SEA. In this case where all the fibres were aligned axially,

by changing the orientation to $\pm 15^\circ$ increases the hoop constraint, the stability of the crush and the SEA.

However, with too much hoop constraint the tendency to splay can be considerably reduced. This was seen by Ramakrishna [84], who tested knitted fibre composites in both warp and weft directions. The weft knitted carbon fibre/epoxy tubes had higher SEAs (65.5kJ/kg) than weft knitted glass fibre/epoxy tubes (54.0kJ/kg). The warp direction provides greater hoop constraint and hinders splaying leading to greater fragmentation. The weft direction has lower hoop constraints favouring splaying. The splaying failure mode is more efficient leading to higher SEAs. The SEA of the knitted fabric composite increased with increased fibre content. Volume fraction increases for glass from 14% - 26% saw an increase in SEA from 46kJ/kg to 54kJ/kg. For carbon the increase was from 54kJ/kg to 65.5kJ/kg for a fibre volume fraction increase from 19% - 31%, following the general trend established in the previous section.

2.2.3 Geometric properties

Cross sectional shape

Thornton [71, 85] states that for simple cross-sections, the SEA of fabric lay-up tubes of a given size increases in the order rectangular < square < circular. These findings are supported by Mamalis *et al.* [86, 87], Farley [65], Chadwick [88], Chiu [89] and Price [90]. This is attributed to the corners acting as stress concentrations leading to the formation of splitting cracks (see Figure 12). Typical SEA's for square samples are 50kJ/kg for carbon and 26kJ/kg for Kevlar® and glass. Thornton's work [91] on glass/epoxy square tubes found that increasing the wall thickness from 1.3mm to 2.8mm increased the SEA from 16kJ/kg to 31kJ/kg.

It has been possible to achieve greater energy absorption potential from conical structures than any other geometry. Cones can be made to crush progressively with an approximately linear increase in load due to an increased area being crushed. Thus it is possible to design energy absorbing structures with controlled load-displacement ramps. However, in the introduction it was stated that the ideal loading situation was

to have a constant deceleration. Therefore tubular structures may be more desirable. Mamalis *et al.* [87, 92, 93] carried out extensive testing on composite frusta and found that the failure mode was affected by shell geometry, fibre architecture and fibre and matrix properties. They also state that increasing the angle of a cone results in lower specific energy. Unstable failure was seen above a threshold semi-apical angle of 15°-20°. It is also possible to initiate crush of cones without a trigger [94]. The energy absorption of cones varies in a complex way with cone angle, diameter and wall thickness, and in some cases exceeds values recorded for axisymmetric tubes.

Price and Hull [94] also found that slotted and sectioned tubes can fail progressively, but SEA is reduced compared to complete tubes. Hamada *et al.* [95, 96] crushed full circle, three-quarter circle, half circle and quarter circle glass cloth/epoxy and carbon/PEEK tubes. As the cross section decreased from full to quarter circle, the SEA decreased by 20% for the glass specimens. The reduction for the carbon/PEEK samples was far less (3.6%). Duckett [97] found similar trends for CoFRM E-glass / polyester tubes with a quarter section tube exhibiting a 19% lower SEA than a full circle. The SEA of half section samples was 5% lower and three-quarter sections was less than 1% lower than the full circular sample.

Mamalis *et al.* [98] investigated an hourglass cross section frame rail for use in the apron construction of the car in order to achieve higher loading capacity at this location of the car body when subjected to axial collapse and/or bending. However, a problem with the design was found associated with the delaminations and residual stresses developed in the curved regions of the beam during fabrication, which may cause severe limitations in its load-carrying capacity by initiation of micro cracking sites in the beam.

It has been shown in this section that it is important to have closed section tubes as the part sections always exhibit lower SEA capability than a complete section. Circular section tubes absorb more energy than equivalent square tubes, although Browne [99] states that it is easier to incorporate a square crash structure rather than a cylindrical crash structure into the design of a vehicle.

Dimensional Effects

With carbon fibre / PEEK tubes Hamada *et al.* [100] found that SEA was dependent on the absolute value of t rather than the t/D ratio. However, the absolute value of t affects the t/D ratio and it can be seen in Figure 18 that graphs of both SEA vs t and SEA vs t/D show similar trends for carbon/PEEK tubes. t/D results for this material showed unstable failure for ratios of less than 0.015, and highest SEA values for wall thicknesses in the range of $t=2-3\text{mm}$.

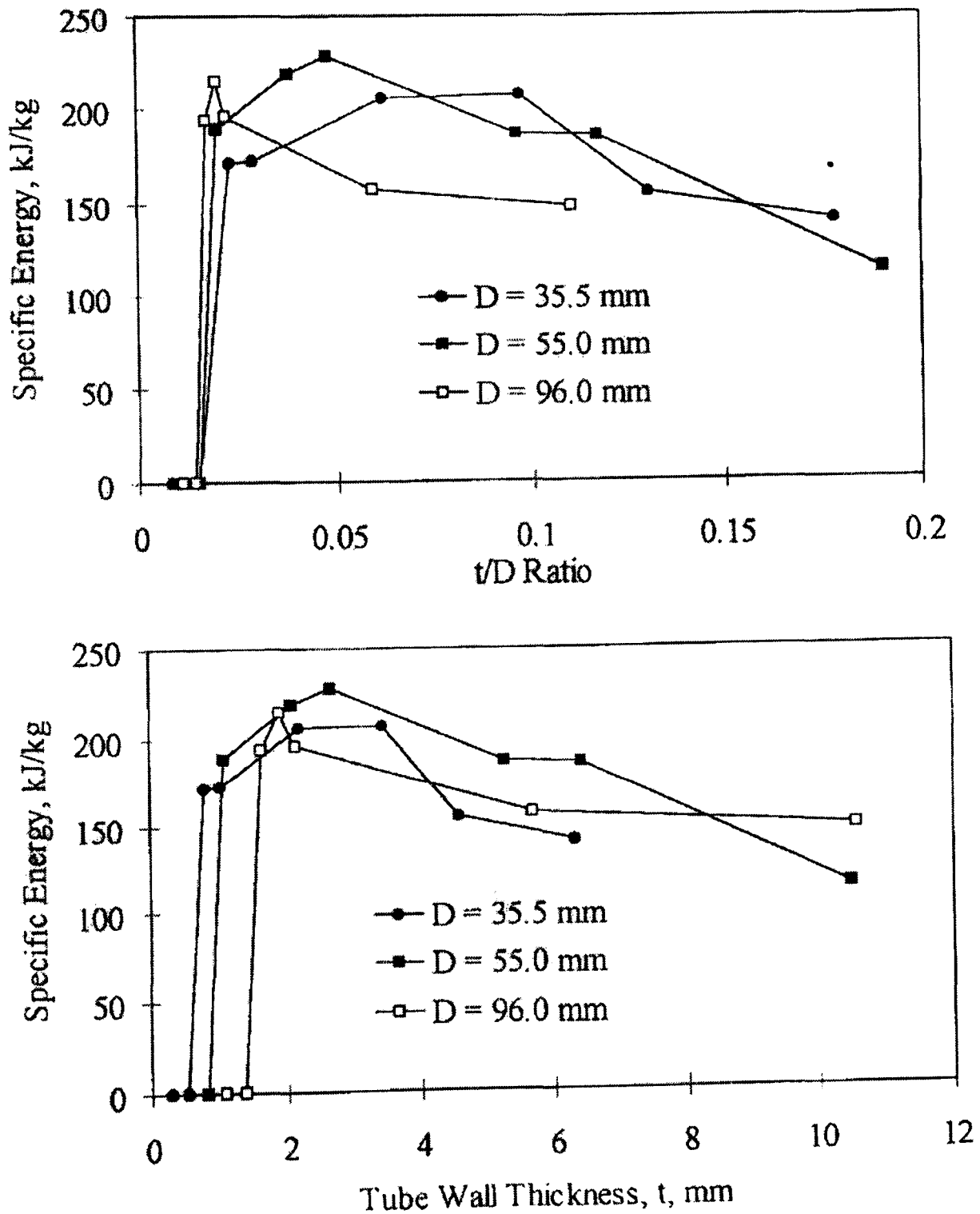


Figure 18: Variation of SEA with Tube t/D Ratio and Wall Thickness (t) [50]

Johnson *et al.* [101] and Browne *et al.* [102, 103] tested structural reaction injection moulded (SRIM) and resin transfer moulded (RTM) glass/vinylester tubes with architectures ranging from random chopped mat to triaxial braid. The results showed that increasing the wall thickness of a tubular crush structure increased the SEA. Fairfull and Hull [104] saw a similar trend from their work with glasscloth / epoxy tubes, with SEA also increasing with increasing t/D ratio up to 0.20, above which it decreased. Farley [105] reported a similar non-linear trend with elliptical cross-section tubes. Farley [73] also found that as the t/D ratio increased the SEA capability increased non-linearly for graphite / epoxy tubes. At the lowest t/D ratios unstable buckling of the composite tubes were observed, which led to low SEA values. In the next range of stable failure a linear increase in SEA with t/D was observed. At the highest t/D ratios an almost constant SEA was seen.

Thornton [71] used relative density (ratio of the density of the tube to the density of a solid cylinder of the same diameter) as a measure for the relative difference between wall thickness and specimen size. His work found that for square and rectangular graphite tubes the relative density required to guarantee stable failure was higher than that for circular tubes with values of 0.075 and 0.025 respectively.

There is a definite trend between wall thickness, t/D ratio and SEA. The thinnest tubes and tubes with the lowest t/D ratio fail by unstable buckling. This leads to decreased energy absorption capability. It is possible to increase the SEA by increasing the wall thickness and t/D ratio. However, above a critical level the SEA then decreases. The optimal wall thickness and t/D ratio were shown by Ramakrishna and Hamada to be 2-3mm and approximately 0.6 respectively. These values will vary for different materials, but provide a good basis for tube geometry design. It is also important to note that square tubes may require a greater wall thickness to ensure stable crush.

Trigger mechanism

A trigger is required at one end of a structure to initiate stable crush. It will act as a stress concentration, usually by reducing the cross sectional area of the tube. This can be done by machining a bevel (chamfer) or tulip shape at one end of the crush

structure (see Figure 19). This leads to a gradual initial increase in load and the growth of a stable crush zone. Without a trigger mechanism composites can fail by unstable axial collapse or compressive shear (as seen in Figure 10). Grundy [106] found that at high speeds composites without an initiator fail catastrophically by shattering the material. This does not provide optimal energy absorption so a trigger is required to cause the fragmentation at the microscopic level, which will initiate stable crushing. Farley [107] found that by introducing a chamfer the peak load can be greatly reduced without affecting the sustained crushing load.

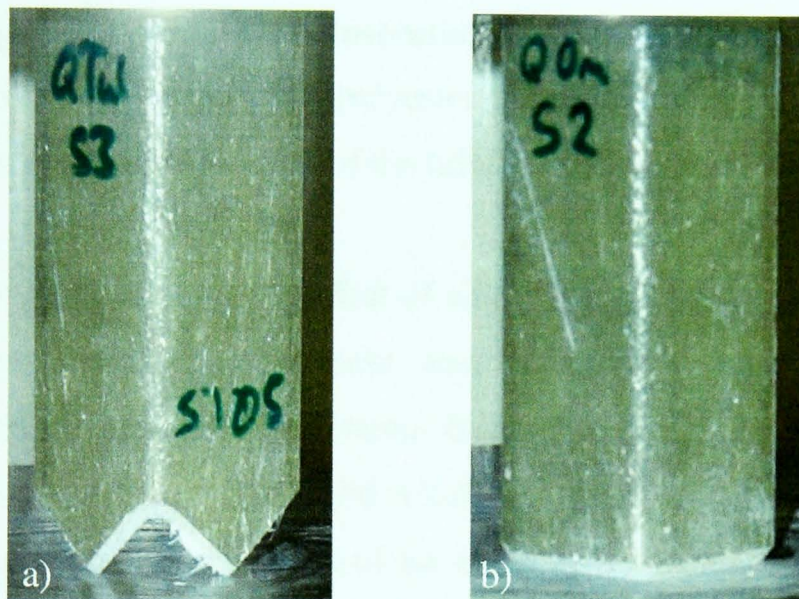


Figure 19: a) 45° Tulip Trigger, and b) 45° Bevel or Chamfer Trigger

Czaplicki *et al.* [108] found that the use of a tulip trigger rather than a bevel trigger on E-glass/polyester and E-glass/vinylester pultruded tubes can increase the SEA by up to 100%. This was attributed to deeper crack penetration and larger distance between fracture lines for bevel triggered samples (a schematic illustration of fracture lines can be seen in Figure 20). Nearly all the fracture that takes place in the surface glass mats occurs at the fracture lines. Therefore, more closely spaced fracture lines result in more total fracture in the tube and hence more energy absorbed. Once initiated by the trigger the pattern continues for the length of the crush.

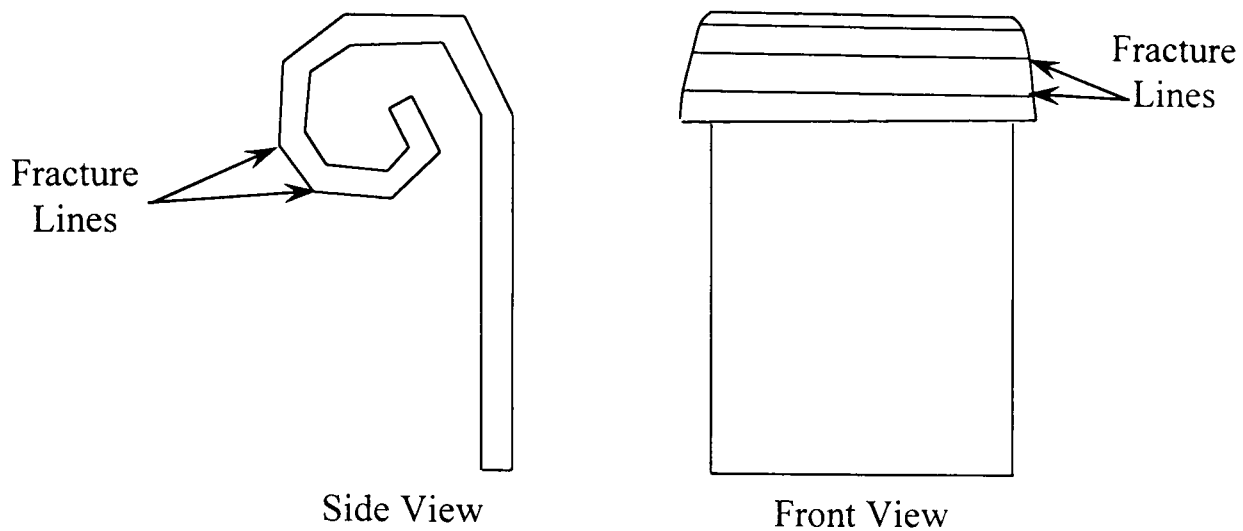


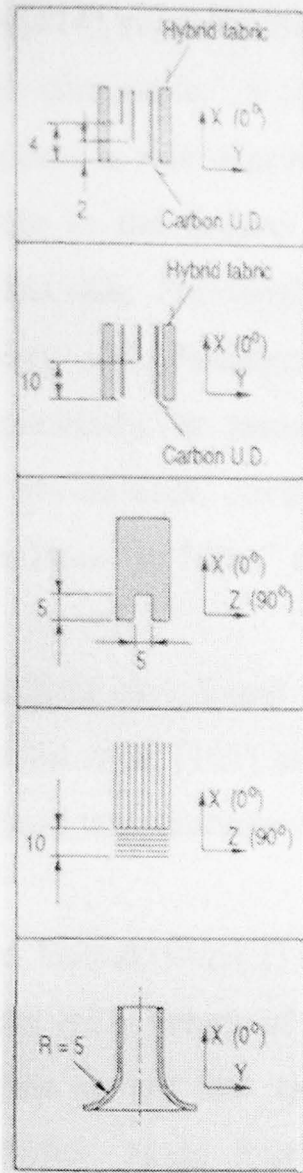
Figure 20: Schematic illustration of fracture lines [108]

Jimenez *et al.* [109] also tested glass/polyester pultruded tubes and found that there was little difference between the SEA of the tulip and bevel triggered samples.

Sigalas *et al.* [110] investigated the effect of chamfer angles from 10° to 90° . In the glass/epoxy tubes the crushing process was initiated by local bending of the chamfered parts of the tubes and by internal cracking. These events gave rise to the generation of wedges of crushed material which were pushed to the inside of the tube wall. The stresses generated at the root of the wedge gave rise to lateral cracks, which caused small rings of material to be sheared off. This sequence of events dominated the initial stages of crush before the crush mode changed to a frond-wedge-frond geometry. The angle of the chamfer did not affect the steady state crush load achieved once the crush zone had progressed beyond the chamfered region.

Hull and Coppola [111] found that for tube crush against a flat platen, the initial chamfer angle has a significant effect on the crush load required to initiate crush, but as found by Sigalas *et al.* it does not affect the progressive crush load.

Thuis and Metz [112] tested various trigger mechanisms by cutting the preform at different plies at the end of the tube to initiate crush (see Figure 21). They found that the different trigger configurations affected the failure mode and energy absorption, with the configuration which simulates the chamfer having the best efficiency. They also found that splaying failure absorbed more energy than fragmentation, and that the use of unidirectional axial fibres is essential to promote splaying.



Trigger no. 1:
Shortening the unidirectional layers by 0, 2 and 4mm respectively

Trigger no. 2:
Shortening of the middle layer of the unidirectional carbon layer by 10mm

Trigger no. 3:
Removing rectangles of 5mm x 5mm in the unidirectional carbon layers

Trigger no. 4:
Shortening of the unidirectional carbon layer by 10mm and replacing it by 10mm 90 degrees unidirectional layers

Trigger no. 5:
Adding a radius of 5mm at one end of the cylinder

Figure 21: Different trigger configurations [112]

There appears to be no significant improvement in SEA for one trigger type over another. Tulip triggers remove more of the sample than bevel triggers and this will lead to an overall reduction in energy absorbed. A 45° bevel was used by Curtis, Duckett, Fernie and Turner [48, 70, 97, 113] to trigger crush on similar CoFRM/polyester tubes. This trigger mechanism was therefore used to enable direct comparison with their data if required.

2.2.4 Testing conditions

Test speed (Quasi-static / Impact)

The matrix materials used in composites are viscoelastic. This means that their response to loading will be rate dependent. The fibres used (carbon and E-glass) are linear elastic so they will be less susceptible to a change in properties with loading

rate. Farley [114] suggests that the effect of test rate on SEA is related to the failure mode of the composite. It depends on whether the mechanism that controls the crushing process is rate dependent. So for sample failure where the fibres play the dominant role in the failure mechanisms the energy absorption should not be a function of test rate. Previously Farley [107] had found from tests on graphite/epoxy, Kevlar®/epoxy and glass/epoxy tubes that the static and dynamic (7.6m/s) tests produced essentially the same energy absorption, failure modes and post crushing integrity. Tests on SMC circular tubes by Snowdon and Hull [57] also found that in the range 0.004ms^{-1} to 14ms^{-1} there was no significant effect on energy absorption.

Many researchers have found that the SEA of samples decreases with increased test speed. Johnson *et al.* [101] and Browne *et al.* [102, 103] found this to be true apart from at elevated temperatures when the static performance degraded.

Hamada and Ramakrishna [115] also observed an SEA reduction. Carbon/PEEK tubes that had SEA values of approximately 200 kJ/kg when tested quasi-statically saw reductions to half that value when tested at 8.5m/s. This was attributed to a change in failure mode from splaying to more fragmentation of the tube wall. Mamalis *et al.* [87] also found that higher crush speeds significantly affect the behaviour of polyester and vinylester resin. Random chopped mat glass / polyester composites were seen to absorb some 35% less specific energy at increased crush speed (21m/s). It was clear that at higher crush speeds the crushing mechanisms of tubular specimens with large thickness differ from the static cases. Mamalis *et al.* [92] suggests that the reduction seen in the energy absorption of dynamically tested fibreglass composite square frusta is probably due to higher values of static friction coefficients between the wedge and the fronds and the crush platen and the fronds.

Results by Schmueser and Wickliffe [72] show that the SEA decreases with a test speed increase by as much as 30%, and suggests that studies based entirely on quasi-static test data can over-estimate the energy absorption levels obtainable in a dynamic application. A 20% decrease was also seen by Ramakrishna [50] for both the knitted carbon and glass fabric/epoxy tubes as the testing speed increased from quasi-static to dynamic (13m/s).

Fernie and Duckett [48, 97, 116] tested braided carbon/vinylester tubes with a range of orientations and wall thicknesses and found that both circular and square section tubes with thin walls (~2mm) were more susceptible to the folding mode (or a combination of folding and splaying) resulting in lower SEA. The folding mode in thin-walled tubes changed to progressive splaying at 5m/s, resulting in higher SEA. However, for tubes that crushed by progressive splaying quasi-statically, the SEA was seen to decrease with increased test rate, which was attributed to the viscoelastic nature of the resin, where at high rates the resin becomes more brittle and fractures earlier, leaving the fibres unconstrained. The tensile and compressive strengths increased at dynamic loading rates (5m/s) by up to 37% and 102% respectively. Work on CoFRM E-glass / polyester showed similar trends with a tensile strength increase of 115% and a compressive strength increase of 26%. This compared to values of 74% and 112% for pure resin samples. Geary [117] found that fracture toughness also increased, by a factor of 2.5 to 3, at higher test speeds. This was attributed to a change in fracture mode from fibre fracture to fibre pull-out.

Similar changes in failure modes at rate were observed by Russell *et al.* [118]. They found that thin-walled tubes that failed unstably by buckling at quasi-static test speeds had these instabilities suppressed at higher compression rates. The instability problem was also overcome by foam filling the tubes. Brachos and Douglas [119] also found that it was possible to stabilise the crush mode of samples which buckled by inclusion of a foam core, and thus increased the energy absorption capability of a tube. With a core the cylindrical samples absorbed more energy than rectangular samples with the same braided structure.

Hamada *et al.* [95, 96] managed to change the failure mode of samples by varying the sizing on the fibres. Aminosilane or acrylsilane treated glass cloth/epoxy specimens were tested. Aminosilane is a suitable coupling agent for epoxy and acrylsilane is not. The aminosilane treated glass cloth/epoxy tubes crushed by splaying and the acrylsilane treated specimens crushed by fragmentation independently of cross section shape. Further testing by Hamada *et al.* [120, 121] on glass cloth treated with either aminosilane or acrylsilane/epoxy composite tubes was done quasi-statically at 1mm/min and dynamically at 8.5m/s and found that the aminosilane treated tubes

crushed progressively by splaying at both test rates and exhibited no change in SEA. The acrylsilane treated tubes saw a 15% increase in SEA with test speed attributed to the change in crushing mechanism from fragmentation to splaying.

The mode of failure has been seen to be the most important factor in influencing the SEA of a tubular structure. For polymer composites, clearly defined modes of failure have been identified, and it has been shown that the progressive splaying mode results in the highest SEA in each case. However, samples that splay quasi-statically tend to show more signs of fragmentation at higher test speeds and a subsequent reduction in SEA. Samples that fail by buckling quasi-statically may fail more by splaying dynamically and therefore have higher SEA levels. This can explain why some researchers have seen SEA increases with rate, while others have seen SEA decreases and some have seen no change at all. The majority of the work observes SEA decreases with test rate so it is important to test samples dynamically as this represents closer the conditions they will see in their application.

Off-axis testing

Fleming and Vizzini [122] looked at the effect of side loads on the energy absorption of composite structures. They took a very slightly tapered (1°) graphite/epoxy cone and crushed them at off axis angles up to 20° . For small levels of side load (5%) the energy absorption was improved. At higher levels ($10^\circ - 20^\circ$) it is reduced significantly especially at the highest angle where all the samples toppled.

Crush platen condition

Fairfull and Hull [59] investigated the role of friction on the energy absorption of glass cloth/epoxy tubes when crushed against four hardened steel platens of different surface roughness. They found that friction can account for more than half of the overall energy absorption of composite tubes. Fairfull [61] showed how an interlayer of PET film, causing the debris wedge to pass between two smooth surfaces, reduced the SEA by 23% and reduced the serrations in the force-displacement trace.

Farley *et al.* [123] investigated 50 different combinations of fibre, matrix, and ply orientation on the effect of two different crushing surface roughnesses on energy absorption. They found that samples that failed by lamina bending were the only ones that were affected by surface roughness. If the failure strain of the fibre exceeds that of the matrix then increasing the surface roughness increased the energy absorbed. If the failure strain of the matrix exceeds that of the fibre then the opposite is seen. When the failure strain of the fibre was similar to that of the matrix there was no change.

Instead of using flat crush platens internal plugs with different radii of curvature have been used to control the way tubes crush. These can be used in addition to varying the angle of the chamfered trigger (see Figure 22). Hull and Coppola [111] investigated the use of internal plugs and found that the geometry of the internal mandrel trigger has a significant effect on the progressive crush load. Maximum crush loads were observed when the crushed material was constrained to move through a sharp radius of curvature at the crush zone. This work is backed up by work by Cooper [124], who was able to increase the SEA of CoFRM E-glass / polyester circular tubes from 65.8 to 95.9kJ/kg, by optimising the radius of a plug initiator to be close to the wall thickness of the sample. Another advantage of using a plug initiator is that the stroke efficiency of the composite will be approximately 1.0 as all the debris will be dispersed to the outside of the tube.

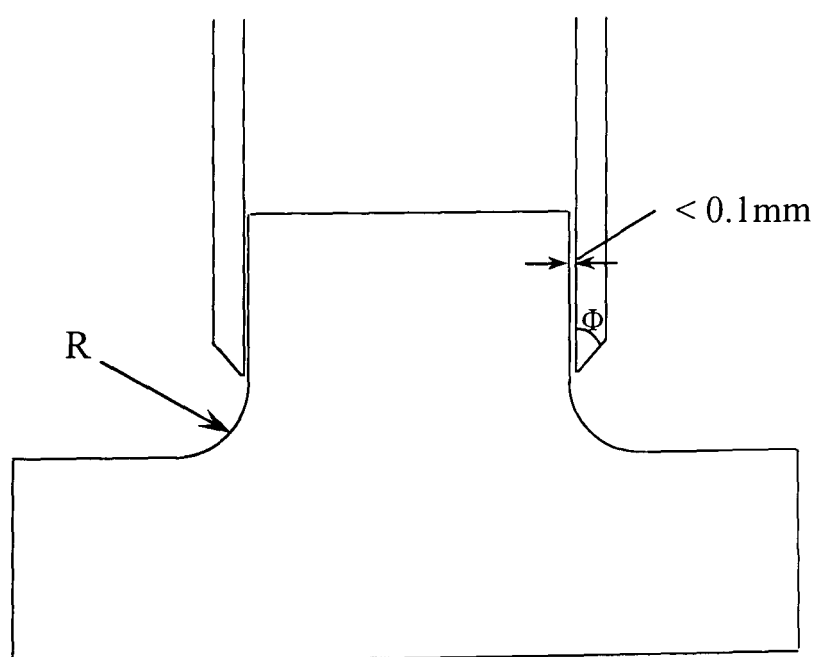


Figure 22: Internal mandrel trigger illustrating chamfer angle, Φ , and radius of curvature, R [111]

2.3 Conclusions

It has been shown in the literature that by changing either specimen geometry or constituent materials it is possible to affect the energy absorption potential of a composite structure. Progressive splaying achieved the highest SEA. It was therefore deemed necessary to keep as many of these factors constant in this study. For all the geometries tested the fibre volume fraction was kept constant. The circular and square samples were also designed to have constant cross-sectional areas.

Quasi-static testing is important to provide a basis for comparison, but it is more important to test samples at dynamic rates as this will provide an understanding into how the structure will react during crash conditions. It has been shown that both constituent material properties and energy absorption are affected by test rate. Samples that splay quasi-statically were seen to experience a reduction in SEA dynamically.

CAI research shows that an impact will reduce the residual compressive strength of a composite, but the research does not investigate fully the failure mechanisms caused by an impact or look at the threshold impact energy level to cause a reduction in properties. All the CAI tests are conducted quasi-statically on plaque samples. It is therefore proposed to investigate the effect of an impact on tubular specimens. Impacted samples will be tested at both quasi-static and dynamic rates to determine threshold energy levels, below which the impact damage has no effect.

It was seen as important in this project to improve the damage tolerance of the composite crash structures tested. However, improved damage tolerance is often coupled with reduced SEA capability, so a balance is likely to be required. Many methods have been used to increase the damage tolerance of composites. These include using toughened matrices, high strain fibres, stitching and interleaves. The first two methods change the constituent materials and stitching was not seen to improve the damage tolerance in all cases. For these reasons it was chosen to use interleaves in this project to investigate a way of improving the damage tolerance of the composite. It was also seen that geometric effects can improve damage tolerance, with one such way being to increase the wall thickness of the composite.

3 Experimental Methods

It is apparent from the literature that changing any of the material variables shown in section 2.2.2 affects the SEA. This is why throughout the test programme only one variable was changed at any time to enable direct comparison between results. It was also emphasised how important the dynamic testing of composites is. Every sample type is therefore tested at both quasi-static and dynamic rates. Although CAI work gives an insight into the behaviour of a composite after impact, it can not be directly related to tubes which are designed to crush rather than fail by compressive shear. The CAI work also does not investigate the threshold damage level before it affects the composite. This is why a range of impact damage levels will be investigated with emphasis on finding the threshold level, below which the effect of the damage is negligible. Having established a threshold damage level, investigations will be carried out to improve the damage tolerance of the composite.

3.1 Experimental Objectives

The objective of this work is to provide an understanding of the effects of a range of non-service type defects on the mode of failure and consequent energy absorption characteristics of tubes manufactured from glass reinforced polymer composites. The damage types investigated were a hole drilled in the test sample, a delamination moulded into the sample, or an area of impact damage imparted using a dropped weight.

Circular and square section tubes will be manufactured by RTM. Simulated damage will be introduced and the samples will be tested at both quasi-static and dynamic test rates. The characteristic failure modes will be observed, and the SEA capability of the composite will be recorded. Having shown how the applied damage affects the crush behaviour of samples a second phase of testing will be implemented to look into ways of improving the damage tolerance of the parts. The methods investigated in this work will be the introduction of a thermoplastic interleaf, which has been shown in the literature to reduce the damage area and improve the CAI properties of the composite [34-37]. Also wall thickness will be varied to investigate the effects on SEA and damage tolerance. The complete test programme is illustrated in Table 1.

Q-S denotes samples tested quasi-statically on an Instron test machine and D denotes samples tested on a Rosand instrumented falling weight (IFW5) test machine.

	Circular Tube (t=2mm)		Circular Tube (t=4mm)		Square Tube (t=2mm)		Square Tube (t=4mm)	
	Q-S	D	Q-S	D	Q-S	D	Q-S	D
No Damage	✓	✓	✓	✓	✓	✓	✓	✓
Holes – Size	✓	✓	✓	✓	✓	✓	✓	✓
Holes – Axial Position	✓	✓	✓	✓	✓	✓	✓	✓
Holes at Corner – Size					✓	✓	✓	✓
Holes at Corner – Axial Position					✓	✓	✓	✓
Multiple Holes	✓	✓	✓	✓	✓	✓	✓	✓
Delamination – Size	✓	✓			✓	✓		
Delamination – Multiple Inserts	✓	✓			✓	✓		
Impact Damage – Levels	✓	✓	✓	✓	✓	✓	✓	✓
Impact Damage – Axial Position	✓	✓	✓	✓	✓	✓	✓	✓
Impact Damage at Corner – Levels					✓	✓	✓	✓
Impact Damage at Corner – Axial Position					✓	✓	✓	✓
Interleaf – No Damage	✓	✓	✓	✓	✓	✓	✓	✓
Interleaf – Impact Damage Levels	✓	✓	✓	✓	✓	✓	✓	✓
Interleaf – Impact Damage at Corner					✓	✓	✓	✓

Table 1: Tube Crush Test Programme

Cylindrical tubes were used to avoid the issue of discontinuity at corners of square section tubes. Square tubes were then designed to have the same wall thickness and cross sectional area, giving an outer width of 30mm. These may prove to be easier to

incorporate into the vehicle design, but it is well documented (see 2.2.3) that there is reduced performance observed related to the square geometry.

For the test programme the constituent materials, manufacturing process, volume fraction, wall thickness and cross sectional area were all kept constant to enable direct comparison between the geometries. Another set of moulds was manufactured to create both circular and square tubes with 4mm wall thicknesses.

3.2 Materials

The reinforcement was a continuous filament random mat (CoFRM) E-glass, with an areal mass of 450 g/m² (Vetrotex Ltd U750-450), which contains 8% thermoplastic binder. The resin system was unaccelerated orthophthalic polyester (Reichhold Norpol 420-100: 41-45% styrene content) with 0.5% Akzo-Nobel NL-49P accelerator and 1% Akzo-Nobel methyl ethyl ketone peroxide (MEKP) Butanox M50 catalyst. These constitutive materials were chosen to facilitate the RTM process with the fibres having relatively high permeability and the resin chosen for its low viscosity. This combination also provides a relatively low cost part at approximately £1.50/kg for the raw materials. This compares to steel at £0.50/kg and carbon/epoxy raw materials which start at approximately £8/kg.

3.3 Specimen Manufacture

The cylindrical tubes were 80mm long and had an outer diameter of 38.1mm and 2mm wall thickness. This was chosen to allow 30mm of crush when using a 45kg drop weight and testing at 5m/s. The drop tower available at the time had a maximum payload of 45kg, which equates to potential drop energy of 561J when dropped from 1.27m (an impact speed of 5m/s (11.2mph)). Approximately 30mm of crush was required to ensure that steady state crush had been achieved. Previous work by Curtis and Duckett [70, 97] tested circular tubes of outer diameter 88.9mm and 4mm wall thickness. These samples absorbed 2900J in 30mm of crush when tested quasi-statically. A ratio of this energy level to the energy potential of the drop weight was used to scale down the dimensions of the tube. A D/t ratio of approximately 16 was chosen to maximise SEA (see 2.2.3). The wall thickness of 2mm was chosen to keep

the volume fraction the same as for Curtis and Duckett by keeping the number of plies an integer in the scaling process. It was also noted by Hamada *et al.* [100] that the optimum wall thickness is 2-3mm. A preliminary study consisted of the manufacture of a prototype part by wrapping pre-wet-out fibres onto a 30mm diameter steel mandrel and using heat shrink tubing to consolidate the part. These samples did not have uniform cross section with the wall thickness varying from 2.6 to 5.2mm and the average fibre volume fraction was 12%. They crushed progressively both quasi-statically and dynamically and the dynamic test samples crushed 25-30mm (see Figure 23). With the size of the outer mandrel restricted to the size of steel hydraulic tubing available it was decided to manufacture tubes with outer diameter 38.1mm (1 1/2") and a 2mm wall thickness. Although scaling effects are seen to be dependent on a number of factors (see 2.2.3) this method enabled the design of cylindrical structures that could be tested at dynamic rates.

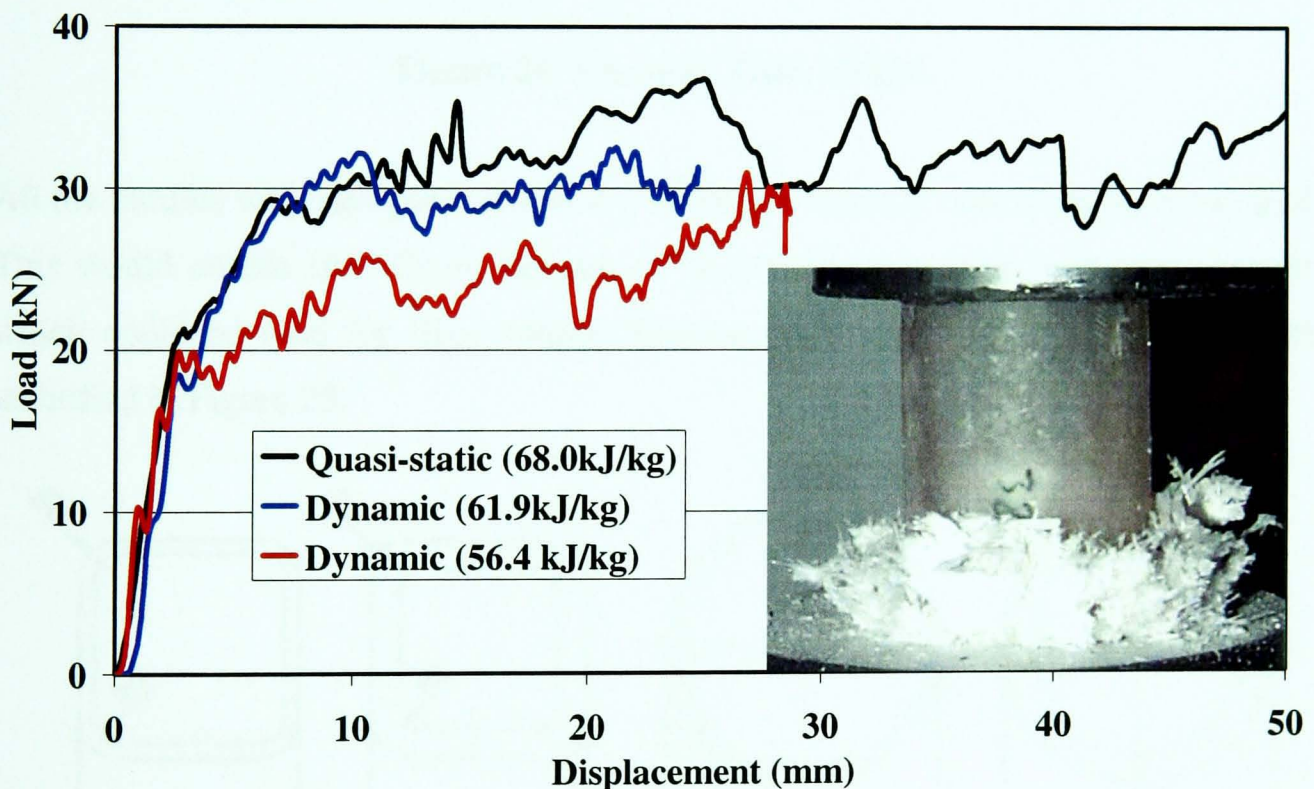


Figure 23: Test Results for Dynamic Tests with Prototype Shrink Wrapped Cylindrical Tube

The circular tube moulds were manufactured with the outer mandrel made from bright seamless steel hydraulic tubing with an inner diameter of 38.1mm. To provide 2mm and 4mm wall thickness specimens, two inner mandrels were manufactured with a ground surface finish, and two sets of end caps were produced to seal the mould and ensure a uniform cavity.

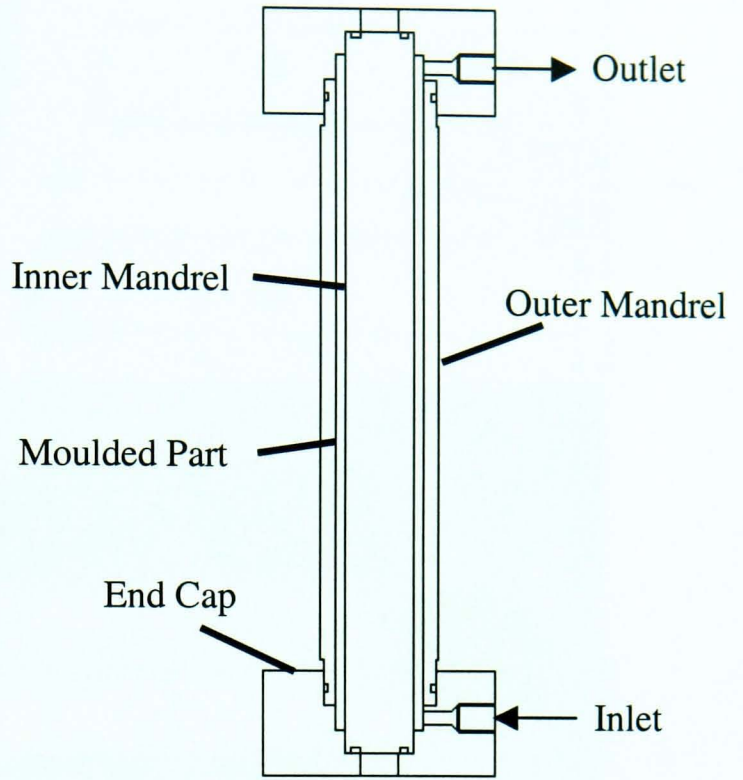
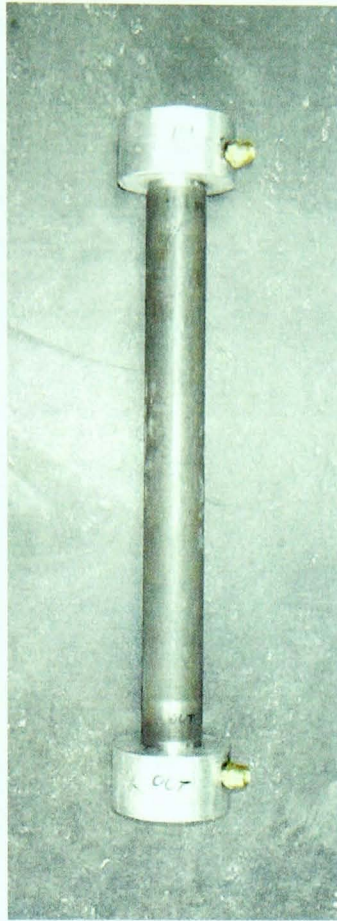


Figure 24: Circular Tube Mould

All the moulds were designed to enable a 500mm composite tube to be manufactured. This would enable five 80mm samples to be cut from the tube with some excess, which could be used for fibre volume fraction tests. Specimen cross sections are identified in Figure 25.

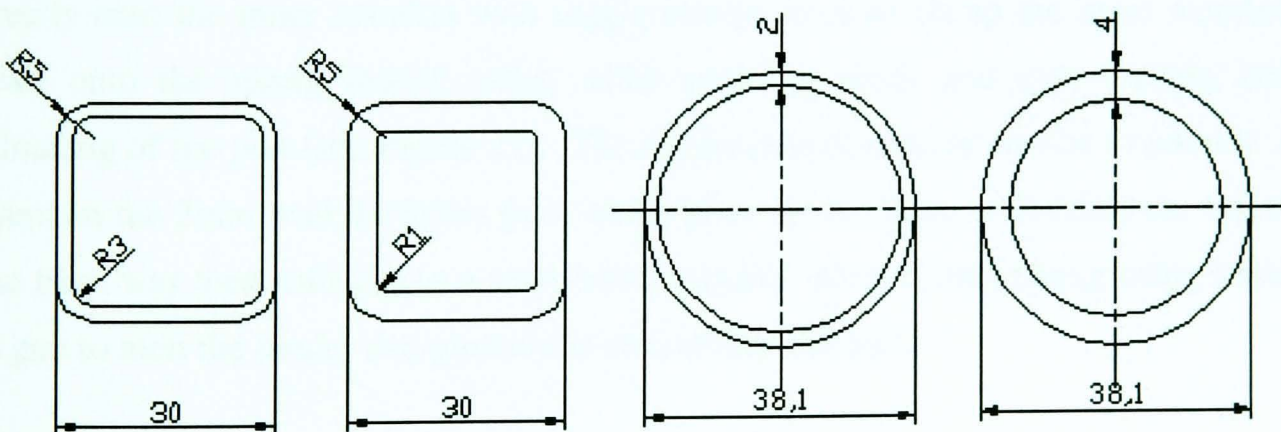


Figure 25: Specimen Cross Sections (all dimensions in mm)

The square tube mould outer mandrel was fabricated in two halves providing a 30mm square specimen (see Figure 26). Again two inner mandrels and sets of end caps were manufactured to provide moulds for 2mm and 4mm wall thickness parts.

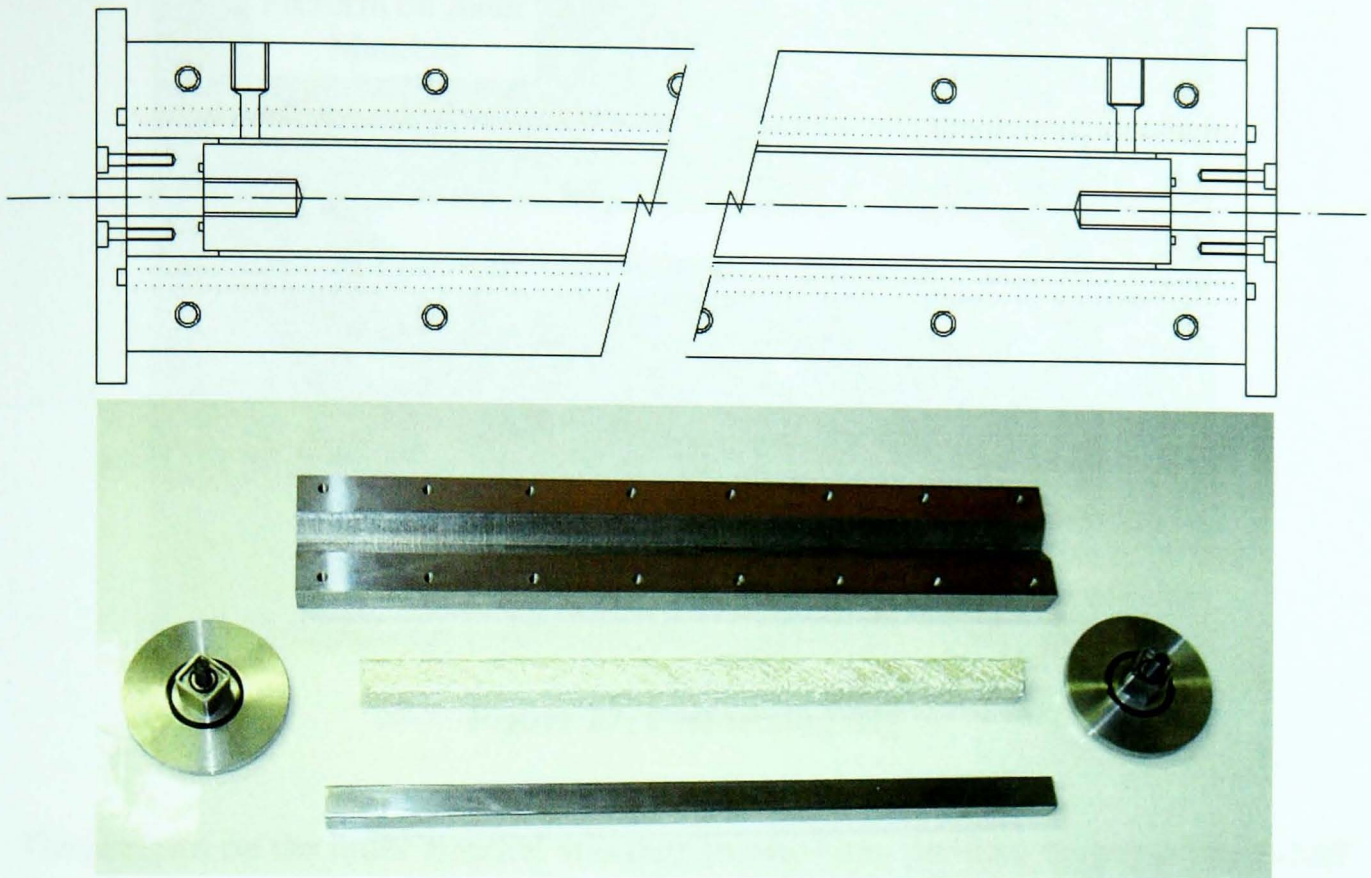


Figure 26: Square Tube Mould

This fabrication process evolved from work by Corden and Macmillan [125, 126]. To manufacture the tubular specimens, firstly the inner and outer mandrels were coated with 5 layers of Chemlease PMR-90 release agent to facilitate extraction of the finished part. A preforming rig was designed to allow the preform to be rolled directly onto the inner mandrel with toggle clamps used to clamp the inner mandrel down onto the spring loaded roller, while enabling quick and easy loading and unloading of the part (see Figure 27). The reinforcement was cut to size to provide 3 layers on the 2mm wall thickness parts and 6 plies for the 4mm wall thickness tubes. The fibre was then rolled onto a steel inner mandrel while consolidating using a hot air gun to melt the binder and pressure to consolidate the part.

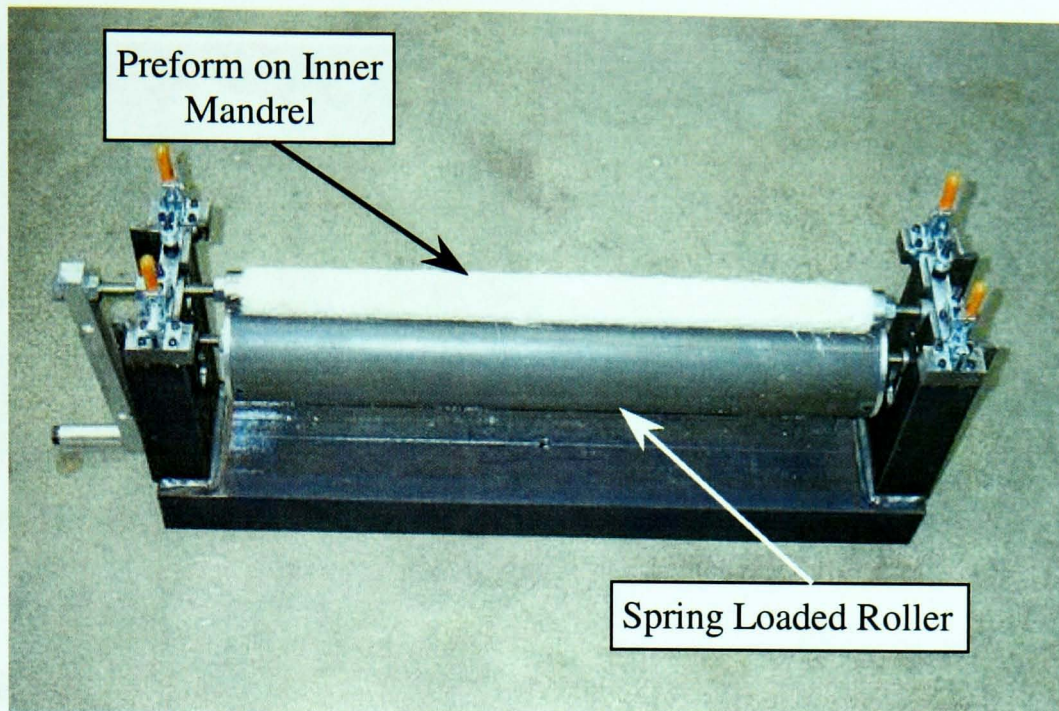


Figure 27: Preforming Rig

The preform on the inner mandrel was then inserted into the steel outer mandrel. End caps seal the mould and hold the mandrels in place providing a uniform cavity, ensuring a constant wall thickness part. Resin was injected at room temperature into the mould through one end cap. The mouldings were left to cure overnight at room temperature inside the tool before being extracted and then post cured for 2 hours at 80°C. This process provides parts with a fibre volume fraction of 25% and a wall thickness variation of less than 0.1mm.

The tubes were then cut to 80mm lengths using a diamond tipped cutting wheel, and a 45° chamfer was ground onto one end of each specimen as a stress concentration to initiate crush.

3.4 Damage Characterisation

In this study damage is represented in three ways Figure 28. Holes are used to simulate point strength reduction, Melinex® inserts are used to simulate delamination between plies, and impact damage is used to represent damage situations.



Figure 28: (a) Hole, (b) Multiple holes, (c) Delamination, (d) Impact Damage

3.4.1 Holes

Initial testing identified a 5mm hole to be the threshold hole size, where holes smaller than 5mm produced similar crushing behaviour to undamaged tubes. The holes were produced with a spur drill of diameter 5mm and 10mm centred at axial positions of 15mm, 30mm and 45mm (see Figure 29). The axial position of the holes was tested after observing that the effect of the holes at dynamic rates was localised.

The effect of using blunt drill bits was emphasised in section 2.1. To minimise the effect of this the old drill bits were regularly replaced, with five 10mm drill bits used in total. With the square samples the same set of tests was carried out for holes on the face as for holes at the corner. The same fixtures were used to hold the tubes for drilling as were used to hold the tubes being impacted (see Figure 31). Further testing was done to see the effect of two holes of diameter 5mm drilled at the same axial position of 30mm, with a circumferential spacing of centres of 10mm. This was done to compare the effect of multiple holes with the effect of a larger single hole.

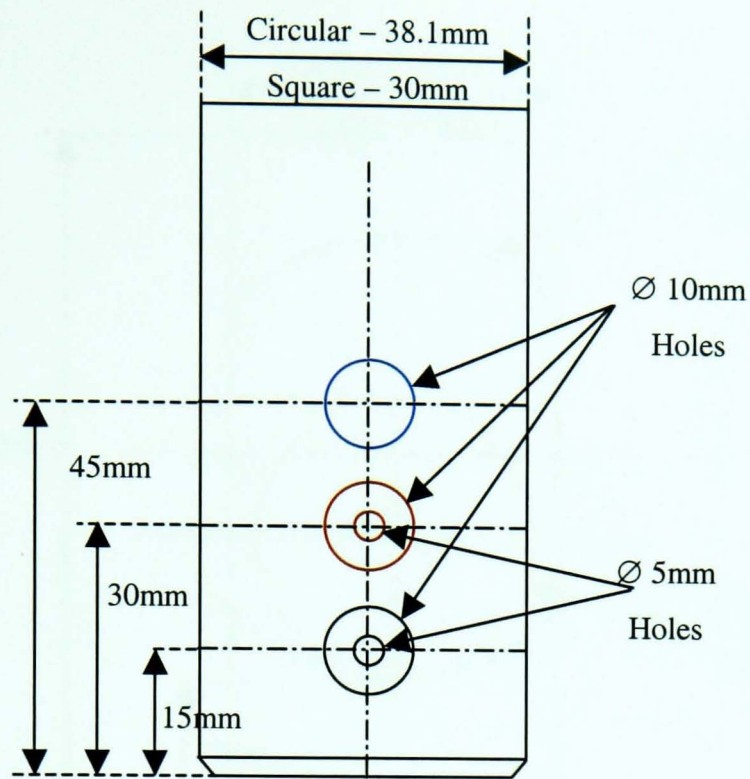


Figure 29: Hole Position in Specimens

3.4.2 Delaminations

Melinex® is a thin (50 μ m) clear PET film, which does not adhere to polyester resins. The Melinex® inserts were placed on the reinforcement prior to preforming to create an inclusion between the plies of the composite. The smallest insert used was a single 32mm diameter insert between the inner and centre ply. The next set of tests took two 32mm diameter inserts, positioned so as to be coincident between the first and second, and the second and third plies. The final set of testing had a single 50.8mm diameter insert placed between the inner and centre ply. Specimens were cut to length ensuring the insert was positioned starting 15mm from the chamfered end of the tube (see Figure 30).

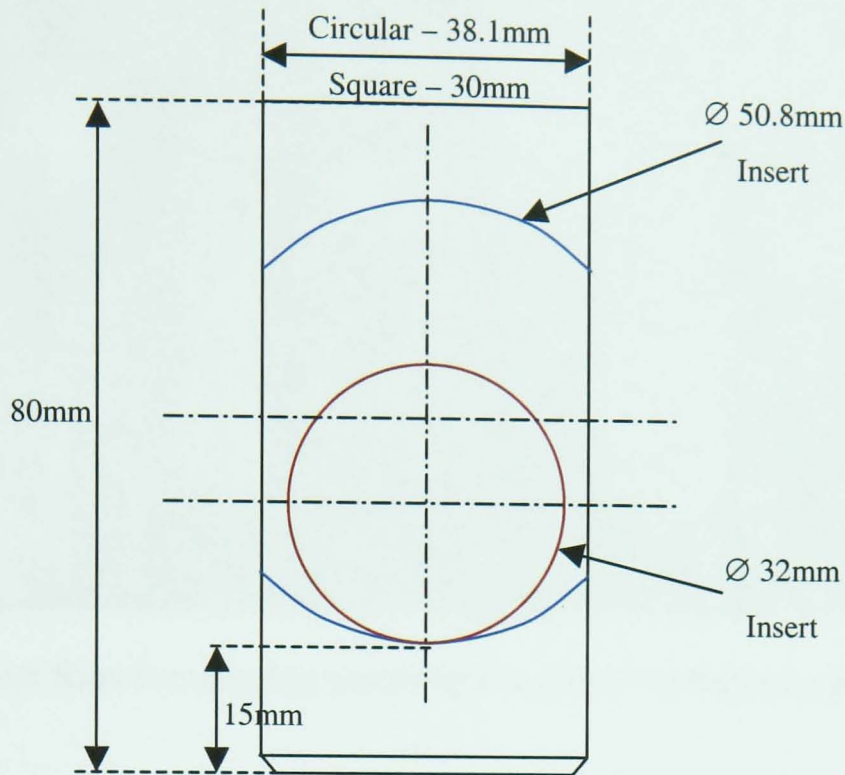


Figure 30: Delamination Position in Specimens

3.4.3 Impact Damage

The testing of impact damaged parts was used to simulate damage that could be acquired during service or assembly. Typical causes of such damage are stones or debris being thrown up off the road and hitting the part, or a tool being dropped during manufacture or service. Low energy impacts such as these involve energies of 5-10J, so it was decided to introduce impact levels of up to 12J. As a simple example an impact involving a 10g stone (approximate dimensions 35mm x 20 x 15) travelling at 100mph (44.7ms^{-1}) would equate to impact energy of 10.0J. Similarly a 1kg tool dropped from 1 metre would produce an impact with 9.8J of energy. This assumes that there is a 100% energy transfer from the impactor. Once initial testing was done it was decided to increase the energy levels to the point where it caused unstable failure.

The tubes were damaged by dropping a fixed weight from a controlled height using the Rosand instrumented falling weight drop tower. A tup with hemispherical end of diameter 12.7mm was used as the impactor (see Figure 31). The fixtures holding the specimens during impact were designed to constrain the sample and ensure that all the energy from the impact was absorbed by the sample.

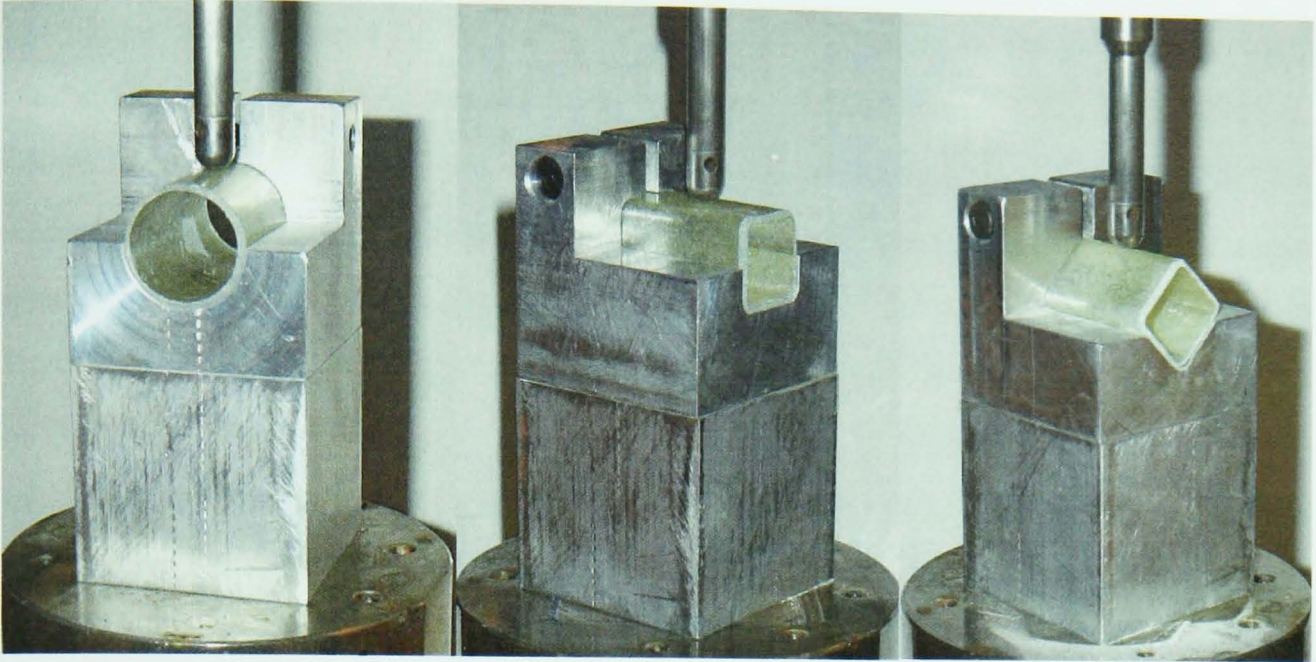


Figure 31: Test Rigs for causing controlled impact damage to composite tubes

The area of the damaged zone was measured visually. Measurements were taken of the delamination through the sample, and the area estimated. The areas recorded are shown in Table 23.

3.4.4 Interlaminar Toughening via Interleaves

Section 2.1 reviewed ways of improving the damage tolerance of composite materials. Interleaves between each ply should increase the interlaminar fracture toughness and therefore impact performance. Testing was done to determine the effect of moulding interleaves between the plies of the CoFRM composite tubes.

The interleaf used was a Xiro 36.004 40g/m² polyester-PU adhesive film supplied by Cornelius Chemical Co. Ltd. It was applied in sheet form to the reinforcement at the preforming stage – resulting in a tube with an interleaf between each ply. A control test was carried out with no impact damage. The rest of the samples were impacted as described in section 3.4.3 at incremental energy levels until unstable failure was observed.

3.5 Test Methods

The main part of the work in this thesis is the crush testing of tubular composite structures. For the majority of the dynamic testing, a high speed camera was used to

observe the failure mode of the sample and verify the speed of the tests. The fibre volume fraction was determined for all the sample geometries. The coefficient of friction between the crush platen and the crush zone of the sample was established for samples of each geometry and test speed. Micrographs were taken for every sample type to examine the crush zone morphology. Environmental Scanning Electron Microscopy (ESEM) was used to look at the differences in the matrix and fibre in the fronds of the quasi-statically and dynamically crushed samples. Testing was completed to find the ultimate compressive strength of the composite to determine how close to the maximum potential crush load the samples were crushing at.

3.5.1 Quasi-Static Tube Crush

The tube specimens were crushed onto a steel platen with a surface ground finish ($0.4\mu\text{m } R_a$). The same crush platen was used for all quasi-static tests. Both sides of the platen were used and the surfaces were reground once during the testing programme to maintain the crush surface. Quasi-static tube crush specimens were tested on an electro-mechanical loading frame (Instron 1195 – see Figure 32) with a 100 kN load cell at 5mm/min. For samples for which the crush load exceeded 100 kN the Instron 8500 servo-hydraulic test machine was used with a 1000 kN load cell.



Figure 32: Instron 1195 Electro-Mechanical Test Machine

Load-displacement data were recorded during all tests on the test machine. All samples were crushed 50mm. Mean crush loads were calculated by finding the average crush load after the first 5mm of crush (the first 5mm of crush was discounted to eliminate the effects of the 45° chamfer). SEA values were then determined by dividing the mean crush load by the mass per unit length of the uncrushed specimens. A minimum of 3 specimens of each sample type was tested.

Digital photographs of each test type were taken at equal intervals (5mm) to record the mode of failure for the samples.

3.5.2 Dynamic Tube Crush

Dynamic tests were done on a Rosand instrumented falling weight machine (IFW5 – see Figure 33) at a nominal impact speed of 5m/s. Energy levels were chosen to ensure that there was at least 30mm of crush.

The Kodak HS4540 high-speed video-imaging camera was loaned from the engineering instrument pool of the Engineering and Physical Sciences Research Council (EPSRC) and was used to verify the speed of the drop tests and to observe the failure modes of the test specimen crushing onto the crush platen. The camera was set up to sample at 4500 frames per second, which enabled an accurate assessment of the velocity of the impactor and provided an image of sufficient magnification and resolution to observe the failure mode of the sample.

A test rig was designed (see Figure 34) with a Kistler 9051A 120kN load cell pretensioned between the ground crush platen and the base. A pretensioning bolt applied a 5kN load to ensure no vibration in the system. The sample would then be attached to the drop weight using cyanoacrylate before being raised to the drop height and released.



Figure 33: Rosand Instrumented Falling Weight Machine (IFW5)

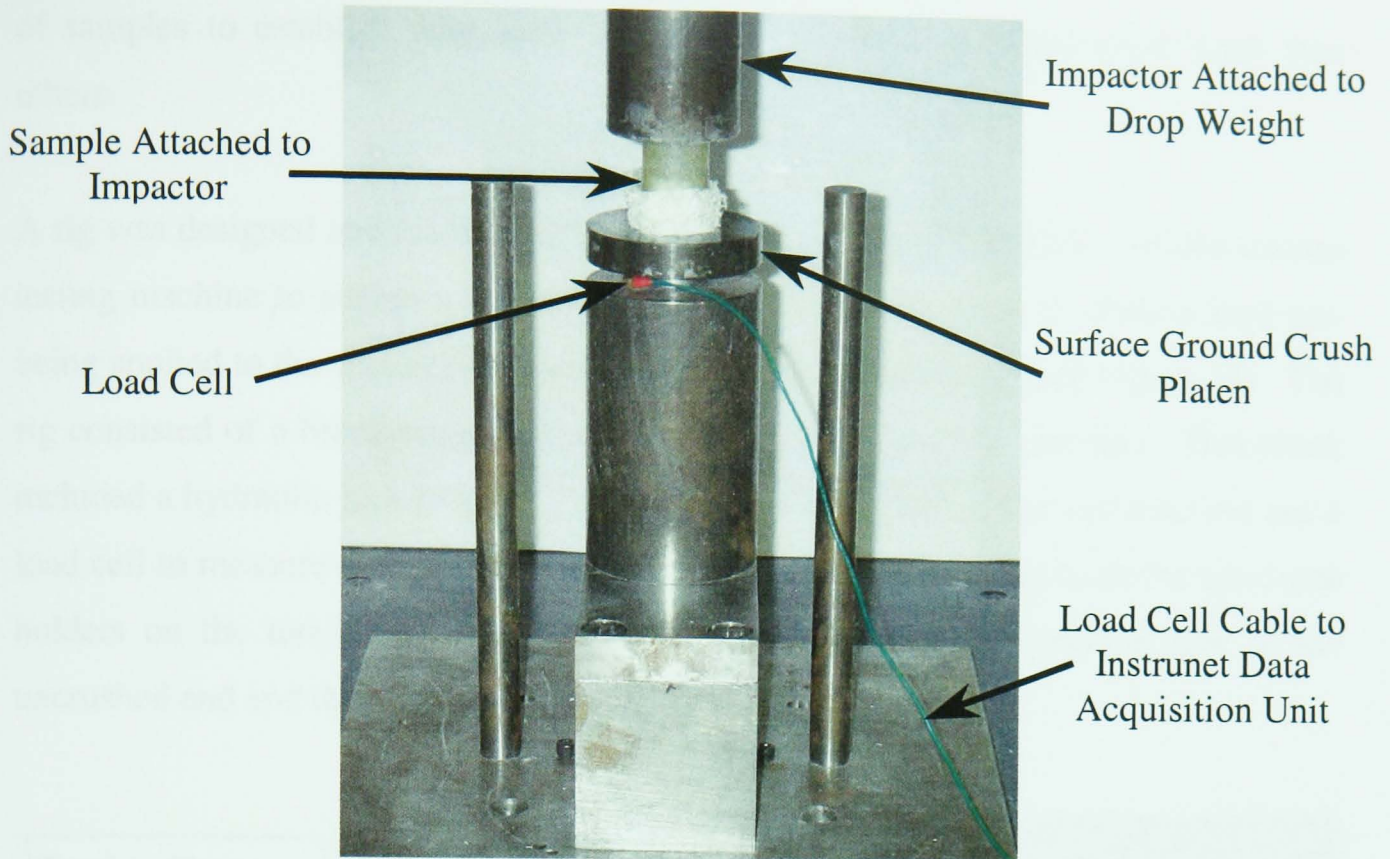


Figure 34: Test Rig for Dynamic Crush Tests in Drop Tower

An Instronet data recording system recorded the load data at a rate of 40kHz. These data are then used to plot the load against displacement and then calculate the SEA as for the quasi-static tests.

3.5.3 Determination of Ultimate Compressive Stress

The ultimate compressive stress was obtained for each sample type. In these tests no chamfer was machined at either end of the sample to act as a crush initiator. The test was stopped as soon as the sample failed and the maximum load was used to calculate the ultimate compressive stress. Tests were carried out both quasi-statically and dynamically. The unstable failure mode associated with the presence of damage is similar to compressive failure, and so looking at how the steady state crush level compares with the ultimate compressive load may give an insight into why some samples are more damage tolerant than others.

3.5.4 Friction Testing

Fairfull and Hull [59] suggest that as much as half the energy absorbed in the crushing process is due to frictional effects. It was necessary to investigate the friction effects

of samples to establish why some specimens crushed at a higher crush load than others.

A rig was designed and manufactured to attach to an Avery 6609CGG reverse torsion testing machine to enable a torque reading to be obtained while a constant load was being applied to the specimen, pushing it against a ground platen (see Figure 35). The rig consisted of a block securely fastened to the bed of the test machine. This block included a hydraulic jack to apply the load to the sliding bed of the test machine and a load cell to measure the applied load. Two fixtures were designed to fit the specimen holders on the torsion testing machine. One held a partially crushed tube at the uncrushed end and the other was the crush platen.

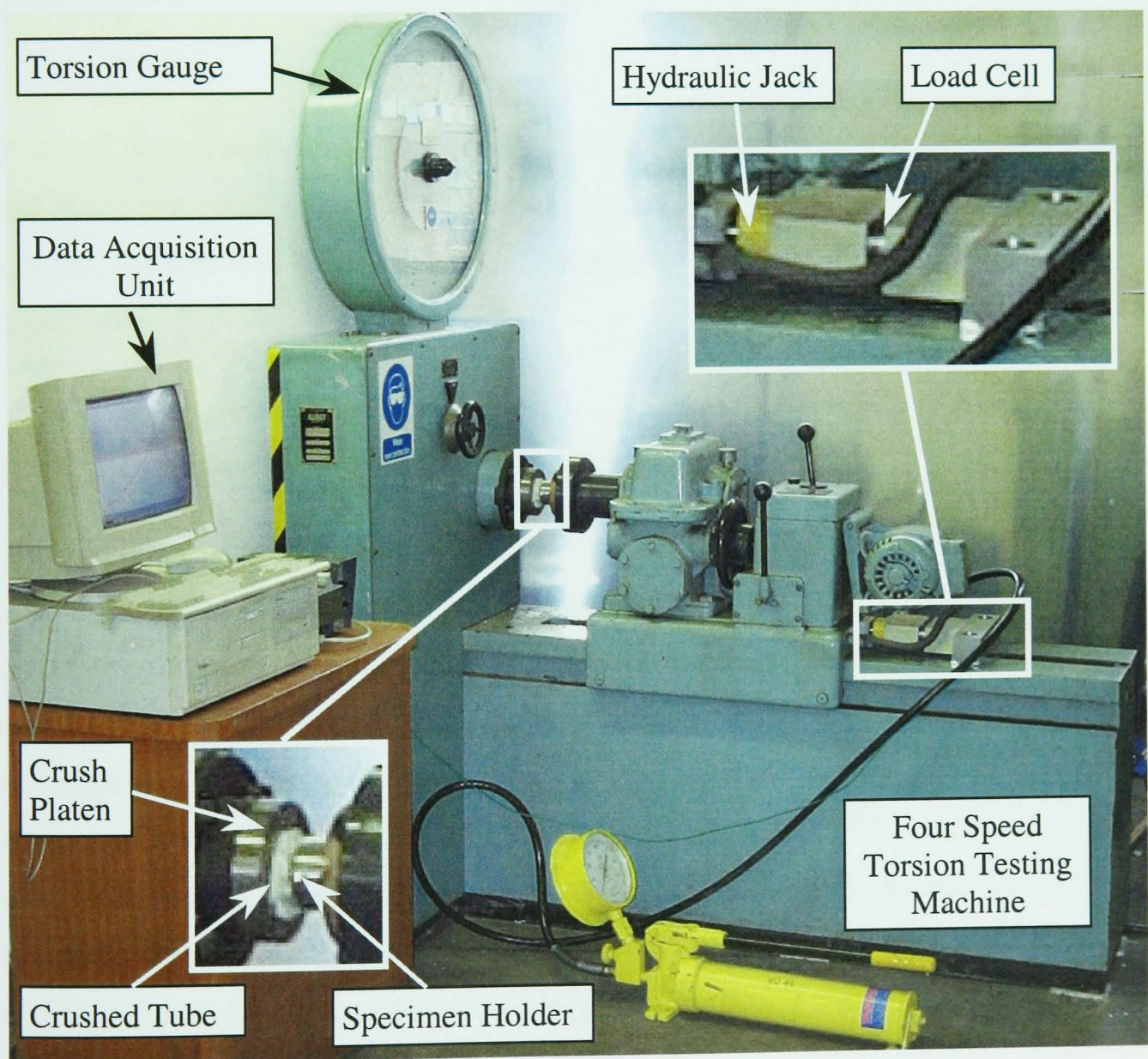


Figure 35: Friction Testing Rig

45mm long specimens of each undamaged sample type were manufactured with the same 45° chamfered initiator as the crush test samples. These were then crushed 17mm quasi-statically or dynamically before being set up as shown in Figure 35. The specimen was set rotating at 10° per minute, which gave a speed of rotation at the crush zone of approximately 3mm/min (the closest setting to the 5mm/min crush speed for quasi-static testing). The load was then applied to the sample in 0.5kN increments up to 5kN and then 1kN intervals up to 10kN, a level of loading that would not induce further crushing of any of the samples. At each increment the torque reading was taken off the gauge. From these readings the coefficient of friction could be easily calculated:

$$\mu = \frac{T}{P \times R_{eff}} \quad (6)$$

Where μ is the coefficient of friction, T is the measured torque, P is the applied load and R_{eff} is the effective radius for the sample, taken as the centre wall radius for the circular samples and the average radial dimension of the centre of the wall for the square tubes.

3.5.5 Determination of Fibre Volume Fraction

The fibre volume fraction for each type of tube was determined by resin burn off tests, similar to ASTM D2584-94. These were carried out on samples taken from each of the types of tube tested. The samples, typically weighing 3 – 5g were weighed to an accuracy of ± 0.01 g. The samples were then placed in an electric furnace at 625°C for 45 minutes to remove all the resin. The samples were weighed again and their fibre mass fractions calculated. These values were then converted to volume fractions using the density values taken from the manufacturers' data (see Figure 36). At least 3 samples were tested for each sample type. The samples were taken from different tubes to account for any variation between tubes.

	Vetrotex U750-450 CoFRM E-glass	Norpol 420-100 Polyester Resin
Density (kg/m ³)	2540	1100

Figure 36: Fibre and Resin Density Data from Manufacturers' Data Sheets

3.5.6 Microscopy

For each of the specimen types tested a micrograph of the crush zone was constructed so as to observe the mechanisms involved in absorbing energy. The sample was crushed and then set in casting resin in situ. This provided the most accurate representation of the crush zone as it would be during testing. A section was then cut across the crush zone, which in turn was cut down and re-potted in 40mm diameter pots. This new sample would then be machined down to a thickness 13mm thick before polishing on the Struers Dap-7 polishing machine. Silicon carbide paper grades from 240-2500 grit were used to polish each specimen. Alumina was used to obtain the final surface finish. After cleaning, each sample type was observed under a Zeiss optical microscope with Aphelion imaging software. Photographs were taken for the whole of the specimen. A collage of these was put together to enable analysis of the crush zone morphology.

3.5.7 Environmental Scanning Electron Microscope (ESEM)

ESEM work was carried out to look at the extent of fibre breakage and matrix fragmentation in the fronds of the quasi-statically and the dynamically tested specimens. A small area of the crush zone and frond were bonded to specimen holders using carbon pads. The samples were then loaded into the environmental chamber where they were viewed and the images captured.

4 Results

This chapter will look at the tube crush test results and develop an understanding of the failure modes associated with different levels of simulated damage. A threshold level will be obtained, below which the specimen will crush as if undamaged. Above this level a change in failure mode will cause a reduction in SEA. This will be followed by the results of testing of the ultimate compressive stress, friction testing, optical microscopy, environmental scanning electron microscopy (ESEM) and fibre volume fraction. The trends observed will be discussed in detail in the chapter 5.

With over 650 samples tested in this work it was necessary to use notation for the tubes as shown in Table 2.

Tube Geometry		Interleaf	Damage Quantity	Damage Type			Damage Position (Corner)	Axial Position	Test Speed	
Circular	Square			Hole	Delamination	Damage			5mm/min	5m/s
C	Q	IL	2x	10m	32mx	3J	c	30	S	D

Table 2: Specimen Classification Notation

The first letter is used to denote the geometry of the tube, C for circular and Q for square tubes. If there is a 4 after this letter it means that the tube has a 4mm wall thickness, otherwise it has a 2mm wall thickness. An IL means that there is an interleaf in the sample. The damage quantity applies if there are two Melinex® inserts or two holes drilled. A hole size is illustrated by an “m” preceded by the hole size in mm. “0m” means no hole. A delamination is denoted by an “mx” preceded by the insert size in mm. The impact damage level is expressed in terms of the energy applied in Joules. If the tube is square a “c” will mean that the damage type is applied to the corner of the tube otherwise it will have been applied to the face. The axial position of the damage is denoted next in mm. An “S” implies a quasi-static test rate of 5mm/min, and a “D” implies a dynamic test rate of 5m/s. Any number at the end of a sample name indicates the test number of a particular specimen.

For example:

C_5m30S is a circular tube with a 2mm wall thickness with a 5mm hole 30mm from the chamfered end of the tube tested quasi-statically.

Q_2x32mxD is a square tube with a 2mm wall thickness with two 32mm Melinex® inserts moulded into the sample tested dynamically.

Q4_IL6J45c is a square tube with a 4mm wall thickness with interleaf, damaged with a 6J impact at the corner 45mm from the chamfer.

4.1 Tube Crush Test Results

The following sections look at the quasi-static and dynamic tube crush results. They have been divided into five sections. The first looks at the difference between the two loading rates for undamaged samples. The next three sections look at each of the damage types. Once this work was completed work was started to investigate ways of improving the damage tolerance of the tubes, and the fifth section looks at one of these methods, the effect of using thermoplastic interleaf moulded into the tubes.

4.1.1 Rate Effects

As the test speed was increased from a quasi-static rate of 5mm/min to a dynamic rate of 5m/s, every geometry of tube tested showed a decrease in SEA (see Table 3 – the figures in brackets are % standard deviation).

	Circular (t=2mm)	Circular (t=4mm)	Square (t=2mm)	Square (t=4mm)
Quasi-Static SEA (kJ/kg)	74.5 (3.7)	87.0 (5.5)	58.8 (10.3)	69.2 (3.7)
Dynamic SEA (kJ/kg)	70.2 (2.8)	76.0 (2.1)	48.5 (1.9)	64.1 (4.5)
% decrease	5.8	12.6	17.5	7.4

Table 3: Rate Effects – No Damage

The results show the same trend as stated by Thornton [71, 85], Mamalis *et al.* [86, 87], Farley [65], Chadwick [88], Chiu [89] and Price [90] in section 2.2.3 with the circular tubes exhibiting higher SEA values than the square tubes of the same cross-

sectional area and wall thickness. The quasi-statically tested samples saw a decrease of 21% between the circular and square samples, while dynamically tested samples saw a decrease of 16% for the thicker section tube and 31% for the thinner section tube. These levels of SEA reduction were also observed by Mamalis *et al.* [87], Schmueser and Wickliffe [72], and Ramakrishna [84].

4.1.1.1 Circular Tubes

Both quasi-statically and dynamically tested samples crush progressively with a steady increase in load as the tube starts to crush at the chamfered trigger, before reaching a steady state crushing load (see Figure 37).

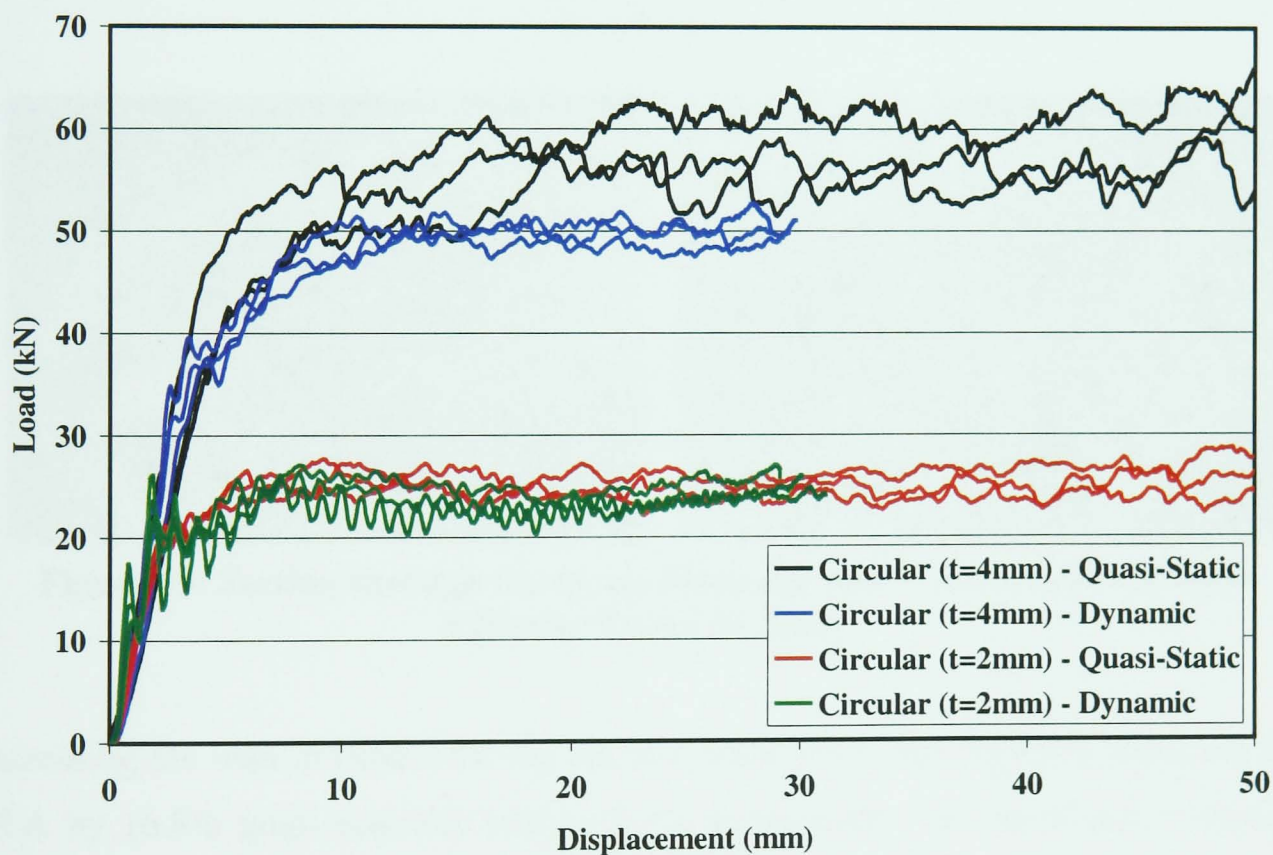


Figure 37: Load vs Displacement for all Circular Tubes

A debris wedge and central wall crack are formed leading to the development of internal and external fronds, signifying a splaying failure mode as described by Fairfull and Hull [59] in section 2.2.1. It is obvious by visual inspection that there is a distinct difference in the appearance of the fronds of the samples tested at the two rates (see Figure 38 and Figure 39). This is observed at the microscopic level using ESEM in section 4.5. The fronds of the quasi-statically tested samples exhibit greater

curvature of the fronds and splitting to form a number of individual petals. The fronds of the dynamically tested samples exhibit no splitting into petals and are less rigid with more individual fibres protruding from the matrix.

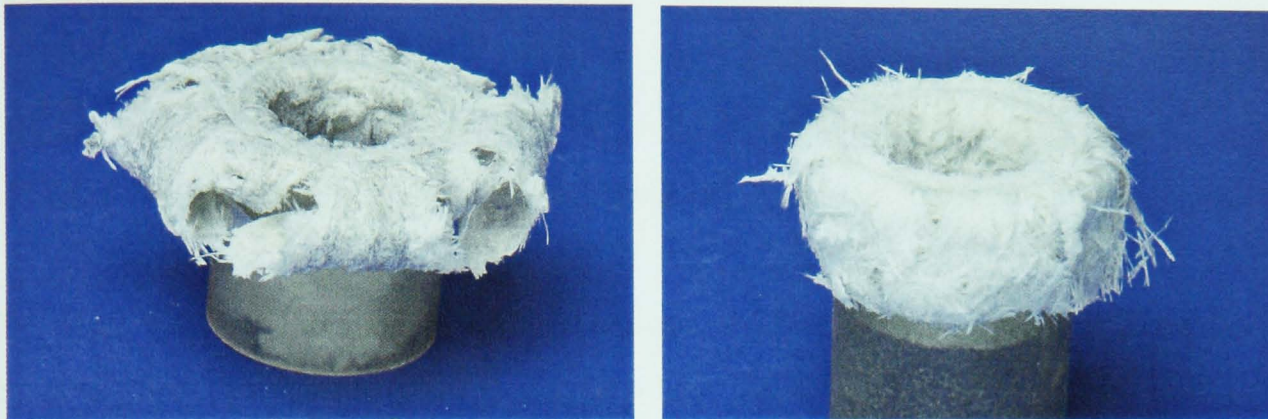


Figure 38: Quasi-Statically and Dynamically Crushed Circular Tubes (t=2mm)



Figure 39: Section through the Quasi-Statically and Dynamically Crushed Circular Tubes (t=2mm)

Increasing the wall thickness for the circular tubes from 2mm to 4mm increased the SEA by 16.8% quasi-statically and by 8.3% dynamically. It was found in section 2.2.3 that the SEA increased with t/D up to a threshold level, so it is not unexpected to see an increase in SEA with wall thickness.

4.1.1.2 Square Tubes

The square tubes also observed a stable progressive failure mode. The fronds of all the samples split at the corners of the tube into 4 petals, but there is still an obvious difference between the quasi-statically tested samples and the dynamically tested samples (see Figure 40).



Figure 40: Quasi-Statically and Dynamically Crushed Square Tubes ($t=4\text{mm}$)

The load displacement trace for the square samples exhibits a greater degree of serration than that of the circular samples (see Figure 41). This is due to the start – stop tearing Mode II fracture at the corners.

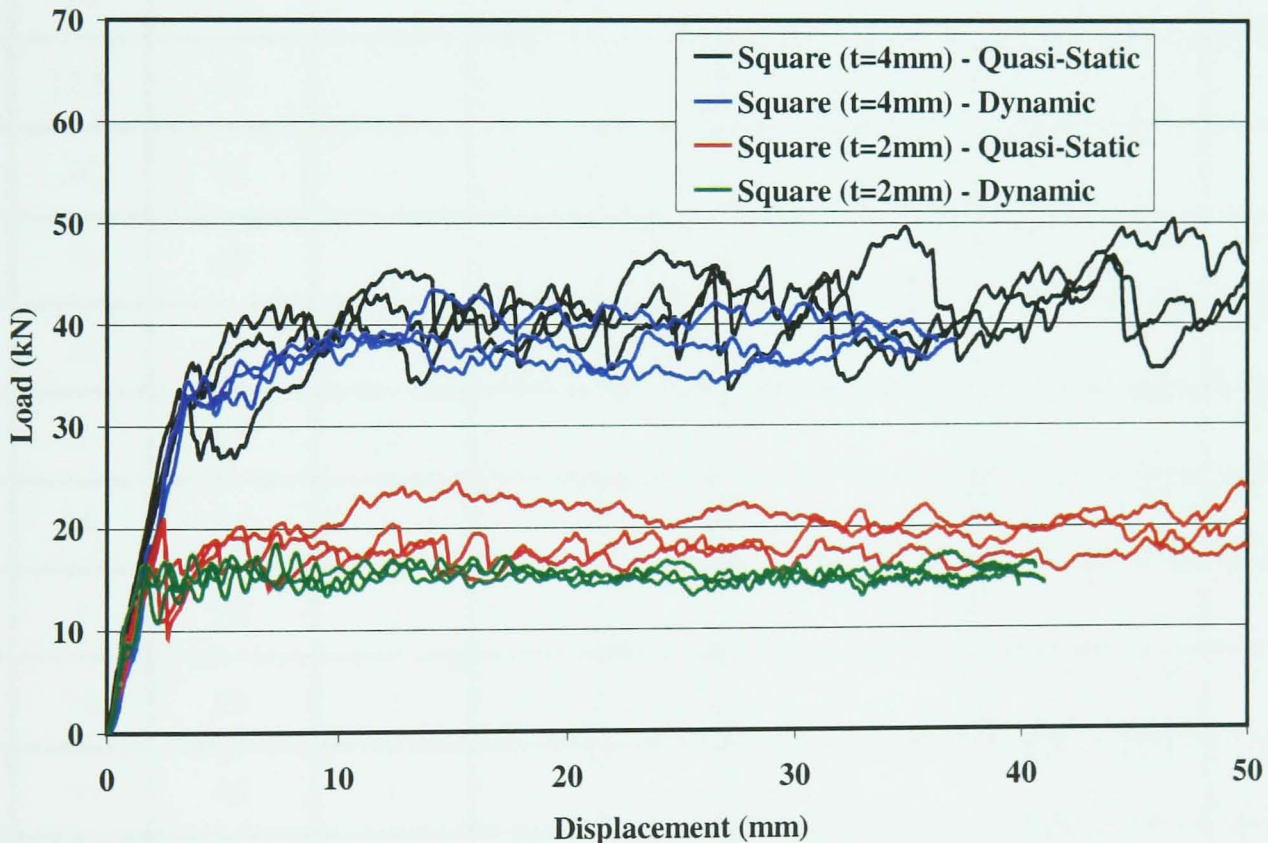


Figure 41: Load vs Displacement for all Square Tubes with No Damage

Increasing the wall thickness for the square tubes from 2mm to 4mm increased the SEA by 17.7% quasi-statically and by 32.2% dynamically.

4.1.2 Damage - Holes

Table 4 shows a summary of the tests completed with inclusion of a hole and results for all the geometries tested. The load vs displacement graphs for all of the results can be found in Appendix 1. There is limited work in the literature on the quasi-static crushing of tubes with holes, and none on the dynamic crushing of anything other than an undamaged tube. This makes comparison with other sources difficult.

Specimen ID	Hole Size (mm)	Axial Position (mm)	Position (Corner)	Circular Tube (t=2mm)		Circular Tube (t=4mm)		Square Tube (t=2mm)		Square Tube (t=4mm)	
				Q-S	D	Q-S	D	Q-S	D	Q-S	D
0m	—	—	—	74.5 (3.7)	70.2 (2.8)	87.0 (5.5)	76.0 (2.1)	58.8 (10.3)	48.5 (1.9)	69.2 (3.7)	64.1 (4.5)
5m15	5	15	—	66.7 (12.7)	69.7 (6.7)	74.5 (12.3)	71.9 (0.8)	57.3 (10.1)	52.4 (5.3)	70.2 (3.2)	59.6 (4.6)
10m15	10	15	—	48.7 (16.8)	48.6 (19.2)	62.8 (15.3)	68.7 (3.2)	58.1 (6.0)	48.7 (2.9)	67.1 (2.9)	56.0 (1.4)
12.5m15	12.5	15	—	—	—	—	—	49.9 (12.9)	47.3 (6.6)	—	—
16m15	16	15	—	—	—	—	—	43.2 (9.3)	47.3 (9.1)	—	—
10m30	10	30	—	21.7 (24.7)	56.7 (10.0)	39.5 (25.4)	60.4 (8.5)	43.8 (29.5)	49.0 (2.5)	53.3 (16.0)	58.5 (1.3)
10m45	10	45	—	26.1 (14.0)	62.5 (1.8)	30.4 (11.1)	75.0 (2.7)	48.9 (25.2)	51.5 (2.3)	49.5 (25.9)	61.3 (6.1)
5mc15	5	15	c	—	—	—	—	57.1 (3.4)	50.3 (6.3)	68.7 (1.4)	64.8 (2.9)
10mc15	10	15	c	—	—	—	—	52.6 (2.9)	43.6 (5.2)	59.0 (9.5)	59.1 (4.2)
5mc30	5	30	c	—	—	—	—	—	—	71.0 (8.3)	63.2 (5.0)
10mc30	10	30	c	—	—	—	—	31.0 (2.0)	35.2 (12.3)	33.3 (6.9)	46.1 (18.9)
10mc45	10	45	c	—	—	—	—	25.8 (16.1)	46.6 (6.1)	30.4 (7.1)	45.7 (41.2)
5m30	5	30	—	58.4 (39.7)	62.8 (2.7)	62.2 (21.1)	72.7 (6.2)	57.3 (2.8)	48.2 (5.4)	72.7 (2.0)	66.4 (5.4)
2x5m30	(2x) 5	30	—	68.2 (46.5)	61.0 (2.3)	42.6 (28.6)	71.5 (4.5)	51.8 (7.9)	46.5 (5.4)	67.0 (4.7)	65.7 (6.1)

Table 4: SEA Results (kJ/kg) for all Tests with Holes

Specimens were seen to fail in three characteristic modes:

Failure mode A is the typical splaying mode of progressive crushing displayed by composite tubes (see [60]). The load versus displacement behaviour is as seen in Figure 42 where the load gradually rises to a steady-state and remains at that level until compaction of the debris inside the tube causes it to rise again.

Failure mode B is a global failure. Before steady-state crushing is reached, a through-thickness crack, originating at the damage zone, propagates circumferentially causing the tube to split and collapse. The load carrying capacity is reduced to a very low level and only increases again once the fracture surface becomes in contact with the crush platen (see Figure 43).

Failure mode C exhibits an initial progressive crushing mode (as in Failure Mode A) followed by a drop-off in load being observed in the immediate vicinity of the damaged region. The drop-off in load is larger than could be accounted for by reduction in area, but is smaller than in mode B. In most cases a similar unstable crack forms to mode B, but the crack may progress into the crush zone, or it may be engulfed by the crush zone before it is able to affect the tube significantly and therefore causes only a slight drop in load. The load recovers to the steady-state level after the crush zone passes through the damage area (see Figure 44). The initiation of the crack in this case is usually due to the crush front interacting with the damage zone causing further weakening. With the square samples the crack's progression is temporarily arrested at the corners of the tube, so if the crack initiates with the crush front in the vicinity of the damage zone the unstable failure may be obvious visually, but may cause little or no reduction in load as the remainder of the tube will be unaffected.

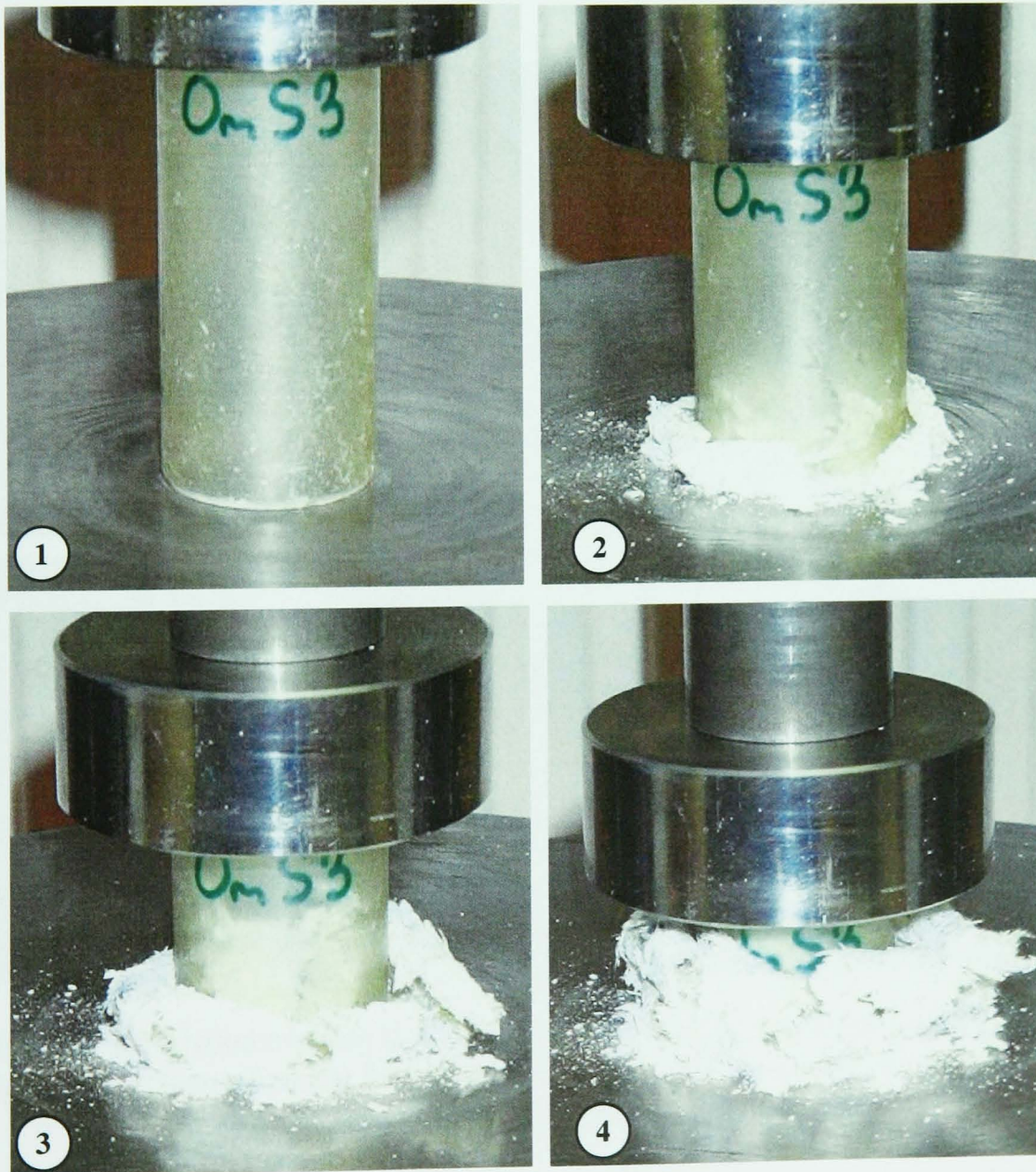
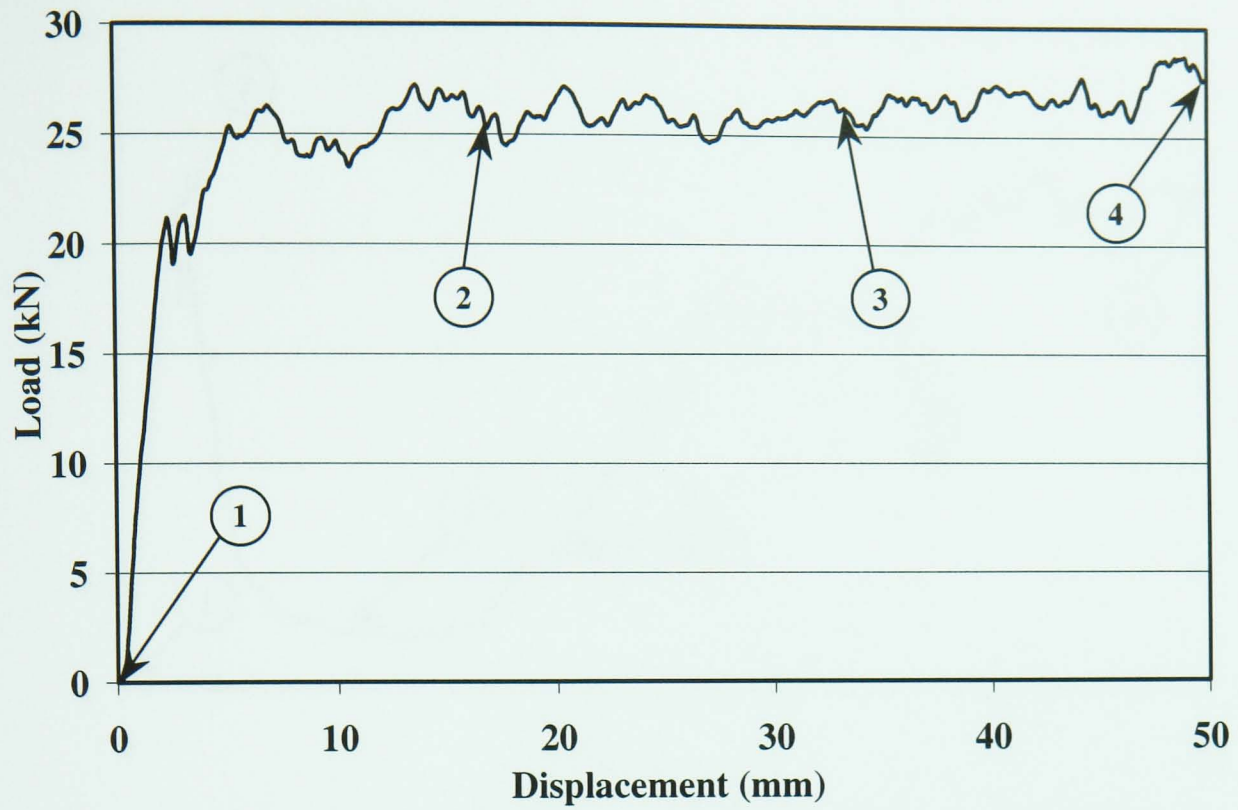


Figure 42: Failure Mode A – Progressive Crush of Cylindrical Sample ($t=2\text{mm}$) Tested Quasi-Statically (C_0mS3)

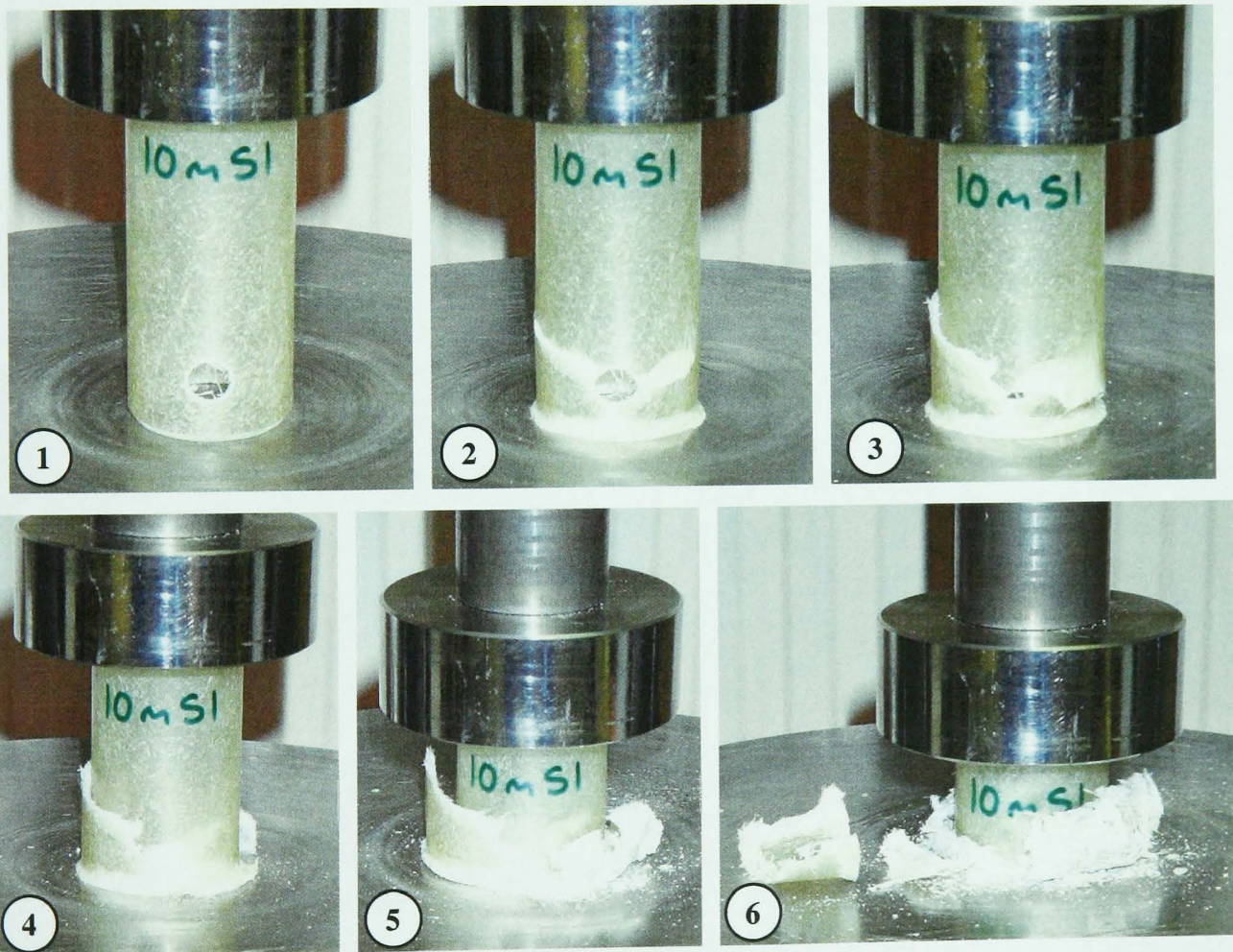
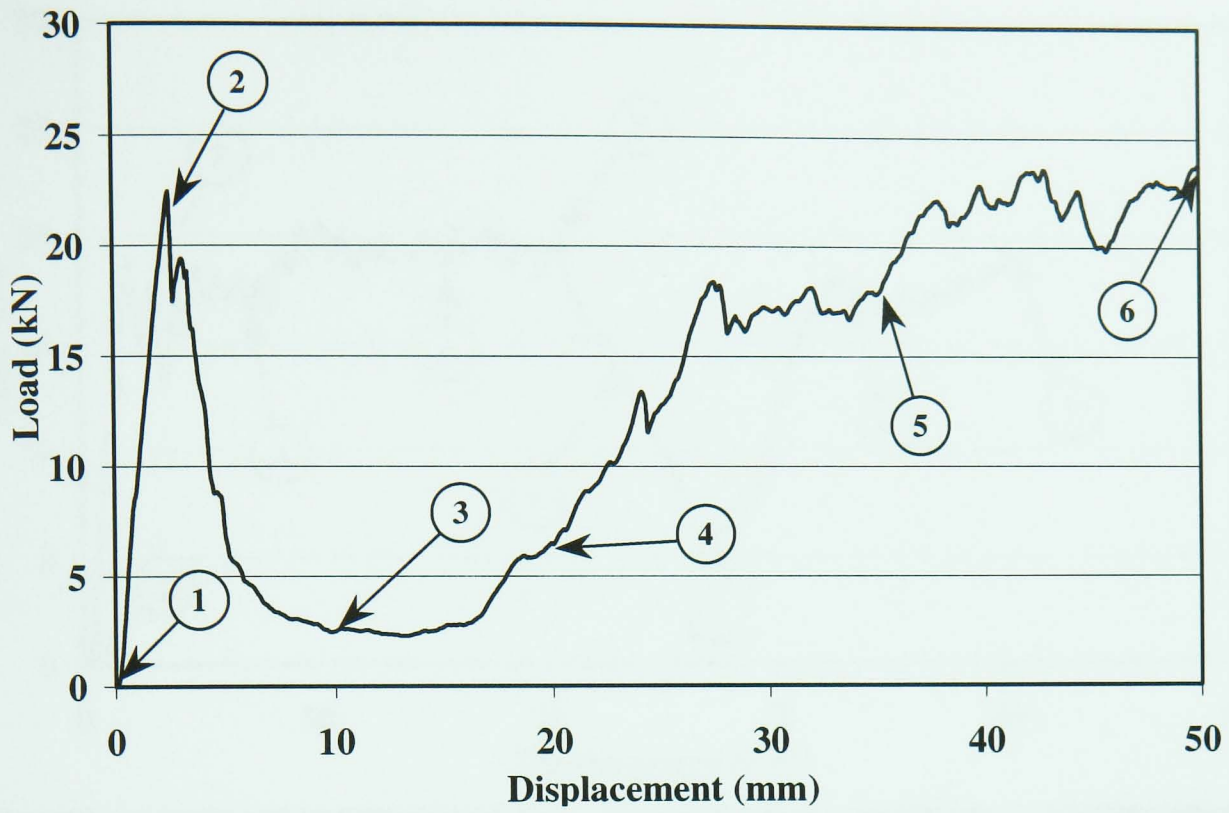


Figure 43: Failure Mode B – Global Failure at Stress Concentration of Cylindrical Sample with 10mm Hole 15mm from Chamfer Tested Quasi-Statically (C_10m15S1)

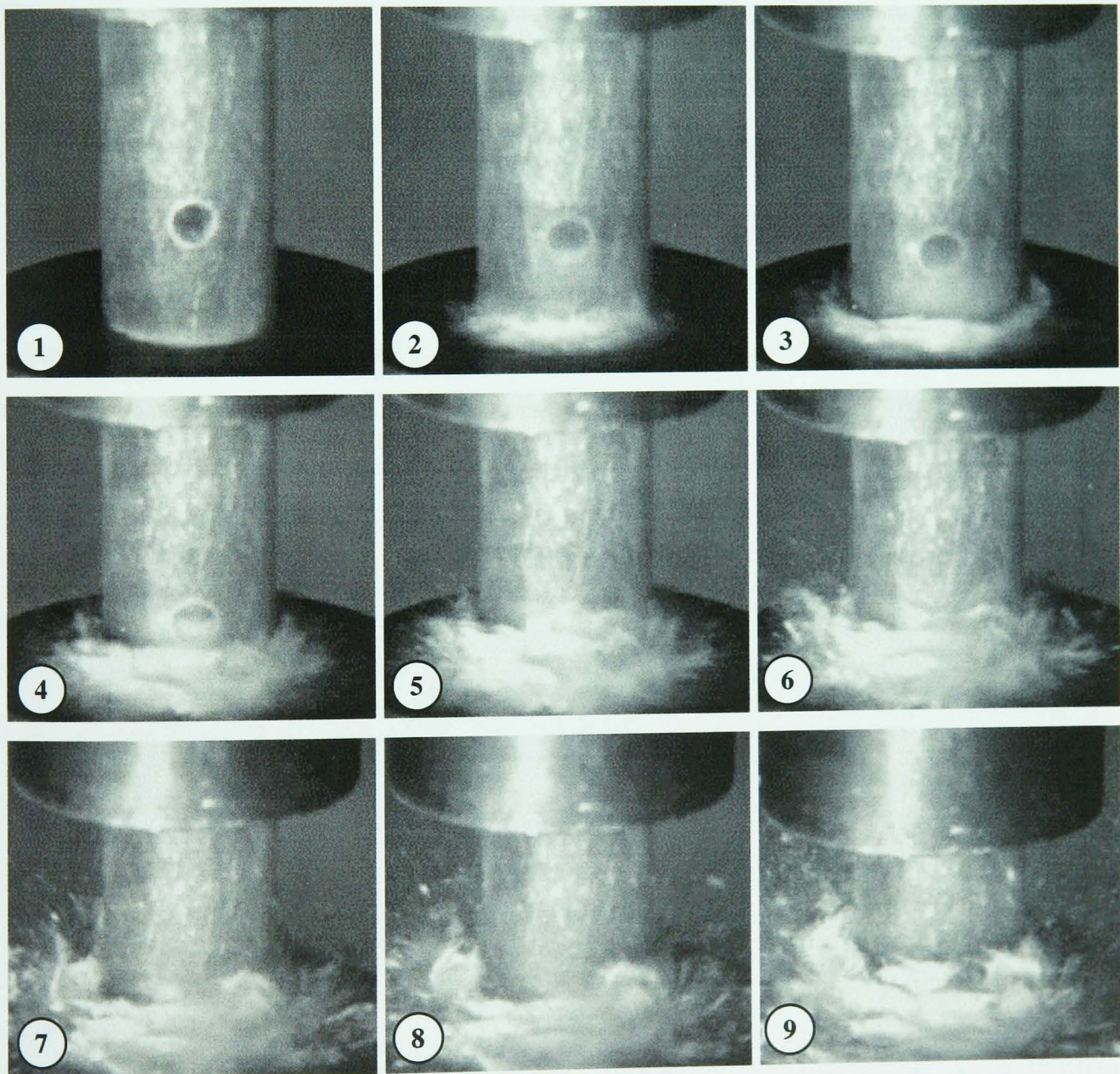
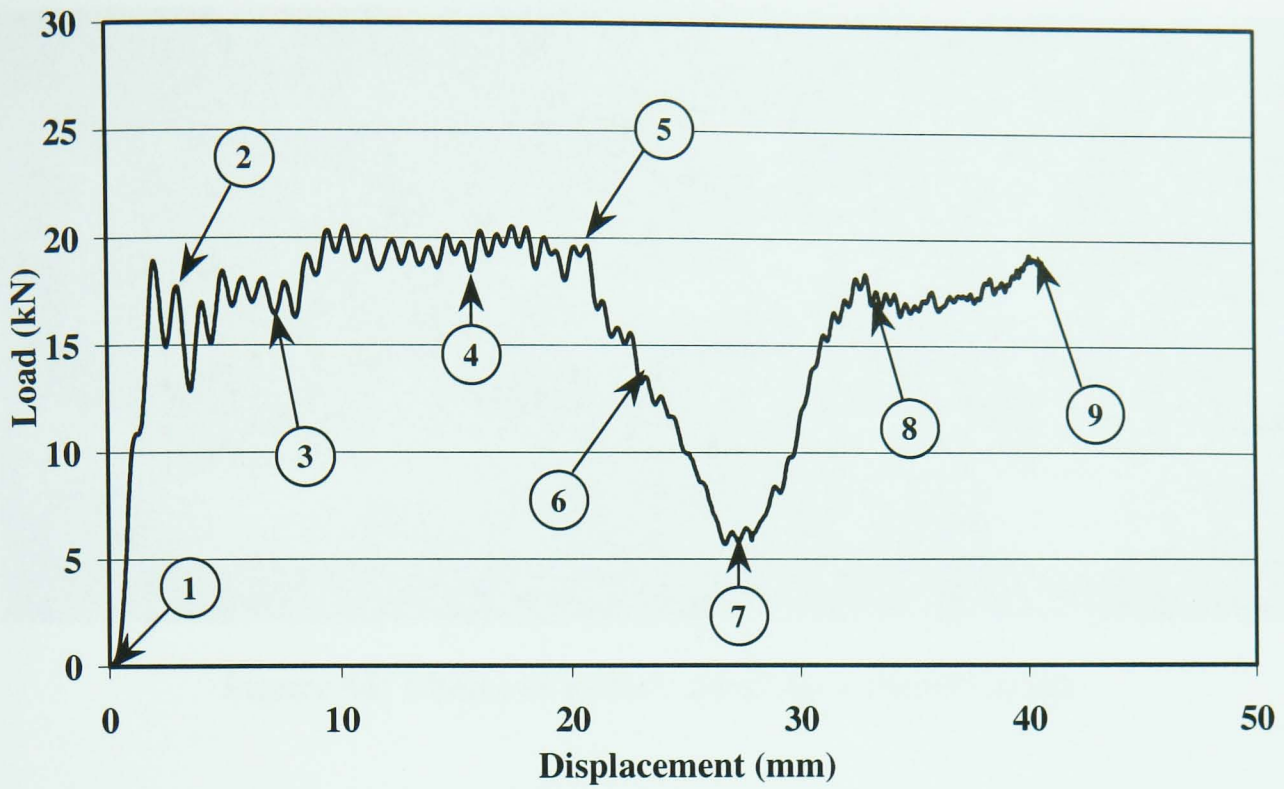


Figure 44: Failure Mode C – Local Failure at Stress Concentration of Cylindrical Tube ($t=2\text{mm}$) with 10mm Hole 30mm from Chamfer Tested Dynamically (C_10m30D1)



Figure 45: Modes of Failure at Stress Concentration

Figure 45 shows the way the samples fail as the stress concentration size reaches the threshold level. The sample on the left shows no effect due to the hole. The middle sample shows a crack forming at the hole propagating at 45° down to the crush zone where it would be quickly engulfed with very little drop in load. The third sample shows a circumferential crack forming. This crack has been arrested at the corners of the tube so only a small amount of the tube will break off and not absorb energy. Above the threshold size, failure similar to the third sample occurs away from the crush zone and continues to propagate around the circumference of the tube bisecting it (see Figure 46). This causes a large drop in load and large sections of the tube are removed uncrushed.

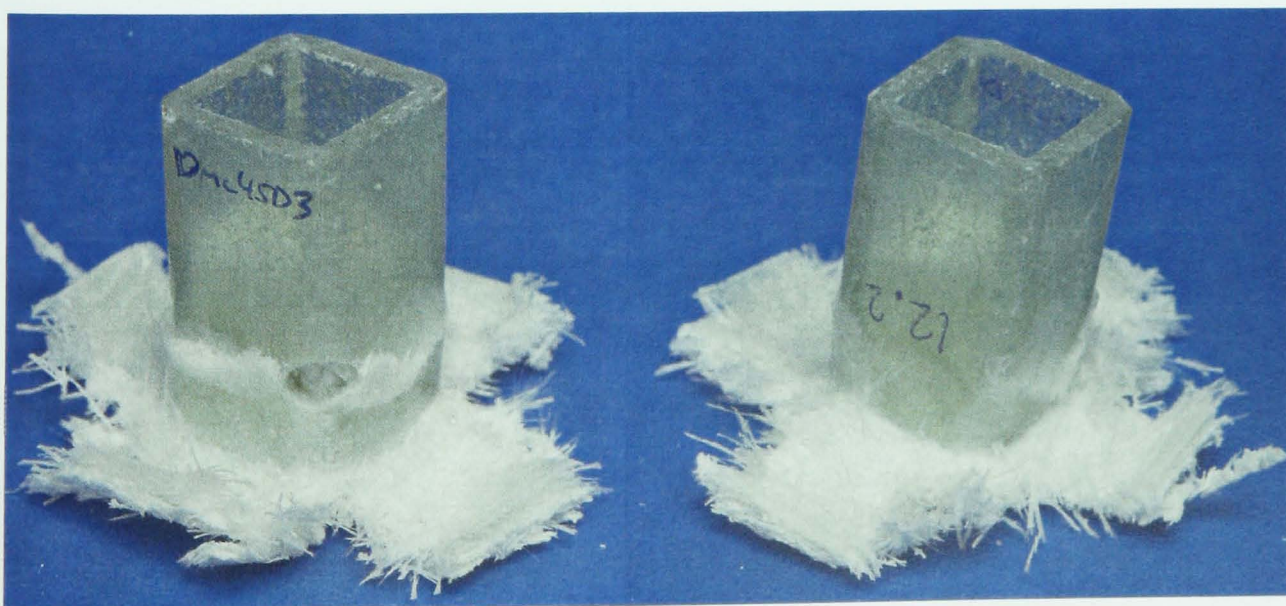


Figure 46: Circumferential Crack Propagated around 3 Sides of Sample

4.1.2.1 Hole Size

For these tests all the holes were positioned with their centres 15mm from the chamfered end of the tubes. It is expected that a critical hole size will be found that will cause a stress concentration, leading to unstable failure.

Circular (t=2mm)

From observing the tests it was established that a hole had either little effect or caused a large drop in SEA, due to an unstable crush mode where a crack initiated at the hole and then propagated around the circumference of the tube.

Damage Type	Static SEA (kJ/kg) (Std. Dev. (%))	Dynamic SEA (kJ/kg) (Std. Dev. (%))
No Damage	74.5 _(3.7)	70.2 _(2.8)
5mm Hole 15mm from chamfer	66.7 _(12.7)	69.7 _(6.7)
10mm Hole 15mm from chamfer	48.7 _(16.8)	48.6 _(19.2)

Table 5: Results for Hole Size in Circular Tubes (t=2mm)

Under quasi-static loading, samples with a 5mm hole showed a mixture of failure modes. Two of the three samples failed progressively by mode A, and one third of samples by mode C, with only a slight drop in SEA. Samples with a 10mm hole all failed globally (mode B). Under dynamic loading, all samples with the 5mm hole failed progressively, not affecting the load-displacement response. The 10mm hole caused a load drop off in the vicinity of the hole for two of the samples. High speed camera images confirm an unstable failure mode (Figure 47).

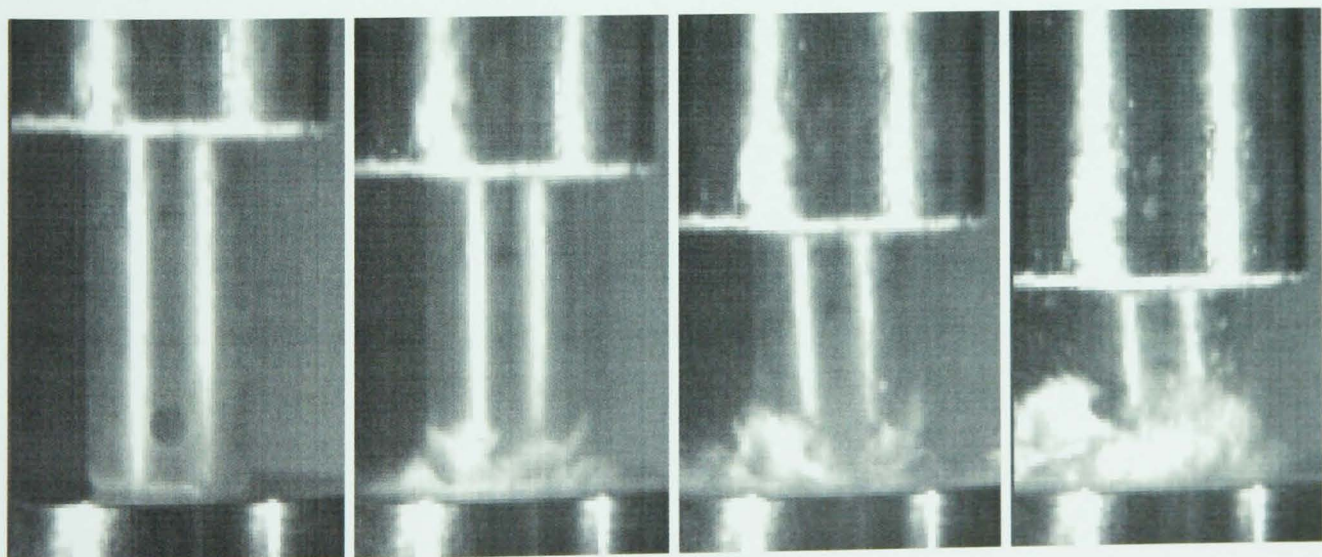


Figure 47: High Speed Camera Images Confirming Unstable Failure of Circular Sample with 10mm Hole.

Circular (t=4mm)

Damage Type	Static SEA (kJ/kg) (Std. Dev. (%))	Dynamic SEA (kJ/kg) (Std. Dev. (%))
No Damage	87.0 _(5.5)	76.0 _(2.1)
5mm Hole 15mm from chamfer	74.5 _(12.3)	71.9 _(0.8)
10mm Hole 15mm from chamfer	62.8 _(15.3)	68.7 _(3.2)

Table 6: Results for Hole Size in Circular Tubes (t=4mm)

Circular tubes with a 4mm wall thickness exhibited similar characteristics to the 2mm wall thickness tubes with three failure modes seen. The cracks that formed at the damage zone had varying effects on the crush depending on the size and direction that they formed.

In the quasi-statically tested tubes the 10mm holes caused unstable failure for all of the specimens. The 5mm holes caused two of the samples to fail with the crack propagating to the crush zone and one sample failing in a similar way to the 10mm hole samples (mode B) and the crack spiralled circumferentially round the tube and caused a much larger reduction in SEA.

As the rate of the test increases the effect of the holes on the SEA decreased. For most of the dynamically tested specimens the load drop due to the effect of the hole was restricted to the vicinity of the hole with the load returning to the pre-hole level by the end of the test. Dynamically there is a negligible difference between the SEAs for the tubes with no hole and those with a 5mm hole. The 10mm holes caused a similar mode of failure as for the quasi-static tests with cracks forming around the tubes and a larger drop in SEA values.

Square (t=2mm) on Face

Damage Type	Static SEA (kJ/kg) (Std. Dev. (%))	Dynamic SEA (kJ/kg) (Std. Dev. (%))
No Damage	58.8 (10.3)	48.5 (1.9)
5mm Hole 15mm from chamfer	57.3 (10.1)	52.4 (5.3)
10mm Hole 15mm from chamfer	58.1 (6.0)	48.7 (2.9)

Table 7: Results for Hole Size in Square Tubes (t=2mm) on the Face

During the quasi-static crush of the square tubes with a 5mm hole two of the samples tested showed no sign of damage crushing progressively through where the hole had been manufactured. On one of the specimens a crack propagated from the hole, but its progression was arrested at the two adjacent corners and only a small piece of the sample broke off without being crushed. This caused a slight reduction in load around the position of the hole, which was quickly recovered, which can account for the very similar SEA values between the specimens with the 5mm hole and those with no damage.

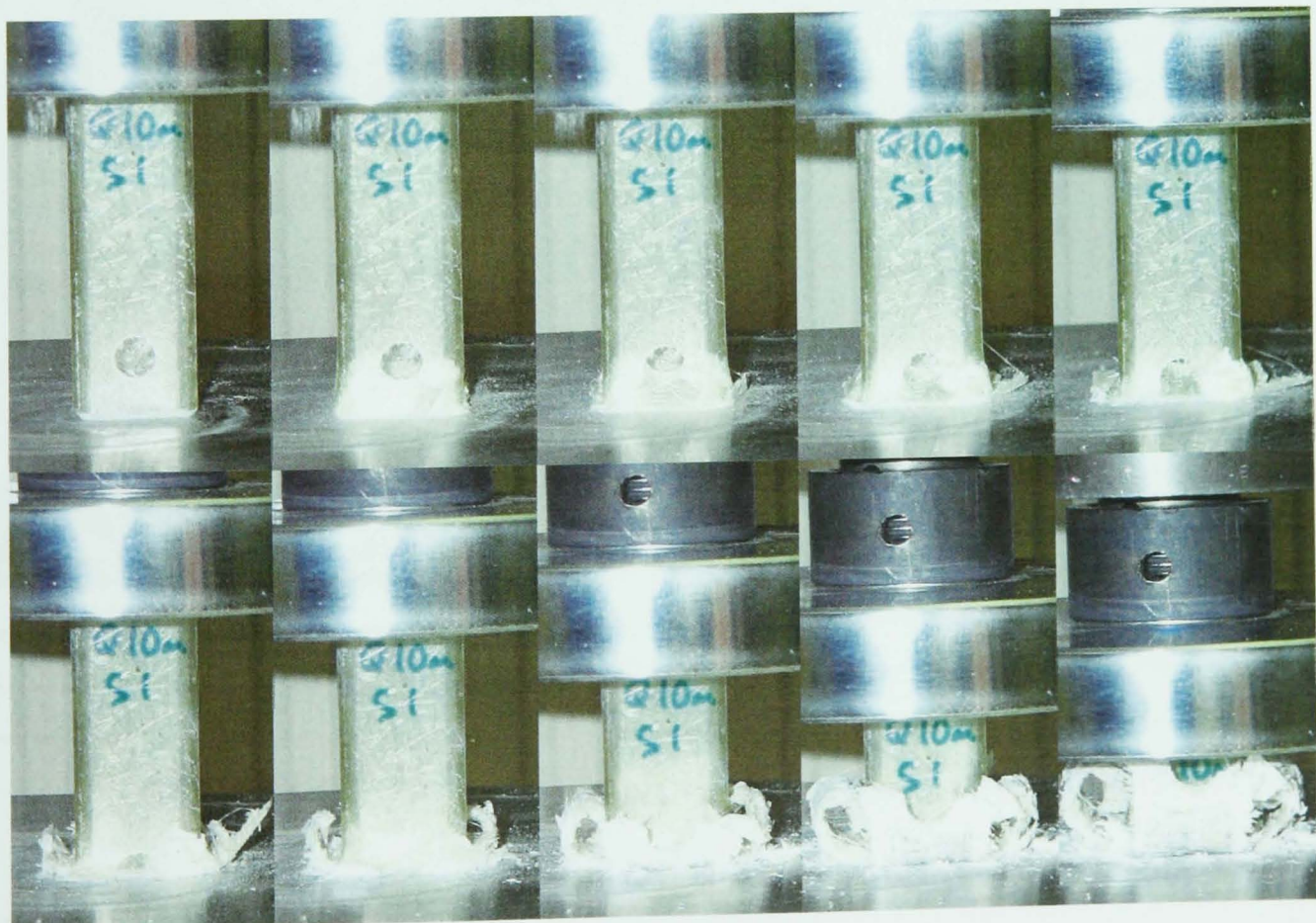


Figure 48: Progressive crush of square tube with 10mm hole (photos at 0, 2.5, 5, 7.5, 10, 15, 20, 30, 40 and 50mm of crush)

The tubes containing a 10mm hole all crushed in a similar way, again with an unstable mode of failure. Figure 48 above shows an example of this and the crack can be clearly seen in the second image. The progression of the crack is again arrested at the corners, enabling the tube to return to a progressive crush mode after engulfing the hole. The drop in load is noticeable, but the rapid return to stable crush enables the SEA values to be comparable to undamaged specimens.

When tested dynamically the hole appeared to have no effect, being clearly visible in one of the fronds of the post-crushed samples (see Figure 49).



Figure 49: Hole in Frond of Square Tube Post Crush

Square (t=4mm) on Face

Damage Type	Static SEA (kJ/kg) (Std. Dev. (%))	Dynamic SEA (kJ/kg) (Std. Dev. (%))
No Damage	69.2 (3.7)	64.1 (4.5)
5mm Hole 15mm from chamfer	70.2 (3.2)	59.6 (4.6)
10mm Hole 15mm from chamfer	67.1 (2.9)	56.0 (1.4)

Table 8: Results for Hole Size in Square Tubes (t=4mm) on the Face

Observations of the quasi-static crush of the square tubes were the same for tubes with a 4mm wall thickness and a 2mm wall thickness.

When tested dynamically the hole appeared to have only a small effect. It can be seen in Figure 45 the way an unstable crack forming may only cause a small drop in load in the vicinity of the damage. Again the geometry of the holes remained unchanged post-crush and could be clearly observed in the fronds of the crushed samples.

Square (t=2mm) at Corner

Damage Type	Static SEA (kJ/kg) (Std. Dev. (%))	Dynamic SEA (kJ/kg) (Std. Dev. (%))
No Damage	58.8 (10.3)	48.5 (1.9)
5mm Hole 15mm from chamfer at Corner	57.1 (3.4)	50.3 (6.3)
10mm Hole 15mm from chamfer at Corner	52.6 (2.9)	43.6 (5.2)

Table 9: Results for Hole Size in Square Tubes (t=2mm) at the Corner

The quasi-static crush of the square tubes with a 5mm hole at the corner is the same as for samples where the hole is on the face of the tube.

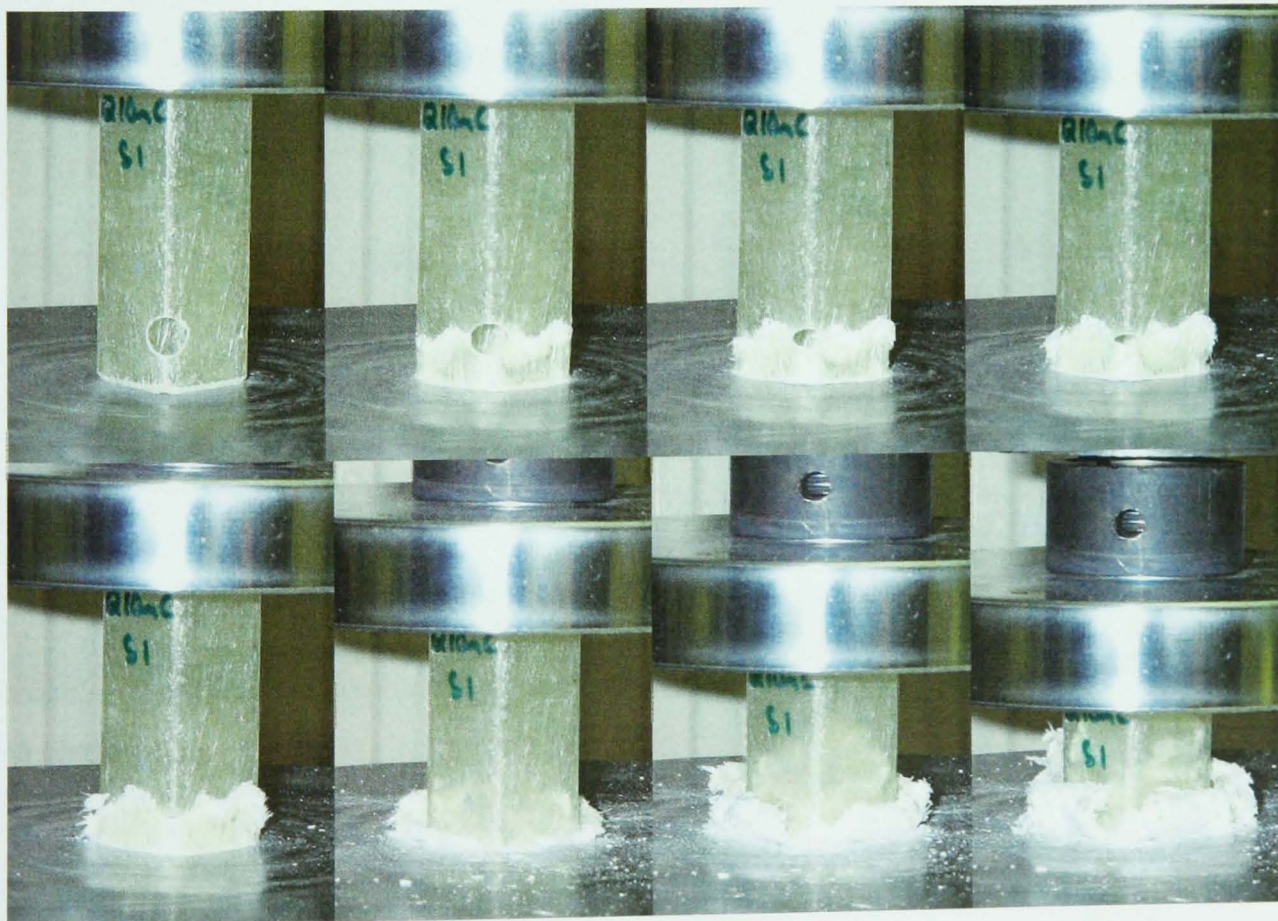


Figure 50: Crush of square tube with 10mm hole at corner (photos at 0, 2.5, 5, 7.5, 10, 20, 30 and 40mm of crush)

The tubes containing a 10mm hole at the corner all crushed in a similar way, again with an unstable mode of failure. Figure 50 above shows an example of this and the crack can be clearly seen. The progression of the crack is again arrested at the corners leaving the back two faces intact. The tube returns to a progressive crush mode after engulfing the hole. The drop in load is greater than when the hole was on one of the faces as two faces are removed uncrushed rather than one. This leads to a lower SEA value compared to undamaged specimens.

When tested dynamically the hole causes a section of the tube to be removed uncrushed by the formation of cracks similar to the quasi-static samples (see Figure 51). Again it is only from two of the faces. The 10% drop in SEA is similar to the quasi-static results.

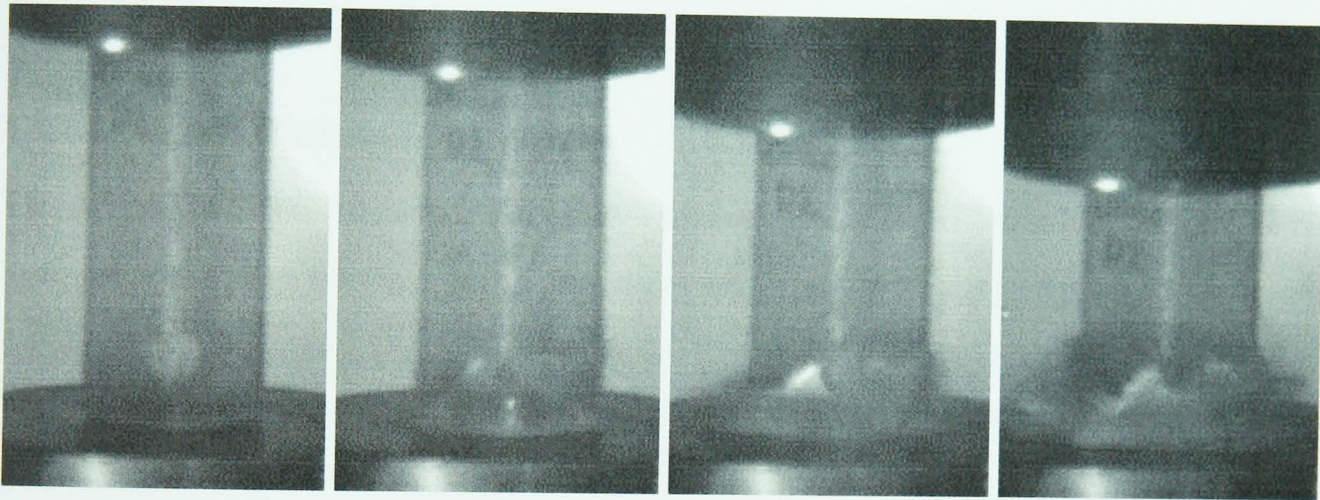


Figure 51: Unstable Failure of Dynamically Crushed Square Tube with 10mm Hole in Corner

Square (t=4mm) at Corner

Damage Type	Static SEA (kJ/kg) (Std. Dev. (%))	Dynamic SEA (kJ/kg) (Std. Dev. (%))
No Damage	69.2 (3.7)	64.1 (4.5)
5mm Hole 15mm from chamfer at corner	68.7 (1.4)	64.8 (2.9)
10mm Hole 15mm from chamfer at corner	59.0 (9.5)	59.1 (4.2)

Table 10: Results for Hole Size in Square Tubes (t=4mm) at the Corner

During the quasi-static crush of the square tubes with a 5mm hole at the corner a crack propagated from the hole and along the two adjacent sides, but its progression was arrested at the next corners and only a small piece of the sample broke off without being crushed. This caused a slight reduction in load around the position of the hole, which was quickly recovered, which can account for the very similar SEA values between the specimens with the 5mm hole and those with no damage.

The 10mm hole caused the same unstable failure as with the 2mm wall thickness samples with the progression of the crack again arrested at the corners leaving the back two faces intact. When tested dynamically the hole again causes a piece of the tube to be removed uncrushed by the formation of cracks similar to the quasi-static samples. Again it is only from two of the faces. The drop in SEA is similar to the quasi-static results.

4.1.2.2 Hole Position – Axially

The dynamically tested samples with holes seemed to exhibit localised reductions in load. The effect of moving the axial position of the hole was used to see whether the effect of the hole was truly localised, or just because the hole was positioned close to the end where crush was initiated. This testing would therefore determine the difference between mode B and mode C failure.

Circular (t=2mm)

Damage Type	Static SEA (kJ/kg) (Std. Dev. (%))	Dynamic SEA (kJ/kg) (Std. Dev. (%))
10mm Hole 15mm from chamfer	48.7 _(16.8)	48.6 _(19.2)
10mm Hole 30mm from chamfer	21.7 _(24.7)	56.7 _(10.0)
10mm Hole 45mm from chamfer	26.1 _(14.0)	62.5 _(1.8)

Table 11: Results for Hole Axial Position in Circular Tubes (t=2mm)

Under quasi-static testing, the axial position of the hole did not affect the mode of failure (mode B). Failure was seen at the hole, remote from the crush zone. After the initial drop the tubes only started to take load again once the crush zone had progressed beyond the position of the hole and a portion of the tube was once again in

contact with both crush platens. This meant that the samples with the axial position of the hole further along the tube exhibited longer periods crushing at lower loads before recovering to the same levels observed in undamaged tubes. The increase in load above the steady state crush load at the end of the tests for samples with a 10mm hole positioned 45mm from the chamfer (10m45S) is due to the two halves of the tube, formed by the circumferential crack, being crushed as though they were two individual tubes and accounts for the greater SEA than samples with a 10mm hole positioned 30mm from the chamfer (10m30S).

The dynamically tested samples again show a drop in load at the position of the hole and then recover to undamaged levels (failure mode C). Undamaged dynamic specimens only crush approximately 30mm due to the load and height of the dropped weight. Due to the damage the specimens crush further to absorb the same amount of energy, as shown in Appendix 1. As the effect of the hole is localised, the specimens with the 10mm diameter hole 45mm from the chamfered end acted as though they were undamaged. They did not exhibit any drop in load and peeling away the fronds from crushed specimens revealed that the geometry of the hole was unchanged.

Circular (t=4mm)

Damage Type	Static SEA (kJ/kg) (Std. Dev. (%))	Dynamic SEA (kJ/kg) (Std. Dev. (%))
10mm Hole 15mm from chamfer	62.8 _(15.3)	68.7 _(3.2)
10mm Hole 30mm from chamfer	39.5 _(25.4)	60.4 _(8.5)
10mm Hole 45mm from chamfer	30.4 _(11.1)	75.0 _(2.7)

Table 12: Results for Hole Axial Position in Circular Tubes (t=4mm)

The effects of the axial position of the hole are the same as for a tube with a 2mm wall thickness.

Under quasi-static testing, the axial position of the hole did not affect the mode of failure (mode B). Failure was seen at the hole, remote from the crush zone.

Dynamically, these cases show a drop in load only at the position of the hole and then recover to undamaged levels (i.e. mode C). With the hole at an axial position of 45mm the crush zone did not progress to the position of the hole during the test and the specimens behaved as though undamaged.

Square ($t=2\text{mm}$) on Face

Damage Type	Static SEA (kJ/kg) (Std. Dev. (%))	Dynamic SEA (kJ/kg) (Std. Dev. (%))
10mm Hole 15mm from chamfer	58.1 _(6.0)	48.7 _(2.9)
10mm Hole 30mm from chamfer	43.8 _(29.5)	49.0 _(2.5)
10mm Hole 45mm from chamfer	48.9 _(25.2)	51.5 _(2.3)

Table 13: Results for Hole Axial Position in Square Tubes ($t=2\text{mm}$) on the Face

Quasi-statically, all the specimens with the 10mm hole fail by a circumferential crack propagating from the hole. With the hole positioned further from the chamfered end, although the corners did arrest the progression of the crack they could not stop it from eventually continuing around the faces of the tube, causing unstable failure by cutting the sample in two. The tube returns to a progressive crush mode after engulfing the hole when once again two surfaces of the tube are in contact with the crush platen. The drop in load causes the SEA values to be lower than undamaged specimens.

However, dynamically none of the specimens fail in an unstable manner. Where the hole has been engulfed it is clearly visible in one of the fronds, while in the specimens where the crush zone has not reached the hole peeling back the frond reveals the hole in its original state. This explains the similar SEA values for all the samples.

Square (t=4mm) on Face

Damage Type	Static SEA (kJ/kg) (Std. Dev. (%))	Dynamic SEA (kJ/kg) (Std. Dev. (%))
10mm Hole 15mm from chamfer	67.1 _(2.9)	56.0 _(1.4)
10mm Hole 30mm from chamfer	53.3 _(16.0)	58.5 _(1.3)
10mm Hole 45mm from chamfer	49.5 _(25.9)	61.3 _(6.1)

Table 14: Results for Hole Axial Position in Square Tubes (t=4mm) on the Face

Again the quasi-static results are the same as the samples manufactured from the 2mm wall thickness tubes. However, dynamically the unstable failure mode causes only a small drop in SEA, with any crack initiating at the hole only in the vicinity of the crush zone (mode C).

Square (t=2mm) at Corner

Damage Type	Static SEA (kJ/kg) (Std. Dev. (%))	Dynamic SEA (kJ/kg) (Std. Dev. (%))
10mm Hole 15mm from chamfer at Corner	52.6 _(2.9)	43.6 _(5.2)
10mm Hole 30mm from chamfer at Corner	31.0 _(2.0)	35.2 _(12.3)
10mm Hole 45mm from chamfer at Corner	25.8 _(16.1)	46.6 _(6.1)

Table 15: Results for Hole Axial Position in Square Tubes (t=2mm) at the Corner

Quasi-statically, all the specimens failed by a circumferential crack propagating from the hole in the same manner as samples with the hole on the face of the tube.

When tested dynamically the hole causes a piece of the tube to be removed, uncrushed, by the formation of cracks similar to the quasi-static samples. Use of a high-speed camera confirms the unstable failure mode (see Figure 52).

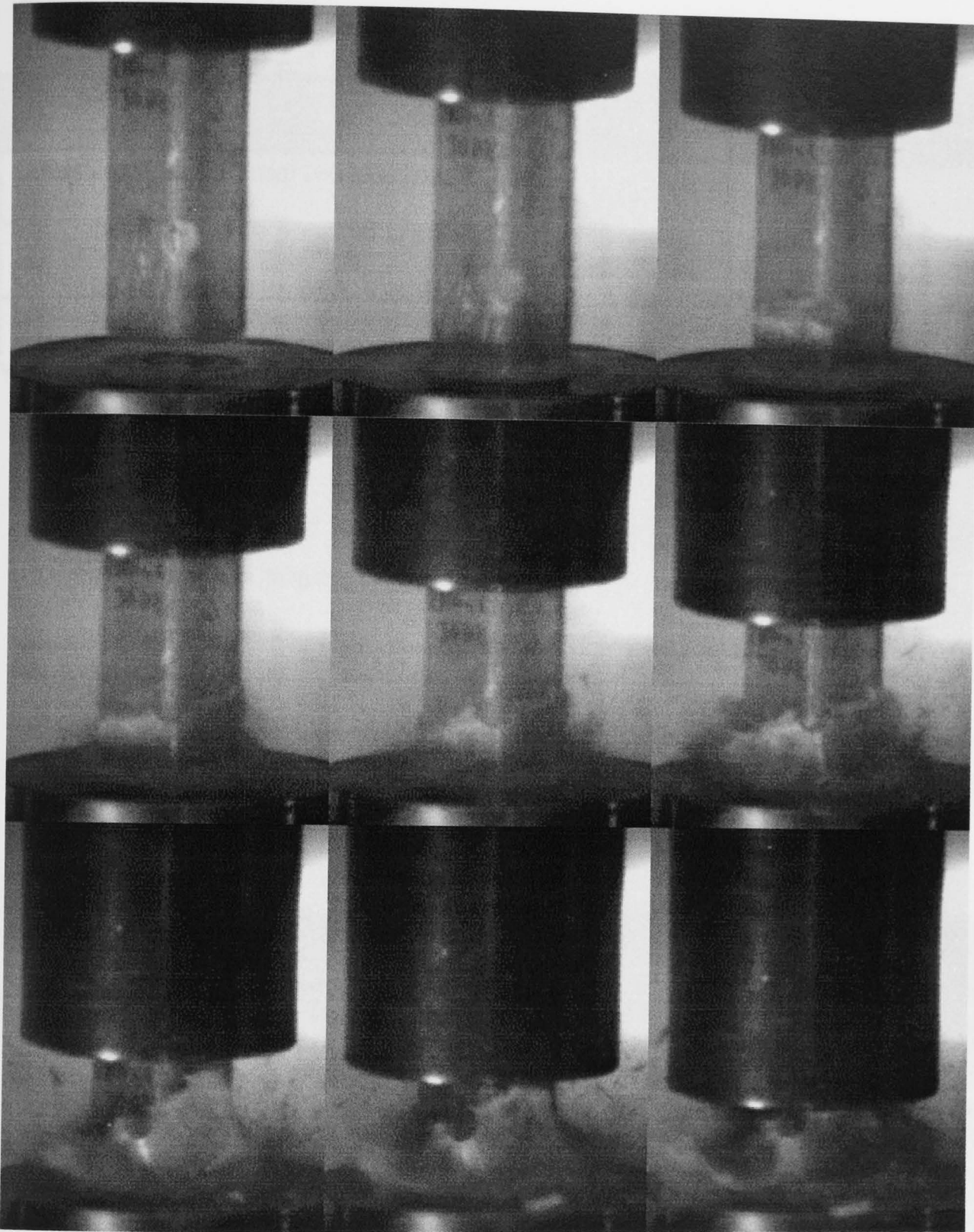


Figure 52: Unstable Failure of Square Tube ($t=2\text{mm}$) with 10mm Hole at the Corner of the Tube 30mm from the Chamfer tested Dynamically (Q_10mc30D2) Captured Using a High Speed Camera

Square (t=4mm) at Corner

Damage Type	Static SEA (kJ/kg) (Std. Dev. (%))	Dynamic SEA (kJ/kg) (Std. Dev. (%))
10mm Hole 15mm from chamfer at Corner	59.0 _(9.5)	59.1 _(4.2)
10mm Hole 30mm from chamfer at Corner	33.3 _(6.9)	46.1 _(18.9)
10mm Hole 45mm from chamfer at Corner	30.4 _(7.1)	45.7 _(41.2)

Table 16: Results for Hole Axial Position in Square Tubes (t=4mm) at the Corner

As with the thinner walled samples all the quasi-statically tested specimens failed by a circumferential crack propagating from the hole.

When tested dynamically the hole causes a section of the tube to be removed uncrushed by the formation of cracks similar to the quasi-static samples. Use of a high-speed camera shows failure at the hole by crack formation either at 45° (as seen in Figure 51 and Figure 52) or parallel to the advancing crush zone (see Figure 53).

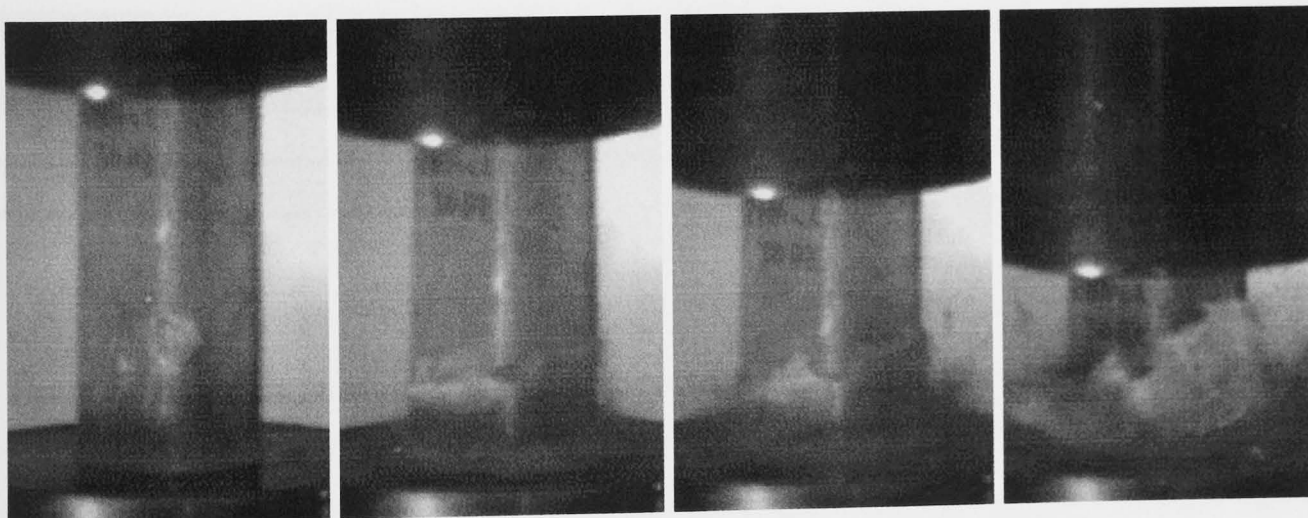


Figure 53: Unstable Crack Propagating Parallel to the Advancing Crush Zone in Dynamically Tested Square Sample with 10mm Hole in Corner of Tube

4.1.2.3 Multiple Holes

The testing of multiple holes was decided to compare the effect of larger holes with that of a number of smaller holes. Testing was done using 5mm holes after

preliminary tests with 3mm holes were shown to have no effect. The holes were positioned with centres 10mm apart, and 30mm axially from the chamfered edge.

Circular (t=2mm)

Damage Type	Static SEA (kJ/kg) (Std. Dev. (%))	Dynamic SEA (kJ/kg) (Std. Dev. (%))
5mm Hole 30mm from chamfer	58.4 _(39.7)	62.8 _(2.7)
2x 5mm Holes 30mm from chamfer	68.2 _(46.5)	61.0 _(2.3)

Table 17: Results for Multiple Holes in Circular Tubes (t=2mm)

Quasi-statically, all samples with two 5mm holes failed in an unstable manner, two by mode B, and one by mode C, although with the third sample the load did not recover within the 50mm crush length. Dynamically tested specimens crushed and failed by mode C and exhibited a drop in load of up to 25% at the position of the holes, whereas the reduction in cross sectional area is 8.5% suggesting unstable failure.

Circular (t=4mm)

Damage Type	Static SEA (kJ/kg) (Std. Dev. (%))	Dynamic SEA (kJ/kg) (Std. Dev. (%))
5mm Hole 30mm from chamfer	62.2 _(21.1)	72.7 _(6.2)
2x 5mm Holes 30mm from chamfer	42.6 _(28.6)	71.5 _(4.5)

Table 18: Results for Multiple Holes in Circular Tubes (t=4mm)

The results are the same as for the 2mm wall thickness samples. Quasi-statically all the tubes with two holes crushed in an unstable manner, although the initial crack occurred at different displacements during the tests. Similarly to the samples with a single 5mm hole at 15mm specimens exhibited mode B failure.

Dynamically tested specimens exhibited a slight drop in load at the position of the holes, but the effect is not as marked as with the single 10mm hole samples. The observed drop in load is equivalent to the proportional loss in cross sectional area caused by the introduction of the holes (8.5%).

Square (t=2mm)

Damage Type	Static SEA (kJ/kg) (Std. Dev. (%))	Dynamic SEA (kJ/kg) (Std. Dev. (%))
5mm Hole 30mm from chamfer	57.3 _(2.8)	48.2 _(5.4)
2x 5mm Holes 30mm from chamfer	51.8 _(7.9)	46.5 _(5.4)

Table 19: Results for Multiple Holes in Square Tubes (t=2mm)

Quasi-statically all the tubes with a single 5mm hole cracked at the hole just prior to being engulfed by the crush zone. This caused a slight drop in load. With this being a localised drop and the SEA being calculated over the full crush length the effect on SEA was negligible. With two holes the specimens crushed in a similar unstable manner. The initial crack occurred approximately 5mm before the crush zone reached the holes, before propagating around the tube removing up to 3 sides of the sample. The resulting drop in load accounts for the reduction in SEA recorded for these specimens.

The dynamic results show a similar trend with only a slight drop in load with the introduction of a second hole.

Square (t=4mm)

Damage Type	Static SEA (kJ/kg) (Std. Dev. (%))	Dynamic SEA (kJ/kg) (Std. Dev. (%))
5mm Hole 30mm from chamfer	72.7 _(2.0)	66.4 _(5.4)
2x 5mm Holes 30mm from chamfer	67.0 _(4.7)	65.7 _(6.1)

Table 20: Results for Multiple Holes in Square Tubes (t=4mm)

A similar trend is observed to the 2mm wall thickness samples with only a localised drop in load both quasi-statically and dynamically, which is more pronounced for the samples with a second hole.

4.1.3 Damage – Delaminations

The testing with Melinex® inserts was chosen to represent delamination between the plies. The work involved the moulding of an insert into the preform prior to moulding. The tests included a single 32mm insert, two 32mm inserts positioned between the first and second, and the second and third plies, and a larger 50.8mm single insert. It is expected that a delamination will reduce the wall thickness at the insert position making it more prone to buckling.

Specimen ID	Insert Size (mm)	Axial Position to start of insert (mm)	Circular Tube (t=2mm)		Square Tube (t=2mm)	
			Q-S	D	Q-S	D
0m	–	–	74.5 _(3.7)	70.2 _(2.8)	58.8 _(10.3)	48.5 _(1.9)
32mx	32	15	72.5 _(2.8)	66.5 _(3.4)	57.6 _(1.6)	49.3 _(5.2)
2x32mx	32	15	60.5 _(4.1)	61.1 _(6.4)	27.2 _(16.8)	44.8 _(3.9)
50mx	50.8	15	64.6 _(9.3)	62.7 _(4.7)	33.6 _(16.2)	44.8 _(4.5)

Table 21: SEA Results (kJ/kg) for all Tests with Melinex® Inserts

Circular (t=2mm)

All quasi-statically tested samples crushed with a progressive crush mode, except for one of the specimens with a 50.8mm diameter insert. This specimen exhibited a delamination of part of the first ply, which led to the slight drop in load. In general the specimens with the two 32mm Melinex® inserts crushed with the lowest steady state load. The overall SEA values are only marginally lower than the specimens with no damage, suggesting that the inclusion of deliberate delaminations, even those with large areas have little or no effect on the energy absorbing behaviour of the composite.

The dynamically tested samples showed a similar slight drop in load around the position of the inserts, but again the SEA results are almost identical to those of the undamaged specimens.

Square (t=2mm)

During quasi-static testing the effect of the Melinex® insert was easily visible. The delamination was seen to separate the plies and leave the individual layers more susceptible to local buckling. With the single 32mm insert the samples experienced a surface ripple at the position of the insert. Although this did not lead to unstable failure it did cause a localised reduction in steady state load. Adding a second 32mm Melinex® insert or having a single 50.8mm insert causes buckling at the insert. As each single ply area buckles a crack formed, which propagated around the circumference of the tube in an unstable failure mode (see Figure 54). This causes a drop in load and a corresponding reduction in SEA.

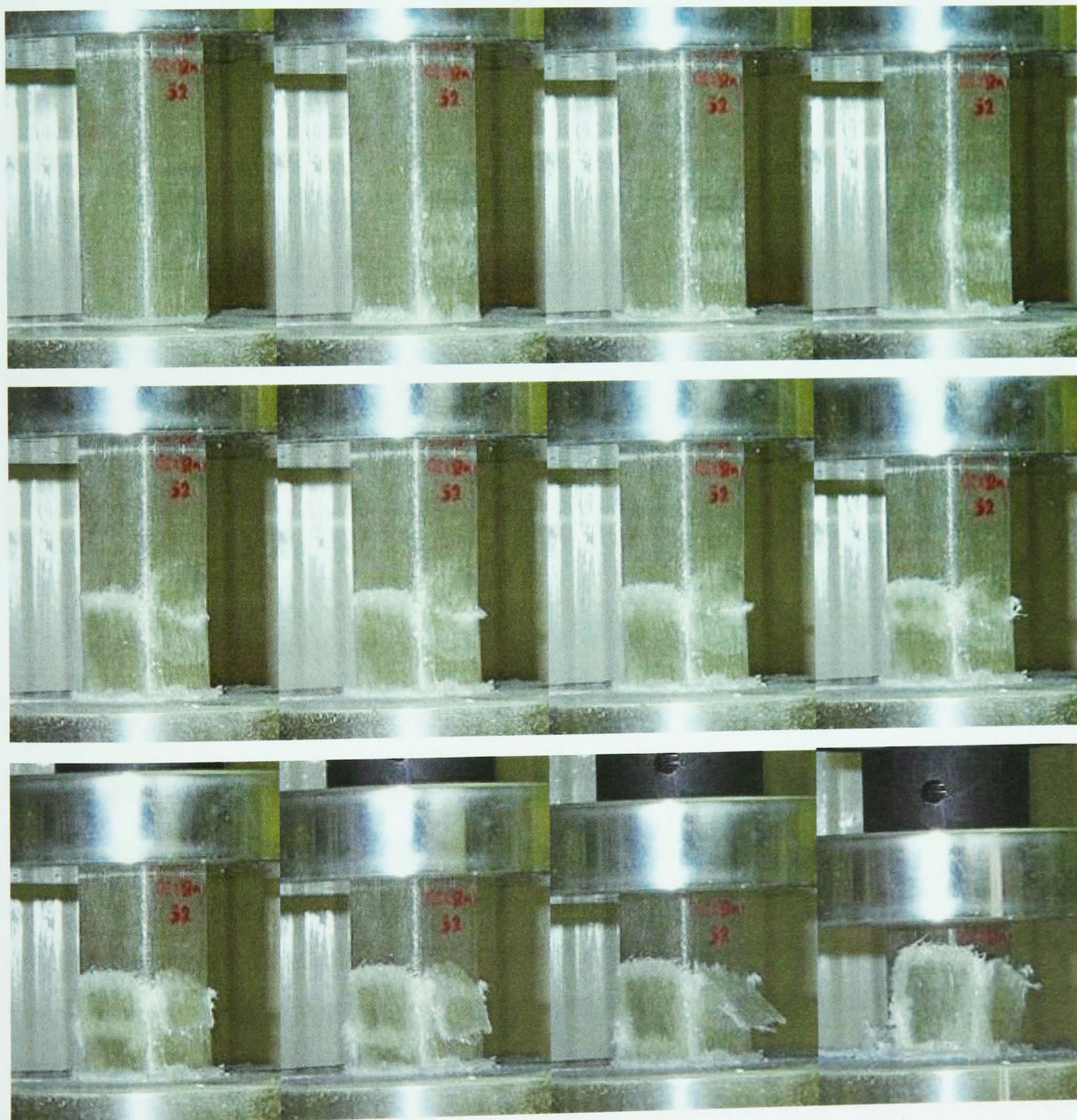


Figure 54: Unstable Failure of Quasi-Statically Tested Sample with Two 32mm Melinex® Inserts

None of the dynamically tested samples showed the same unstable failure mode as the statically tested samples. It was possible to see with the high-speed camera that the samples experienced a surface ripple at the position of the insert (Figure 55). Although this localised buckling did not lead to unstable failure in the form of crack growth it did cause a slight reduction in steady state load and suggest that this amount of delamination is getting close to the threshold level where unstable failure would be seen.

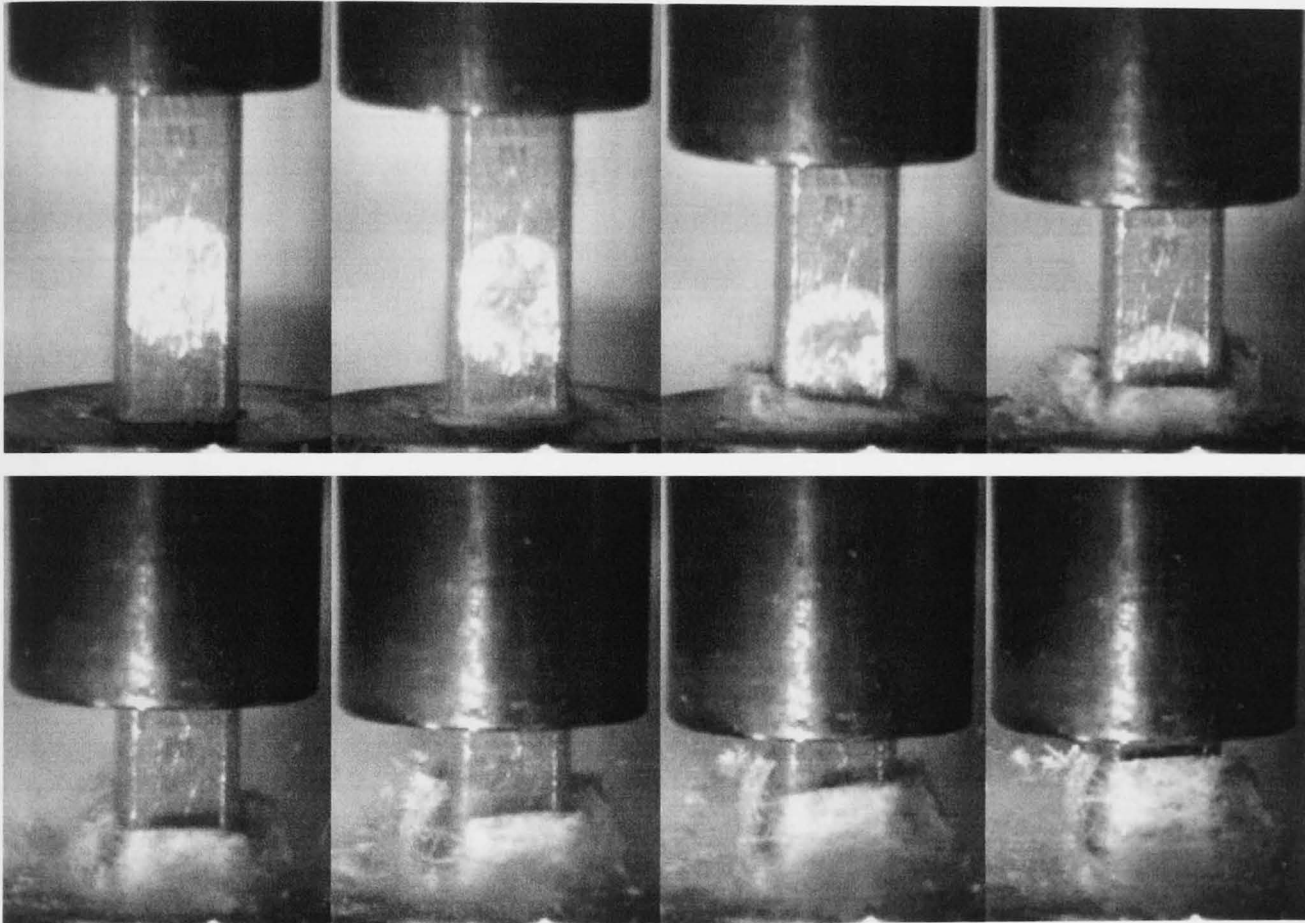


Figure 55: Rippling of Tube Surface during Stable Failure of Dynamically Tested Sample with Two 32mm Melinex® Inserts

4.1.4 Damage - Impact Damage

The testing of impact damaged parts was used to simulate damage that could be acquired during service or manufacture conditions. The tubes were damaged by dropping a fixed weight from a controlled height using the Rosand instrumented falling weight drop tower. A tup with hemispherical end of diameter 12.7mm was used as the impactor. It is expected that the damage will reduce the strength of the composite and provide an initial crack, which could develop once loaded to a critical level.

Specimen ID	Impact Damage (J)	Axial Position (mm)	Position (Corner)	Circular Tube (t=2mm)		Circular Tube (t=4mm)		Square Tube (t=2mm)		Square Tube (t=4mm)	
				Q-S	D	Q-S	D	Q-S	D	Q-S	D
0m	–	–	–	74.5 (3.7)	70.2 (2.8)	87.0 (5.5)	76.0 (2.1)	58.8 (10.3)	48.5 (1.9)	69.2 (3.7)	64.1 (4.5)
1.5J30	1.5	30	–	46.7 (50.6)	67.2 (5.6)	61.8 (31.2)	73.5 (5.4)	57.7 (3.5)	46.4 (5.0)	–	–
3J30	3	30	–	24.8 (9.6)	41.6 (37.4)	49.0 (17.9)	73.9 (5.0)	41.2 (37.6)	46.9 (4.7)	55.9 (28.4)	63.3 (6.3)
6J30	6	30	–	29.3 (11.5)	33.6 (5.3)	40.7 (19.5)	74.0 (2.5)	32.4 (16.7)	49.4 (6.5)	39.2 (22.8)	58.1 (10.5)
9J30	9	30	–	22.0 (32.0)	37.9 (9.7)	38.3 (22.8)	43.0 (2.0)	27.3 (29.7)	37.6 (26.3)	45.5 (24.7)	61.3 (6.7)
1.5J45	1.5	45	–	56.6 (42.7)	65.2 (5.8)	89.3 (2.9)	74.6 (2.4)	55.3 (10.1)	47.2 (2.8)	–	–
3J45	3	45	–	22.0 (15.2)	49.8 (43.6)	58.2 (31.2)	75.0 (1.3)	38.5 (35.1)	48.4 (1.8)	67.9 (7.1)	64.5 (3.3)
6J45	6	45	–	25.5 (12.4)	29.8 (6.1)	33.3 (7.9)	74.5 (3.8)	25.9 (8.4)	47.9 (4.2)	35.8 (7.0)	62.0 (6.9)
9J45	9	45	–	–	–	31.4 (4.8)	45.9 (20.1)	23.2 (7.5)	33.4 (24.9)	33.6 (12.3)	60.4 (5.4)
1.5Jc30	1.5	30	c	–	–	–	–	57.8 (3.6)	47.3 (1.5)	–	–
3Jc30	3	30	c	–	–	–	–	56.7 (5.8)	52.0 (6.4)	–	–
6Jc30	6	30	c	–	–	–	–	43.5 (31.2)	49.1 (1.0)	71.2 (4.3)	65.4 (2.4)
9Jc30	9	30	c	–	–	–	–	28.0 (28.2)	42.8 (11.7)	–	–
12Jc30	12	30	c	–	–	–	–	24.9 (12.1)	27.9 (29.3)	72.0 (3.1)	63.6 (4.9)
18Jc30	18	30	c	–	–	–	–	–	–	70.0 (6.0)	65.2 (7.7)
24Jc30	24	30	c	–	–	–	–	–	–	59.0 (16.7)	62.9 (4.1)
30Jc30	30	30	c	–	–	–	–	–	–	59.6 (14.4)	58.9 (6.9)

Table 22: SEA Results (kJ/kg) for all Tests with Impact Damage

Table 22 shows a summary of the tests completed with impact damaged parts and SEA results for all the geometries tested. The load vs displacement graphs for all the tests can be found in Appendix 1.

The impact damaged parts exhibit the same three modes of failure seen in the samples with holes. When unstable failure occurred it was in the form of a crack initiating at

the damage zone. Its progression was again either circumferential or towards the crush zone. The former case causing a greater reduction in SEA than the latter.

Energy Level	C	CIL	Q	QIL	Qc	QILc	C4	C4IL	Q4	Q4IL	Q4c	Q4ILc
1.5J	147	–	144	–	111	–	61	–	–	–	–	–
3J	330	285	264	–	197	–	129	–	171	–	–	–
6J	620	615	575	467	369	–	242	380	423	–	299	–
9J	789	–	554	913	340	604	433	576	723	445	–	334
12J	–	–	–	768	647	705	–	637	–	–	349	–
15J	–	–	–	1632	–	776	–	673	–	778	–	747
18J	–	–	–	–	–	–	–	–	–	–	643	–
21J	–	–	–	–	–	–	–	–	–	1291	–	830
24J	–	–	–	–	–	–	–	–	–	–	615	–
27J	–	–	–	–	–	–	–	–	–	1237	–	–
30J	–	–	–	–	–	–	–	–	–	–	613	–

Table 23: Area of Damage Zone Caused by Impactor (mm²)

Increasing the level of impact energy generally created a larger damage zone. However, in some cases at the higher energy levels there was greater indentation and even penetration rather than the increase in size of the damage zone, as seen in Figure 56. This makes it hard to characterise the level of impact energy that has caused a zone of damage by visual inspection.



6J impact 9J impact 12J impact 15J impact

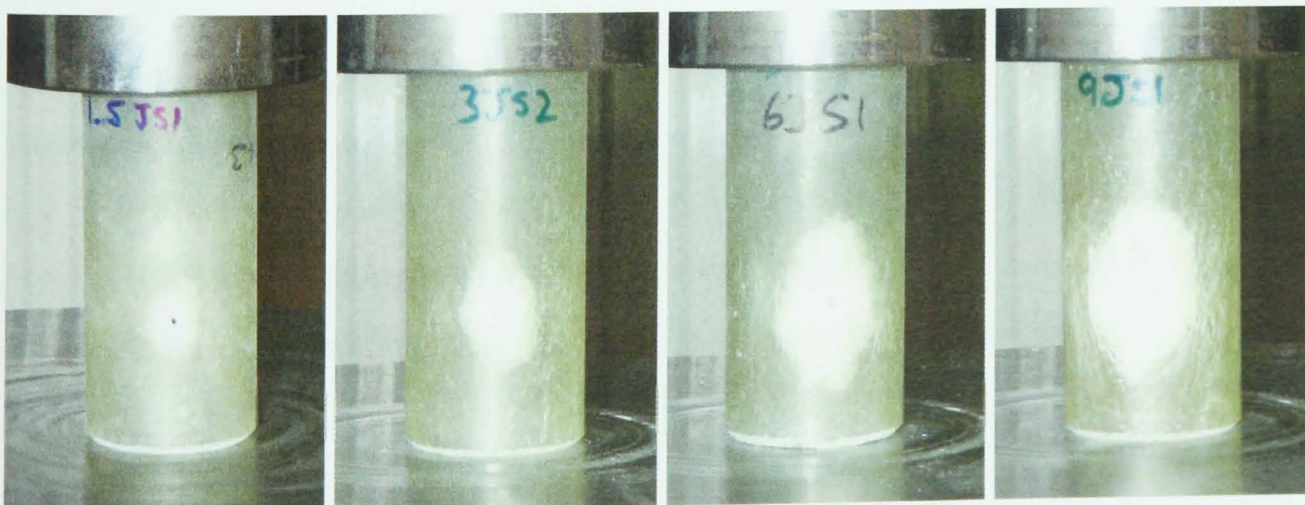
Figure 56: Damage Levels in Square Tubes with Interleaf Demonstrating Penetration and Delamination

4.1.4.1 Damage Levels

Circular (t=2mm)

Damage Type	Static SEA (kJ/kg) (Std. Dev. (%))	Dynamic SEA (kJ/kg) (Std. Dev. (%))
No Damage	74.5 (3.7)	70.2 (2.8)
1.5J Impact 30mm from chamfer	46.7 (50.6)	67.2 (5.6)
3J Impact 30mm from chamfer	24.8 (9.6)	41.6 (37.4)
6J Impact 30mm from chamfer	29.3 (11.5)	33.6 (5.3)
9J Impact 30mm from chamfer	22.0 (32.0)	37.9 (9.7)

Table 24: Results for Impact Damage Levels in Circular Tubes (t=2mm)



1.5J impact 3J impact 6J impact 9J impact

Figure 57: Damage levels in Circular Tube Test Specimens after Impacts

The energy levels of impact tested were 1.5J, 3J, 6J, and 9J. The area of the damage zone has been estimated (see Figure 57 and Table 23).

The impact damaged samples show a similar trend to samples damaged by the inclusion of holes with the quasi-statically tested specimens more sensitive to damage than the dynamically tested samples. The 1.5J samples observed a similar failure mode to the single 5mm hole specimens. Quasi-statically both stable and unstable failure modes were observed in different samples, while dynamically all samples crushed in a stable manner. All the quasi-statically tested samples with 3 – 9J failed unstably. The 3J samples at 5m/s showed a less marked drop in load to the specimens impacted at higher energy levels.

Circular (t=4mm)

Damage Type	Static SEA (kJ/kg) (Std. Dev. (%))	Dynamic SEA (kJ/kg) (Std. Dev. (%))
No Damage	87.0 _(5.5)	76.0 _(2.1)
1.5J Impact 30mm from chamfer	61.8 _(31.2)	73.5 _(5.4)
3J Impact 30mm from chamfer	49.0 _(17.9)	73.9 _(5.0)
6J Impact 30mm from chamfer	40.7 _(19.5)	74.0 _(2.5)
9J Impact 30mm from chamfer	38.3 _(22.8)	43.0 _(2.0)

Table 25: Results for Impact Damage Levels in Circular Tubes (t=4mm)

Again the quasi-statically tested specimens were more sensitive to damage than the dynamically tested samples. A 1.5J impact has a similar effect to a 5mm hole with a mix of stable and unstable failure modes when crushed quasi-statically. At a higher test rate this level of damage has no effect. With damage levels of 9J all dynamically tested specimens failed in an unstable manner causing lower SEA values.

Square on Face (t=2mm)

Damage Type	Static SEA (kJ/kg) (Std. Dev. (%))	Dynamic SEA (kJ/kg) (Std. Dev. (%))
No Damage	58.8 (10.3)	48.5 (1.9)
1.5J Impact 30mm from chamfer	57.7 (3.5)	46.4 (5.0)
3J Impact 30mm from chamfer	41.2 (37.6)	46.9 (4.7)
6J Impact 30mm from chamfer	32.4 (16.7)	49.4 (6.5)
9J Impact 30mm from chamfer	27.3 (29.7)	37.6 (26.3)

Table 26: Results for Impact Damage Levels in Square Tubes (t=2mm)

The reduction in damage area between the 6J and the 9J samples can be explained by two of the 9J samples exhibiting greater indentation and less lateral delamination. Apart from this the damage zone sizes are similar to those experienced by the round tubes.

The quasi-statically tested specimens were more sensitive to damage than the dynamically tested samples. The 1.5J samples observed a slight drop in load in the vicinity of the damage zone. At 3J there was a mix in failure modes between stable and unstable, while dynamically all samples crushed in a stable manner. All the quasi-statically tested samples with 6J and above failed unstably with a circumferential crack initiating at the damage zone and then propagating around the rest of the tube. With the dynamically tested samples a marked drop in load was only experienced in samples that were impacted at 9J.

Square on Face (t=4mm)

Damage Type	Static SEA (kJ/kg) (Std. Dev. (%))	Dynamic SEA (kJ/kg) (Std. Dev. (%))
No Damage	69.2 (3.7)	64.1 (4.5)
3J Impact 30mm from chamfer	55.9 (28.4)	63.3 (6.3)
6J Impact 30mm from chamfer	39.2 (22.8)	58.1 (10.5)
9J Impact 30mm from chamfer	45.5 (24.7)	61.3 (6.7)

Table 27: Results for Impact Damage Levels in Square Tubes (t=4mm)

Again the quasi-statically tested specimens were more sensitive to damage than the dynamically tested samples. The quasi-static threshold for stable and unstable crush was seen at 3J with a mix of stable and unstable failure modes. Above this level all samples exhibited unstable circumferential cracking. The dynamic threshold is hard to observe with the drop in load localised to the position of the damage and only a small reduction in SEA compared to the undamaged samples. A 6J sample exhibited a greater drop in load than any of the 9J samples.

Square on Corner (t=2mm)

Damage Type	Static SEA (kJ/kg) (Std. Dev. (%))	Dynamic SEA (kJ/kg) (Std. Dev. (%))
No Damage	58.8 (10.3)	48.5 (1.9)
1.5J Impact 30mm from chamfer at Corner	57.8 (3.6)	47.3 (1.5)
3J Impact 30mm from chamfer at Corner	56.7 (5.8)	52.0 (6.4)
6J Impact 30mm from chamfer at Corner	43.5 (31.2)	49.1 (1.0)
9J Impact 30mm from chamfer at Corner	28.0 (28.2)	42.8 (11.7)
12J Impact 30mm from chamfer at Corner	24.9 (12.1)	27.9 (29.3)

Table 28: Results for Impact Damage Levels in Square Tubes (t=2mm) at the Corner

The quasi-statically tested specimens were more sensitive to damage than the dynamically tested samples. At 6J there was a mix in failure modes between stable and unstable. All the samples with 9 – 12J failed unstably with a circumferential crack initiating at the damage zone and then propagating around the rest of the tube. With the dynamically tested samples a marked drop in load was only really experienced in samples that were impacted at 12J (only one 9J specimen experienced unstable failure).

Square on Corner (t=4mm)

Damage Type	Static SEA (kJ/kg) (Std. Dev. (%))	Dynamic SEA (kJ/kg) (Std. Dev. (%))
No Damage	69.2 (3.7)	64.1 (4.5)
6J Impact 30mm from chamfer at Corner	71.2 (4.3)	65.4 (2.4)
12J Impact 30mm from chamfer at Corner	72.0 (3.1)	63.6 (4.9)
18J Impact 30mm from chamfer at Corner	70.0 (6.0)	65.2 (7.7)
24J Impact 30mm from chamfer at Corner	59.0 (16.7)	62.9 (4.1)
30J Impact 30mm from chamfer at Corner	59.6 (14.4)	58.9 (6.9)

Table 29: Results for Impact Damage Levels in Square Tubes (t=4mm) at the Corner

Far higher energy level impacts were required at the corners of the 4mm wall thickness samples to cause unstable failure. The quasi-static threshold damage size was 24J, while dynamically tested samples were only starting to show localised drop off in load at 30J. The size of the damage zone caused by the impact at the corners is also far less than a similar impact on the face of the tube.

The threshold damage level for unstable failure at the corners of the square tube were generally higher than on the face, but when unstable failure occurred there were fewer corners remaining to arrest the propagation of the crack so the drop in load was seen to be greater than for samples damaged on the face of the tube.

4.1.4.2 Damage Position – Axially

It was found in the tests with holes that positioning the hole further from the chamfered end of the tube increased their performance under dynamic loading. Tests were done to see if this were the same for tubes with impact damage.

For all the samples tested the quasi-statically tested specimens were more sensitive to damage than the dynamically tested samples.

Circular (t=2mm)

Damage Type	Static SEA (kJ/kg) (Std. Dev. (%))	Dynamic SEA (kJ/kg) (Std. Dev. (%))
No Damage	74.5 _(3.7)	70.2 _(2.8)
1.5J Impact 45mm from chamfer	56.6 _(42.7)	65.2 _(5.8)
3J Impact 45mm from chamfer	22.0 _(15.2)	49.8 _(43.6)
6J Impact 45mm from chamfer	25.5 _(12.4)	29.8 _(6.1)

Table 30: Results for Axial Position of Impact Damage in Circular Tubes (t=2mm)

There was very little difference caused by the position of the damage zone being 45mm rather than 30mm from the chamfered end of the tube. The dynamic threshold is observed to be the same for the dynamically tested samples regardless of the axial position of the damage zone.

Circular (t=4mm)

Damage Type	Static SEA (kJ/kg) (Std. Dev. (%))	Dynamic SEA (kJ/kg) (Std. Dev. (%))
No Damage	87.0 _(5.5)	76.0 _(2.1)
1.5J Impact 45mm from chamfer	89.3 _(2.9)	74.6 _(2.4)
3J Impact 45mm from chamfer	58.2 _(31.2)	75.0 _(1.3)
6J Impact 45mm from chamfer	33.3 _(7.9)	74.5 _(3.8)
9J Impact 45mm from chamfer	31.4 _(4.8)	45.9 _(20.1)

Table 31: Results for Axial Position of Impact Damage in Circular Tubes (t=4mm)

Under quasi-static loading unstable failure was observed in all samples impacted at 3J and above. This is the same as for samples impacted at 30mm, although none of the 1.5J samples failed unstably, which had previously exhibited a mix of failure modes.

With damage levels of 9J and above all dynamically tested specimens failed in an unstable manner causing lower SEA values. This is the same threshold level as for previous testing.

Square on Face (t=2mm)

Damage Type	Static SEA (kJ/kg) (Std. Dev. (%))	Dynamic SEA (kJ/kg) (Std. Dev. (%))
No Damage	58.8 _(10.3)	48.5 _(1.9)
1.5J Impact 45mm from chamfer	55.3 _(10.1)	47.2 _(2.8)
3J Impact 45mm from chamfer	38.5 _(35.1)	48.4 _(1.8)
6J Impact 45mm from chamfer	25.9 _(8.4)	47.9 _(4.2)
9J Impact 45mm from chamfer	23.2 _(7.5)	33.4 _(24.9)

Table 32: Results for Axial Position of Impact Damage in Square Tubes (t=2mm)

The same threshold damage levels are observed as for samples impacted at 30mm. With damage levels of 3J and above all quasi-statically tested specimens failed in an unstable manner causing lower SEA values. Dynamically tested samples did not exhibit this effect at impact levels below 9J.

Square on Face (t=4mm)

Damage Type	Static SEA (kJ/kg) (Std. Dev. (%))	Dynamic SEA (kJ/kg) (Std. Dev. (%))
No Damage	69.2 (3.7)	64.1 (4.5)
3J Impact 45mm from chamfer	67.9 (7.1)	64.5 (3.3)
6J Impact 45mm from chamfer	35.8 (7.0)	62.0 (6.9)
9J Impact 45mm from chamfer	33.6 (12.3)	60.4 (5.4)

Table 33: Results for Axial Position of Impact Damage in Square Tubes (t=4mm)

The quasi-static threshold for stable and unstable crush was seen at 3J with unstable failure being observed in the vicinity of the damage zone. This can be seen more clearly in the load vs displacement graphs in Appendix 1 than in the SEA values in Table 33. The dynamic threshold is hard to observe with the drop in load localised to the position of the damage and only a small reduction in SEA compared to the undamaged samples. However, looking at the samples with a 9J impact at 45mm post test (see Figure 58) it is clear that the samples have started to fail at the damage zone and that the crack is only present on the front face of each of the samples.



Figure 58: Square Samples ($t=4\text{mm}$) with 9J impact at 45mm Post Test

The axial position of the damage zone does not affect the threshold damage levels to cause unstable failure. This is true for both quasi-statically and dynamically tested samples. Figure 58 shows the localised unstable failure of dynamically tested square ($t=4\text{mm}$) samples impacted 45mm from the chamfer with 9J of energy. Observing these samples helps to understand what happened during the crush of samples impacted at 30mm, for which we have load vs displacement traces for crush through the damage zone, and how the position of the damage relates to a reduction in sustained load.

4.1.5 Interlaminar Toughening via Interleaves

Interleaves were used to improve the damage tolerance of the composite structure. The interleaf is moulded between each ply in the test specimens and would increase the interlaminar fracture toughness and therefore impact performance. Testing was done quasi-statically and dynamically for each of the tube geometries. Impact energy levels were tested to find the threshold level above which unstable failure occurred. It is expected that interleaves will improve the damage tolerance by reducing the area of damage caused by a given level of impact. However, it has been shown in section 2.1 that this is likely to reduce the SEA performance of the composite. SEA results are shown below in Table 34.

Specimen ID	Impact Damage (J)	Axial Position (mm)	Position (Corner)	Circular Tube (t=2mm)		Circular Tube (t=4mm)		Square Tube (t=2mm)		Square Tube (t=4mm)	
				Q-S	D	Q-S	D	Q-S	D	Q-S	D
IL	–	–	–	53.2 (1.8)	55.6 (2.7)	45.3 (4.3)	53.6 (5.6)	34.6 (11.7)	39.6 (4.5)	41.4 (2.9)	48.0 (5.4)
IL3J30	3	30	–	43.4 (27.0)	50.5 (6.4)	–	–	–	–	–	–
IL6J30	6	30	–	29.2 (21.6)	36.1 (22.3)	41.8 (3.5)	52.0 (5.9)	32.0 (1.1)	39.2 (1.3)	–	–
IL9J30	9	30	–	–	–	46.3 (7.9)	50.6 (2.3)	26.3 (43.8)	32.6 (10.4)	41.4 (6.1)	48.8 (6.7)
IL12J30	12	30	–	–	–	36.8 (22.3)	44.5 (22.1)	23.9 (37.5)	35.2 (4.8)	–	–
IL15J30	15	30	–	–	–	29.6 (40.8)	42.1 (18.9)	21.8 (9.4)	35.6 (14.1)	37.7 (2.1)	46.3 (3.8)
IL21J30	21	30	–	–	–	–	–	–	–	39.9 (4.1)	46.5 (2.8)
IL27J30	27	30	–	–	–	–	–	–	–	35.3 (6.1)	46.6 (5.7)
IL9Jc30	9	30	c	–	–	–	–	32.8 (2.9)	32.4 (24.1)	–	–
IL12Jc30	12	30	c	–	–	–	–	25.4 (40.5)	28.1 (17.3)	44.8 (6.9)	47.9 (5.0)
IL15Jc30	15	30	c	–	–	–	–	15.0 (1.5)	26.7 (28.8)	–	–
IL18Jc30	18	30	c	–	–	–	–	–	–	37.3 (8.4)	48.0 (6.5)
IL24Jc30	24	30	c	–	–	–	–	–	–	42.7 (0.5)	47.8 (7.0)

Table 34: SEA Results (kJ/kg) for all Tests with Interleaves

4.1.5.1 No Damage – Rate Effects

The inclusion of an interleaf did not change the failure modes. The samples still failed progressively by splaying, but the inclusion of the interleaf affected the appearance of the crushed samples. In the circular tubes it can be seen that more fronds are formed and there is some delamination between the plies in the fronds (see Figure 59 and Figure 60). The square samples exhibit similar delamination in the fronds, but the number of fronds is still four, separated at the corners.

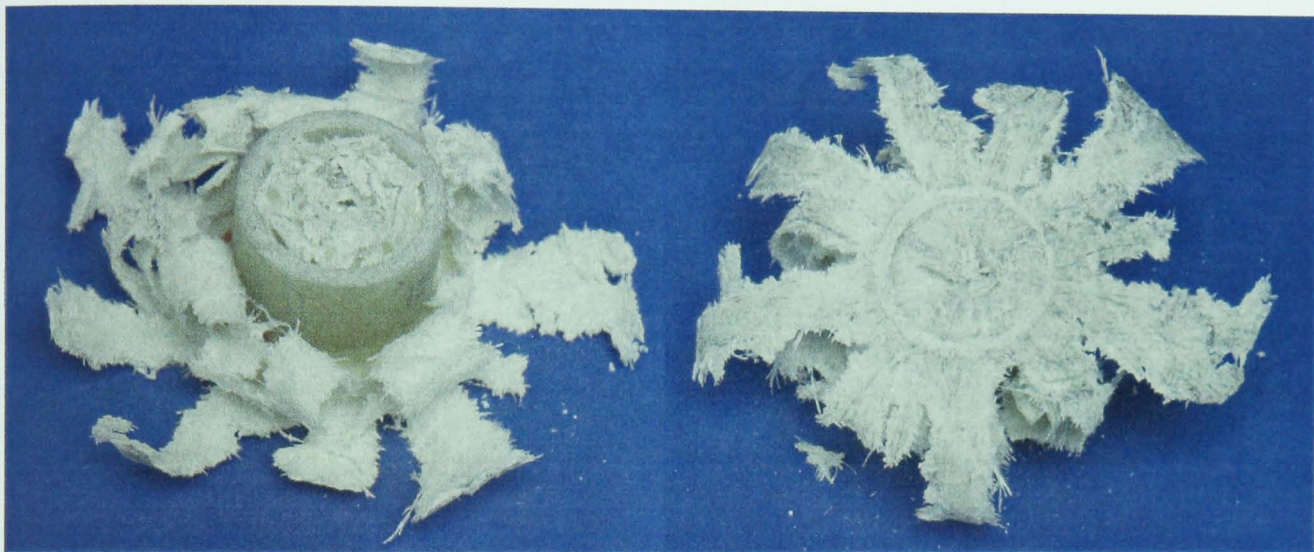


Figure 59: Quasi-Statically Crushed Circular ($t=4\text{mm}$) Sample with Interleaf



Figure 60: Quasi-Statically Crushed Circular ($t=4\text{mm}$) Sample without Interleaf

The introduction of the interleaf reduced the amount of serration of the load vs displacement trace. However, its inclusion reduced SEA for both quasi-statically and dynamically tested samples (see Table 35). This was expected after research by Sohn *et al.* [34] observed a reduction in compressive strength of the composite samples they

tested with interleaves. The rate effects are seen to reverse, with dynamically tested samples absorbing higher energy levels than the quasi-statically tested samples.

Specimen ID	Circular Tube (t=2mm)		Circular Tube (t=4mm)		Square Tube (t=2mm)		Square Tube (t=4mm)	
	Q-S	D	Q-S	D	Q-S	D	Q-S	D
SEA - No Interleaf	74.5 (3.7)	70.2 (2.8)	87.0 (5.5)	76.0 (2.1)	58.8 (10.3)	48.5 (1.9)	69.2 (3.7)	64.1 (4.5)
SEA - Interleaf	53.2 (1.8)	55.6 (2.7)	45.3 (4.3)	53.6 (5.6)	34.6 (11.7)	39.6 (4.5)	41.4 (2.9)	48.0 (5.4)
% Decrease with Interleaf	28.6	20.8	48.0	29.4	41.1	18.2	40.2	25.2

Table 35: Effect of Interleaf on SEA

4.1.5.2 Damage Levels with Interleaf

Circular (t=2mm)

Damage Type	Static SEA (kJ/kg) (Std. Dev. (%))	Dynamic SEA (kJ/kg) (Std. Dev. (%))
Interleaf – No Damage	53.2 _(1.8)	55.6 _(2.7)
Interleaf – 3J Impact 30mm from chamfer	43.4 _(27.0)	50.5 _(6.4)
Interleaf – 6J Impact 30mm from chamfer	29.2 _(21.6)	36.1 _(22.3)

Table 36: Results for Impact Damage Levels in Circular Tubes (t=2mm) with Interleaf

During the quasi-static testing it was observed that in the specimens where the circumferential crack did appear the growth of this crack was slower than with the specimens without the interleaf. The inclusion of the interleaf only reduced the size of the damage zone slightly caused by the impact (see Table 23). This was not seen to be the case for all geometries tested, as was suggested by Kim [35] and Masters [36].

By including the interleaf it is possible to increase the damage tolerance of the tubes, but it is at the expense of energy absorption performance. The damage threshold, above which the specimens start to fail in an unstable manner due to circumferential cracking, doubles from 1.5J to 3J quasi-statically with the inclusion of an interleaf, and from 3J to 6J dynamically.

Circular (t=4mm)

Damage Type	Static SEA (kJ/kg) (Std. Dev. (%))	Dynamic SEA (kJ/kg) (Std. Dev. (%))
Interleaf – No Damage	45.3 _(4.3)	53.6 _(5.6)
Interleaf – 6J Impact 30mm from chamfer	41.8 _(3.5)	52.0 _(5.9)
Interleaf – 9J Impact 30mm from chamfer	46.3 _(7.9)	50.6 _(2.3)
Interleaf – 12J Impact 30mm from chamfer	36.8 _(22.3)	44.5 _(22.1)
Interleaf – 15J Impact 30mm from chamfer	29.6 _(40.8)	42.1 _(18.9)

Table 37: Results for Impact Damage Levels in Circular Tubes (t=4mm) with Interleaf

The results for the 4mm wall thickness specimens also show greater performance post impact than the samples without the interleaf. The damage threshold increased from 1.5J to 12J quasi-statically with the inclusion of an interleaf, and from 9J to 15J dynamically.

Square on Face (t=2mm)

Damage Type	Static SEA (kJ/kg) (Std. Dev. (%))	Dynamic SEA (kJ/kg) (Std. Dev. (%))
Interleaf – No Damage	34.6 _(11.7)	39.6 _(4.5)
Interleaf – 6J Impact 30mm from chamfer	32.0 _(1.1)	39.2 _(1.3)
Interleaf – 9J Impact 30mm from chamfer	26.3 _(43.8)	32.6 _(10.4)
Interleaf – 12J Impact 30mm from chamfer	23.9 _(37.5)	35.2 _(4.8)
Interleaf – 15J Impact 30mm from chamfer	21.8 _(9.4)	35.6 _(14.1)

Table 38: Results for Impact Damage Levels in Square Tubes (t=2mm) with Interleaf

Samples were impacted at energy levels of 6J, 9J and 12J, and 15J. The area of the damage zone has been estimated (see Figure 56 and Table 23).

The reduction in damage area between the 9J and the 12J samples can be explained by all of the 12J samples exhibiting greater indentation and less lateral delamination. The damage size for a 6J sample shown is lower than for corresponding round tubes with interleaf.

During the quasi-static testing it was observed that in the specimens where the circumferential crack did appear the growth of this crack was slower than with the specimens without the interleaf. This improved damage resistance lead to greater resistance to cracking and delamination during crushing.

By including the interleaf it is possible to increase the damage tolerance of the tubes, but it is at the expense of a drop in performance (40% quasi-statically but only 18% dynamically). There is no longer a reduction in SEA as test speed increases. There is even a 9% increase in SEA for the samples tested at 5m/s.

The damage threshold, above which the specimens start to fail in an unstable manner due to circumferential cracking, increases from 3J to 9J quasi-statically with the inclusion of an interleaf, and from 9J to above 15J dynamically.

Square on Face (t=4mm)

Damage Type	Static SEA (kJ/kg) (Std. Dev. (%))	Dynamic SEA (kJ/kg) (Std. Dev. (%))
Interleaf – No Damage	41.4 _(2.9)	48.0 _(5.4)
Interleaf – 9J Impact 30mm from chamfer	41.4 _(6.1)	48.8 _(6.7)
Interleaf – 15J Impact 30mm from chamfer	37.7 _(2.1)	46.3 _(3.8)
Interleaf – 21J Impact 30mm from chamfer	39.9 _(4.1)	46.5 _(2.8)
Interleaf – 27J Impact 30mm from chamfer	35.3 _(6.1)	46.6 _(5.7)

Table 39: Results for Impact Damage Levels in Square Tubes (t=4mm) with Interleaf

The results for the 4mm wall thickness samples show far greater performance post impact than the samples without the interleaf. The damage threshold increased from 3J to around 27J quasi-statically with the inclusion of an interleaf, and from 6J to above 27J dynamically.

Square on Corner (t=2mm)

Damage Type	Static SEA (kJ/kg) (Std. Dev. (%))	Dynamic SEA (kJ/kg) (Std. Dev. (%))
Interleaf – No Damage	34.6 (11.7)	39.6 (4.5)
Interleaf – 9J Impact 30mm from chamfer at Corner	32.8 (2.9)	32.4 (24.1)
Interleaf – 12J Impact 30mm from chamfer at Corner	25.4 (40.5)	28.1 (17.3)
Interleaf – 15J Impact 30mm from chamfer at Corner	15.0 (1.5)	26.7 (28.8)

Table 40: Results for Impact Damage Levels in Square Tubes (t=2mm) at the Corner with Interleaf

The rig used to hold the specimens while damage was impacted is shown in Figure 31. The energy levels of impact tested were 9J, 12J and 15J. The effect of these impact energy levels is shown in Figure 61.



Figure 61: Damage levels in square tube test specimens with interleaf after impacts at corners

The area of damage is smaller at the corners than corresponding impacts on the surface (see Figure 56). With impacts on the face of the tubes the area of damage size

increased more with each incremental rise in impact energy than is observed for impacts at the corners.

There is an obvious threshold value of 12J for the quasi-statically tested samples where there was a mix in failure modes between stable and unstable. Below this value all specimens failed stably and above this value all specimens exhibited an unstable failure mode. Dynamically there appeared to be mixed modes of failure for all sets of tests from 9J to 15J, suggesting a broader threshold damage level.

Square on Corner (t=4mm)

Damage Type	Static SEA (kJ/kg) (Std. Dev. (%))	Dynamic SEA (kJ/kg) (Std. Dev. (%))
Interleaf – No Damage	41.4 _(2.9)	48.0 _(5.4)
Interleaf – 12J Impact 30mm from chamfer at Corner	44.8 _(6.9)	47.9 _(5.0)
Interleaf – 18J Impact 30mm from chamfer at Corner	37.3 _(8.4)	48.0 _(6.5)
Interleaf – 24J Impact 30mm from chamfer at Corner	42.7 _(0.5)	47.8 _(7.0)

Table 41: Results for Impact Damage Levels in Square Tubes (t=4mm) at the Corner with Interleaf

With 4mm wall thickness samples the quasi-statically tested specimens were again more sensitive to damage than the dynamically tested samples with a localised drop in load observed in specimens with damage levels above 18J. The dynamic samples did not experience any drop in performance even at 24J. This shows increased performance quasi-statically. Dynamically the samples without interleaf start to exhibit a drop in load at about 24J, which is not observed in the interleaved samples.

4.2 Ultimate Compressive Stress (UCS)

Having completed the tube crush programme, work was started to determine why some samples were more damage tolerant than others. The mode of failure observed at the damage zone was similar to that observed in compressive coupon samples tested by Fernie [48]. This section shows the results for each of the sample types when tested without any trigger to find the ultimate compressive stress. The coupon samples exhibited a 26% increase in UCS with test rate so similar increases are expected.

Sample Type	Quasi-Static UCS (MPa)	Dynamic UCS (MPa)	% Increase with Rate
Circular Tube (t=2mm)	174.9 _(2.6)	234.0 _(2.3)	33.8
Circular Tube (t=2mm) with Interleaf	132.8 _(1.0)	192.7 _(6.1)	45.1
Circular Tube (t=4mm)	237.2 _(0.7)	-	-
Circular Tube (t=4mm) with Interleaf	168.2 _(2.4)	-	-
Square Tube (t=2mm)	180.4 _(2.4)	265.0 _(5.1)	47.0
Square Tube (t=2mm) with Interleaf	171.2 _(0.8)	269.4 _(2.3)	57.4
Square Tube (t=4mm)	234.0 _(1.6)	291.6 _(1.9)	24.6
Square Tube (t=4mm) with Interleaf	174.3 _(3.4)	248.4 _(2.2)	42.5

Table 42: Ultimate Compressive Stress Results

Table 42 shows that the UCS increased for all geometries tested with and without interleaf, by between 24.6 and 57.4%.

By dividing the average crushing stress by the UCS for each of the undamaged tube types gives the results shown in Figure 62. It can be seen that dynamically tested samples crush at a lower load compared to the ultimate compressive load of the sample. This means that a larger stress concentration is required to cause unstable

failure to occur. This is also shown to be the case for interleaved samples when compared to samples without interleaf.

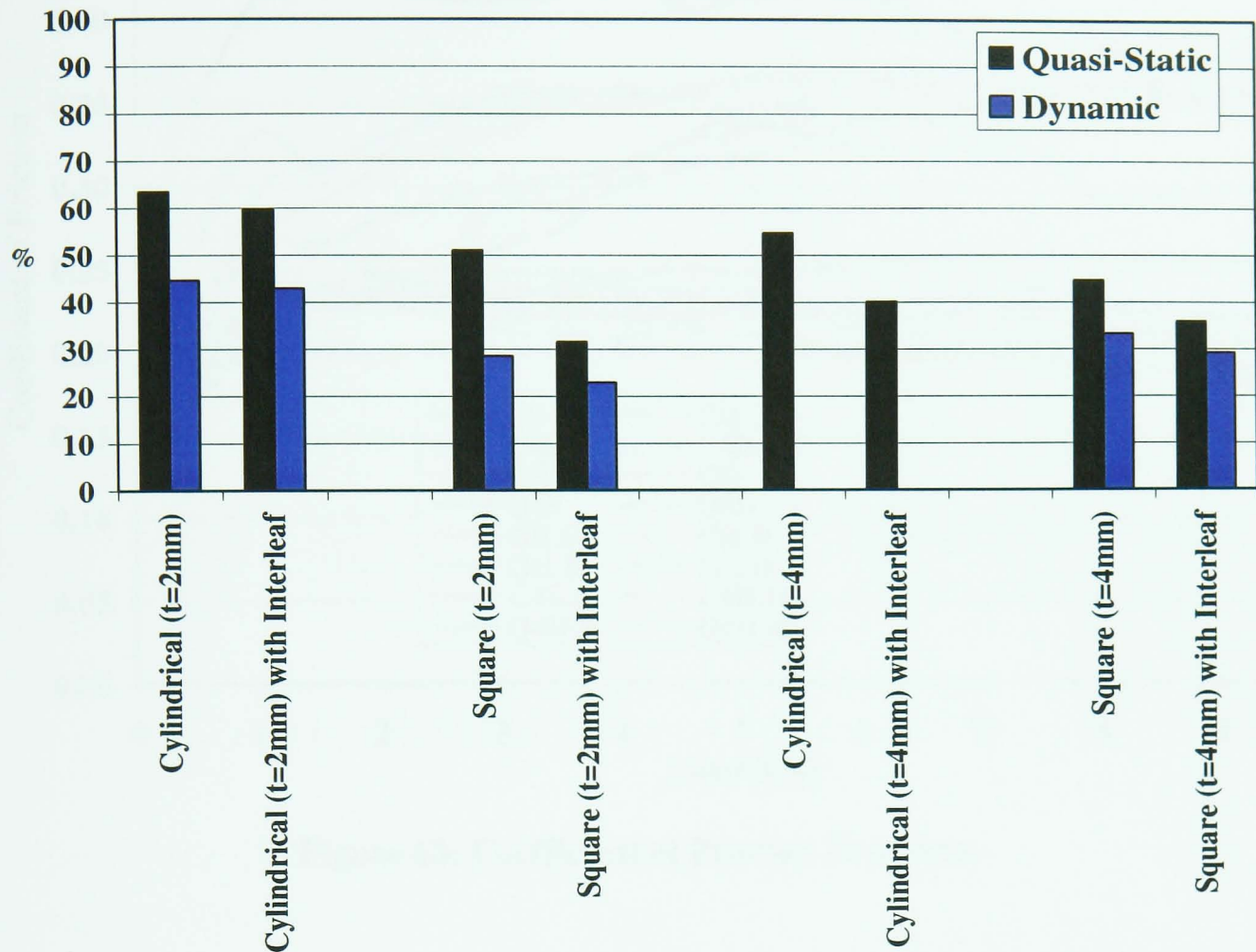


Figure 62: Crush Load as Percentage of Ultimate Compressive Load

4.3 Friction

The introduction of an interleaf improved the damage tolerance of the specimens. However, this was coupled with a reduction in SEA by up to 48%. The main cause of this was suspected to be the reduction in coefficient of friction in the crush zone. Frictional effects have been shown by Fairfull [59] to account for more than half of the energy absorption capability of a crushing tube. This section looks at the results for the coefficient of friction between each of the samples and the ground steel crush platen. The results for the coefficient of friction are shown in Figure 63.

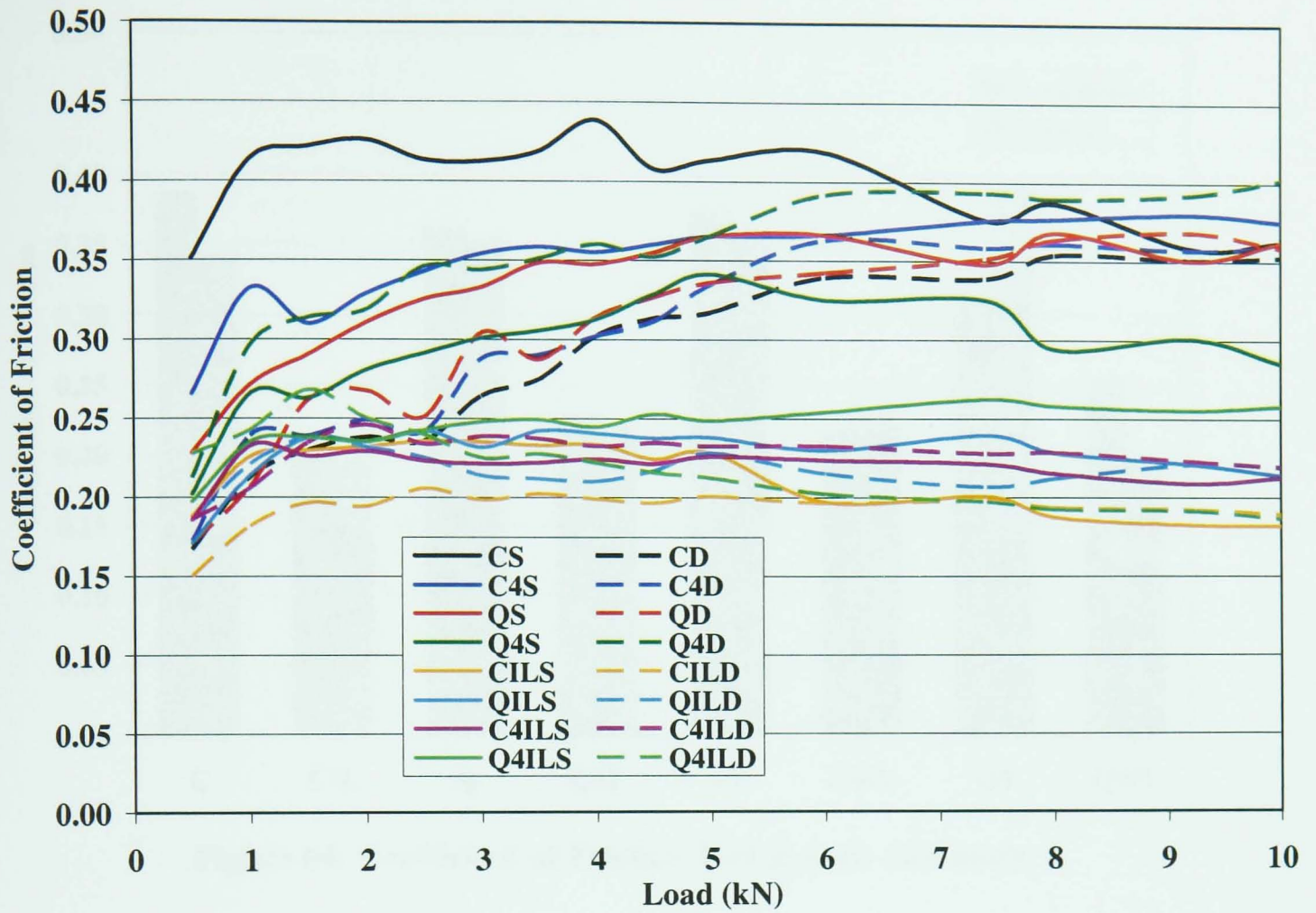


Figure 63: Coefficient of Friction Test Data

The test equipment described in 3.5.4 requires visual readings to be taken for the torque values. Due to smaller values being recorded at lower loads any errors in readings produce a proportionally greater error in the final results. By ignoring the results up to 5kN it is possible to guarantee the results are for kinetic friction only. A summary of these results is shown in Figure 64.

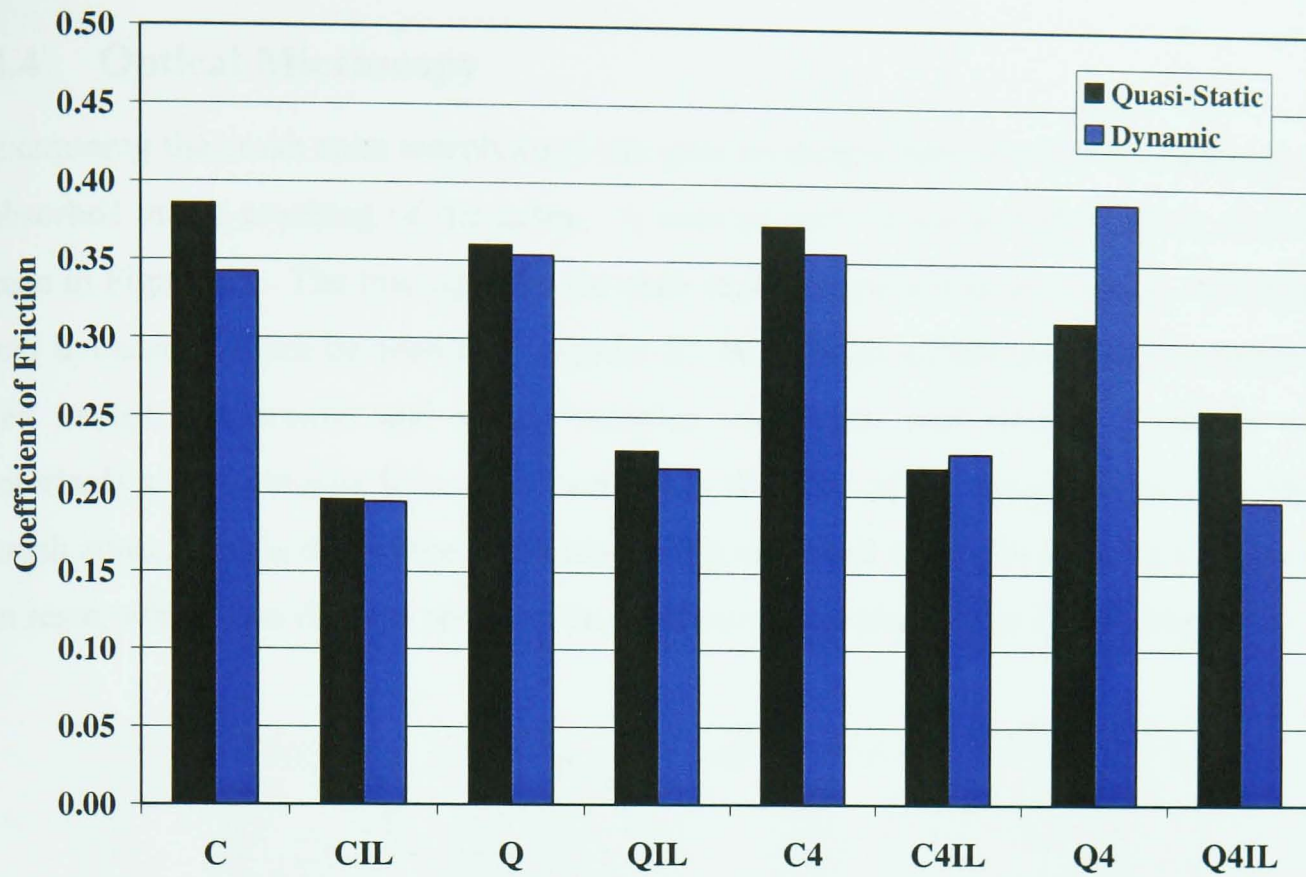


Figure 64: Coefficient of Friction Test Results Summary

It was suggested by Mamalis *et al.* [92] that the reduction seen in the energy absorption at dynamic rates was due to higher values of friction between the wedge and the fronds and the crush platen and the fronds in the static tests. With these results there is no obvious difference between the results for the quasi-statically and the dynamically tested samples, although the friction tests all take place at a quasi-static test rate.

When averaged, samples without an interleaf have a coefficient of friction between the crush zone and the ground steel crush platen of 0.36. Samples with an interleaf have a coefficient of friction of 0.22. These results confirm that the SEA reduction seen through interleaving could be accounted for by a reduced coefficient of friction in the crush zone.

4.4 Optical Microscopy

Examining the crush zone morphology can give an insight into the ways that energy is absorbed in the crushing of the tubes. A scan of each of the potted samples can be seen in Figure 65. The micrographs for each sample type tested, both quasi-statically and dynamically can be seen in Appendix 2. With many of the quasi-static samples (all except the circular and square samples with 4mm wall thickness without an interleaf) a compressive failure is observed in the wall of the sample away from the crush zone. This is due to the crush load being sustained while the samples were cast in resin, which was done to preserve the crush zone morphology as it is during a test.



Figure 65: Scan of Samples with Crush Zone Encapsulated in Resin

The micrographs all exhibit a similar shape to the schematic of the splaying crush mode shown in Figure 12. The debris wedge and the centre wall crack associated with the splaying failure mode are clearly visible in all samples. The micrographs also show flexural damage in the fronds. They confirm the greater curvature seen in the quasi-statically tested samples and the greater degree of fragmentation seen in the fronds of the dynamically tested samples.

The micrographs generally show a shorter centre wall crack in samples with interleaf (although not in the QILs sample). By measuring the crack lengths from the tip of the debris wedge to the end of the crack for all samples the interleaved samples had an average crack length 20% shorter than samples without interleaf. This is to be expected as the interleaf will increase the interlaminar fracture toughness. This leads to a tighter angle through which the fronds bend at the crush platen and can result in a greater amount of delamination, which has been observed in the fronds of the interleaved samples. However, micrographs are only representative of one point around the perimeter of the tube and may not be representative of the entire specimen.

4.5 Environmental Scanning Electron Microscopy (ESEM)

ESEM images of the crush zone and fronds of quasi-statically and dynamically tested samples were taken. Images from the fronds of quasi-statically and dynamically tested cylindrical tubes ($t=2\text{mm}$) without any damage are shown in this section. The aim of this work is to show the difference between the fibre and the matrix from the fronds of quasi-statically and dynamically tested samples

It was possible to observe the change in crush mode as specimens were crushed quasi-statically and dynamically. It was also obvious that the change in crush mode caused a reduction in SEA as test speed increased. By using an Environmental Scanning Electron Microscope (ESEM) it was possible to observe the crush zone morphology and obtain an insight into why the quasi-statically tested samples had higher SEA values than the dynamically tested ones.

Geary [117] found that the fracture toughness increased by a factor of 2.5 to 3 at increased test rate. Work by Fernie [116, 127] also showed that as the test speed increases the ultimate tensile and compressive strengths of the polyester resin used increased by 74% and 112% respectively, as well as an increase in elastic moduli by up to 117%. This will account for the greater fragmentation of the matrix at higher test speeds.

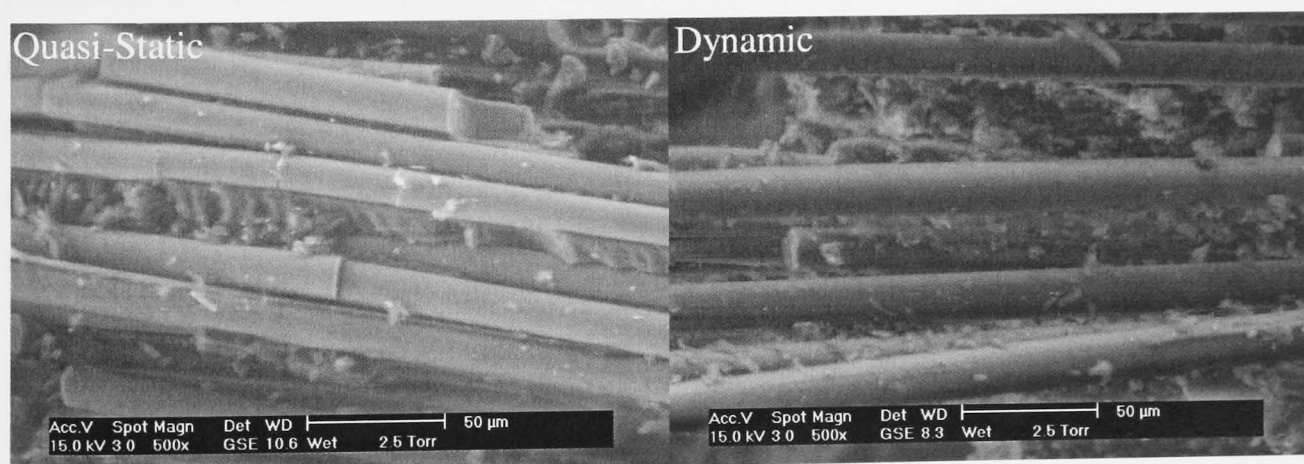


Figure 66: ESEM Images of Fibres in the Fronds (Quasi-Static and Dynamic)

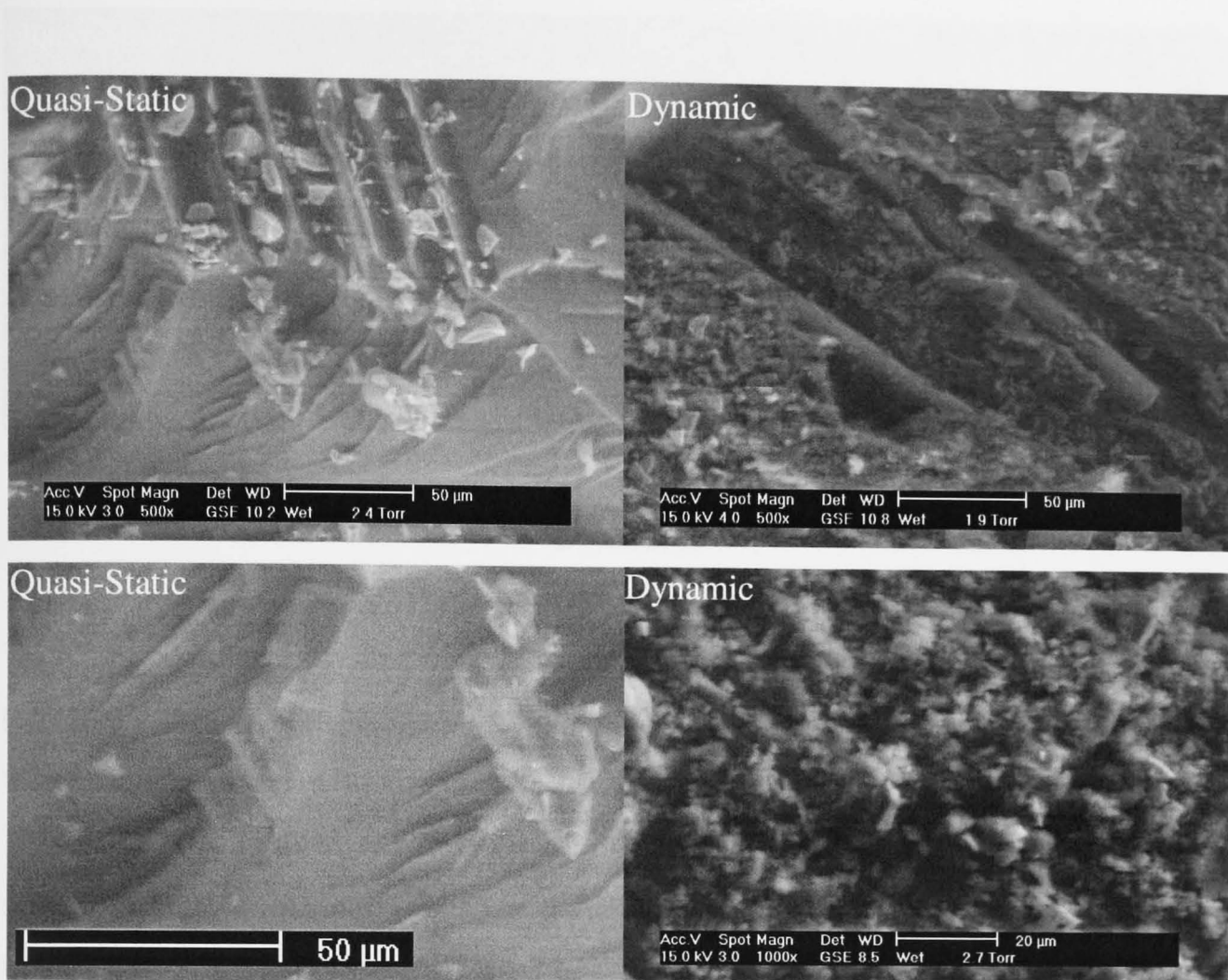


Figure 67: ESEM Images of Resin in the Fronds (Quasi-Static and Dynamic)

From the ESEM images it can be seen that the dynamically tested samples show a greater degree of matrix fragmentation than the quasi-statically tested samples (see Figure 67). The fronds of the quasi-static samples exhibit areas where the resin has remained intact, and it can be seen where fibres have pulled out of the matrix. As the matrix breaks up at higher testing rates the support for the fibres is reduced causing them to buckle, which absorbs less energy than when the fibres are constrained. The resin absorbs more energy dynamically than statically. However, this is at the expense of the fibres, which are capable of absorbing a greater amount of energy.

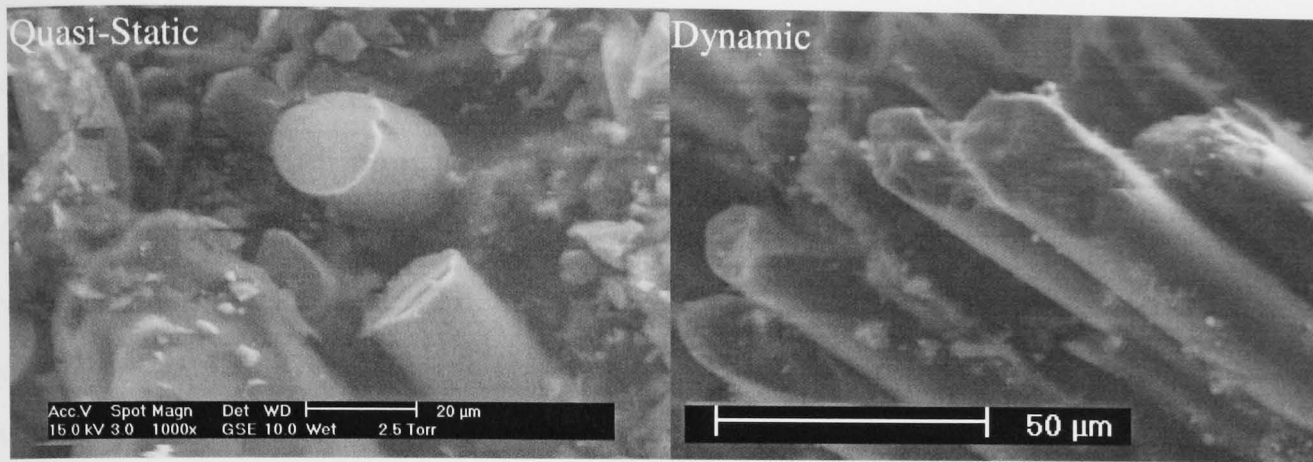


Figure 68: ESEM Images of Glass Fracture Surfaces (Quasi-Static and Dynamic)

The glass strands also show a different fracture surface between the different rates (see Figure 68). Quasi-statically tested samples exhibit tensile fracture of the surface, while the dynamically tested samples are seen to have sheared at the fracture surface. This could be due to higher fracture toughness at higher test rates leading to a shorter centre wall crack, which would force the fronds through a tighter angle and lead to more transverse shear failure of the fronds rather than interlaminar shearing. This is in line with the failure modes in section 2.2.1, with more fragmentation being observed, and therefore less energy absorbed.

4.6 Fibre Volume Fraction

Fibre volume fraction tests were conducted as described in section 3.5.5. The results from the burn off tests are shown in Table 43 below. The results give an average fibre volume fraction of 24.9% with a percentage standard deviation of 4.7%. These results confirm that the fibre volume fraction was indeed kept constant for all geometries tested enabling more reliable comparison of data.

	Circular (t=2mm)	Circular (t=4mm)	Square (t=2mm)	Square (t=4mm)
Without Interleaf	26.1 (4.6)	23.3 (7.1)	26.3 (4.9)	26.0 (5.1)
With Interleaf	24.3 (3.3)	23.5 (2.2)	24.8 (.09)	24.7 (1.9)

Table 43: Fibre Volume Fraction Results (%) from Resin Burn Off Tests (values in brackets are % standard deviation)

5 Discussion

The SEA value recorded for this the CoFRM E-glass/polyester tubes tested of 74.6 – 87.0kJ/kg for the circular geometries tested quasi-statically is significantly higher than the value of 25 – 50kJ/kg typically seen for steel and aluminium tubes. It is also at the top end of the range for glass/polyester (39kJ [57] to 80kJ [60]) as described in section 2.2.2.

Undamaged samples and samples with damage levels below a threshold level crushed progressively (failure mode A). This progressive crush was in the form of splaying, with a greater degree of fragmentation observed in samples crushed at a higher test speed. When the level of pre-existing damage exceeded the threshold level, unstable failure occurred in the form of a crack initiating at the damage zone (failure modes B and C). The crack would propagate either around the tube, bisecting it (failure mode B), to the crush zone or to the corners of the square tubes and then down to the crush zone (failure mode C). This would lead to a reduction in the load taken by the specimen and a section of the tube being removed uncrushed. The extent of the drop in load is determined by the size of the removed section. The effect is greatest when the crack bisects the tube (failure mode B) and least when the crack propagates to the crush zone and is engulfed enabling the crush load to return to undamaged levels (failure mode C). At the threshold damage level there is generally a mix in failure modes between stable and unstable. In some cases the progression of the crush front and central wall crack have to interact with the damage zone to cause further weakening before crack growth is initiated. In these cases the crack generally propagates to the damage zone and is engulfed with only a small localised drop in load being observed. The change in failure mode from stable to unstable indicates the threshold damage level.

5.1 Rate Effects

The crush zone morphology of a CoFRM E-glass /polyester tube tested at dynamic rate is significantly different to that seen under quasi-static loading. More fibre damage is seen under quasi-static conditions, and more matrix damage is seen under impact. The effect is attributed to the viscoelastic nature of the matrix material.

Work by Fernie [116, 127] and Geary [117] found that as the test speed increases the ultimate tensile and compressive strengths, elastic moduli and fracture toughness all increased. At the higher rate the resin is more brittle and fractures earlier, leaving the fibres unsupported, more compliant, and less likely to fail by shearing. This leads to the dynamic SEA being lower than the quasi-static SEA. Early work in the literature suggested that increasing the rate of the tests could cause the SEA to increase [120, 121], decrease [87, 92, 115] or stay the same [57, 107], although more recent research suggests similar results to those outlined in this work where SEA is seen to decrease as test speed increases (e.g. Browne *et al.* [102]). The increases in SEA were generally due to changes in failure mode from buckling or fragmentation to splaying, which would account for the increase in SEA.

Dynamically all samples displayed greater damage tolerance than quasi-statically tested samples. Local fracture at the simulated damage site is driven by local maximum stress. Fernie [116] showed with coupon tests for this material that the ultimate tensile and compressive stresses (UTS and UCS) increased by 115% and 26% at the rate of 5m/s, but also found that at higher speeds (up to 7m/s) a reduction was then seen. Test results in this work for tubular samples without a chamfer as a crush initiator found that the UCS increased by between 25% and 50% at 5m/s. This increase in failure stress therefore increases the load required for onset of failure by fracture at the damage zone at impact rates. Also, at impact rates, samples crush at a lower load. These lower crushing stresses require a greater damage level (or stress concentration) to trigger the tube to fail in the same unstable manner. Unstable failure can also occur when the effects of the local damage and the crush zone morphology interact, when the central wall crack associated with the crush zone is close enough to the damage to cause further weakening, leading to a localised reduction in load. Secondary effects, such as inertia and material damping would also tend to localise the material failure at the crush zone away from the damage under dynamic conditions.

For all geometries tested it was shown that quasi-statically tested samples absorbed more energy than dynamically tested samples. However, dynamically tested samples were shown to be able to absorb greater amounts of impact damage before failing in an unstable manner. This could be explained by the crush load being a lower

percentage of the ultimate crush load and therefore a greater stress concentration is required to cause unstable failure.

5.2 Geometric Effects

A square tube was seen to absorb less energy than a circular tube of similar cross sectional area and wall thickness as was observed in section 2.2.3. Circular tubes were seen to absorb 74.5kJ/kg and 87.0kJ/kg quasi-statically for samples with 2mm and 4mm wall thicknesses respectively. For equivalent square section samples the SEA values are 58.8kJ/kg and 69.2kJ/kg. The SEA value was reduced by approximately 21% for both wall thicknesses tested. This is attributed to the geometric stress raisers of the corners and the reduction in composite material properties, which are generally seen at discontinuities.

With an interleaf the reduction in SEA with a shift from circular to square section is 35% for thin walled samples and 8.5% for thick walled samples. The SEA reduction due to the inclusion of an interleaf for the square tubes is around 40% for samples of both wall thicknesses. The thinner circular tubes show a far lower reduction in SEA than the thick tubes. Possible reasons for this are that the square tubes tear at corners so the reduced friction has less effect because of the failure mode, or that the thicker tubes have 6 layers so the debris wedge slides between plies rather than through a ply. However, more geometries would need to be tested to support these assertions.

Although the square tubes were seen to absorb less energy than circular tubes, they displayed a similar threshold hole size, regardless of the peripheral position of the hole. The threshold hole size was seen to be dependant on loading rate. Larger stress concentrations were tolerated at the higher rate. The square tubes are generally more tolerant to impact damage than circular tubes, especially when impacted at the corners. The corners were also seen to arrest the progression of cracks that formed, which often lead to smaller reductions in load than circular tubes where the crack would progress until it had bisected the tube.

It has been shown in section 2.1 that the load required to initiate delamination is proportional to the thickness of the sample to the power 1.5. Increasing the wall

thickness of the tubes improved the damage tolerance of the samples tested. The increases were not as marked as might be expected from work by Caprino *et al.* [16], Tan and Sun [17], and Schoeppner and Abrate [19] showing a power law, except in the samples with an interleaf.

5.3 Damage

5.3.1 Holes

The presence of a hole in a tube can have a significant effect on the mode of failure, at its worst case triggering a global collapse and reducing the energy absorption properties. A threshold hole size exists, below which progressive crush is seen, and above which global collapse occurs. For the materials and geometries tested in this study, under quasi-static loading the threshold hole size is 5mm, where a mixture of progressive crushing and unstable failure were observed. Under quasi-static loading, above the threshold size, the onset of failure is at the hole and is entirely load dependent (i.e. independent of axial position of the hole). Dynamically, the threshold size was increased to 10mm, and for all samples in this study the load drop was restricted to the vicinity of the hole, where the load returned to the pre-hole level by the end of the test (i.e. the load-displacement behaviour is strongly dependent on axial position of the hole). Multiple holes, where the holes are positioned with centres two diameters apart, are seen to interact under quasi-static loading - a global collapse is seen for all samples where two holes are spaced within two hole diameters. However, no interaction effects were seen under dynamic loading where only a small drop in load around the position of the hole was recorded. Generally, the effect of two 5mm diameter holes is not as marked as a single 10mm diameter hole. It may be necessary to test more hole sizes around the threshold level to confirm the exact threshold hole size.

The hole size required to trigger unstable crush under quasi-static loading (5mm) was seen to be the same for square tubes as in equivalent circular section tubes and was the same for corner holes as for holes on the face. In square tubes the corners act as a means of arresting propagating cracks and led to a less marked reduction in SEA than with circular tubes. The drop in load for tubes with corner holes was greater than that

seen for tubes with face holes as the crack would propagate to at least two faces before being arrested at the next corners, rather than just one face. At impact rates the damage tolerance was increased and the threshold hole size was seen to be above 10mm.

At the threshold hole size a crack did not form in every sample. The unstable failure often causes only a small drop in SEA with the crack being initiated due to the interaction between the crush zone and the stress concentration causing further weakening. The progression of the crack is usually only to the crush front. There is a slight drop caused when the crack forms at the position of the hole, and is not always obvious from SEA data (averaged over the full length of the crush). Above the threshold hole size the hole causes a crack to form in early stages of crush, usually when the load taken by the sample reaches close to the steady state load.

For this material tested, relatively small hole sizes can cause unstable failure to occur, although it has been shown that the damage tolerance of the material increases at higher test rates. This is due to the increased UCS and decreased crush load resulting in the crushing stress of the dynamically tested samples being far lower as a percentage of the ultimate compressive stress of the material.

5.3.2 Simulated Delaminations

In the circular tubes tested simulated delaminations of up to 1.5 times the tube diameter caused a local drop in steady-state crushing load, and no unstable failure modes were seen under quasi-static or dynamic load cases. For the data presented here with single ply delaminations, the energy absorption can be conservatively estimated from the reduction in inter-ply surface area. Stacked delaminations were seen to interact and cause a greater reduction in crush load. The results show that the crush mode is relatively insensitive to local delaminations, and that the SEA is less sensitive to delaminations under dynamic loading rates.

Delamination had a greater effect in square tubes than in circular tubes, causing unstable failure in quasi-statically tested samples with two stacked 32mm Melinex® inserts or a single 50.8mm insert. The delamination reduced the local wall thickness

of the tube. The single ply layer then buckled with a crack forming at the centre of the insert position. This crack then progressed around the circumference of the tube causing a large reduction in SEA. Quasi-statically tested specimens were more sensitive to delamination damage than the dynamically tested samples, which did not experience any crack formation.

It is possible that the localised reduction in load may be attributed to the simulated delamination reducing the friction in the crush zone in the vicinity of the insert, and the delamination separating the tube into thinner sections, which were more susceptible to buckling, which is known to be a less efficient mode of energy absorption as shown by Farley [51]. Square section samples are more likely to be vulnerable to this type of failure because of the combination of strong, rigid corners with weak planar sections. Thornton [71] found that below a certain thickness : section size ratio, Φ , the collapse tends to be unstable. The critical ratio, Φ , was found to be appreciably higher for square and rectangular graphite FRP sections ($\Phi \approx 0.075$) than circular sections ($\Phi \approx 0.025$). This could also be related to the second moment of area, where by calculating the buckling load P_b :

$$P_b = \frac{\pi^2 EI}{L^2} \quad (7)$$

for the circular and square sections tested, the load required to buckle the square tubes is 21% lower than the load required to buckle the circular samples. However, even using Equation 7 the buckling load is 454kN for square tubes and 572kN for cylindrical with 2mm wall thickness, which are over 20 times the crush loads of the samples. E for this material is 10GPa [113].

By examining local buckling of the composite the critical stress for a circular section is:

$$\sigma_{cr,l} = \frac{E}{\sqrt{3(1-\nu^2)}} \left(\frac{t}{R} \right) \quad (8)$$

ν for this material is approximately 0.3. Using Equation 8 gives a critical load of 144kN, which is still in excess of what is experienced by the composite. For a square section:

$$\sigma_{cr,l} = \frac{\pi^2 E}{3(1-\nu^2)} \left(\frac{t}{B} \right)^2 \quad (9)$$

Where B is the width of the plate between the clamped edge restraints (upper bound solution). This equates to a critical load of 42kN. By assuming the delamination divides the wall thickness by 2 the critical load would be 10.5kN, which is now below the actual crushing load of 19kN, and therefore buckling can occur. The delamination will divide the tube into sections of thinner wall thickness. It is therefore likely that local buckling rather than global buckling caused the unstable failure in the square samples with delaminations. It also explains why the cylindrical samples did not exhibit unstable failure and the square samples did.

5.3.3 Impact Damage

Generally as the level of impact energy increased the size of the damage zone increased. However, the main exception to this rule is when the tup penetrates or at least partially penetrates the sample, when the size of the damage zone may be smaller than a lesser impact that has caused a larger area of delamination. These observations are supported by Cantwell and Morton [6].

Impact damage was seen to have a significant effect. There is a far larger range of threshold impact levels associated with geometric and testing parameters than in samples with holes in. Above a threshold impact energy level, unstable failure modes, similar to those seen due to the inclusion of holes, were observed. The threshold damage level for circular tubes loaded quasi-statically was 1.5J of impact energy. For dynamic loading, an impact of 3J for the 2mm wall thickness samples and 9J for the 4mm wall thickness samples lead to unstable failure.

The impact damage threshold of 3J for square tubes tested quasi-statically is twice that seen in circular tubes. The dynamic threshold level of 9J for the 2mm wall

thickness samples is again greater than the equivalent circular tube. For the 4mm wall thickness samples the dynamic threshold appears to be at 6J, but the 9J samples all show greater damage tolerance than the 6J samples with only a slight drop in SEA compared to the undamaged samples. Further testing may be required to determine an absolute threshold level.

The size of damage zone due to an impact at the corner of a square tube is less than that for the same level of impact on the face of the tube. This is due to the geometric effects reducing the level of bending. Damage tolerance was greater at the corners of a square tube, but above the threshold level when the tube failed in an unstable manner, the drop in load was greater than in a face-damaged sample due to the crack growth to at least two of the faces removing them uncrushed. Threshold energy levels for impacts at the corner of the 2mm wall thickness square tubes were 6J quasi-statically and 9J dynamically. For the 4mm wall thickness samples the threshold levels were 24J quasi-statically and 30J dynamically and even at 30J the samples only saw a localised drop in load, not a large drop associated with unstable failure.

The results demonstrate that the axial loading behaviour is highly sensitive to the combination of in-plane damage and delaminations caused by relatively low energy out-of-plane impacts. This sensitivity to damage was reduced at dynamic loading rates and in square samples, especially when damaged at the corners. The axial position of the damage did not make any difference to the threshold energy levels observed.

5.4 Interleaves

Interleaves were seen to reduce the SEA levels by 28.6% to 48.0% quasi-statically and by 18.2% to 29.4% dynamically. Reductions in compressive strength with the inclusion of interleaves was observed by Sohn *et al.* [34]. It has been shown that the presence of the interleaf reduces the coefficient of friction between the sample and the ground steel crush platen from 0.36 to 0.22. This reduction of friction in the crush zone will result in a reduction in SEA. Interestingly, the SEA level no longer decreases with loading rate.

As the test speed was increased from quasi-static to dynamic the failure mode changed to include a greater degree of matrix fragmentation, which caused reductions in SEA of between 5.8% and 17.6% depending on the geometry. The reduction in SEA for quasi-statically tested samples due to the inclusion of an interleaf was between 28.6% and 48.0% due to a reduction in the coefficient of friction in the crush zone from 0.36 to 0.22. Fragmentation is affected less by frictional effects than splaying and this can account for the SEA increase with rate for samples with interleaf of between 4.6% and 18.4% rather than a decrease. The reduction in SEA for splaying samples due to lower frictional effects seems to outweigh the reduction in SEA associated with the change in failure mode to include more fragmentation. It is important to note that the dynamic failure mode is still splaying dominated. However, the increased level of matrix fragmentation seen in dynamically tested samples may contribute towards this reversal of trends seen with the inclusion of interleaf.

Work by Kim [35] and Masters [36] suggested that the area of damage is less on specimens with interleaves, but this was not always found to be the case. The inclusion of the interleaf did however increase the damage threshold of all samples tested, as it improved the CAI [34-36]. This meant that energy levels of above 9J were required to cause unstable failure. At these higher energy levels massive areas of damage were seen. In some cases the area of damage almost enveloped a whole side of a square sample. In others penetration was seen. Images of these damage zones are shown in the section 4.1.4.

The interleaf increases the damage threshold from 1.5J to 3J under quasi-static conditions and from 3J to 6J for the dynamic rate for the 2mm wall thickness circular samples. With the thicker walled samples there was a similar increase from 1.5J to 12J quasi-statically and from 9J to 15J dynamically. The energy level threshold, increases from 3J to 9J quasi-statically with the inclusion of an interleaf, and from 9J to over 15J at impact rates for square samples with 2mm wall thickness. For the 4mm samples the threshold levels increased from 3J to around 27J quasi-statically and from 6J to above 27J dynamically. By increasing the wall thickness and adding an interleaf it was possible to increase the damage tolerance of this composite energy absorber by a factor of 9.

Again a smaller damage zone is produced for a given impact at the corners when compared to an impact on the face of the square tubes. Threshold energy levels for impacts at the corner of the 2mm wall thickness square tubes increased from 6J to 12J quasi-statically and from 9J to between 9 and 15J dynamically (between 9J and 15J all sets of tests exhibited a mixture of stable and unstable failure modes). With a 4mm wall thickness the quasi-statically tested samples exhibit a reduction in load, but no unstable failure for samples tested with an 18J and a 24J impact. Dynamically, the samples without interleaf start to exhibit a slight drop in load at about 24J, which is not observed in interleaved samples.

For samples without interleaf increasing the test speed from quasi-static (5mm/min) to dynamic (5m/s) caused a reduction in SEA regardless of specimen geometry. However, the dynamically tested samples showed improved damage tolerance, requiring larger energy impacts before failing in an unstable manner when crushed. Samples tested dynamically and samples with interleaf crush at a load which is a lower percentage of the ultimate compressive load of the material than quasi-statically tested samples and samples without interleaf. This means that a greater stress concentration in the form of a larger impact is required to cause unstable failure giving rise to greater damage tolerance.

By including the interleaf it is possible to increase the damage tolerance of the tubes, but it is at the expense of a drop in energy absorption. This is due to the reduced coefficient of friction in the crush zone. The reduced coefficient of friction also causes a smoother load vs displacement trace due to less stick-slip effect in the crush zone.

6 Conclusions

The aim of this project was to consider the effect of damage on the energy absorption potential of continuous filament random mat (CoFRM) E-glass / polyester composite tubes under axial loading. Damage was induced in three ways: drilled holes, Melinex® inserts moulded into the samples to provide a zone of delamination, and impact damage of various energy levels imparted using a hemispherical tup on an instrumented falling weight machine. Circular and square section samples were tested to see whether part geometry affected the energy absorption and damage tolerance of the composite tubes. The wall thickness of the tubes was varied from 2mm to 4mm for both test geometries. Samples were tested both quasi-statically and dynamically. The dynamic tests provide a more realistic loading condition, better simulating the conditions the parts will see in operation. Having observed the failure modes and damage tolerance of the tubes under various testing parameters it was important to look at ways of improving the damage tolerance of the samples. One method investigated was to include an interleaf at the preforming stage.

The 2mm wall thickness circular tubes tested quasi-statically absorbed 74.5kJ/kg. Square samples absorbed on average 21% less energy than the circular samples quasi-statically. Dynamically the decrease in SEA is 31% for the 2mm wall thickness samples and 16% for samples with a 4mm wall thickness. The reduction in SEA seen by the square samples was due to geometric stress raisers at the corners leading to through thickness failure, which left the fronds less constrained allowing them to splay at a lower load.

Increasing the wall thickness (and hence t/D ratio) increased the SEA of the tubes. This could be attributed to a stabilising effect in the crush zone with a better defined debris wedge at the centre of the 6-ply composite, compared to the 3-ply thinner samples.

Quasi-statically tested samples absorb more energy than dynamically tested samples. Decreases were in the order of 6 - 18%. This is attributed to the viscoelastic nature of the matrix. The mode of failure is unchanged in dynamically tested samples, but a

greater degree of matrix fragmentation at the higher test speed will leave the load bearing fibres less well constrained and able to bend further before fracturing. This means that there is less fibre fracture and therefore the samples are unable to absorb the levels of energy seen under quasi-static loading. Tests were only carried out at one quasi-static and one dynamic test rate and it would be necessary to conduct further tests to establish how the SEA was affected at higher test speeds.

Damage, in the form of a hole, a delamination, or an impact will, below a certain damage level have no effect on the progressive crush mode and SEA of a sample. Above the threshold level the damage zone provides a high enough stress concentration to cause a compressive failure to be seen. In the samples with delaminations this was seen to be in the form of local buckling. The failure is initiated at the damage zone, with a crack forming and then propagating around the tube. This leads to a reduction in the SEA of the sample.

There are typically two levels of reduction in SEA. The first type of failure is generally seen above the threshold level where the crack is initiated at the damage zone away from the crush front. The crack then propagates around the tube bisecting it causing a large drop in load. The load taken only recovers to the mean crush load once at least one of the bisected halves has two surfaces of the sample are in contact with the top and bottom crush platens. This caused the greatest reduction in SEA. The second type of failure is seen at the threshold damage level. The crack is initiated by the interaction between the crush zone and the damage zone causing further weakening and leads to a localised reduction in load as the crack gets engulfed before bisecting the tube. The direction of the crack growth associated with this type of failure is typically down to the crush zone rather than circumferentially.

For the material tested, relatively small hole sizes (5mm) can cause unstable failure to occur, although it has been shown that the damage tolerance of the material increases (to 10mm) at higher test rates (5m/s). At the threshold hole size the dynamically tested samples saw only a localised drop in load in the vicinity of the hole. A hole away from the crush front would have no effect on the SEA.

Large delaminations, in the form of Melinex® inserts up to 1.5 times the diameter of the tube, can be tolerated by circular samples with only a slight drop in load at the position of the insert. The inserts only caused unstable failure in square samples with a 2mm wall thickness tested quasi-statically. This occurred due to localised buckling in the region of the insert. It has been shown that square samples are more susceptible to buckling than circular samples.

It has been shown that low levels of impact energy (1.5J – 3J) can cause unstable failure in these composite samples when tested quasi-statically leaving them unable to absorb the energy levels to their potential. Dynamically, the energy levels required to cause unstable failure are still low (3J – 9J), but it is significant that there is improved damage tolerance for this composite at a higher test speed.

Thicker samples are more damage tolerant. They will exhibit a smaller area of damage caused by a given out of plane impact, and will require a higher energy level impact before an unstable failure of the structure occurs under compressive loading.

The square samples, which may be easier to incorporate into vehicle design, were seen to require twice the energy level of a circular tube, from an out of plane impact, to reach the threshold damage level. This doubling rule of impact energy required to cause unstable failure may only be applicable because the levels involved are low. When the threshold level for square tubes was reached, the drop in load experienced due to unstable failure is less than that observed in circular tubes. The cracks that are initiated at the damage zone in square samples are often arrested at the adjacent corners of the tube. This results in a smaller section of the sample being removed uncrushed than if the crack had propagated around the whole perimeter of the tube, as was seen in the cylindrical samples. Therefore a smaller reduction in SEA is experienced than for cylindrical tubes. The corners of square samples are able to absorb higher levels of out-of-plane impact than faces before unstable failure occurs during compressive testing. With the 4mm wall thickness parts an impact energy level of 24 – 30J on the corner of the tube is required to cause unstable failure, whereas 3 – 12J is required on the face of the tube. It would be important to test the damage tolerance of full scale vehicle parts, but this work suggests that the laboratory

scale tests are likely to show a worst case scenario with the thicker specimens being more damage tolerant.

The introduction of an interleaf in the samples caused the SEA to decrease by between 28.6% and 48.0% quasi-statically and between 18.2% and 29.4% dynamically. This is attributable to a reduction in the coefficient of friction in the crush zone. The coefficient of friction between the ground steel crush platen and the sample reduced from 0.36 to 0.22 with the inclusion of an interleaf. This reduced the stick-slip in the crush zone and brought about a smoother load response.

Interleaved samples absorb more energy dynamically than quasi-statically, which is the opposite trend to samples without interleaf. This could be attributed to the mode of failure seen by the samples tested at different rates, with fragmentation being less affected by the reduction in friction in the crush zone than splaying. This is unlikely to be the only factor affecting the energy absorption of the samples with interleaf tested at the different rates.

The circular tubes with interleaf did not exhibit an increase in SEA with wall thickness, but a slight decrease. A possible explanation for this is that the thicker circular samples absorbed the highest energy levels of all geometries tested. The failure mode that absorbs the most energy is splaying. This failure mode is the most affected by the reduced coefficient of friction, so samples with the highest SEA values will be affected the most by the reduced friction in the crush zone.

Samples with interleaf were more damage tolerant than samples without interleaf, by up to 9 times. This improved damage tolerance comes at the price of SEA, which was seen to decrease by between 18% and 48%.

The ultimate compressive stress (UCS) of the samples increases by between 25 - 57% with increased test speed. The mean crush load of the samples is seen to decrease with test speed by between 6 and 18%. The mean crush load of some samples is therefore a lower percentage of the ultimate crush load than others. By looking at how this relates to the damage tolerance of all the samples tested it is clear that the more damage tolerant samples crush at a lower proportion of the ultimate crush load

of the material and therefore require a greater stress concentration to cause ultimate compressive failure, and are therefore more damage tolerant. This hypothesis fits for all the trends shown with increased damage tolerance observed as test speed increased, wall thickness increased, sample geometry was changed from circular to square and interleaves were included in the samples. Other factors, such as inertia and material damping may also influence the damage tolerance due to rate effects.

By incorporating the work from this thesis into the design of a crash structure it will be possible to manufacture a part that is tolerant to the levels of accidental impact damage seen in operation. Then, in the event of a crash situation, there is no doubt that the part will absorb the energy levels it was designed to. If a crash structure were designed using all the means of improving damage tolerance observed in this thesis a concept part would be square, $t/W \geq 0.13$, and with interleaves between the plies. Ideally it would be orientated so that all four sides of the part were at 45° to the road surface. This would mean that any stone coming up off the road, or any object being dropped on the structure would be more likely to hit a corner. By knowing the damage tolerance of a part there is less of a requirement to over design a structure and can therefore lead to a weight reduction of the vehicle.

This work was conducted on laboratory scale tubular samples. It is therefore important to do further testing on automotive scale crash structures. The structures tested exhibited lower SEA capability and greater damage tolerance at dynamic test rates. However, further testing at higher test speeds are required to see whether these trends continue. By using interleaves between plies it was possible to improve the damage tolerance of the structures but this was at the expense of SEA performance. It is therefore important to investigate other means of improving damage tolerance that do not reduce SEA to the same extent.

7 Publications

1. RIBEAUX, M. and N.A. Warrior. *Effect of Impact Damage on the Specific Energy Absorption of Glass/Polyester Composites*. in *Proceedings of the American Society for Composites 17th Technical Conference*. 2002. Purdue University, West Lafayette, Indiana.
2. Warrior, N. A. and M. RIBEAUX, *Effect of Damage on the Energy Absorption of Prismatic Thin-Walled Polymer Composite Structures*. *Key Engineering Materials*, 2003. **245-246**: p. 491-501.
3. Nicholas A. Warrior; Kristofer Bottome and MICHAEL RIBEAUX. *Effects of Fiber Architecture on the Energy Absorption of Damaged Thin-Walled Composite Tube*. in *Proceedings of the American Society for Composites 18th Technical Conference*. 2003. University of Florida, Gainesville, Florida.
4. M. RIBEAUX, N. A. Warrior and D. A. Bailey, *Effect of Stress Concentrations on the Energy Absorption of Thin-Walled CoFRM Composite Tubes*. Accepted for *Fourth International Conference on Thin-Walled Structures*, 22 - 24 June 2004. Loughborough University, Loughborough, England.
5. M. RIBEAUX, N. A. Warrior and D. A. Bailey, *Effect of Impact Damage on the Energy Absorption of Thin-Walled CoFRM Composite Tubes*. In Preparation.
6. M. RIBEAUX and N. A. Warrior, *Effect of Thermoplastic Interleaf on the Damage Tolerance and Energy Absorption Potential of Thin-Walled Composite Tubes*. In Preparation.

8 References

1. *Frontal impact test based on that developed by European Enhanced Vehicle Safety Committee as basis for legislation*, <http://www.euroncap.com/>.
2. Lee, S.M. and P. Zahuta, *Instrumented Impact and Static Indentation of Composites*. Journal of Composite Materials, 1991. **25**: p. 204-222.
3. Choi, H.Y., R.J. Downs, and F.-K. Chang, *A New Approach toward Understanding Damage Mechanisms and Mechanics of Laminated Composites Due to Low-Velocity Impact: Part I - Experiments*. Journal of Composite Materials, 1991. **25**: p. 992-1011.
4. Richardson, M.O.W. and M.J. Wisheart, *Review of low-velocity impact properties of composite materials*. Composites Part A, 1996. **27A**: p. 1123-1131.
5. Liu, D., B.B. Raju, and X. Dang, *Size Effects on Impact Response of Composite Laminates*. International Journal of Impact Engineering, 1998. **21**(10): p. 837-854.
6. Cantwell, W.J. and J. Morton, *The Impact Response of Composite Materials - a Review*. Composites, 1991. **22**(5): p. 347-362.
7. Dear, J.P. and S.A. Brown, *Impact damage processes in reinforced polymeric materials*. Composites Part A, 2003. **34**: p. 411-420.
8. Larsson, F., *Damage tolerance of a stitched carbon/epoxy laminate*. Composites Part A, 1997. **28A**: p. 923-934.
9. Found, M.S., G.J. Holden, and R.N. Swamy, *Static Indentation and Impact Behaviour of GRP Pultruded Sections*. Composite Structures, 1997. **39**(3-4): p. 223-228.
10. Rigas, E.J. and S. Petrie. *Effects of Thickness and Temperature on the Residual Compressive Strength of Polyester S2 Glass Laminates Subjected to Low Energy Impact*. in *Proceedings of the American Society for Composites 17th Technical Conference*. 2002. Purdue University, West Lafayette, Indiana.
11. Corum, J.M., R.L. Battiste, and M.B. Ruggles-Wren, *Low-energy impact effects on candidate automotive structural composites*. Composites Science and Technology, 2003. **63**: p. 755-769.
12. Peijs, *Hybrid composites based on polyethylene and carbon fibres Part 3: Impact resistant structural composites through damage management*. Composites, 1990(24): p. 522-530.
13. Mahfuz, H., M. Saha, R. Biggs, and S. Jeelani, *Damage Tolerance of Resin Infiltrated Composites Under Low Velocity Impact - Experimental and Numerical Studies*. Key Engineering Materials, 1998. **141-143**: p. 209-234.
14. Bibo, G.A. and P.J. Hogg, *Damage Tolerance of Continuous Fibre Composites: Material and Environmental Effects*. Key Engineering Materials, 1998. **141-143**: p. 93-126.
15. Papanicolaou, G.C., A.M. Blanas, A.V. Pournaras, and C.D. Stavropoulos, *Impact Damage and Residual Strength of FRP Composites*. Key Engineering Materials, 1998. **141-143**: p. 127-148.
16. Caprino, G., V. Lopresto, C. Scarponi, and B. Briotti, *Influence of material thickness on the response of carbon-fabric/epoxy panels to low velocity impact*. Composites Science and Technology, 1999. **59**: p. 2279-2286.

17. Tan, T.M. and C.T. Sun, *Use of Statical Indentation Laws in the Impact Analysis of Laminated Composite Plates*. Journal of Applied Mechanics, 1985. **52**: p. 6-12.
18. de Freitas, M. and L. Reis, *Failure mechanisms on composite specimens subjected to compression after impact*. Composite Structures, 1998. **42**: p. 365-373.
19. Schoeppner, G.A. and S. Abrate, *Delamination threshold loads for low velocity impact on composite laminates*. Composites Part A, 2000. **31**: p. 903-915.
20. Swanson, S.R., *Scaling of impact damage in fiber composites from laboratory specimens to structures*. Composite Structures, 1993. **25**: p. 249-255.
21. Sjogren, B.A. and L.A. Berglund, *The effects of matrix and interface on damage in GRP cross-ply laminates*. Composites Science and Technology, 2000. **60**: p. 9-21.
22. Sjogren, A., A. Krasnikovs, and J. Varna, *Experimental determination of elastic properties of impact damage in carbon fibre/epoxy laminates*. Composites Part A, 2001. **32**: p. 1237-1242.
23. Short, G.J., F.J. Guild, and M.J. Pavier, *Post-impact compressive strength of curved GFRP laminates*. Composites Part A, 2002. **33**: p. 1487-1495.
24. Karbhari, V.M., J.E. Haller, P.K. Falzon, and I. Herszberg, *Post-impact crush of hybrid braided composite tubes*. International Journal of Impact Engineering, 1999. **22**: p. 419-433.
25. Rahman, M.T. and G.M. Newaz. *Effect of Impact Damage on Energy Absorption in Cylindrical PMC Tubes*. in *Proceedings of the American Society for Composites 15th Technical Conference*. 2000. College Station, TX.
26. Doyum, A.B. and B. Altay, *Low-velocity impact damage in glass fibre/epoxy cylindrical tubes*. Materials & Design, 1997. **18**(3): p. 131-135.
27. Persson, E., I. Eriksson, and L. Zackrisson, *Effect of hole machining defects on strength and fatigue life of composite laminates*. Composites Part A, 1997. **28A**: p. 141-151.
28. Cowley, K.D. and P.W.R. Beaumont, *Damage Accumulation at Notches and the Fracture Stress of Carbon-Fibre/Polymer Composites: Combined Effects of Stress and Temperature*. Composites Science and Technology, 1997. **57**: p. 1211-1219.
29. Caprino, G., *Residual Strength Prediction of Impacted CFRP Laminates*. Journal of Composite Materials, 1984. **18**: p. 508-518.
30. Falzon, P.J. and I. Herszberg. *Prediction of the Compression-After-Impact Strength of 2-D Braided Composites*. in *ICCM-11*. 1997. Gold Coast, Australia.
31. Clarke, M.P. and M.J. Pavier, *Artificial damage techniques for low velocity impact in carbon fibre composites*. Composite Structures, 1993. **25**: p. 113-120.
32. Hamada, H., K. Sugimoto, H. Saito, and R. Inai. *Design of Integrated FRP Energy Absorber with Bolted Joint*. in *Proceedings of the American Society for Composites 17th Technical Conference*. 2002. Purdue University, West Lafayette, Indiana.
33. Zhong, W. and B.Z. Jang, *Material Design Approach for Improving Impact Resistance of Composites*. Key Engineering Materials, 1998. **141-143**: p. 169-186.

34. Sohn, M.S., X.Z. Hu, J.K. Kim, and L. Walker, *Impact damage characterisation of carbon fibre/epoxy composites with multi-layer reinforcement*. Composites Part B, 2000. **31**: p. 681-691.
35. Kim, J.-K., *Methods for Improving Impact Damage Resistance of CFRPs*. Key Engineering Materials, 1998. **141-143**: p. 149-168.
36. Masters, J., *Improved Damage and Delamination Resistance through Interleafing*. Key Engineering Materials, 1989. **37**: p. 317-348.
37. Matsuda, S., M. Hojo, S. Ochiai, A. Murakami, H. Akimoto, and M. Ando, *Effect of ionomer thickness on mode I interlaminar fracture toughness for ionomer toughened GFRP*. Composites Part A, 1999. **30**: p. 1311-1319.
38. Duarte, A., I. Herszberg, and R. Paton, *Impact Resistance and tolerance of interleaved tape laminates*. Composite Structures, 1999. **47**: p. 753-758.
39. Walker, L., M.S. Sohn, and X.Z. Hu, *Improving impact resistance of carbon-fibre composites through interlaminar reinforcement*. Composites Part A, 2002. **33**: p. 893-902.
40. Kim, J.-K., D.B. Mackay, and Y.-W. Mai, *Drop-weight impact damage tolerance of CFRP with rubber-modified epoxy matrix*. Composites, 1993. **24(6)**: p. 485-496.
41. Bibo, G.A. and P.J. Hogg, *Carbon-Fibre Non-Crimp Fabric Laminates for Cost-Effective Damage-Tolerant Structures*. Composites Science and Technology, 1998. **58**: p. 129-143.
42. Suh, S.S., N. Han, J.-M. Yang, and H.T. Hahn. *The Effect of Stitching on Damage Tolerance of Stiffened Composite Panel*. in *Proceedings of the American Society for Composites 17th Technical Conference*. 2002. Purdue University, West Lafayette, Indiana.
43. Hosur, M.V., M.R. Karim, and S. Jeelani, *Experimental investigations on the response of stitched/unstitched woven S2-glass/SC15 epoxy composites under single and repeated low velocity impact loading*. Composite Structures, 2003. **61**: p. 89-102.
44. Cantwell, W.J., P.T. Curtis, and J. Morton, *An Assessment of the Impact performance of CFRP Reinforced with High-strain Carbon Fibres*. Composites Science and Technology, 1986. **25**: p. 133-148.
45. Hirai, Y., H. Hamada, and J.-K. Kim, *Impact response of woven glass-fabric composites-I. Effect of fibre surface treatment*. Composites Science and Technology, 1998. **58**: p. 91-104.
46. Hirai, Y., H. Hamada, and J.-K. Kim, *Impact response of woven glass-fabric composites-II. Effect of temperature*. Composites Science and Technology, 1998. **58**: p. 119-128.
47. Kessler, M.R. and S.R. White, *Self-activated healing of delamination damage in woven composites*. Composites Part A, 2001. **32**: p. 683-699.
48. Fernie, R., *Loading Rate Effects on the Energy Absorption of Lightweight Tubular Crash Structures*. 2002, Thesis: University of Nottingham.
49. Ramakrishna, S., *Microstructural design of composite materials for crashworthy structural applications*. Materials & Design, 1997. **18(3)**: p. 167-173.
50. Ramakrishna, S. and H. Hamada, *Energy Absorption Characteristics of Crash Worthy Structural Composite Components*. Key Engineering Materials, 1998. **141-143**: p. 585-622.
51. Farley, G.L., *Prediction of the Energy-Absorption Capability of Composite Tubes*. Composite Materials, 1992. **26(3)**: p. 388-404.

52. Thornton, P.H., *Energy Absorption in Composite Structures*. Composite Materials, 1979. **13**: p. 247-262.
53. Farley, G. and R. Jones, *Crushing Characteristics of Continuous Fibre-Reinforced Composite Tubes*. Journal of Composite Materials, 1992. **26**(1): p. 37-50.
54. Abramowicz, W., *The Effective Crushing Distance in Axially Compressed Thin-Walled Metal Columns*. International Journal of Impact Engineering, 1983. **1**(3): p. 309-317.
55. Jones, N., *Structural Impact*. 1989: Cambridge University Press.
56. Thornton, P.H. and C.L. Magee, *The Interplay of Geometric and Materials Variables in Energy Absorption*. Journal of Engineering Materials and Technology, 1977. **99**(2): p. 114-120.
57. Snowdon, P. and D. Hull, *Energy Absorption of SMC Under Crash Conditions*. International Conference - Fibre Reinforced Composites '84, 1984. **5**: p. 1-10.
58. Ramakrishna, S., H. Hamada, Z. Maekawa, and H. Sato, *Energy Absorption Behaviour of Carbon-Fiber-Reinforced Thermoplastic Composite Tubes*. Thermoplastic Composite Materials, 1995. **8**: p. 323-344.
59. Fairfull, A.H. and D. Hull, *Energy Absorption of Polymer Matrix Composite Structures : Frictional Effects*. Symposium on Structural Failure, 1988: p. 255-279, Chapter 8.
60. Hull, D., *A Unified Approach to Progressive Crushing of Fibre-Reinforced Composite Tubes*. Composites Science and Technology, 1991. **44**: p. 376-421.
61. Fairfull, A.H., *Scaling Effects in the Energy Absorption of Axially Crushed Composite Tubes*. 1986, University of Liverpool: Liverpool.
62. Berry, J.P., *Energy Absorption and Failure Mechanisms of Axially Crushed GRP Tubes*. 1984, University of Liverpool: Liverpool.
63. Keal, R., *Post Failure Energy Absorbing Mechanisms of Filament Wound Composite Tubes*. 1983, University of Liverpool: Liverpool.
64. Farley, G.L., *Analogy for the Effect of Material and Geometrical Variables on Energy-Absorption Capability of Composite Tubes*. Journal of Composite Materials, 1992. **26**(1): p. 78-89.
65. Farley, G.L. *Energy absorption in composite materials for crashworthy structures*. in *International Conference of Composite Materials VI*. 1987.
66. Farley, G., *Crushing Response of Energy Absorbing Composite Structure*. Engineering Mechanics, 1992: p. 876-879.
67. Satoh, H., H. Hirakawa, Z. Maekawa, H. Hamada, M. Nakamura, and D. Hull, *Comparison of Energy Absorption Among Carbon/Thermoplastic Tubes*. Proceedings of the 1993 38th International SAMPE Symposium and Exhibition, 1993. **38**(1): p. 952-966.
68. Warrior, N.A., T.A. Turner, F. Robitaille, and C.D. Rudd, *Effect of resin properties and processing parameters on crash energy absorbing composites made by RTM*. Composites Part A, 2003. **34**: p. 543-550.
69. Hamada, H., J. Coppola, D. Hull, Z. Maekawa, and H. Sato, *Comparison of Energy Absorption of Carbon / Epoxy and Carbon / PEEK Composite Tubes*. Composites, 1992. **23**(4): p. 245-252.
70. Curtis, C.D., *Energy Absorption and Crush Behaviour of Composite Tubes*. 2000, Thesis: University of Nottingham.
71. Thornton, P.H. and P.J. Edwards, *Energy Absorption in Composite Tubes*. Journal of Composite Materials, 1982. **16**: p. 521-545.

72. Schmueser, D.W. and L.E. Wickliffe, *Impact Energy Absorption of Continuous Fibre Composite Tubes*. Journal of Engineering Materials and Technology, 1987. **109**: p. 72-77.
73. Farley, G., *Effect of Specimen Geometry on the Energy Absorption Capability of Composite Materials*. Journal of Composite Materials, 1986. **20**: p. 390-400.
74. Farley, G.L., *Effect of Fiber and Matrix Maximum Strain on the Energy Absorption of Composite Materials*. Journal of Composite Materials, 1986. **20**: p. 322-334.
75. Hull, D., *Axial Crushing of Fibre Reinforced Composite Tubes*. Structural Crashworthiness. Lectures Presented at the First International Symposium on Structural Crashworthiness, 1983: p. 118-135.
76. Karbhari, V., P. Falzon, and I. Herzberg, *Energy Absorption Characteristics of Hybrid Braided Composite Tubes*. Journal of Composite Materials, 1997. **31**(12): p. 1164-1186.
77. Karbhari, V., P. Falzon, and I. Herzberg, *Effect of Braid Architecture on Progressive Crush of Composite Tubes*. 41st International SAMPE Symposium, 1996: p. 1409-1416.
78. Karbhari, V. and A. LoCurcio, *Progressive Crush Response of Hybrid Felt/Fabric Composite Structures*. Journal of Reinforced Plastics and Composites, 1997. **16**(3): p. 243-268.
79. Tao, W.H., R.E. Robertson, and P.H. Thornton. *Energy Absorption in Crushing Fiber Composite Materials*. in *ASM International*. 1988. Metals Park, OH.
80. Tao, W.H., R.E. Robertson, and P.H. Thornton, *Effects of Material Properties and Crush Conditions on the Crush Energy absorption of Fiber Composite Rods*. Composites Science and Technology, 1993. **47**: p. 405-418.
81. Farley, G., *Energy Absorption in Composite Material and Structure*. Proceedings of the 43rd American Helicopter Society Annual Forum, 1987. **2**: p. 613-627.
82. Quek, S.C., A.M. Waas, J. Hoffman, and V. Agaram, *Crushing response of braided and CSM glass reinforced composite tubes*. Journal of Composite Structures, 2001. **52**: p. 103-112.
83. Hamada, H., S. Ramakrishna, and H. Sato, *Effect of Fibre Orientation on the Energy absorption Capability of Carbon Fibre / PEEK Composite Tubes*. Composite Materials, 1996. **30**(8): p. 947-963.
84. Ramakrishna, S., *Energy Absorption Characteristics of Knitted Fabric Reinforced Epoxy Composite Tubes*. Reinforced Plastics and Composites, 1995. **14**: p. 1121-1141.
85. Thornton, P.H., J.J. Harwood, and P. Beardmore, *Fiber-Reinforced Plastic Composites for Energy Absorption Purposes*. Composites Science and Technology, 1985. **24**: p. 275-289.
86. Mamalis, A.G., D.E. Manolakos, G.A. Demosthenos, and M.B. Ioannidis, *The Static and Dynamic Axial Crumbling of Thin-Walled Fibreglass Composite Square Tubes*. Composites Part B, 1997. **28B**: p. 439-451.
87. Mamalis, A.G., Y.B. Yuan, and G.L. Viegelaahn, *Collapse of thin-wall composite sections subjected to high speed axial loading*. International Journal of Vehicle Design, 1992. **13**(5/6): p. 564-579.

88. Chadwick, M. and A. Caliskan, *Crush Mechanisms Observed in Polymeric Composite Tubes*. Automotive Composites Consortium Conference, 1997: p. 453-462.
89. Chiu, C.H., C.K. Lu, and C.M. Wu, *Crushing Characteristics of 3-D Braided Composite Square Tubes*. *Composite Materials*, 1997. **31**(22): p. 2309-2327.
90. Price, J.N. and D. Hull, *Crush Behaviour of Square Section Glass Fibre Polyester Tubes*. *How to apply advanced composite technology*, 1988: p. 53-61.
91. Thornton, P.H., *The Crush Behaviour of Glass Fiber Reinforced Plastic Sections*. *Composites Science and Technology*, 1986. **27**: p. 199-223.
92. Mamalis, A.G., D.E. Manolakos, G.A. Demosthenos, and M.B. Ioannidis, *Energy Absorption Capability of Fibreglass Composite Square Frusta Subjected to Static and Dynamic Axial Collapse*. *Thin Walled Structures*, 1996. **25**(4): p. 269-295.
93. Mamalis, A.G., M. Robinson, D.E. Manolakos, G.A. Demosthenos, M.B. Ioannidis, and J. Carruthers, *Crashworthy capability of composite material structures*. *Composite Structures*, 1997. **37**: p. 109-134.
94. Price, J.N. and D. Hull, *The Crush Performance of Composite Structures*. *Composite Structures* 4, 1987. **2**: p. 2.32-2.44.
95. Hamada, H., S. Ramakrishna, Z. Maekawa, M. Nakamura, and T. Nishiwaki, *Energy Absorption Characteristics of Composite Tubes with Different Cross-Sectional Shapes*. *Proceedings of the 10th Annual ASM/ESD Advanced Composites Conference*, 1994: p. 523-534.
96. Hamada, H., J. Coppola, and D. Hull, *Effect of Surface Treatment on Crushing Behaviour of Glass Cloth / Epoxy Composite Tubes*. *Composites*, 1992. **23**(2): p. 93-99.
97. Duckett, M.J., *Rate Dependent Effects on the Energy Absorption and Material Properties of Polymer Composites*. 2001, Thesis: University of Nottingham.
98. Mamalis, A.G., D.E. Manolakos, G.A. Demosthenos, and M.B. Ioannidis, *Analytical and experimental approach to damage and residual strength of fibreglass composite automotive frame rails during manufacturing*. *Composite Structures*, 1995. **32**: p. 325-330.
99. Browne, A.L. and S.A. Iobst. *Dynamic Axial Crush of Automotive Rail-Sized Composite Tubes Part 1: Tubes with Woven Reinforcements (Carbon, Kevlar, and Glass) and Non-Plug Crush Initiators*. in *Proceedings of the American Society for Composites 17th Technical Conference*. 2002. Purdue University, West Lafayette, Indiana.
100. Hamada, H. and S. Ramakrishna, *Scaling Effects in the Energy Absorption of Carbon-Fiber/PEEK Composite Tubes*. *Composites Science and Technology*, 1995. **55**: p. 211-221.
101. Johnson, N., D. Houston, P. Watling, and L. Lalik, *Generic Tube Crush Program: Structural Reaction Injection Molded Tubes*. Automotive Composites Consortium, 1998.
102. Browne, A., D. Houston, P. Watling, and L. Lalik, *Generic Tube Crush Program: Resin Transfer Molded Tubes*. Automotive Composites Consortium, 1998.
103. Browne, A.L., N.L. Johnson, D.Q. Houston, and L. Lalik. *Automotive Composites Consortium generic tube crush program: Processing and molding effects on the axial crush of RTM and SRIM tubes*. in *SAMPE-ACCE-DOE Advanced Composites Conference*. 1999.

104. Fairfull, A.H. and D. Hull. *Effects of Specimen Dimensions on Specific Energy Absorption of Fibre Composite Tubes*. in *International Conference of Composite Materials VI*. 1987.
105. Farley, G.L., *Crushing Characteristics of Composite Tubes with "Near-Elliptical" Cross Sections*. *Composite Materials*, 1992. **26**(12): p. 1741-1751.
106. Grundy, J., J. Blears, and B. Sneddon, *Assessment of Crash-Worthy Car Materials*. Chartered Mechanical Engineer (CME), 1985. **32**(4): p. 31-35.
107. Farley, G.L., *Energy Absorption of Composite Materials*. *Composite Materials*, 1983. **17**: p. 267-279.
108. Czaplicki, M., R. Robertson, and P. Thornton, *Comparison of Bevel and Tulip Triggered Pultruded Tubes for Energy Absorption*. *Composites Science and Technology*, 1991. **40**: p. 31-46.
109. Jimenez, M.A., A. Miravete, E. Larrode, and D. Revuelta, *Effect of trigger geometry on energy absorption in composite profiles*. *Composite Structures*, 2000. **48**: p. 107-111.
110. Sigalas, I., M. Kumosa, and D. Hull, *Trigger Mechanisms in Energy-Absorbing Glass Cloth/Epoxy Tubes*. *Composites Science and Technology*, 1991. **40**: p. 265-287.
111. Hull, D. and J. Coppola, *Performance of Glass Fibre-Vinyl Ester Composite Tubes Crushed Using Internal Mandrels*. *International Conference on Composite Structures*, 1991: p. 129-143.
112. Thuis, H. and V. Metz, *The Influence of Trigger Configurations and Laminate Lay-up on the Failure Mode of Composite Crush Cylinders*. *Composite Structures*, 1993. **28**: p. 37-43 (131-137).
113. Turner, T.A., *The Effect of Processing Variables on the Energy Absorption of Composite Crash Structures*. 2004, Thesis: University of Nottingham.
114. Farley, G., *The Effects of Crushing Speed on the Energy-Absorption Capability of Composite Tubes*. *Composite Materials*, 1991. **25**: p. 1314-1329.
115. Hamada, H. and S. Ramakrishna, *Comparison of Static and Impact Energy Absorption of Carbon Fiber/PEEK Composite Tubes*. *Composite Materials : Testing and Design*, 1986. **12**: p. 182-197.
116. Fernie, R., M.J. Duckett, and N.A. Warrior. *Geometric and Loading Rate Effects on the Energy Absorption of Triaxially Braided Carbon Vinyl Ester Tubes*. in *Proceedings of the American Society for Composites 17th Technical Conference*. 2002. Purdue University, West Lafayette, Indiana.
117. Geary, W., J. Dutton, and D.M. Shuter, *The influence of size effects and dynamic loading on the fracture toughness of commercial GRP materials*. *Composites Science and Technology*, 2000. **60**: p. 633-638.
118. Russell, A., T. Reddy, S. Reid, and P. Soden, *Quasi-Static and Dynamic Axial Crushing of Foam-Filled FRP Tubes*. *Composite Material Technology*, ASME, 1991. **37**: p. 145-152.
119. Brachos, V. and C. Douglas, *Energy Absorption Characteristics of Hybrid Composite Structures*. *Proceedings of the 1995 27th International SAMPE Technical Conference*, 1995. **27**: p. 421-435.
120. Hamada, H. and S. Ramakrishna, *Impact performance of glass cloth/epoxy composite tubes with different surface treatment*. *Composite Interfaces*, 1996. **4**(1): p. 35-44.
121. Hamada, H., S. Ramakrishna, M. Nakamura, Z. Maekawa, and D. Hull, *Progressive Crushing Behaviour of Glass/Epoxy Composite Tubes with Different Surface Treatment*. *Composite Interfaces*, 1994. **2**(2): p. 127-142.

122. Fleming, D. and A. Vizzini, *The Effect of Side Loads on the Energy Absorption of Composite Structures*. Journal of Composite Materials, 1992. **26**(4): p. 486-499.
123. Farley, G., K. Wolterman, and J. Kennedy, *The Effects of Crushing Surface Roughness on the Crushing Characteristics of Composite Tubes*. American Helicopter Society, 1992. **37**(3): p. 53-60.
124. Cooper, E., *An Elastic-Plastic Finite Element Model for Composite Crash Structures*. 2002, Thesis: University of Nottingham.
125. Corden, T.J., *Development of design and manufacturing techniques for glass reinforced plastic waste water treatment equipment*. 1996, Thesis: University of Nottingham.
126. MacMillan, A.R., *Environmental degradation of glass reinforced polyesters in the waste water treatment industry*. 1997, Thesis: University of Nottingham.
127. Fernie, R. and N.A. Warrior, *Impact Test Rigs for High Strain Rate Tensile and Compressive Testing of Composite Materials*. Strain, 2002. **38**: p. 69-73.

9 Appendix 1 – Load vs Displacement Results

9.1 Rate Effects

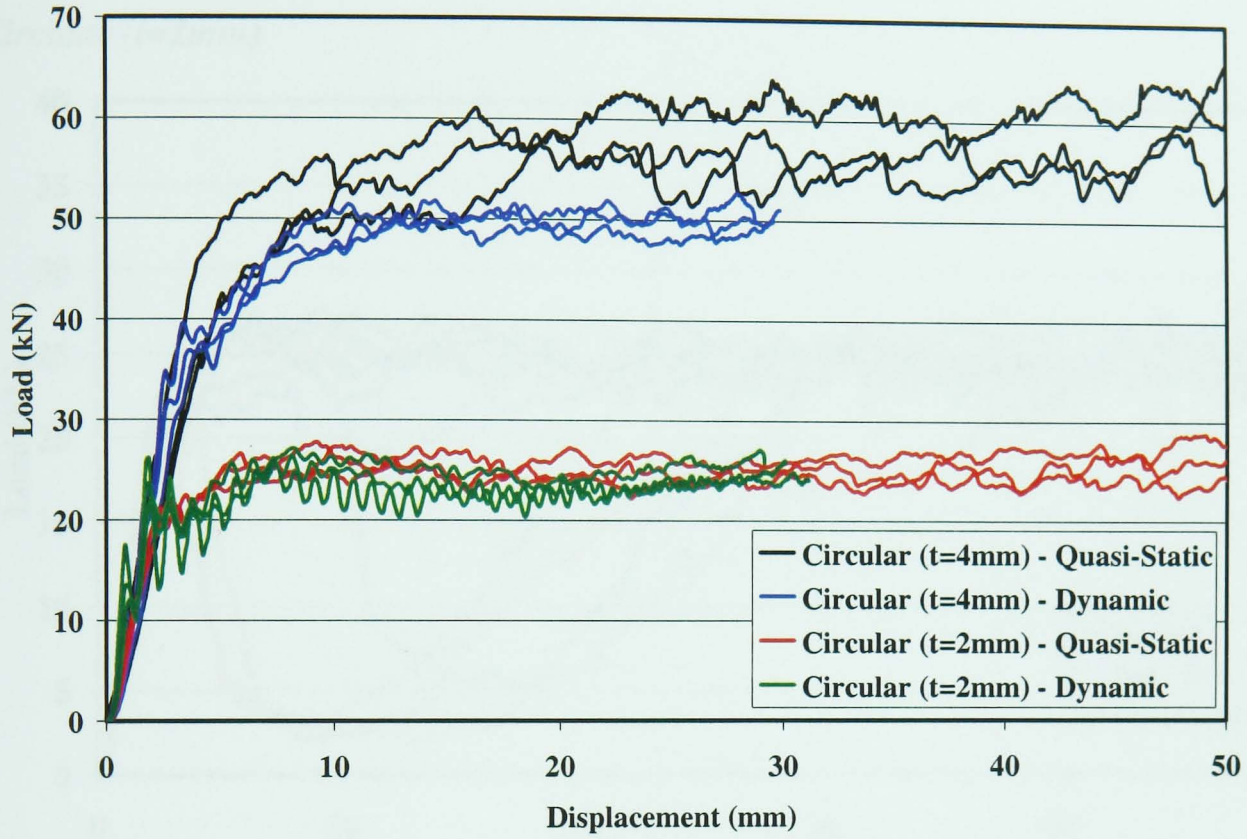


Figure 1: Quasi-Statically and Dynamically Tested Circular Tube Results

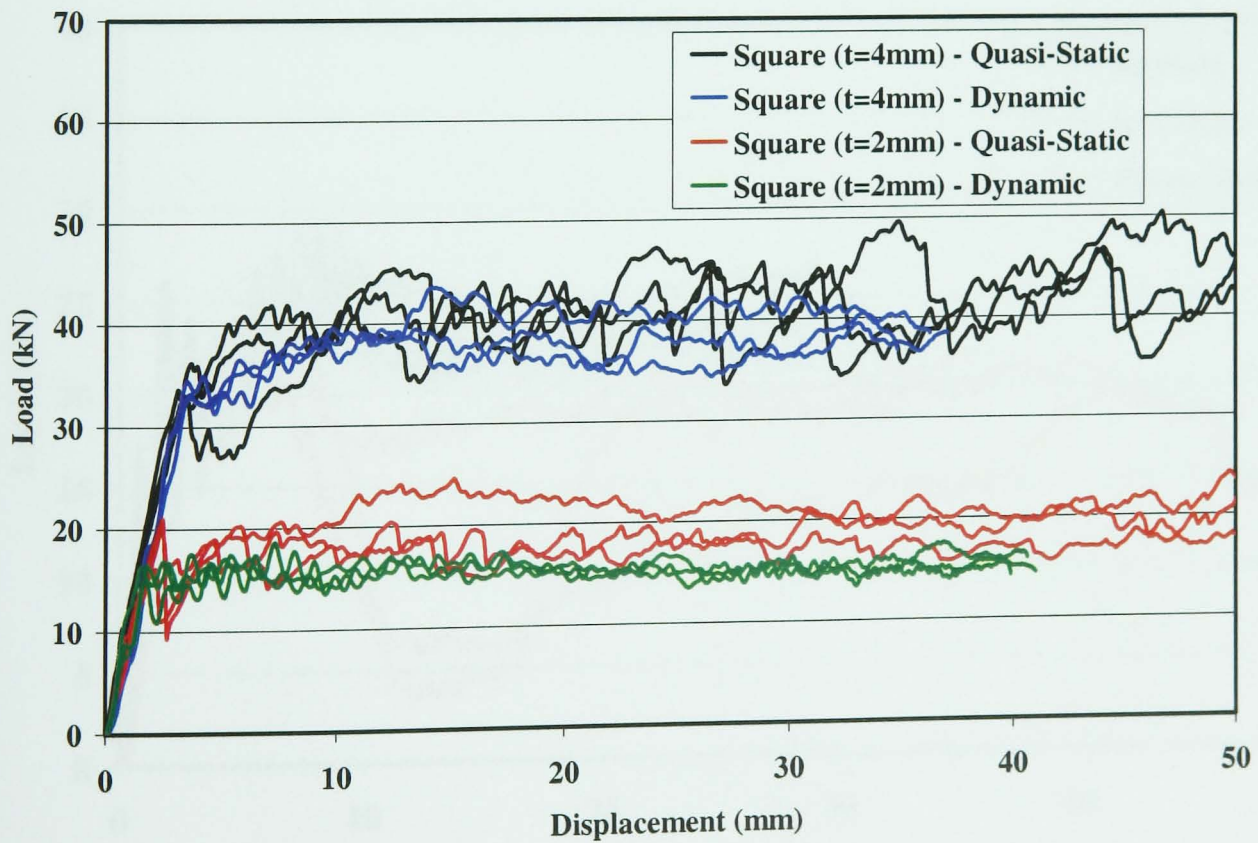


Figure 2: Quasi-Statically and Dynamically Tested Square Tube Results

9.2 Holes

9.2.1 Hole Size

Circular ($t=2mm$)

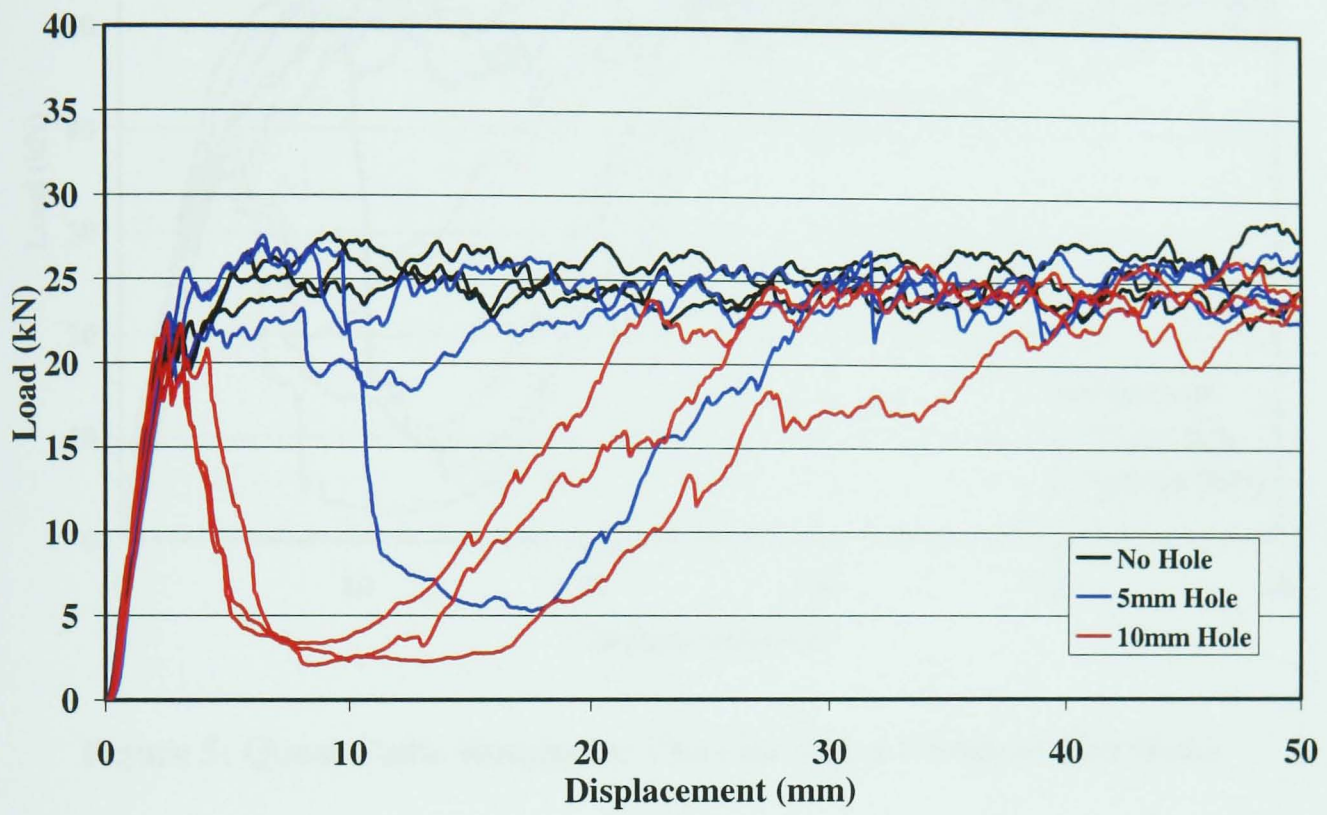


Figure 3: Quasi-Static Results for Circular Tubes ($t=2mm$) with Holes

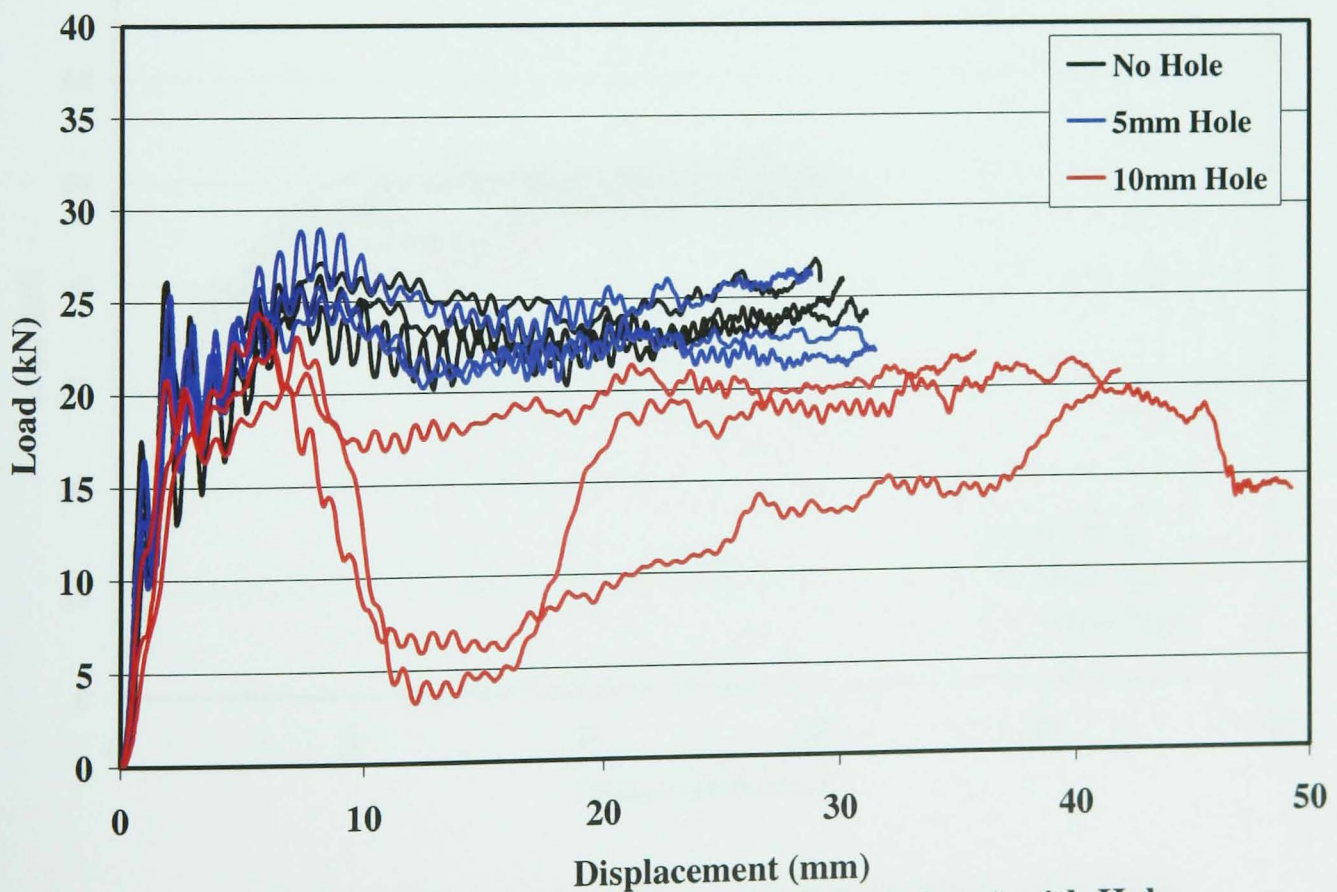


Figure 4: Dynamic Results for Circular Tubes ($t=2mm$) with Holes

Circular (t=4mm)



Figure 5: Quasi-Static Results for Circular Tubes (t=4mm) with Holes

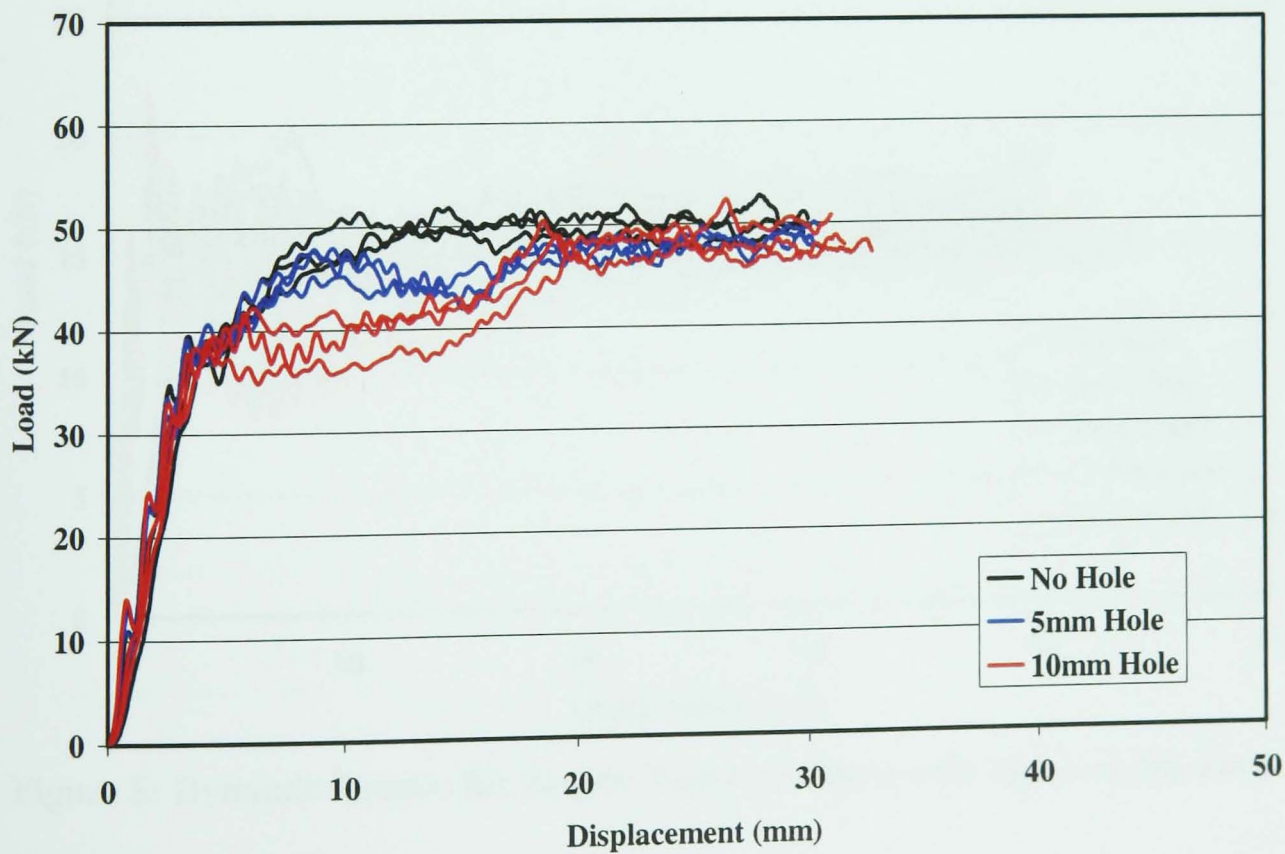


Figure 6: Dynamic Results for Circular Tubes (t=4mm) with Holes

Square (t=2mm) on Face

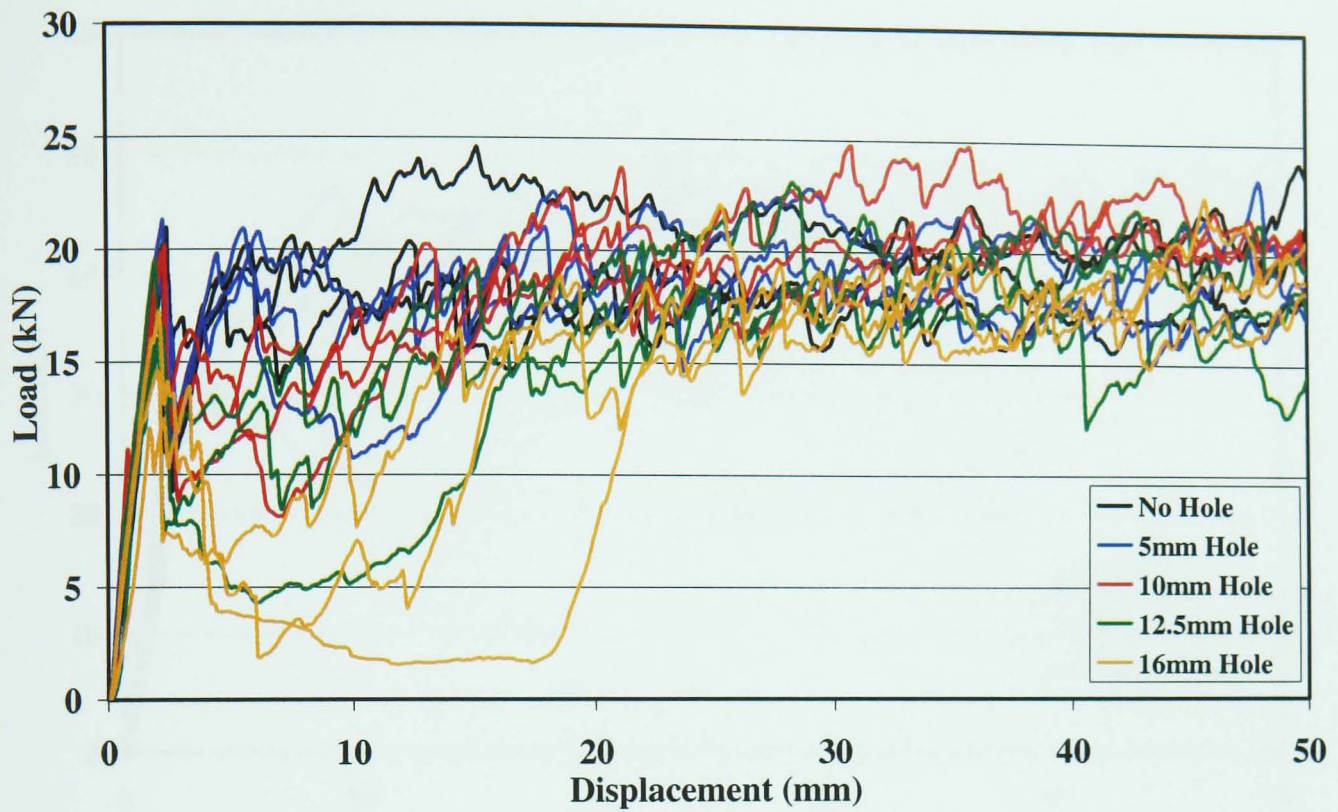


Figure 7: Quasi-Static Results for Square Tubes (t=2mm) with Holes on the Face

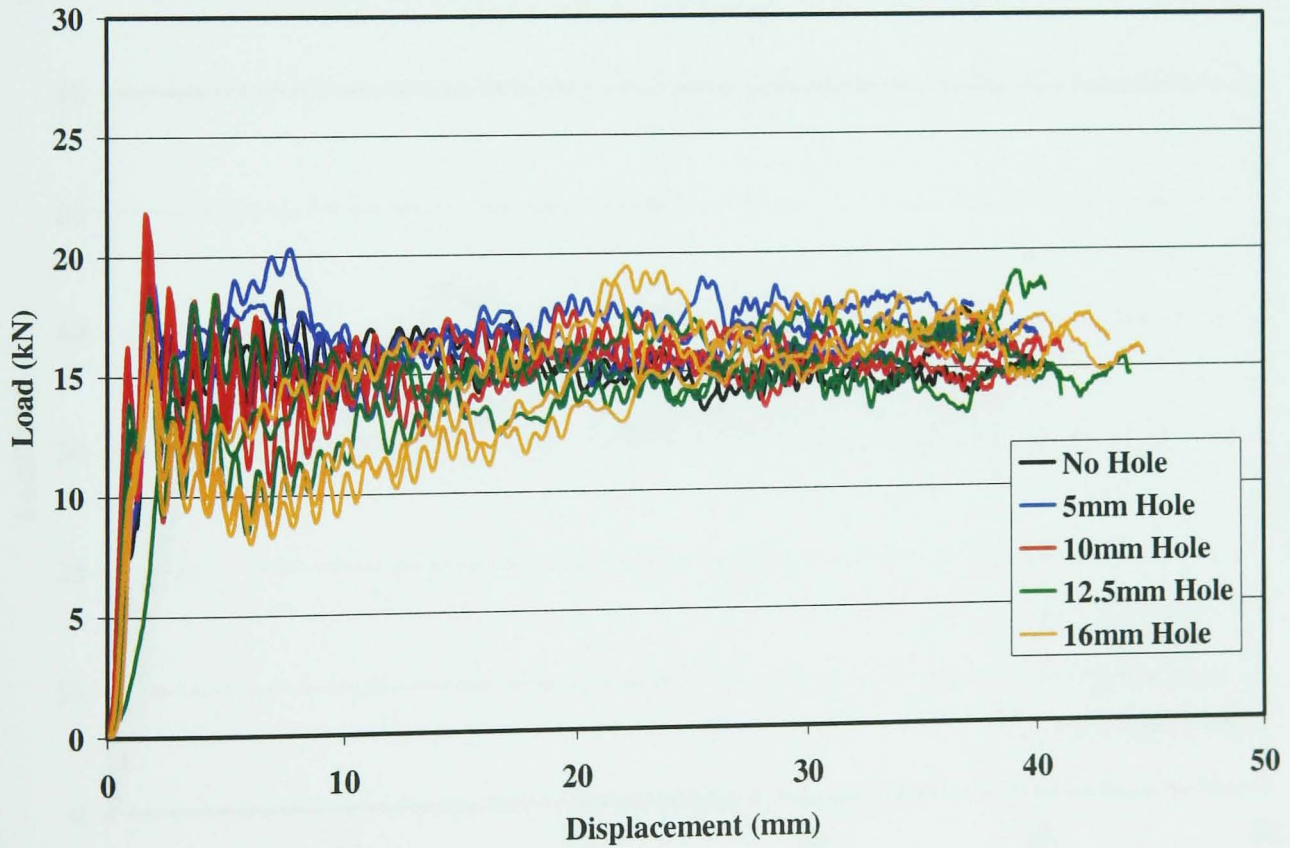


Figure 8: Dynamic Results for Square Tubes (t=2mm) with Holes on the Face

Square (t=4mm) on Face

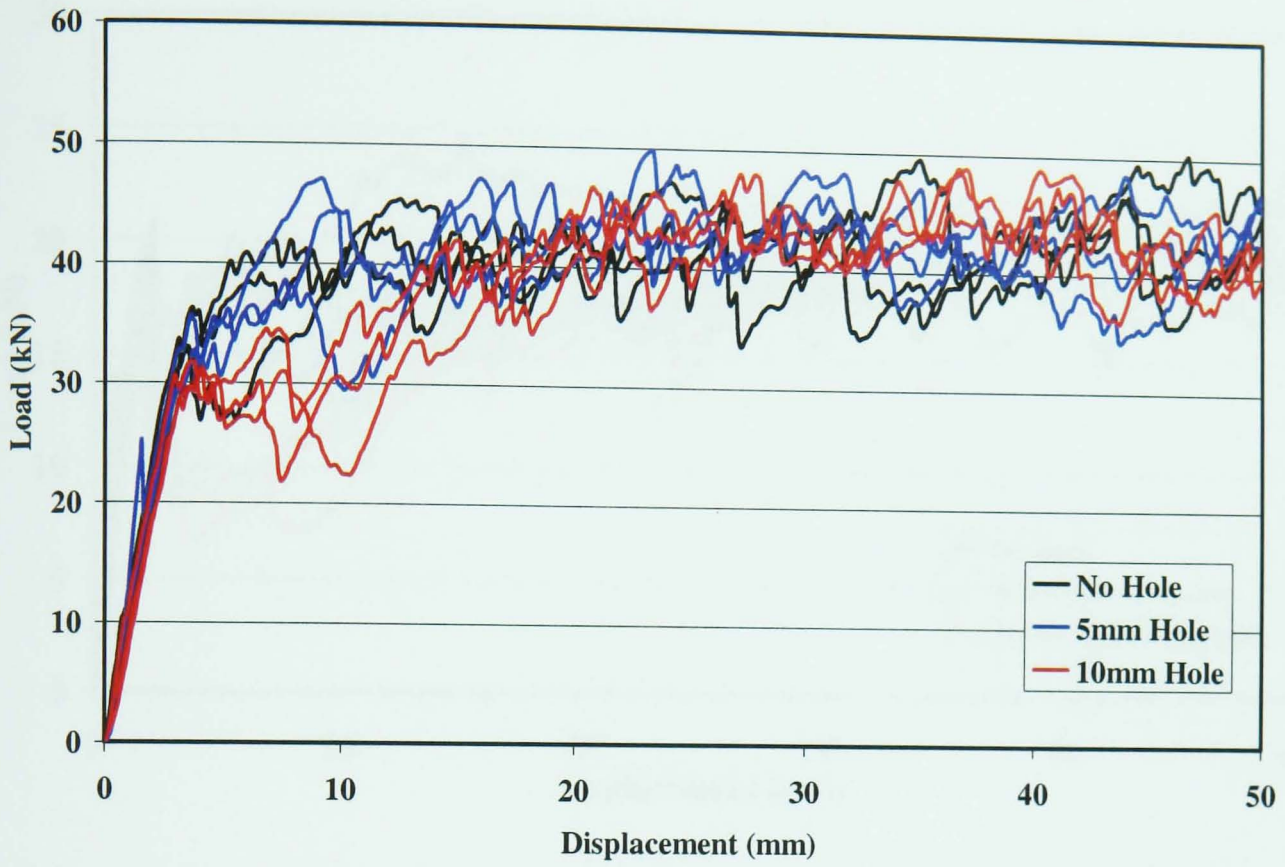


Figure 9: Quasi-Static Results for Square Tubes (t=4mm) with Holes on the Face

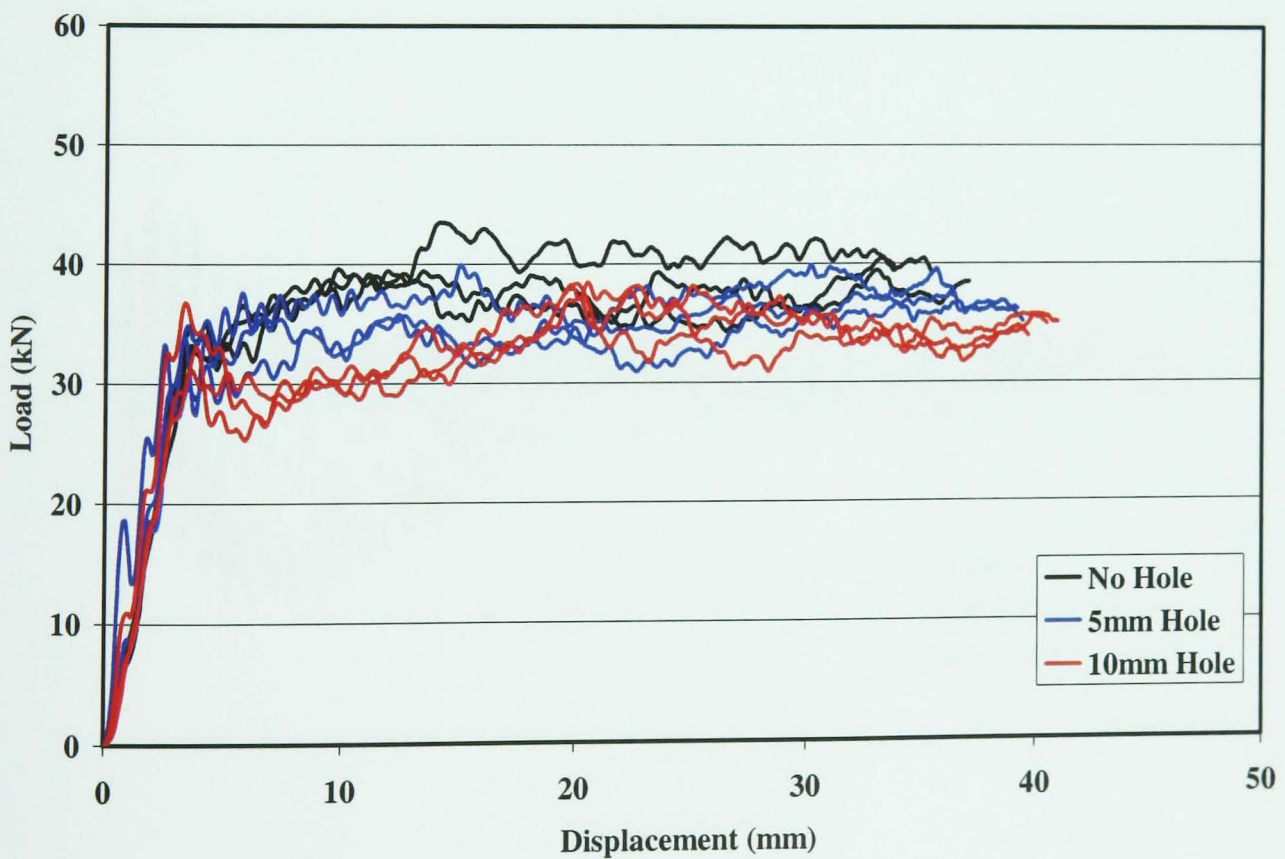


Figure 10: Dynamic Results for Square Tubes (t=4mm) with Holes on the Face

Square (t=2mm) on Corner

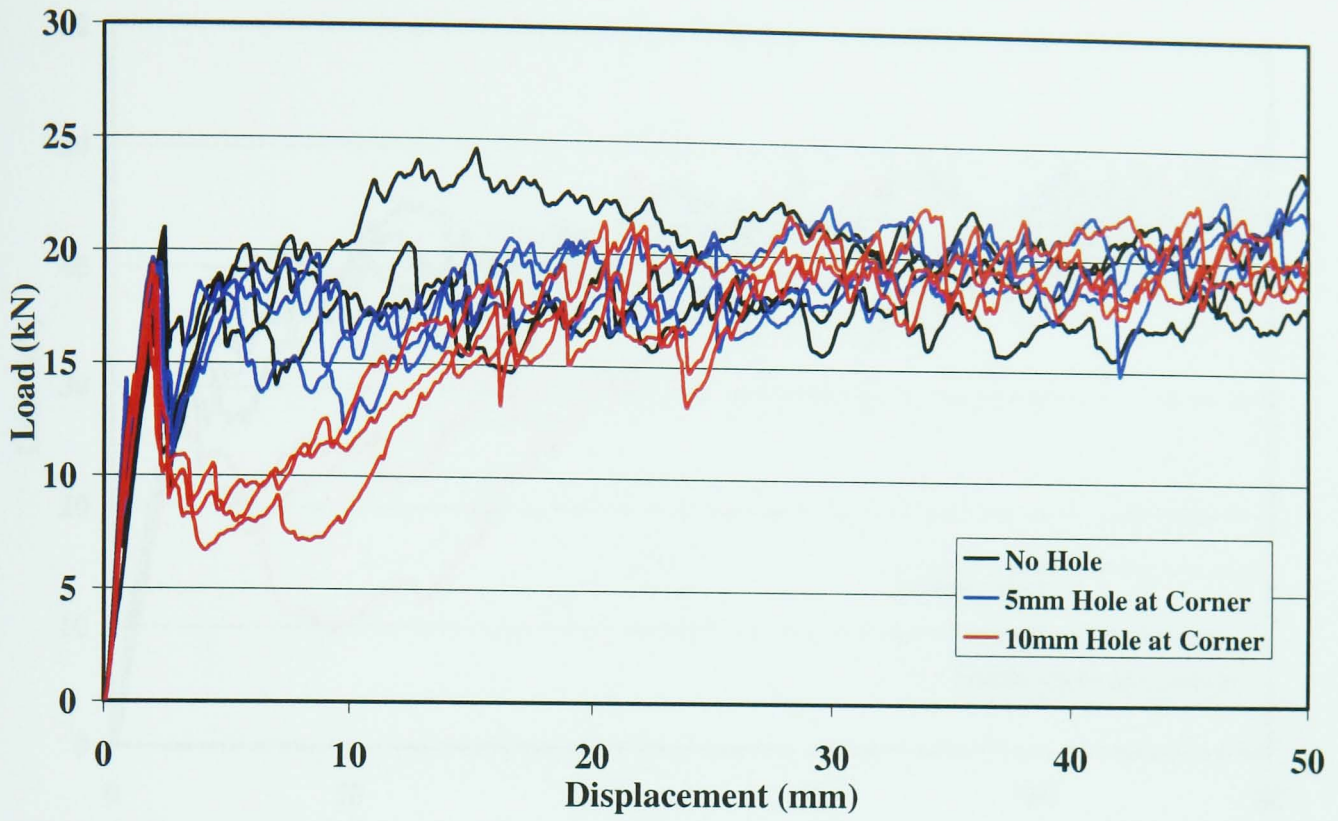


Figure 11: Quasi-Static Results for Square Tubes (t=2mm) with Holes in the Corner

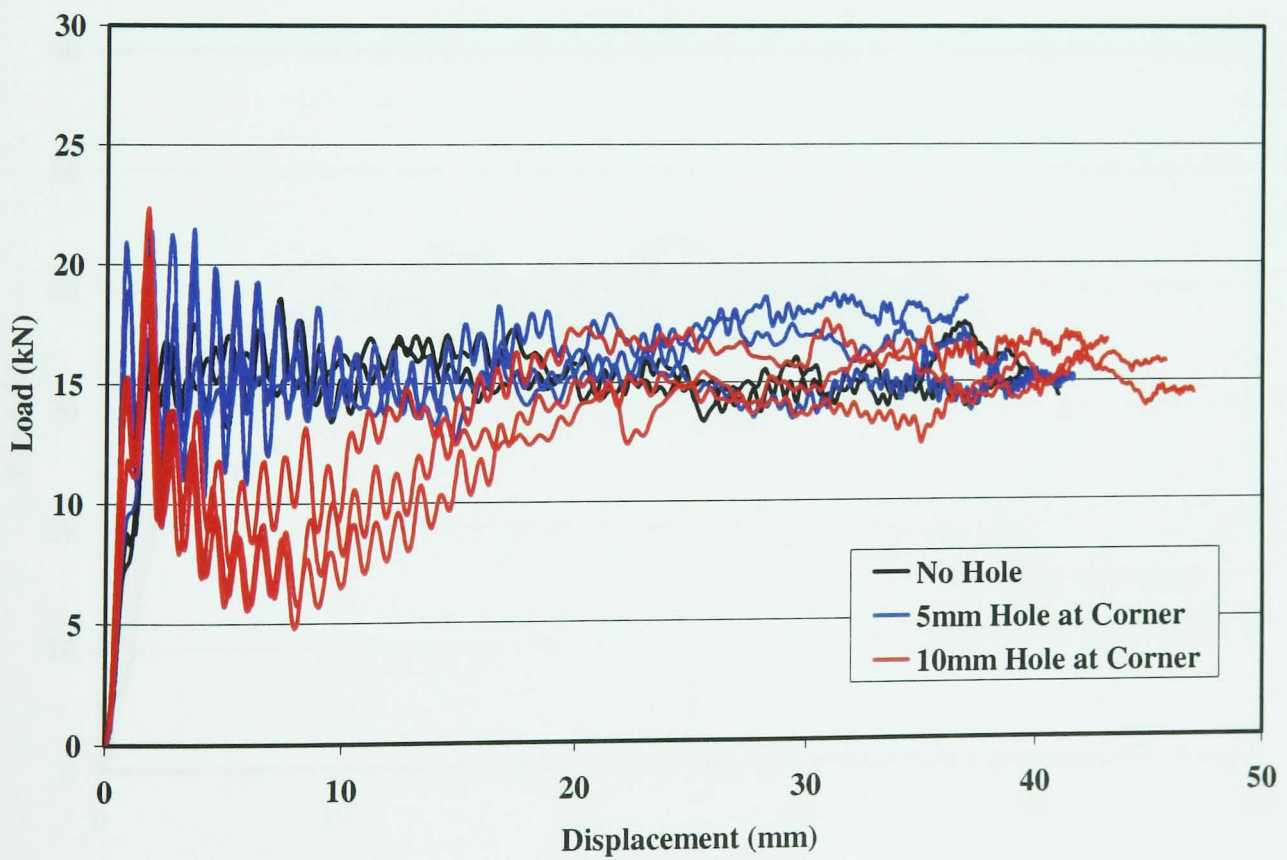


Figure 12: Dynamic Results for Square Tubes (t=2mm) with Holes in the Corner

Square (t=4mm) on Corner

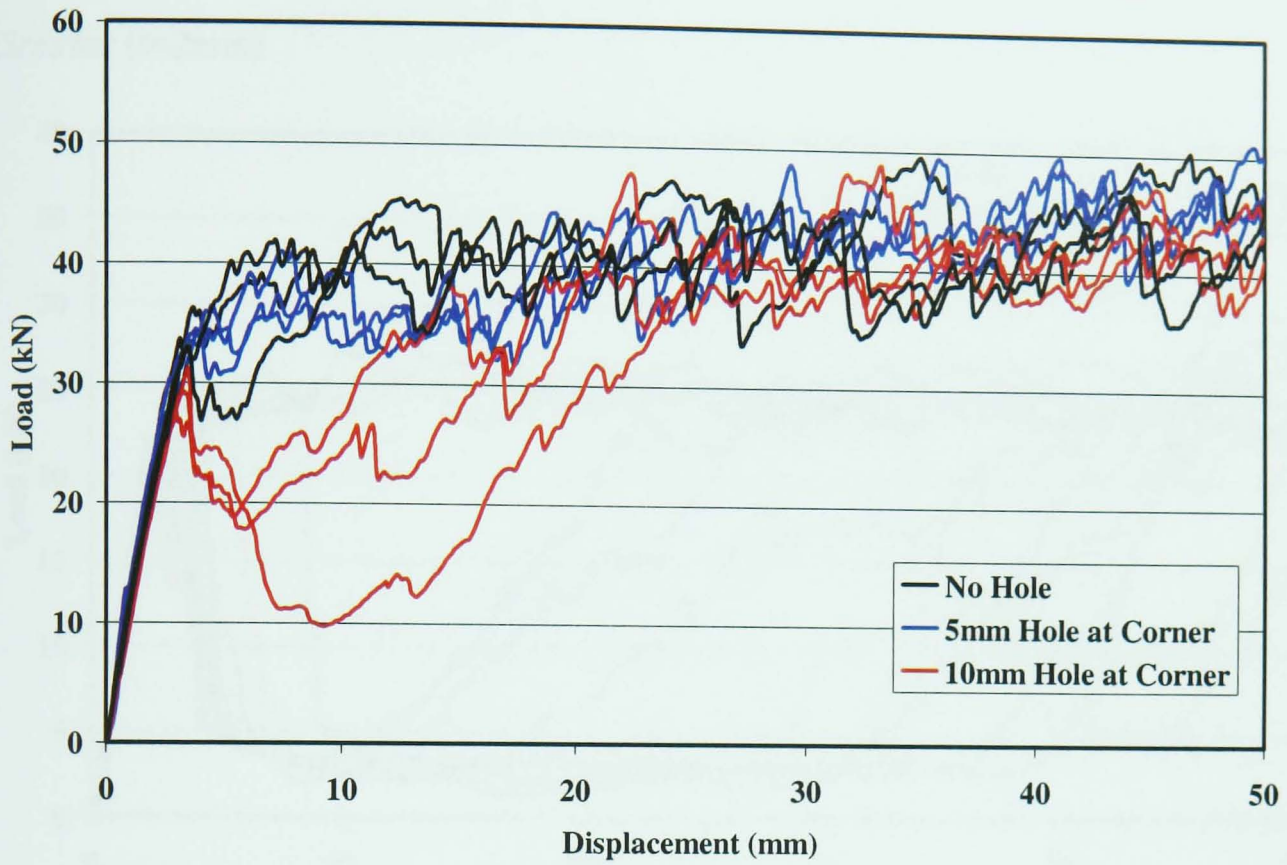


Figure 13: Quasi-Static Results for Square Tubes (t=4mm) with Holes in the Corner

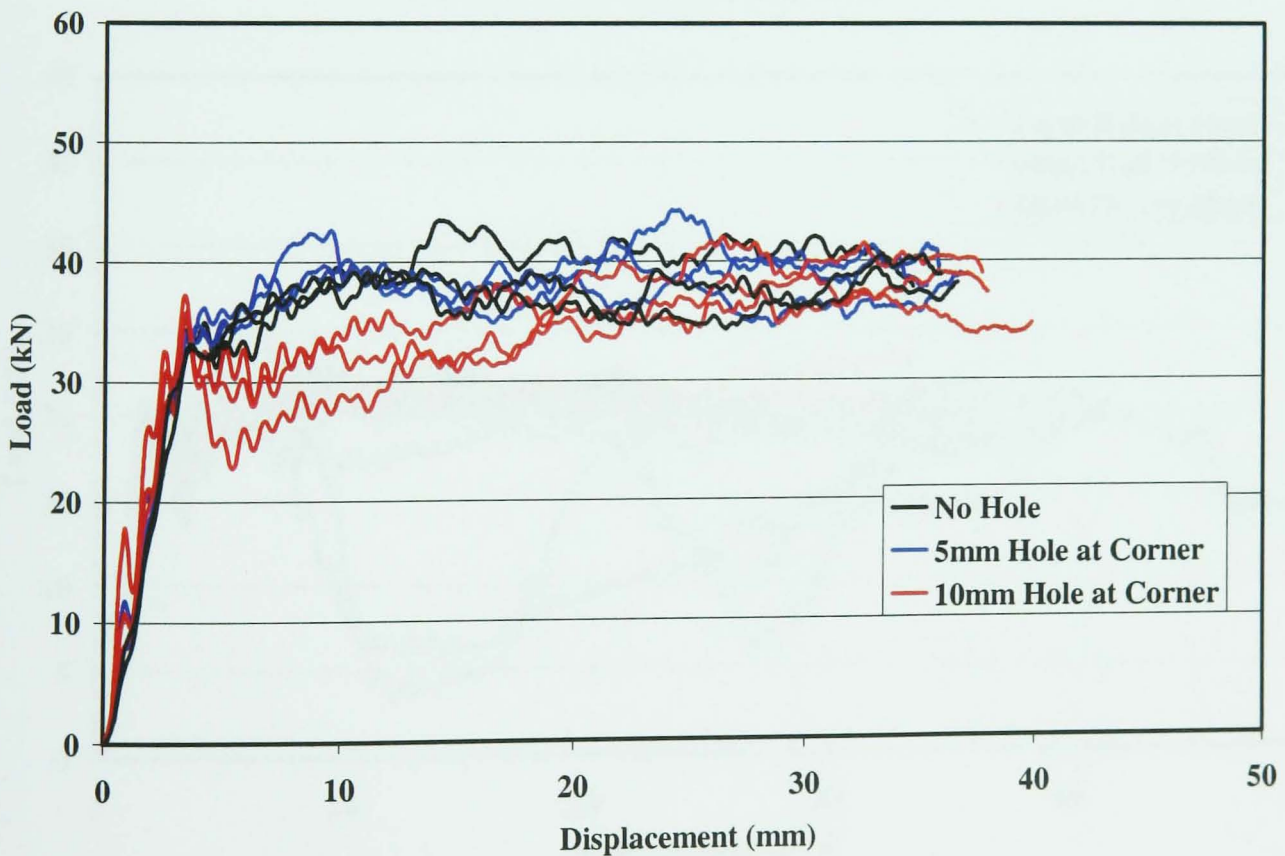


Figure 14: Dynamic Results for Square Tubes (t=4mm) with Holes in the Corner

9.2.2 Hole Position – Axially

Circular (t=2mm)

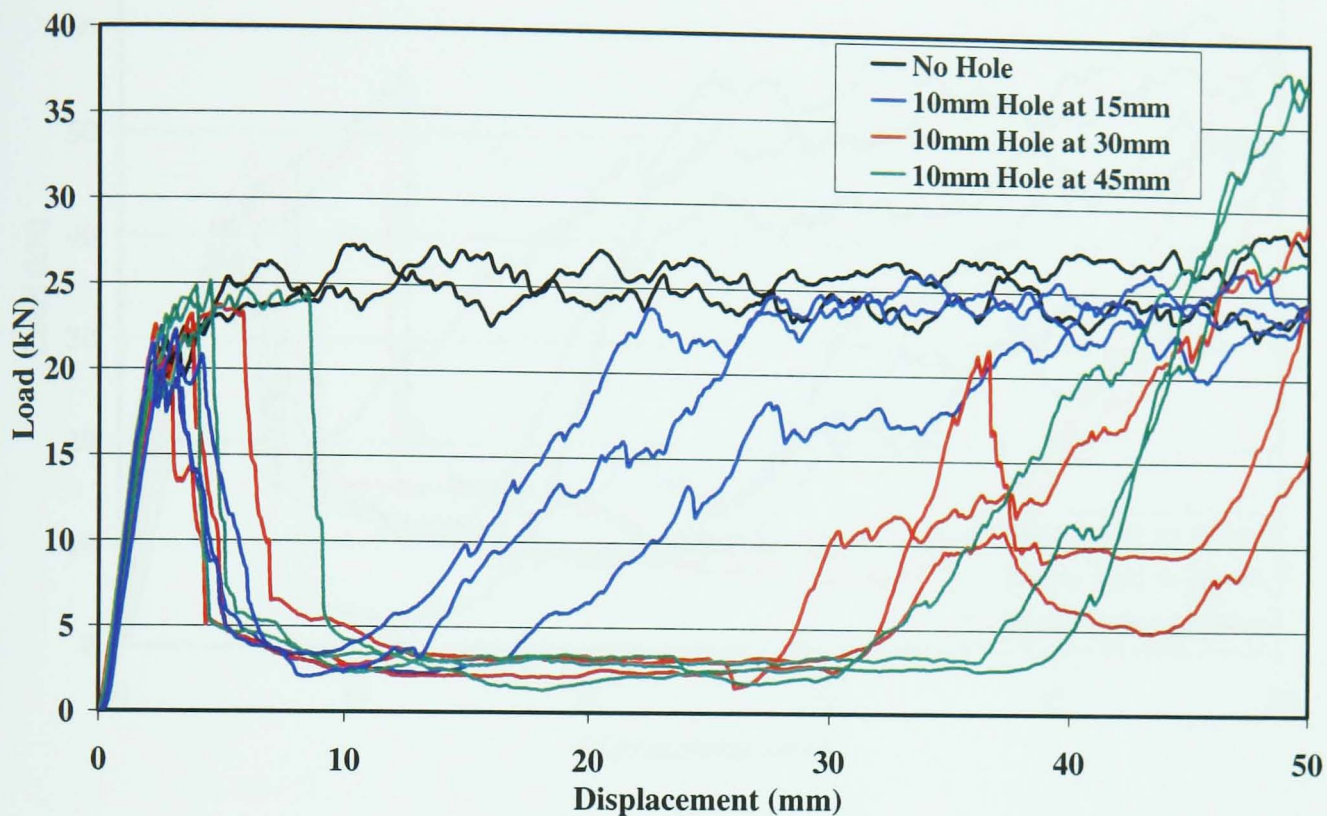


Figure 15: Quasi-Static Results for Circular Tubes (t=2mm) with Holes Positioned Axially along Tube

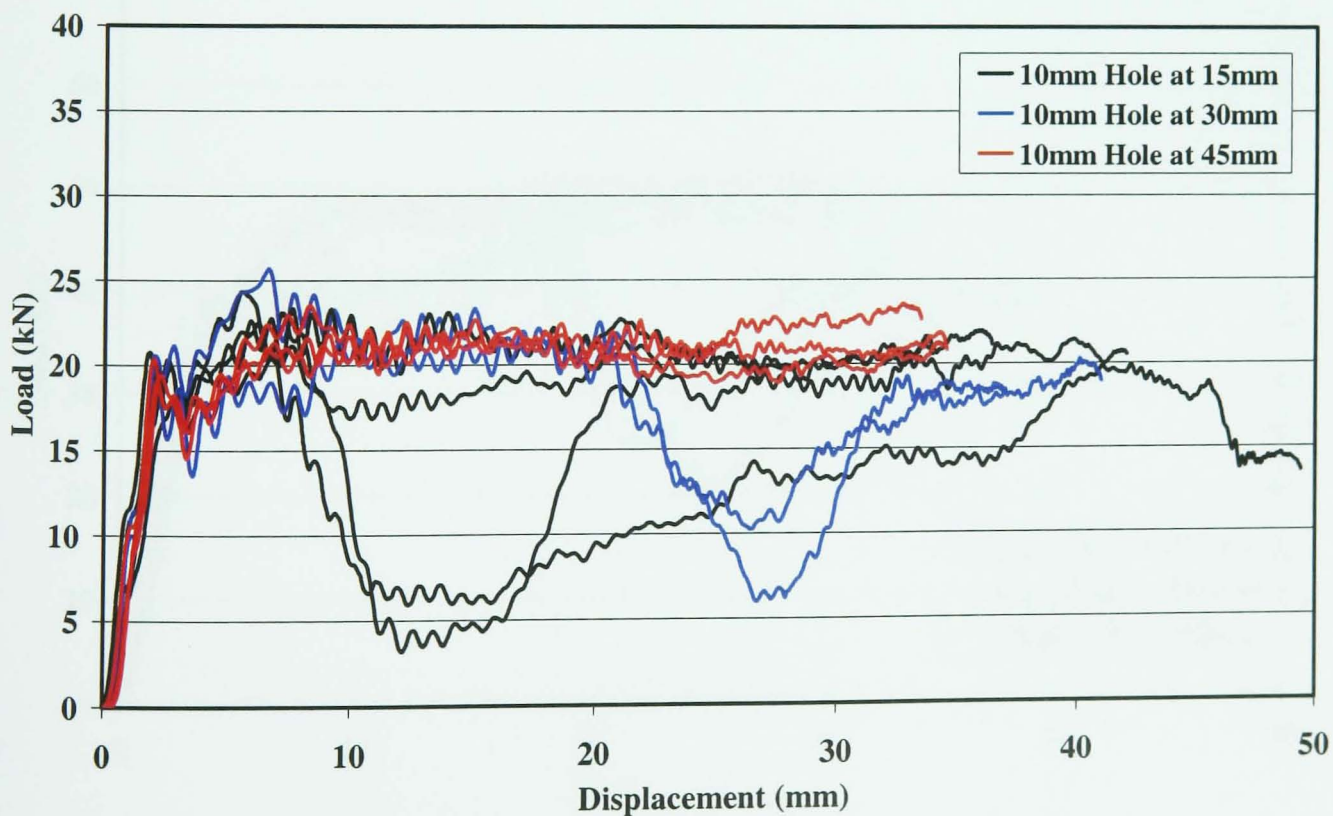


Figure 16: Dynamic Results for Circular Tubes (t=2mm) with Holes Positioned Axially along Tube

Circular (t=4mm)

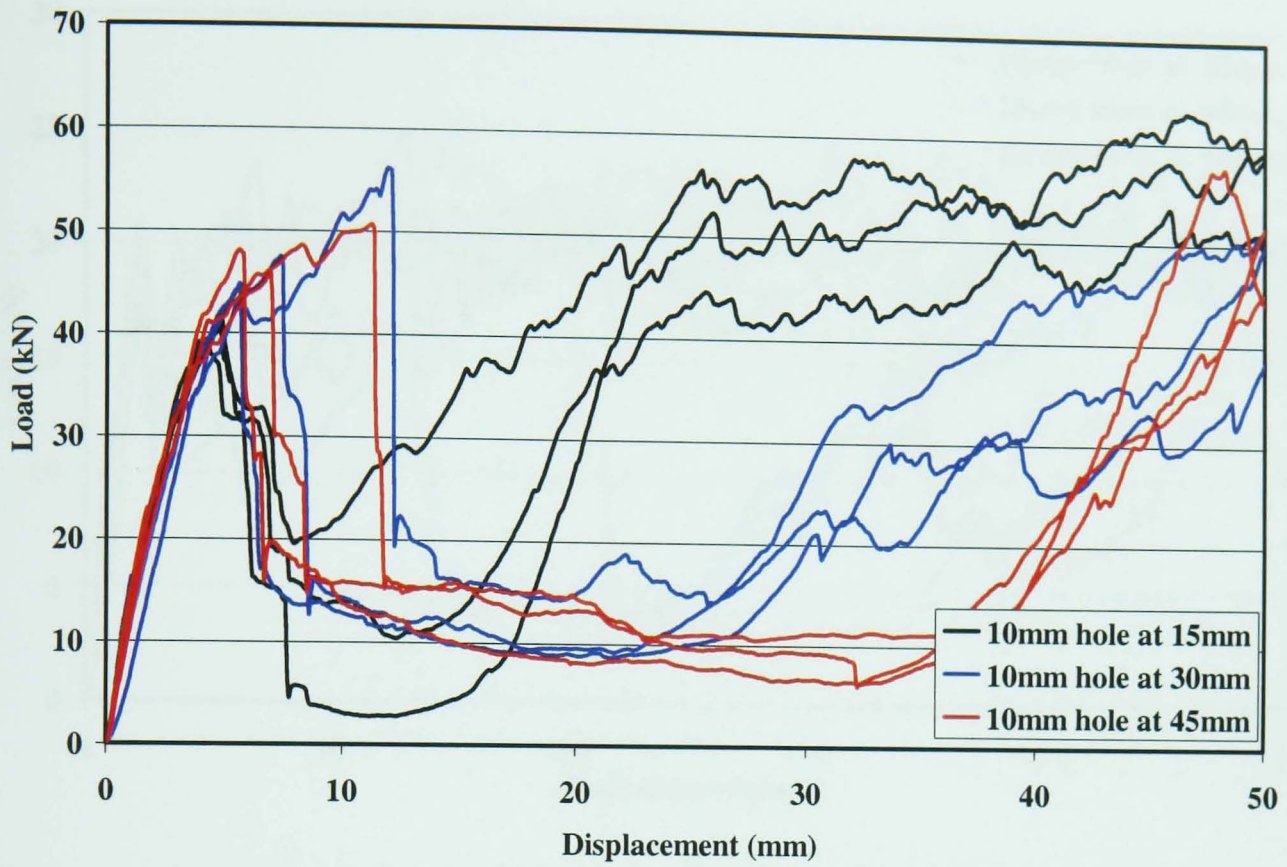


Figure 17: Quasi-Static Results for Circular Tubes (t=4mm) with Holes Positioned Axially along Tube

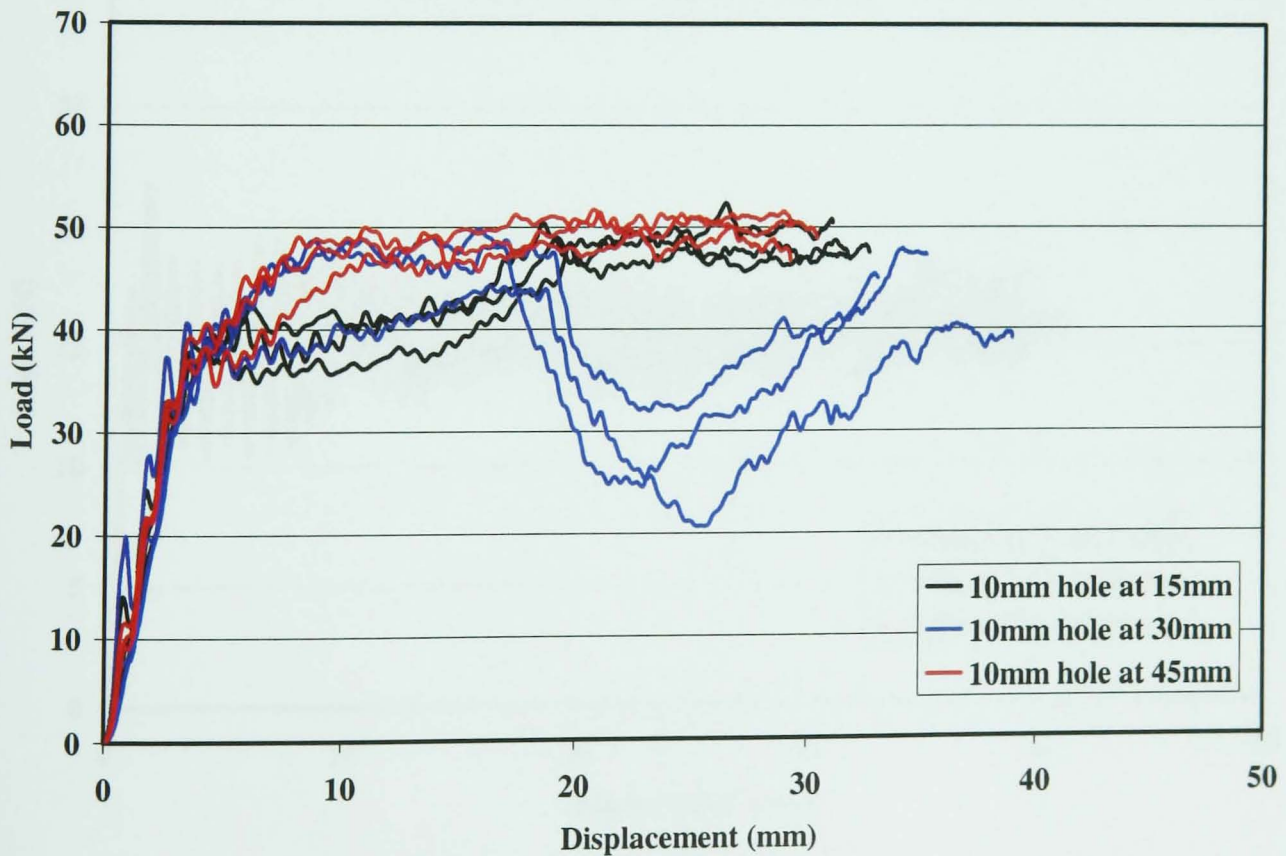


Figure 18: Dynamic Results for Circular Tubes (t=4mm) with Holes Positioned Axially along Tube

Square (t=2mm) on Face

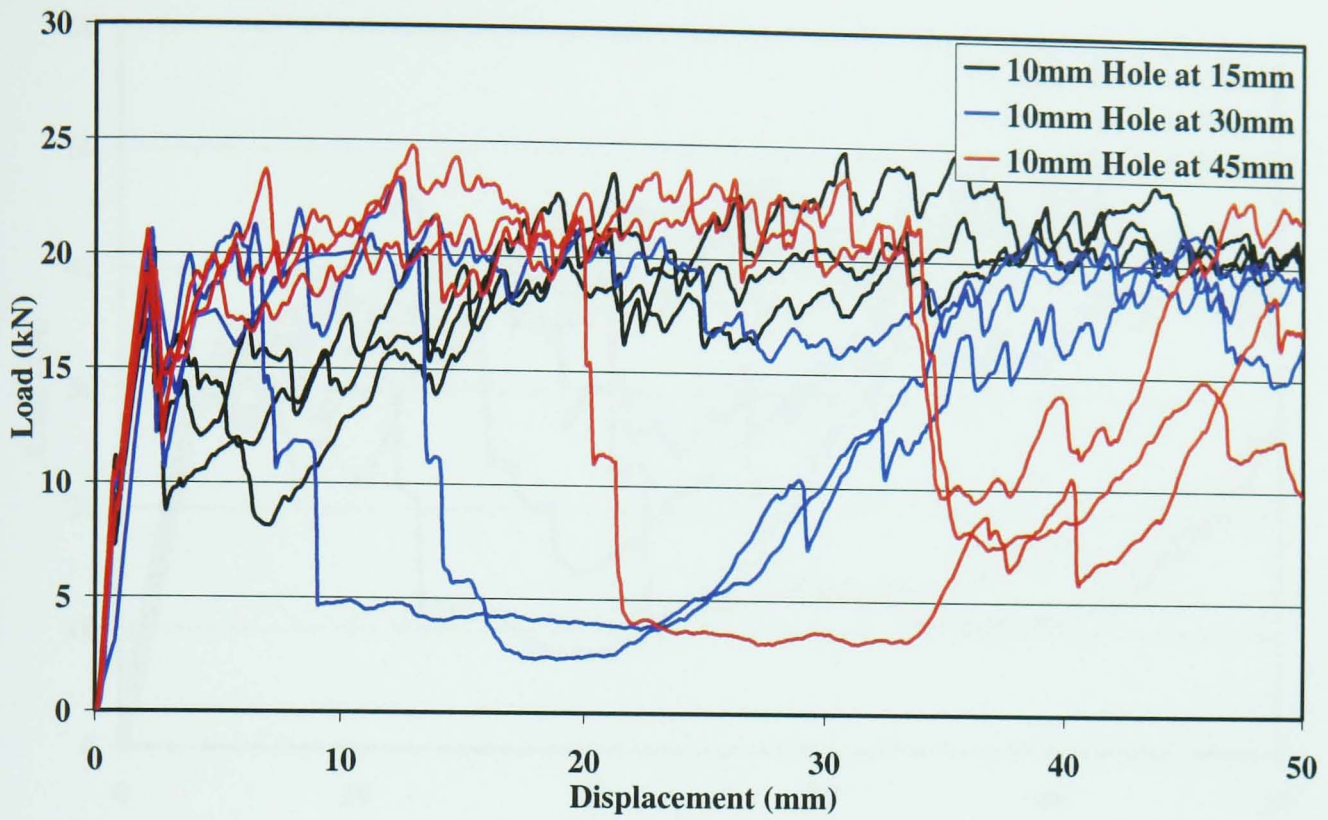


Figure 19: Quasi-Static Results for Square Tubes (t=2mm) with Holes Positioned Axially along the Face of Tube

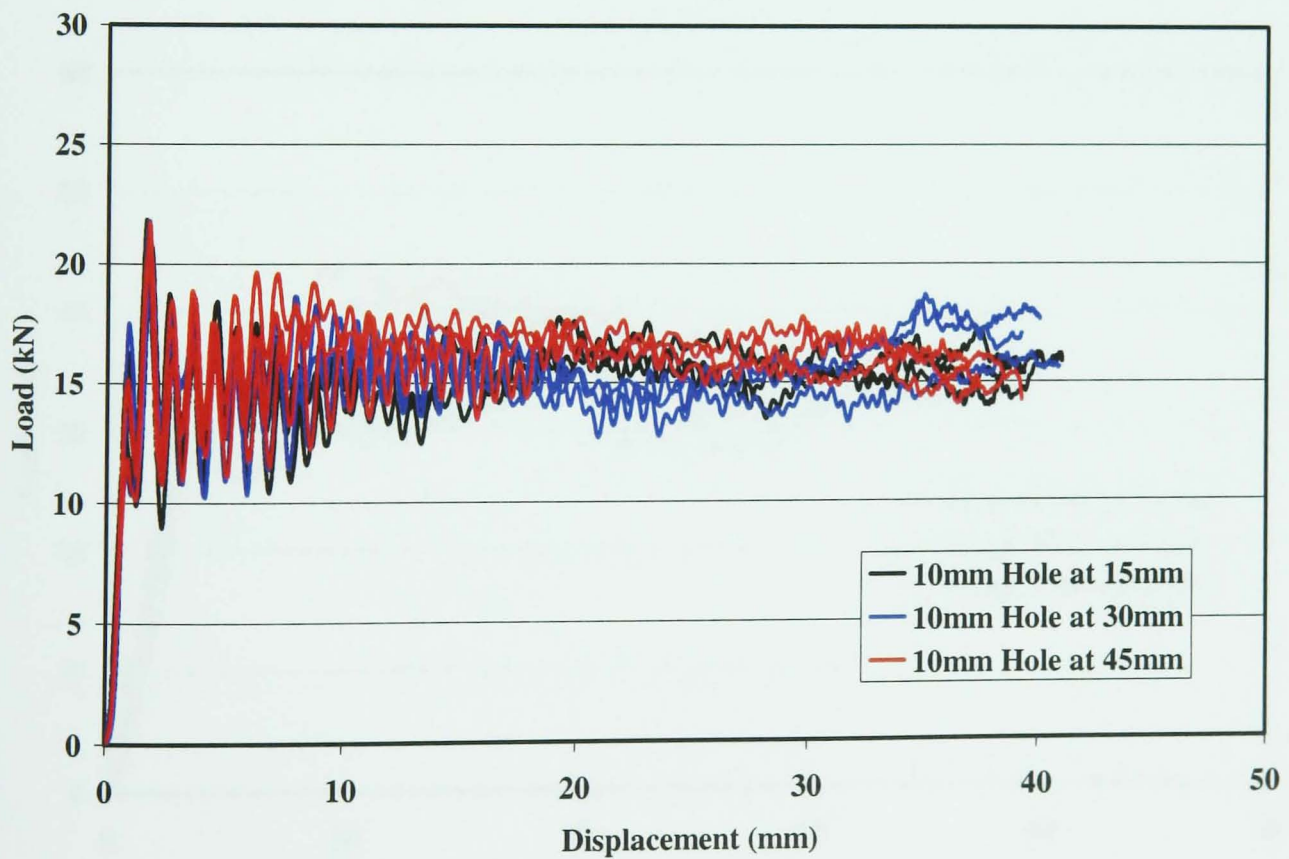


Figure 20: Dynamic Results for Square Tubes (t=2mm) with Holes Positioned Axially along the Face of Tube

Square (t=4mm) on Face

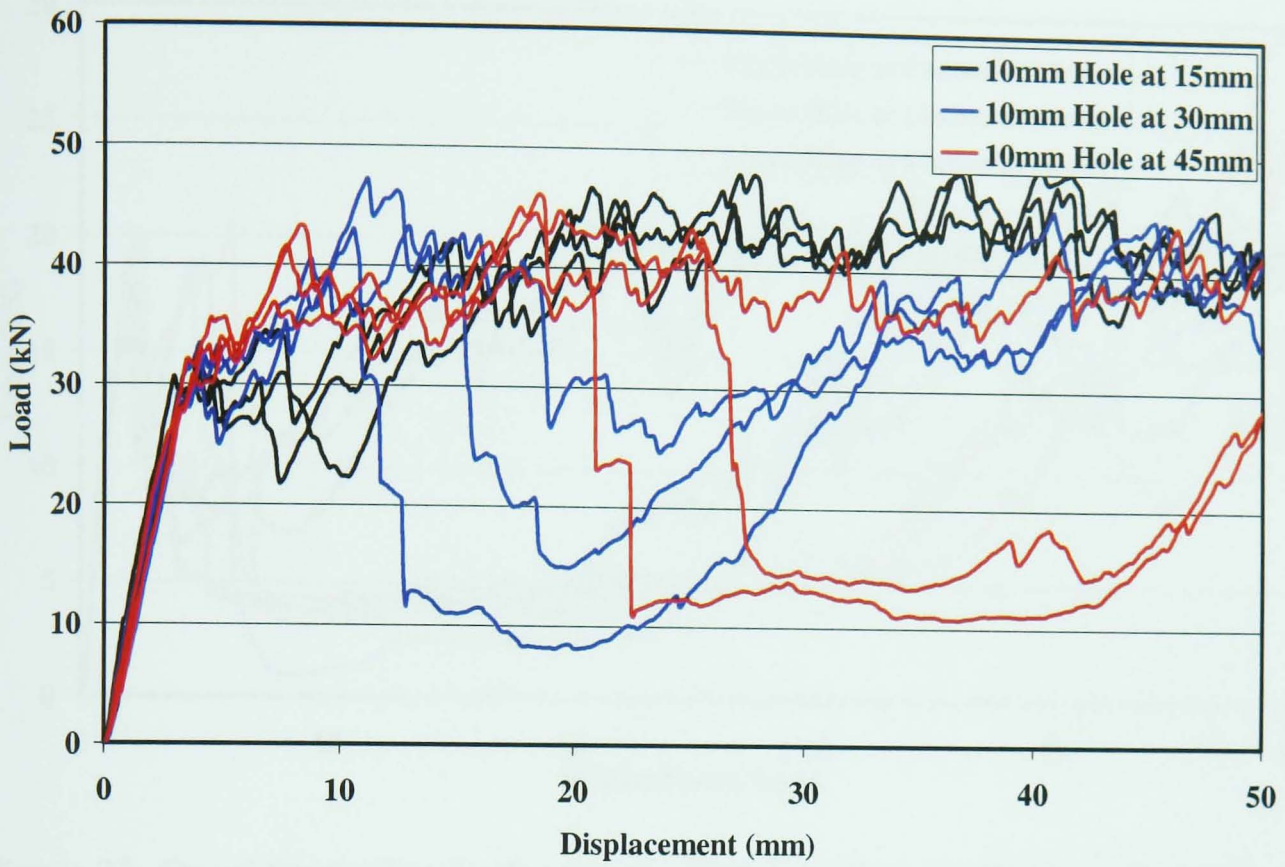


Figure 21: Quasi-Static Results for Square Tubes (t=4mm) with Holes Positioned Axially along the Face of Tube

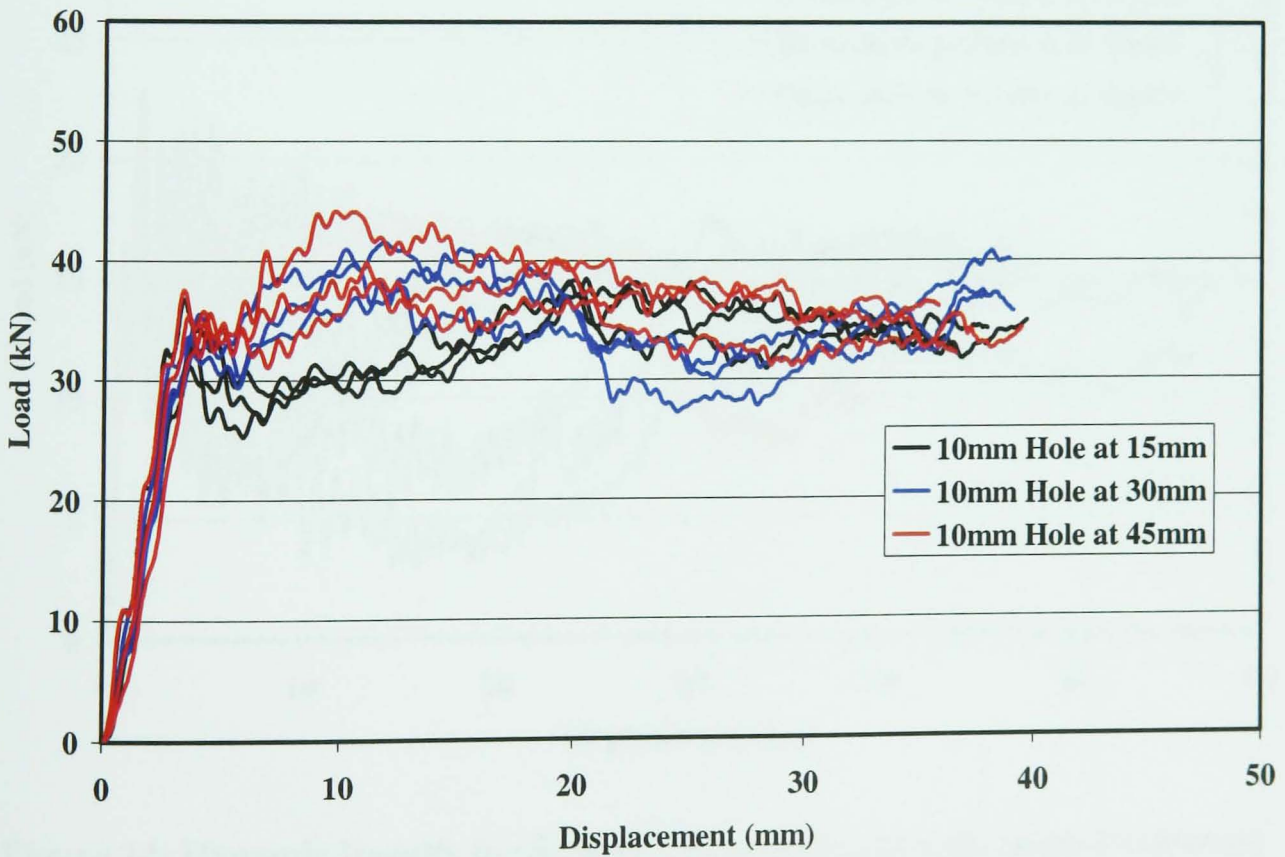


Figure 22: Dynamic Results for Square Tubes (t=4mm) with Holes Positioned Axially along the Face of Tube

Square (t=2mm) on Corner

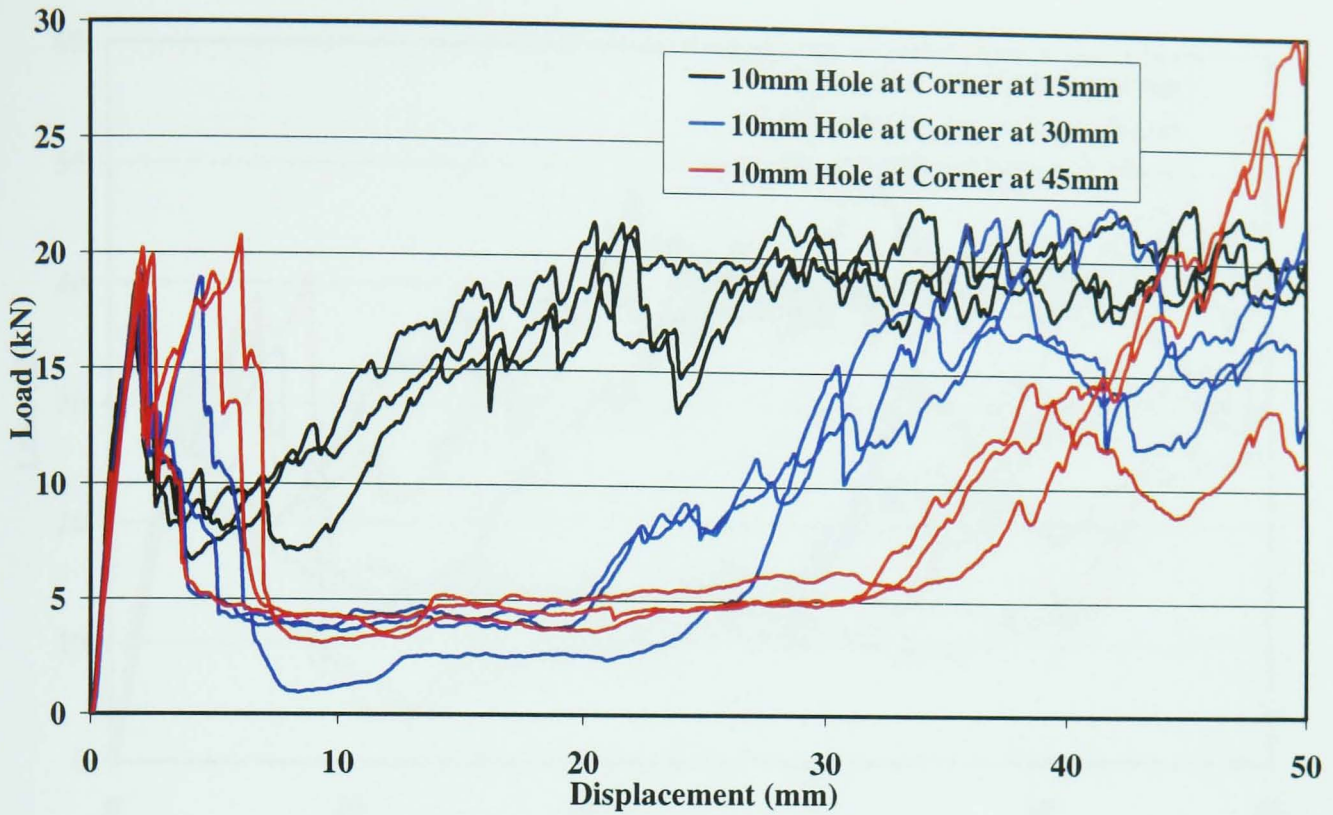


Figure 23: Quasi-Static Results for Square Tubes (t=2mm) with Holes Positioned Axially along the Corner of Tube

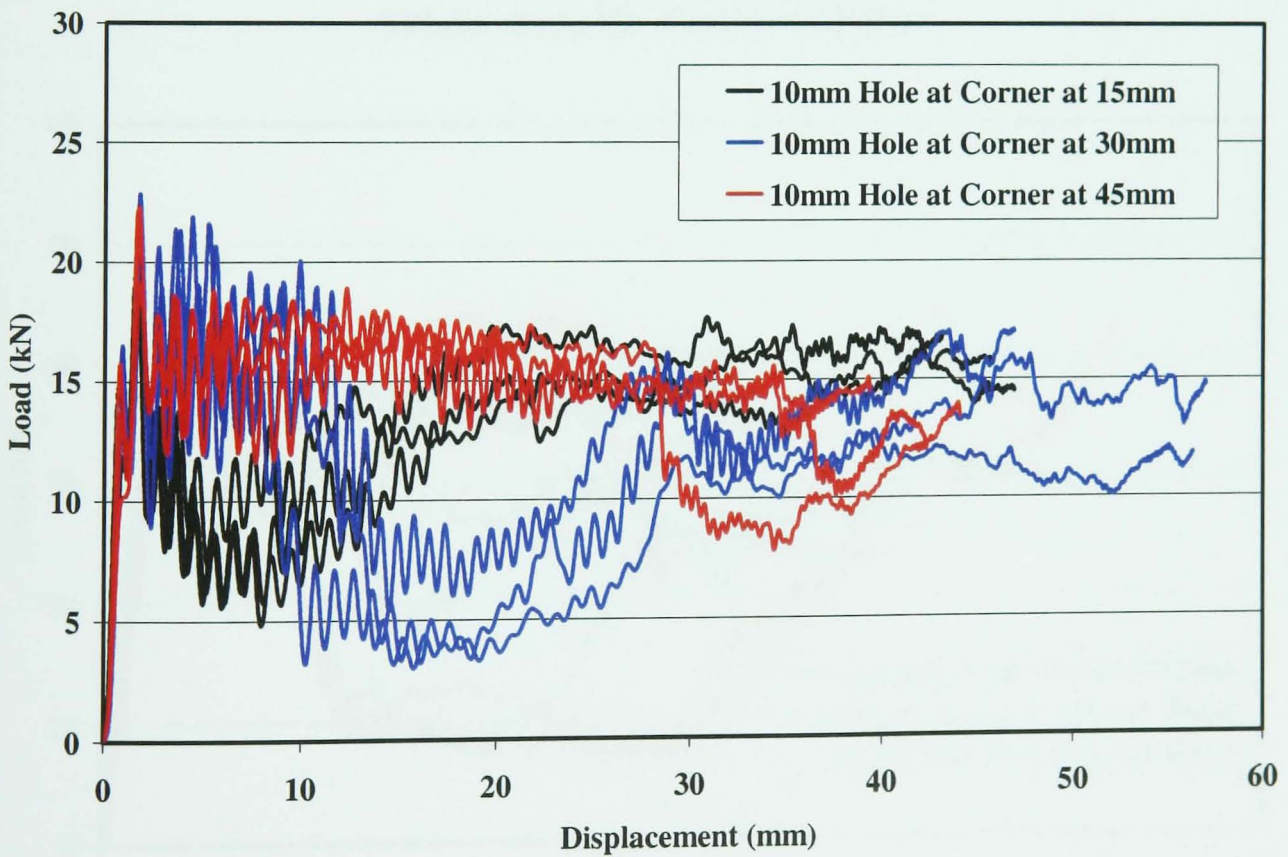


Figure 24: Dynamic Results for Square Tubes (t=2mm) with Holes Positioned Axially along the Corner of Tube

Square (t=4mm) on Corner

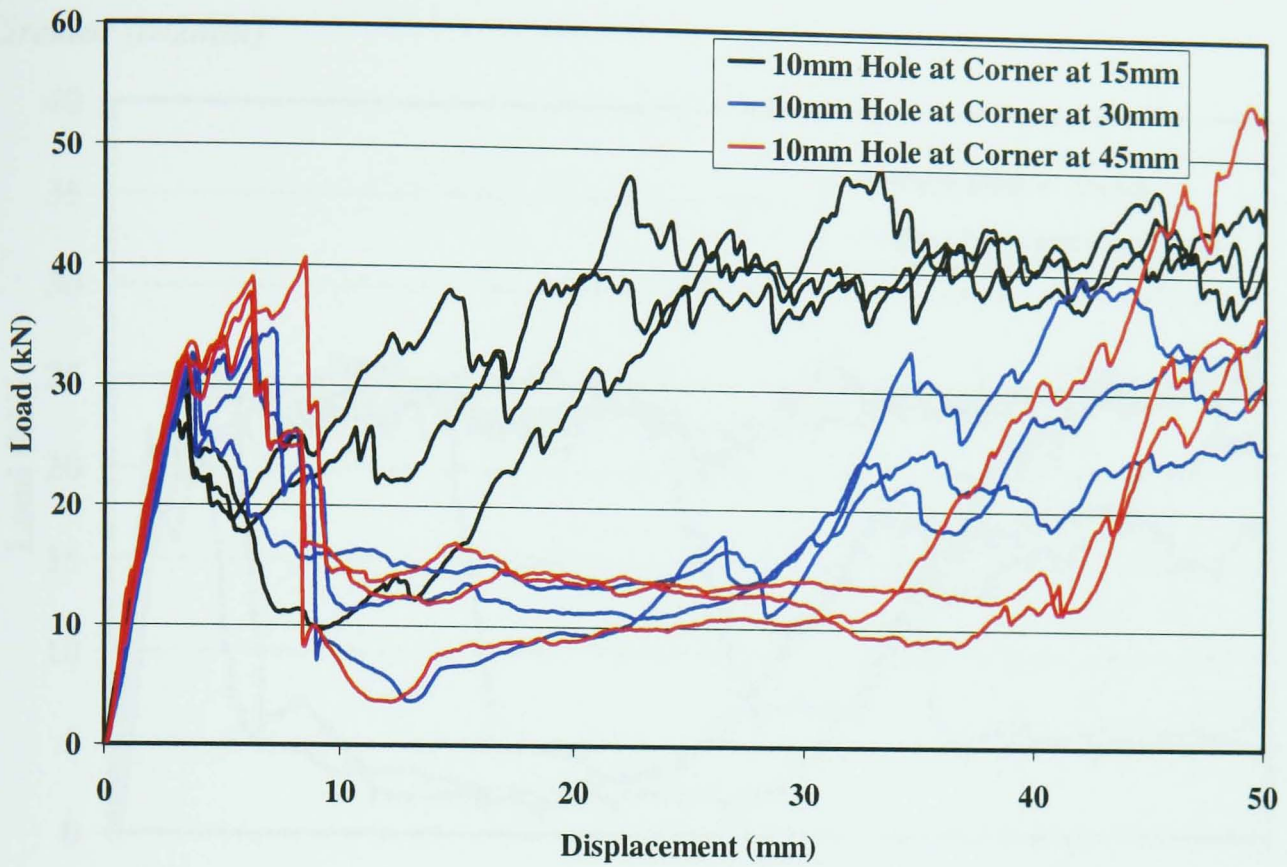


Figure 25: Quasi-Static Results for Square Tubes (t=4mm) with Holes Positioned Axially along the Corner of Tube

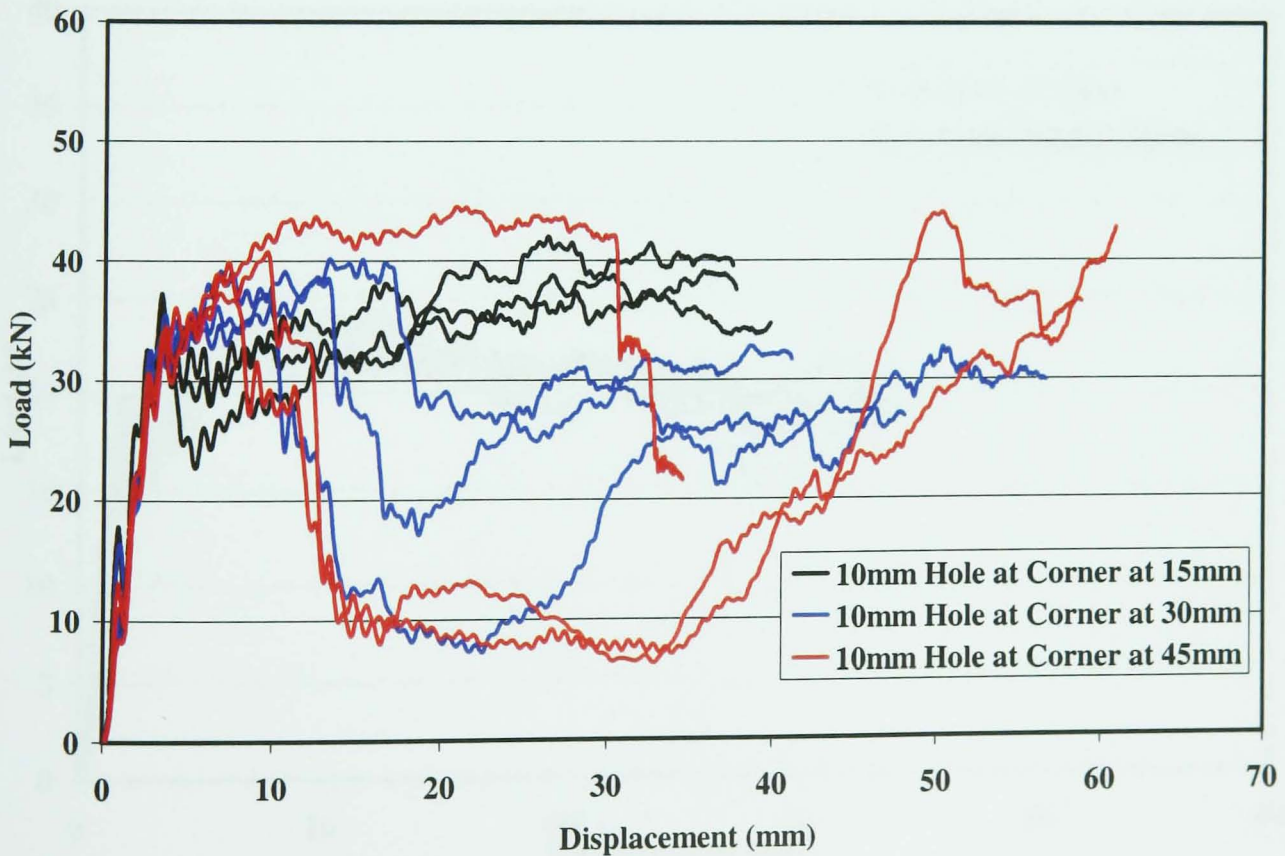


Figure 26: Dynamic Results for Square Tubes (t=4mm) with Holes Positioned Axially along the Corner of Tube

9.2.3 Multiple Holes

Circular ($t=2\text{mm}$)

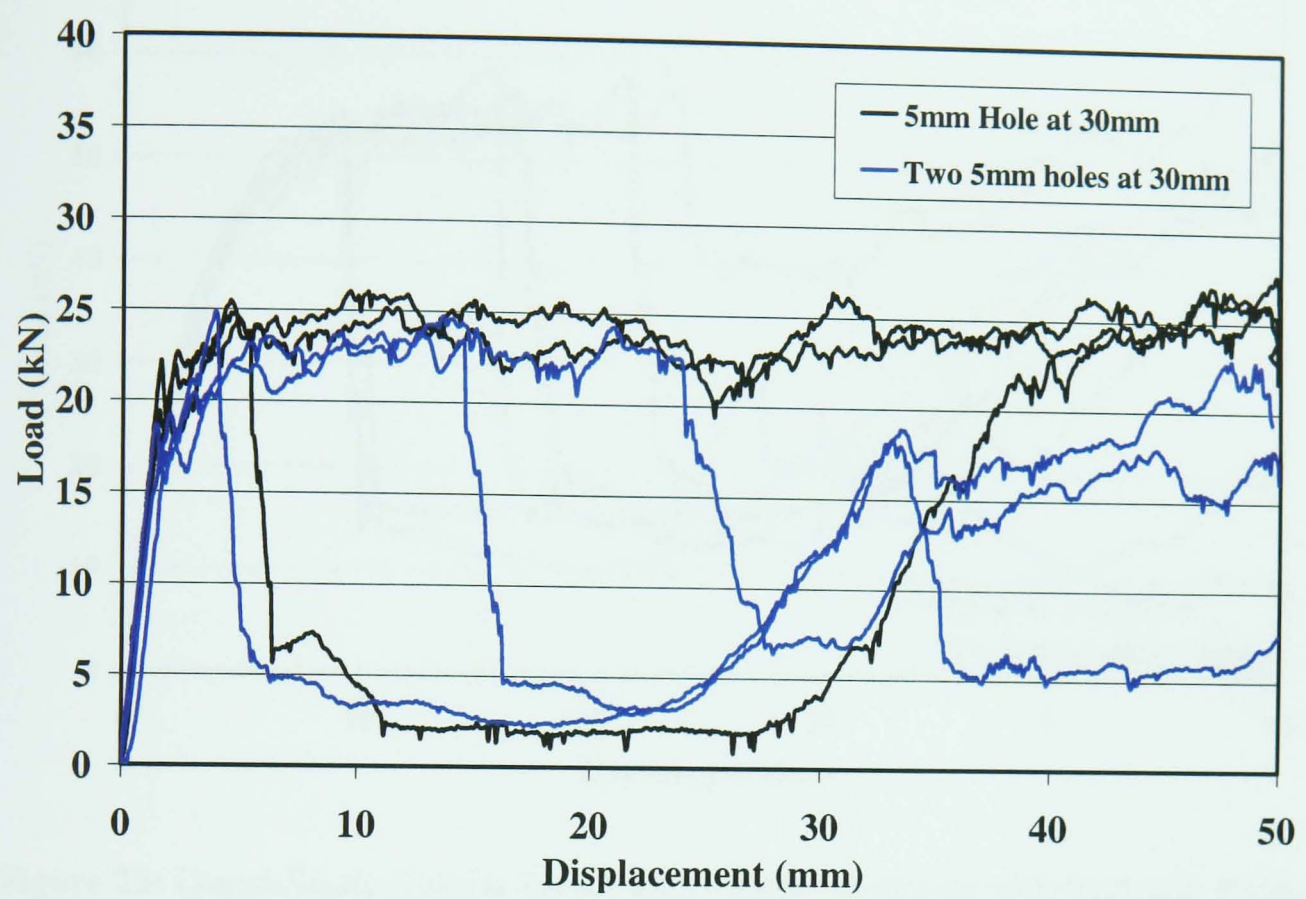


Figure 27: Quasi-Static Results for Circular Tubes ($t=2\text{mm}$) with Multiple Holes

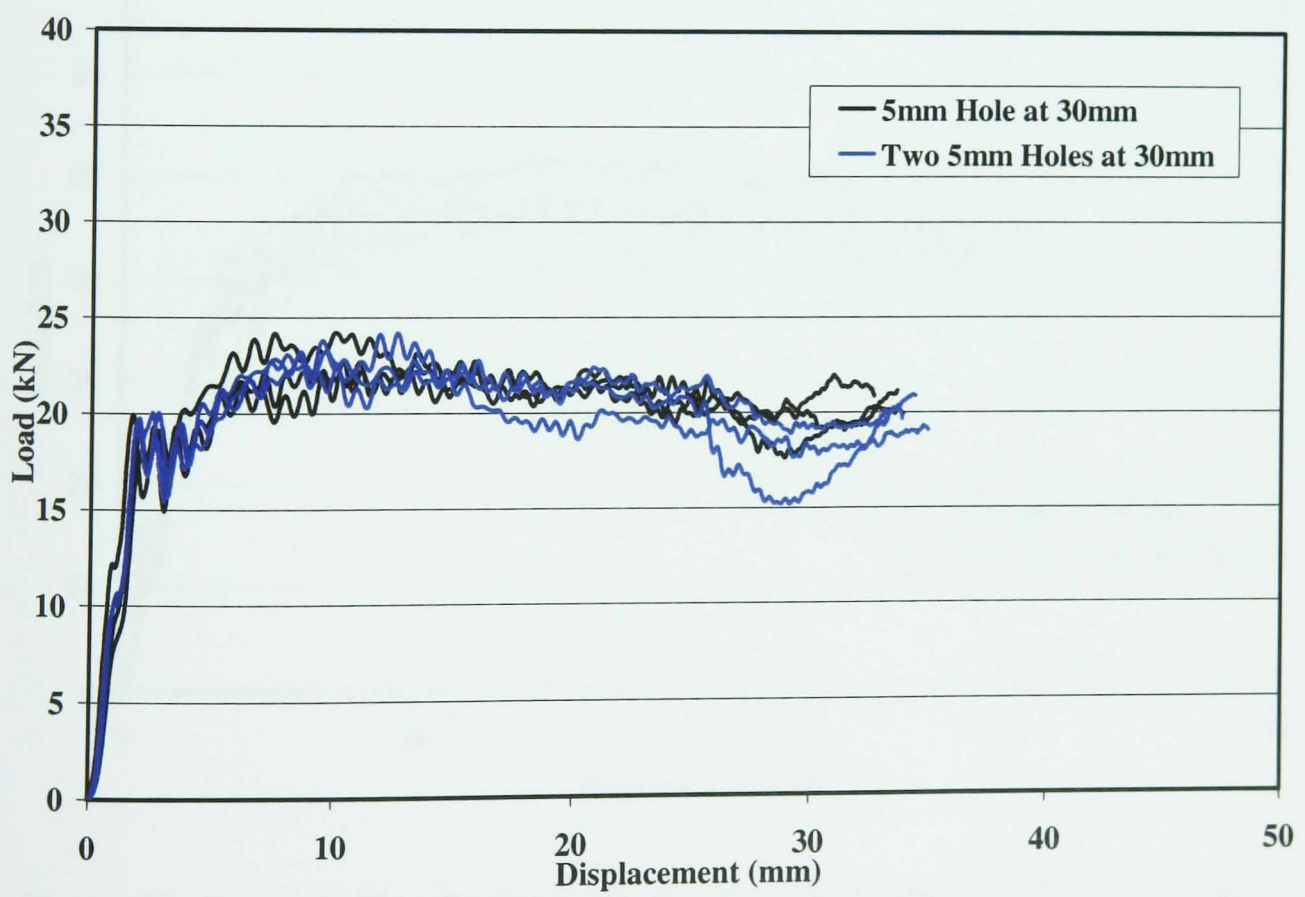


Figure 28: Dynamic Results for Circular Tubes ($t=2\text{mm}$) with Multiple Holes

Circular (t=4mm)

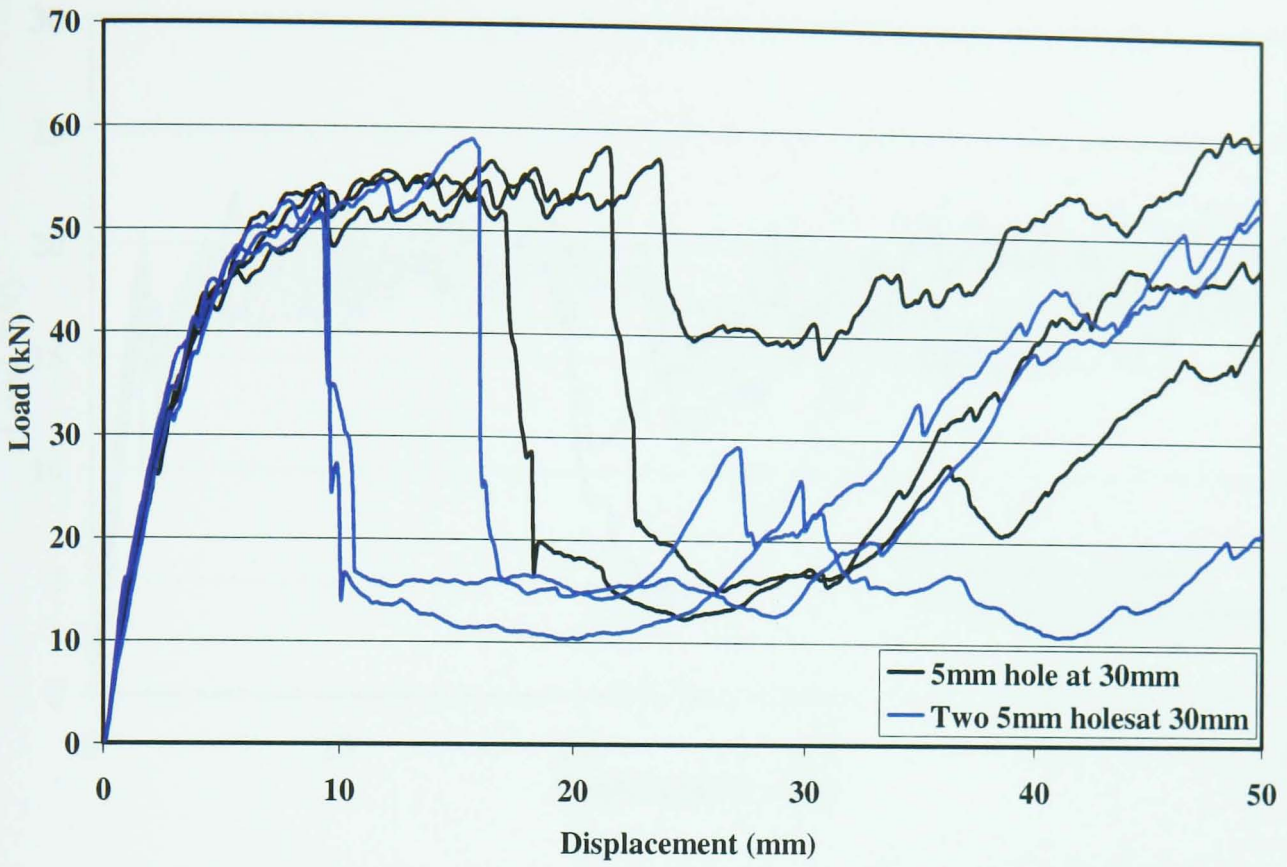


Figure 29: Quasi-Static Results for Circular Tubes (t=4mm) with Multiple Holes

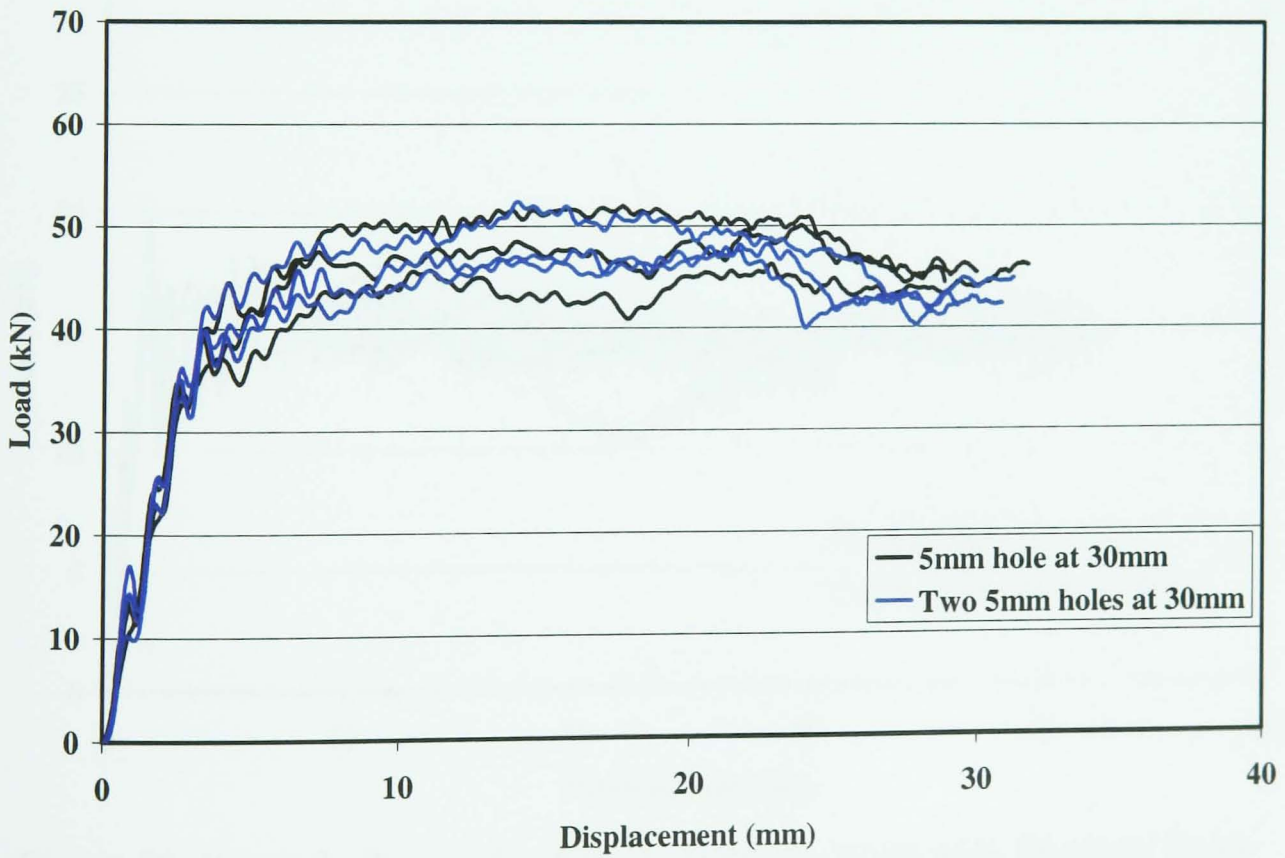


Figure 30: Dynamic Results for Circular Tubes (t=4mm) with Multiple Holes

Square ($t=2\text{mm}$)

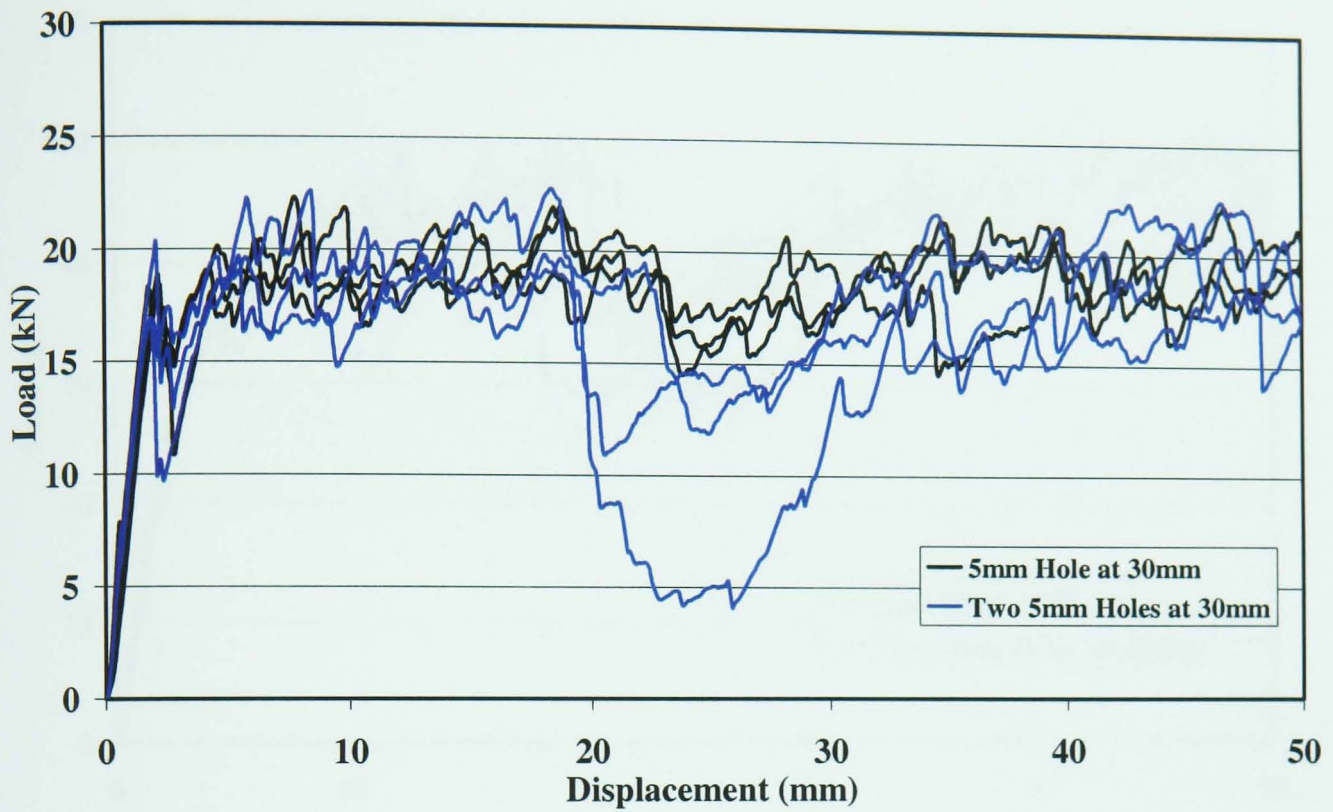


Figure 31: Quasi-Static Results for Square Tubes ($t=2\text{mm}$) with Multiple Holes

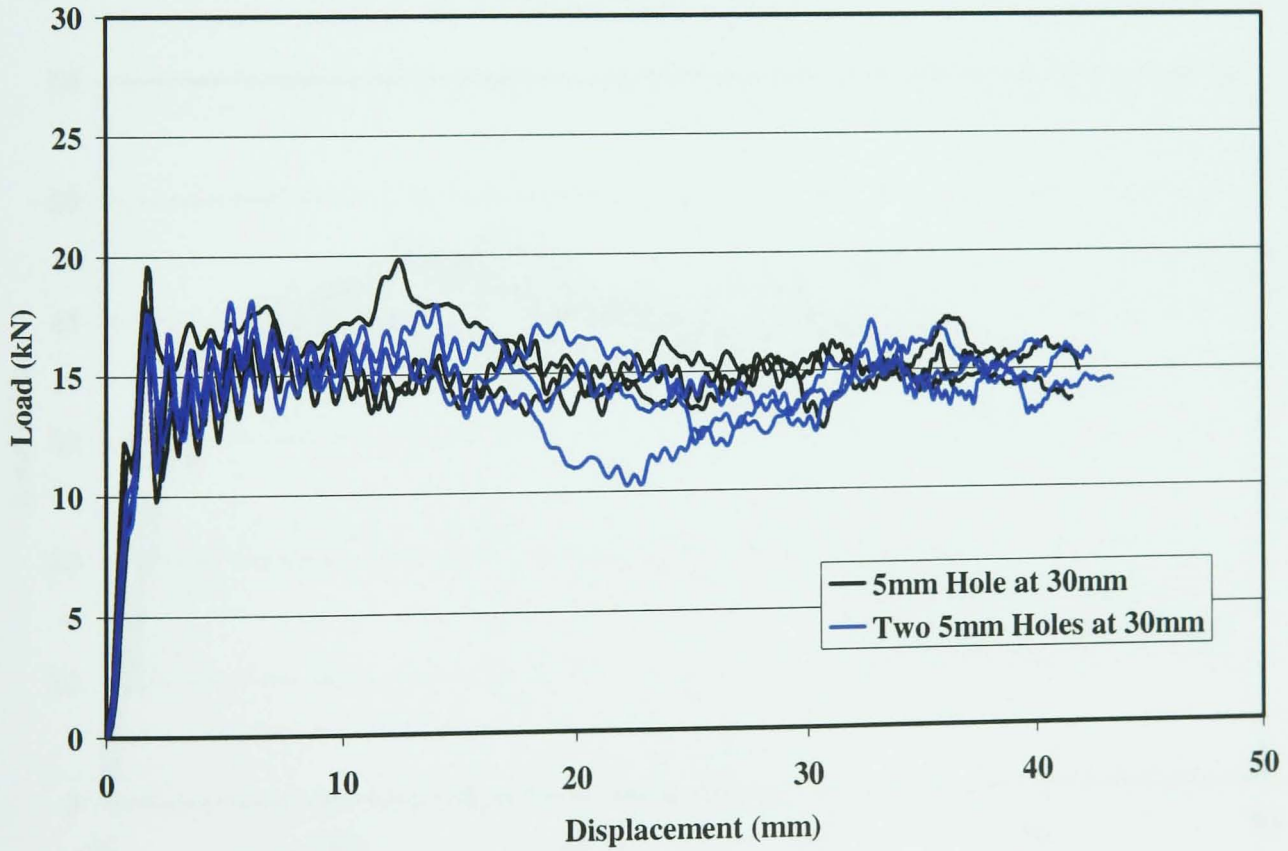


Figure 32: Dynamic Results for Square Tubes ($t=2\text{mm}$) with Multiple Holes

Square (t=4mm)

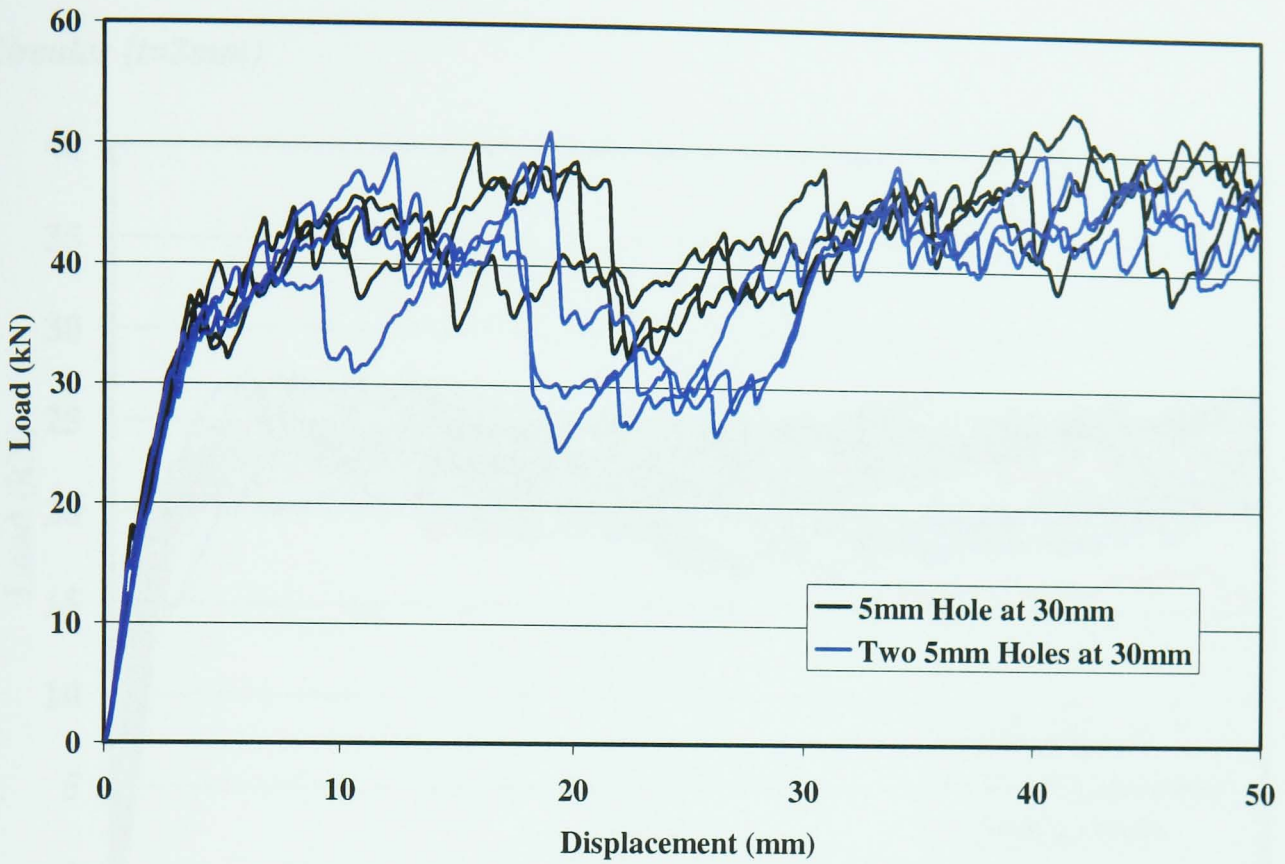


Figure 33: Quasi-Static Results for Square Tubes (t=4mm) with Multiple Holes

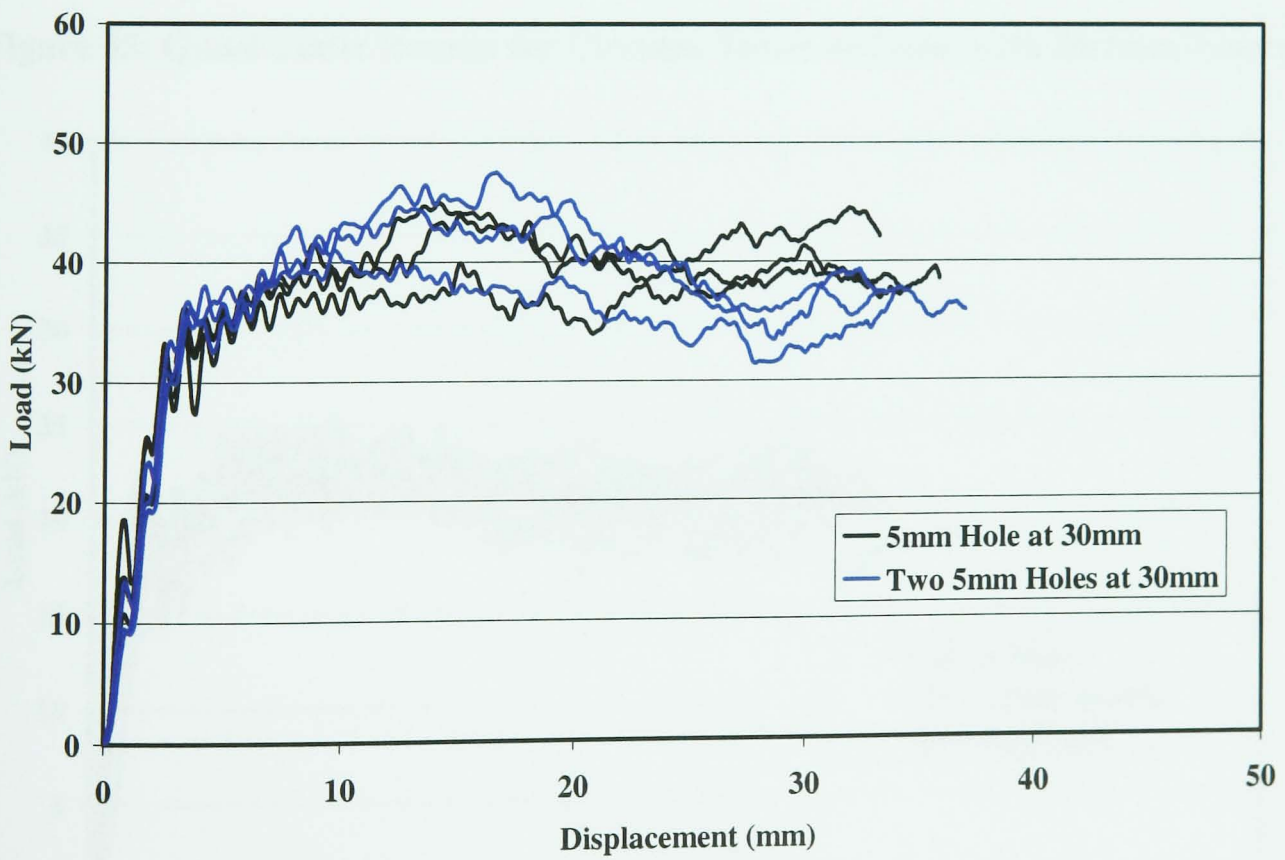


Figure 34: Dynamic Results for Square Tubes (t=4mm) with Multiple Holes

9.3 Melinex Inserts

Circular (t=2mm)

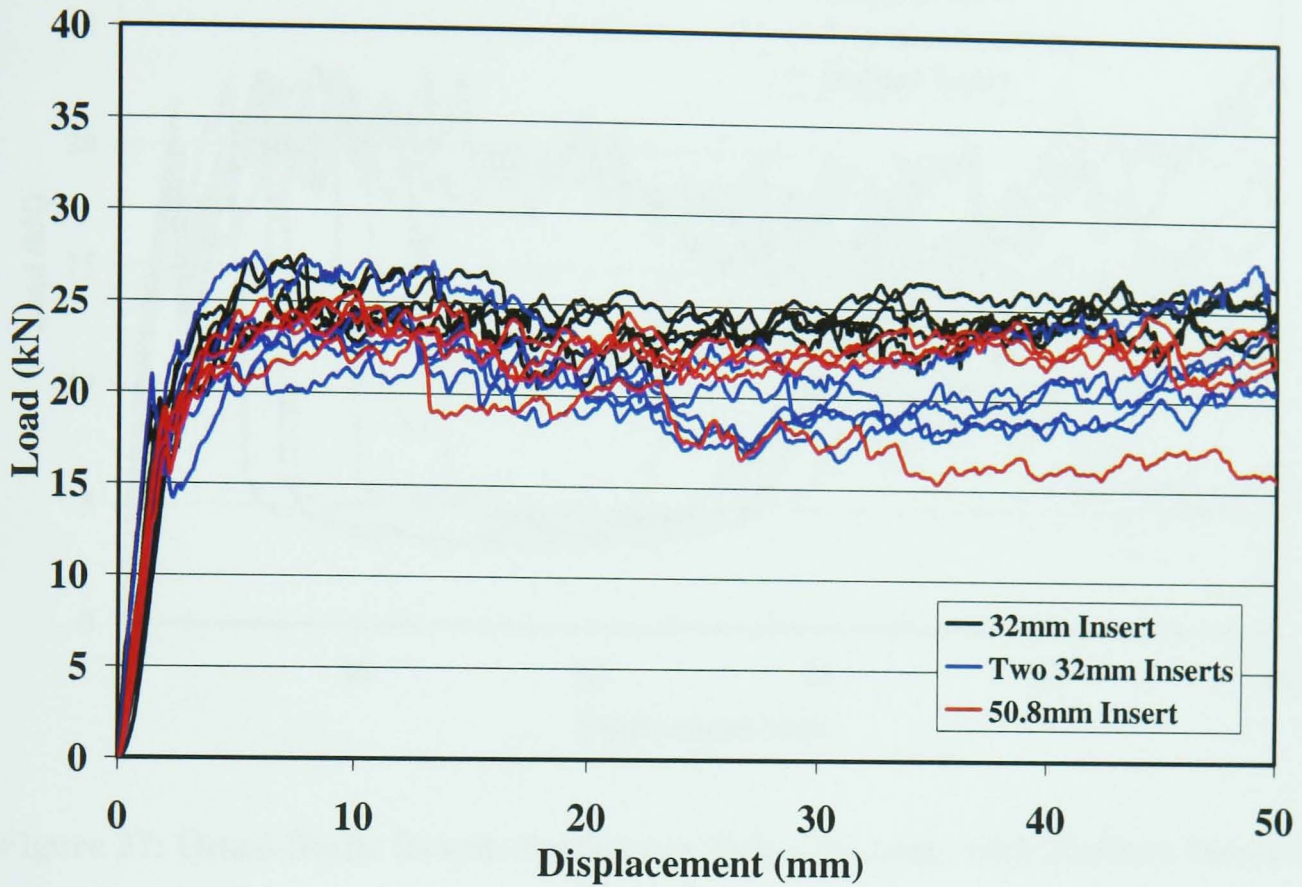


Figure 35: Quasi-Static Results for Circular Tubes (t=2mm) with Melinex Inserts

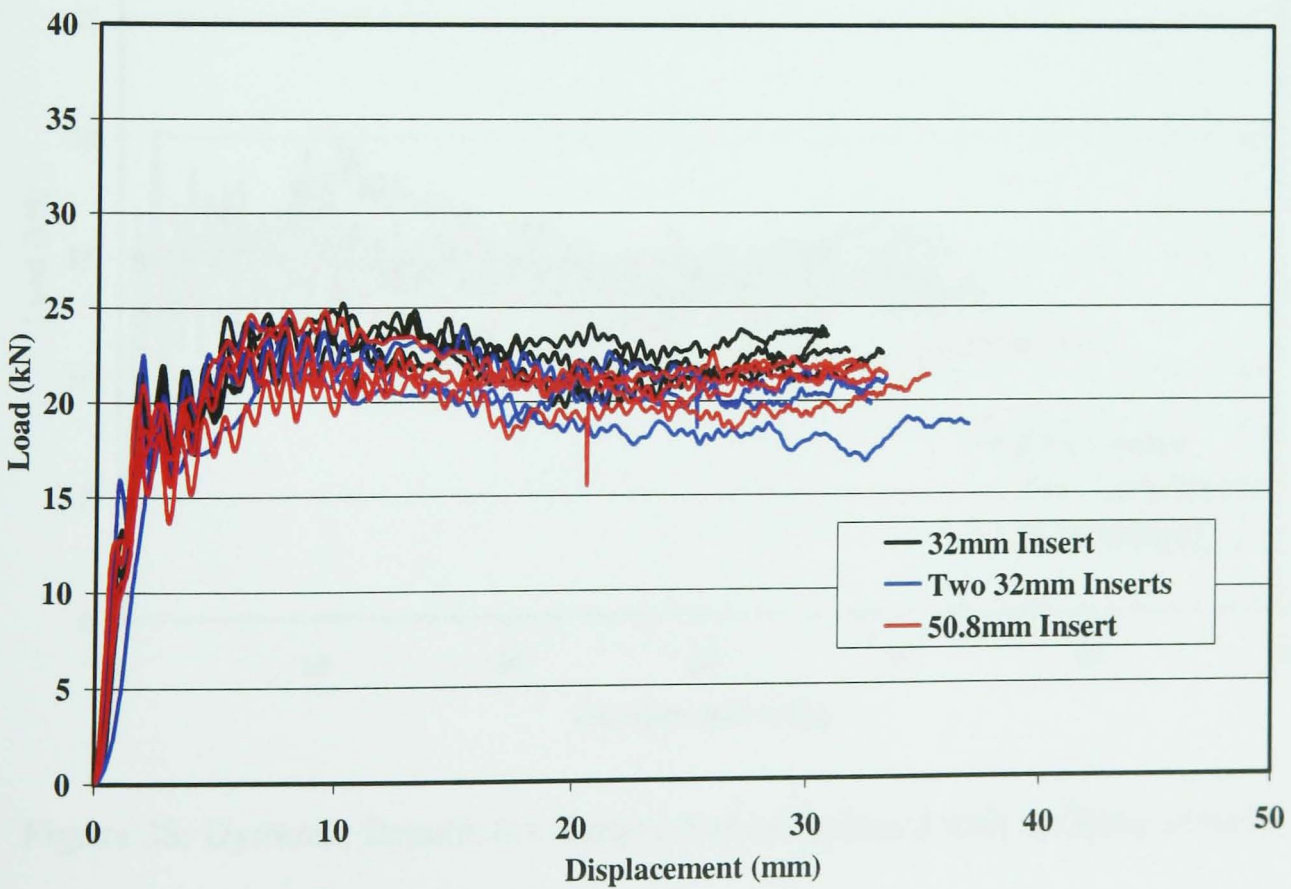


Figure 36: Dynamic Results for Circular Tubes (t=2mm) with Melinex Inserts

Square (t=2mm)

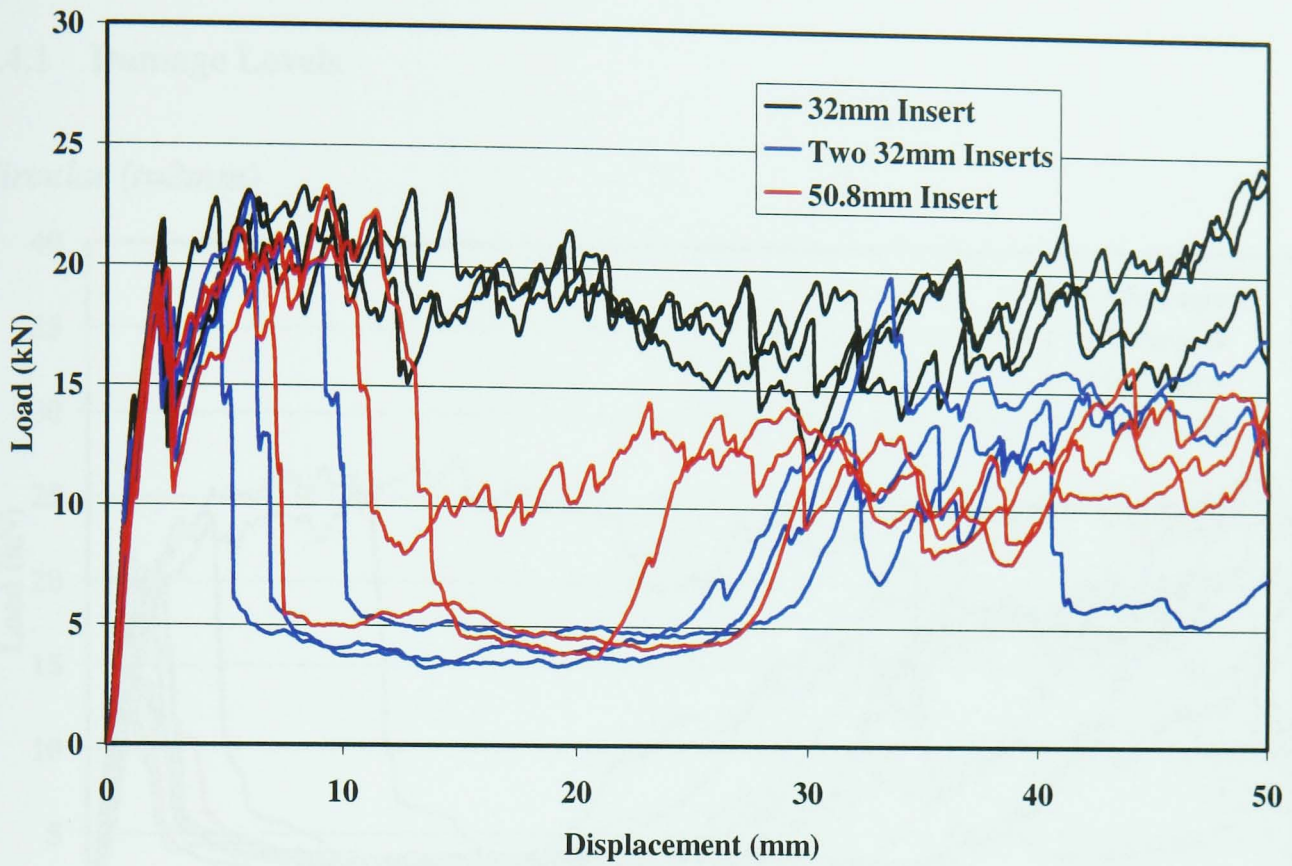


Figure 37: Quasi-Static Results for Square Tubes (t=2mm) with Melinex Inserts

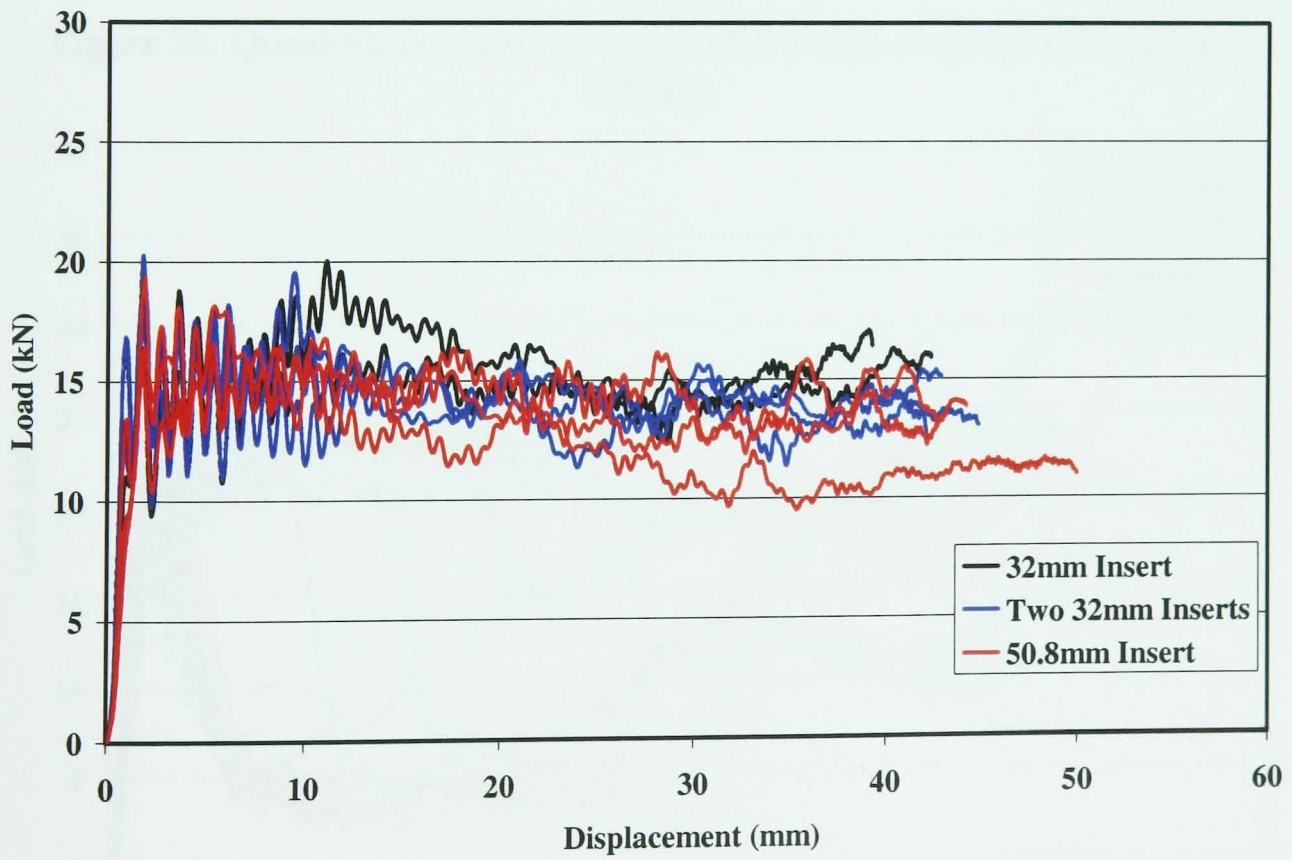


Figure 38: Dynamic Results for Square Tubes (t=2mm) with Melinex Inserts

9.4 Impact Damage

9.4.1 Damage Levels

Circular (t=2mm)

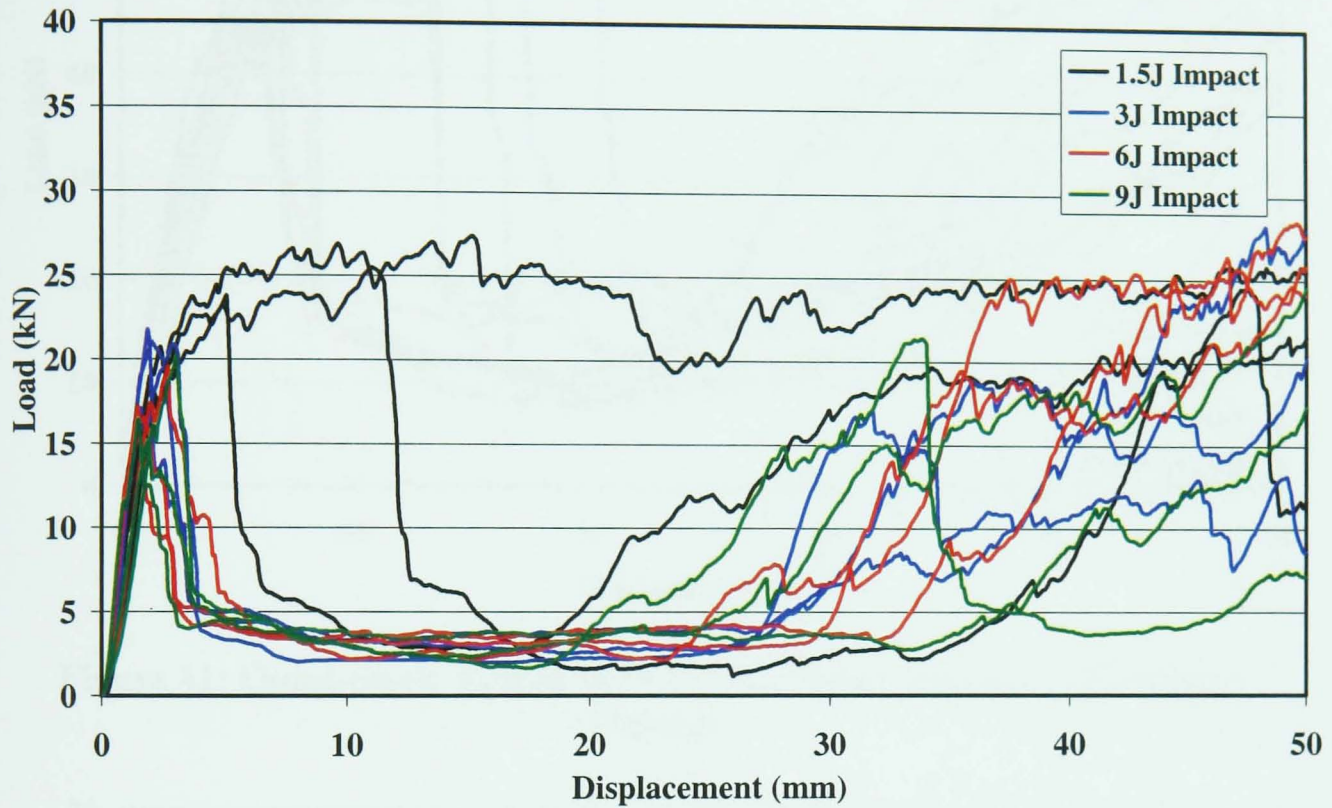


Figure 39: Quasi-Static Results for Circular Tubes (t=2mm) with Impact Damage

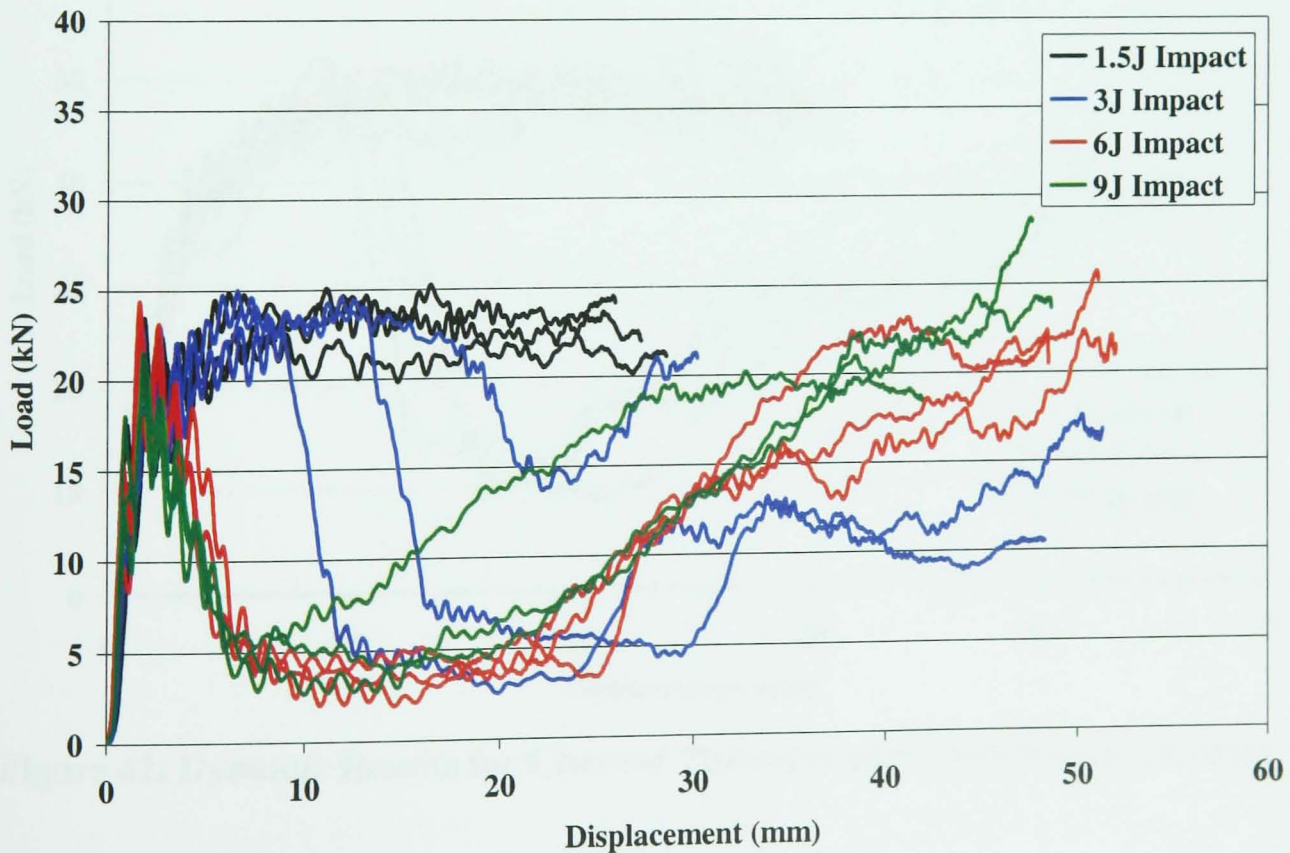


Figure 40: Dynamic Results for Circular Tubes (t=2mm) with Impact Damage

Circular (t=4mm)

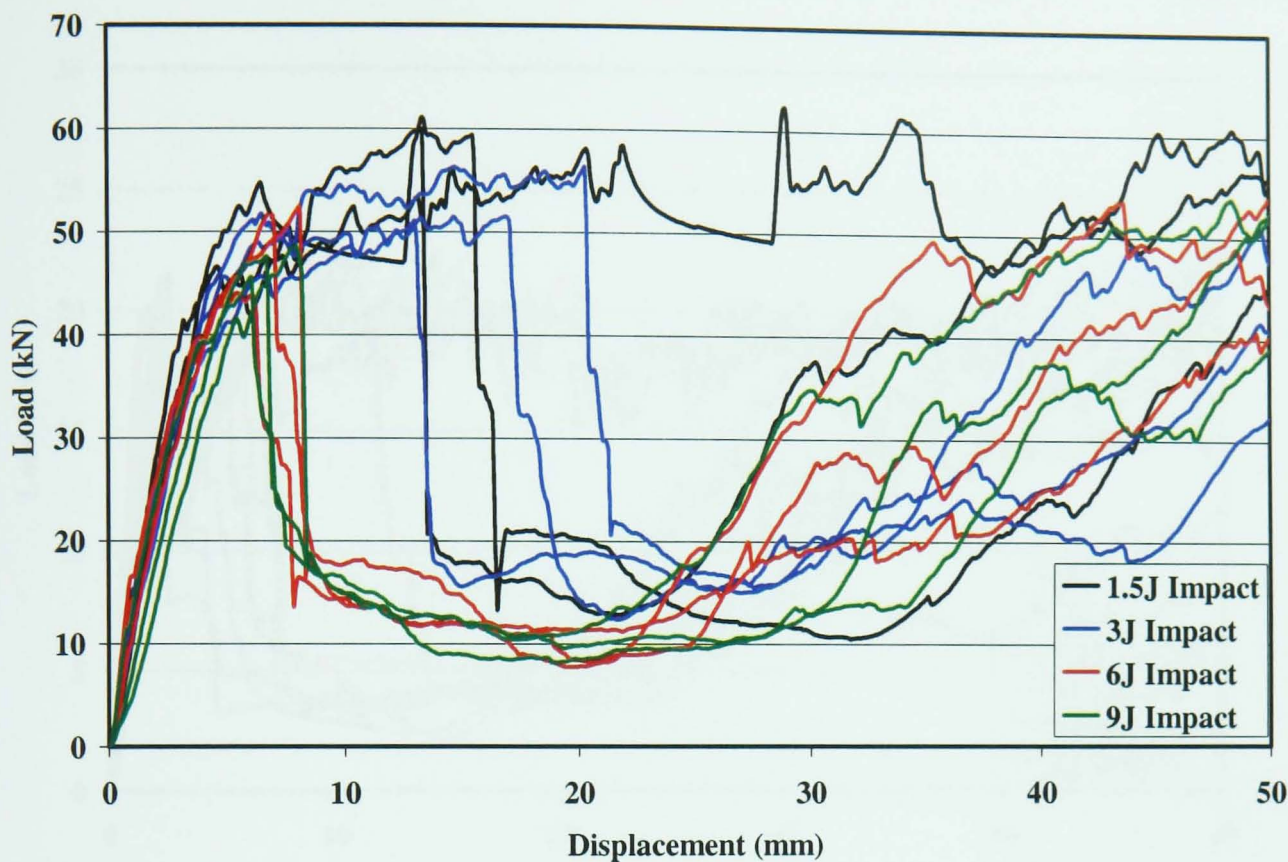


Figure 41: Quasi-Static Results for Circular Tubes (t=4mm) with Impact Damage

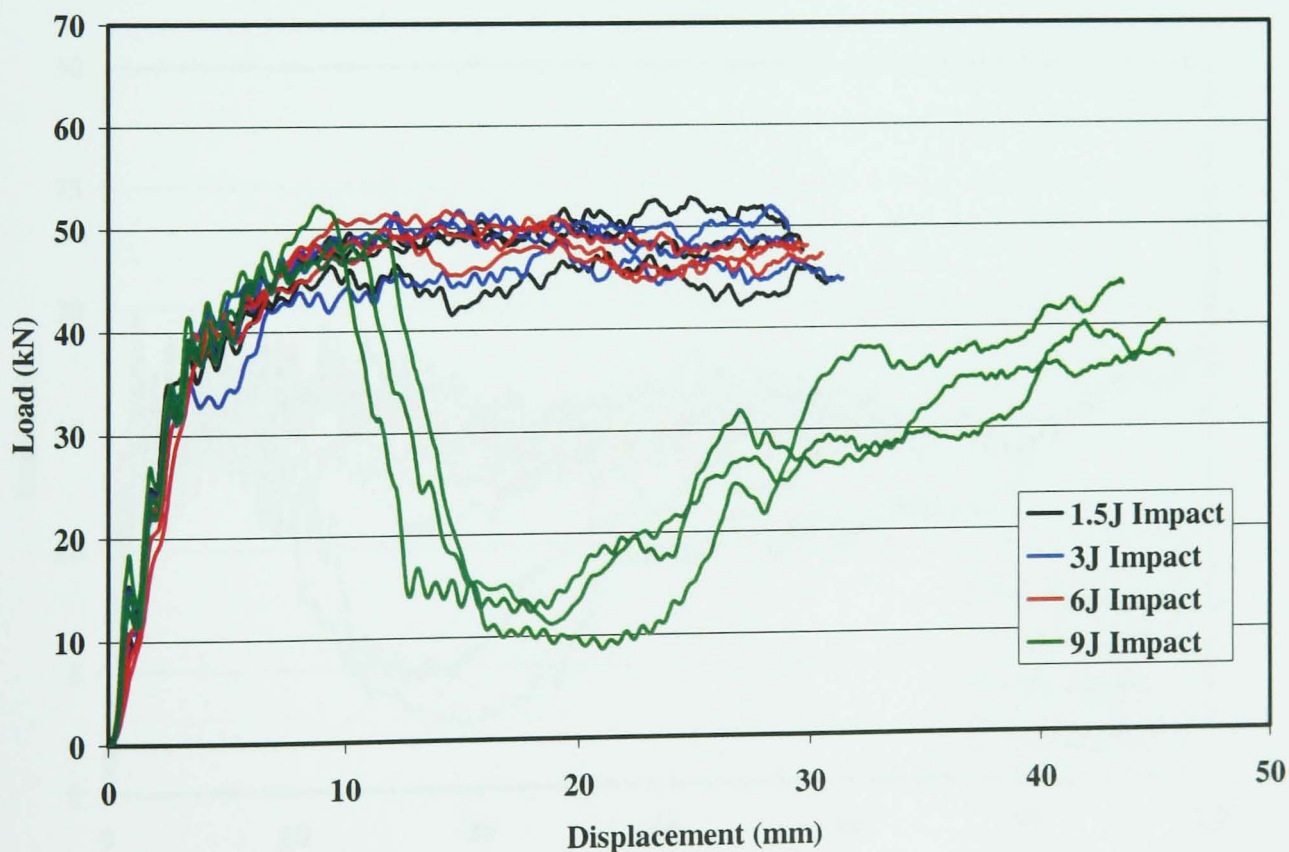


Figure 42: Dynamic Results for Circular Tubes (t=4mm) with Impact Damage

Square on Face (t=2mm)

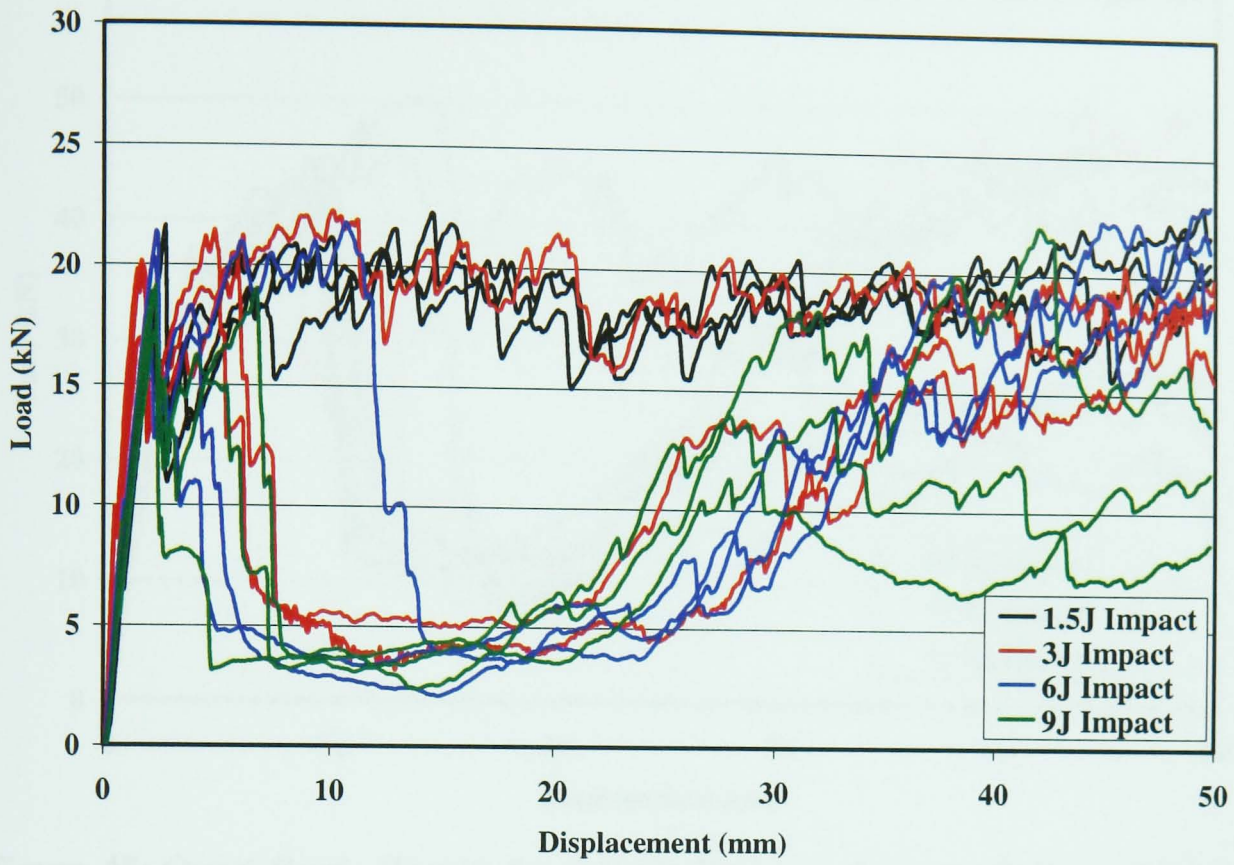


Figure 43: Quasi-Static Results for Square Tubes (t=2mm) with Impact Damage on the Face

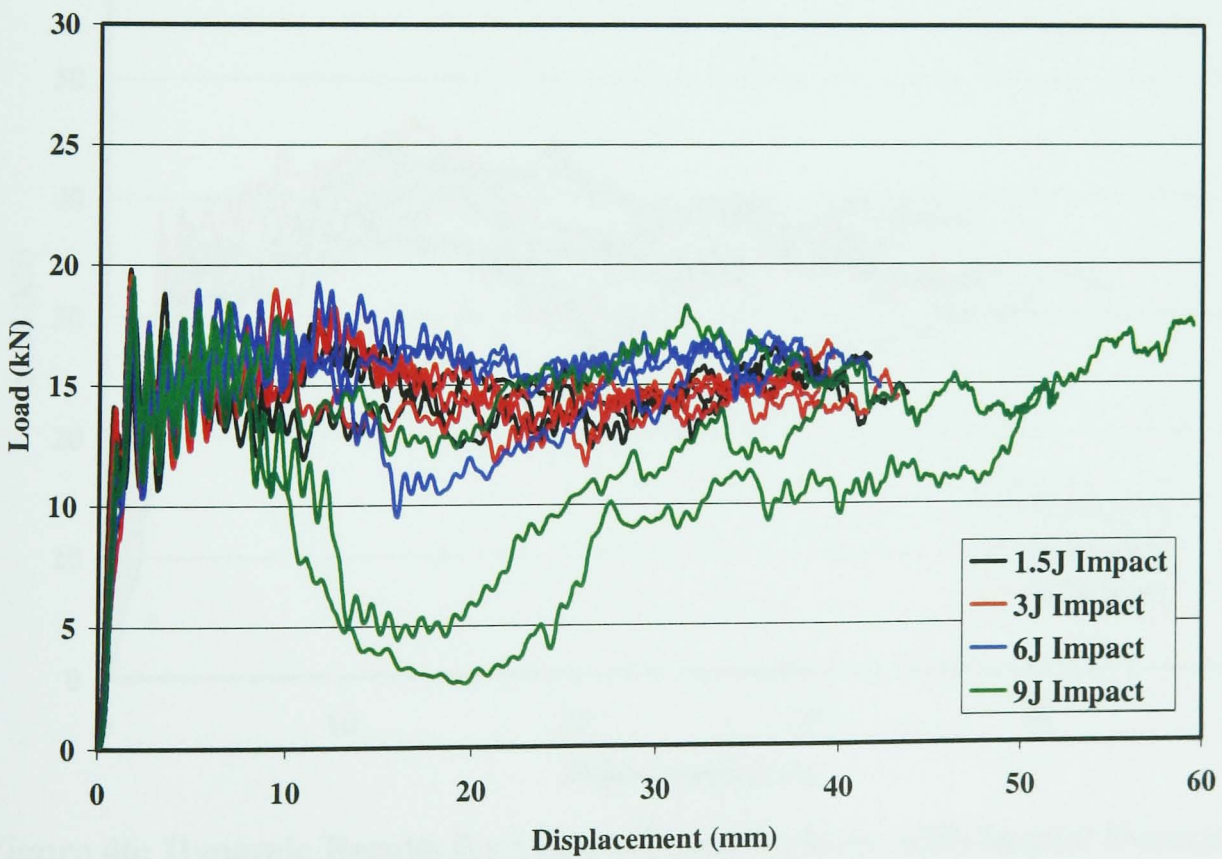


Figure 44: Dynamic Results for Square Tubes (t=2mm) with Impact Damage on the Face

Square on Face (t=4mm)

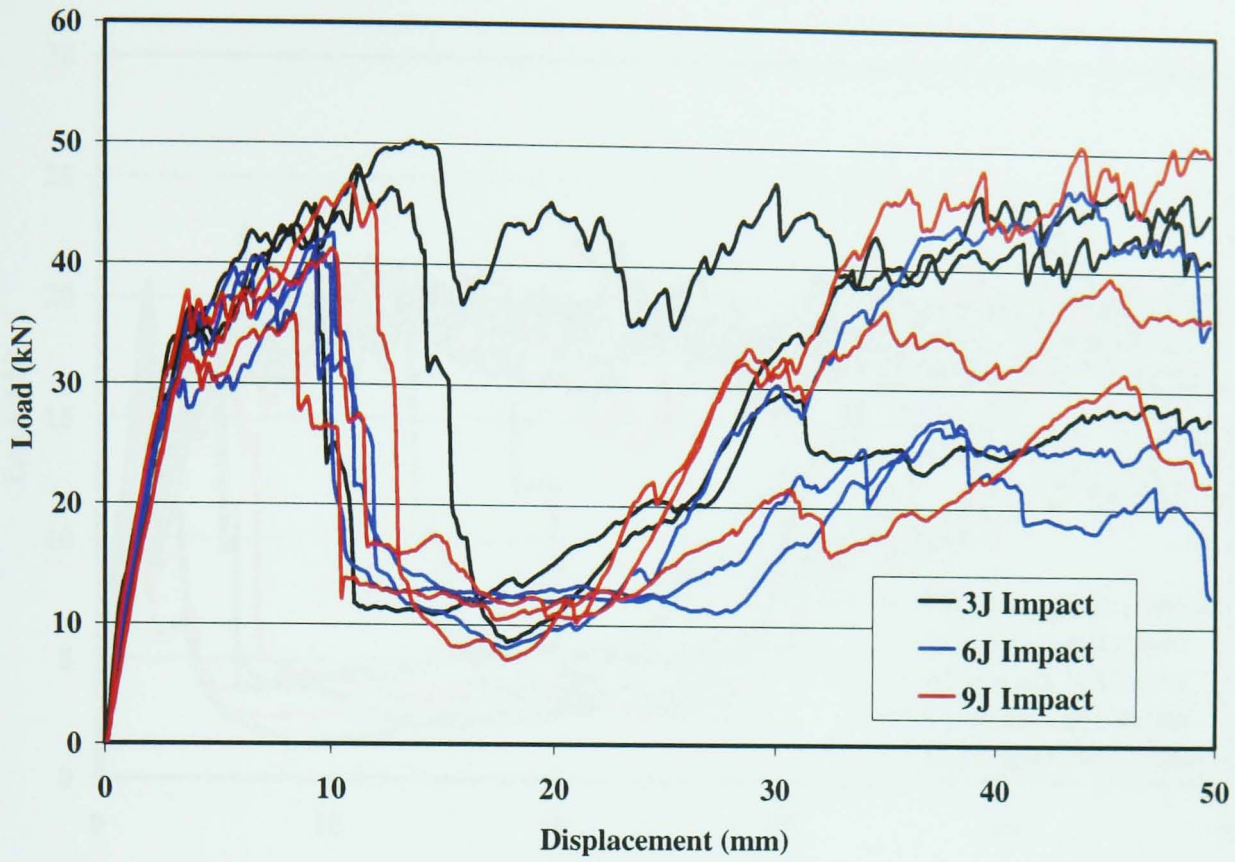


Figure 45: Quasi-Static Results for Square Tubes (t=4mm) with Impact Damage on the Face

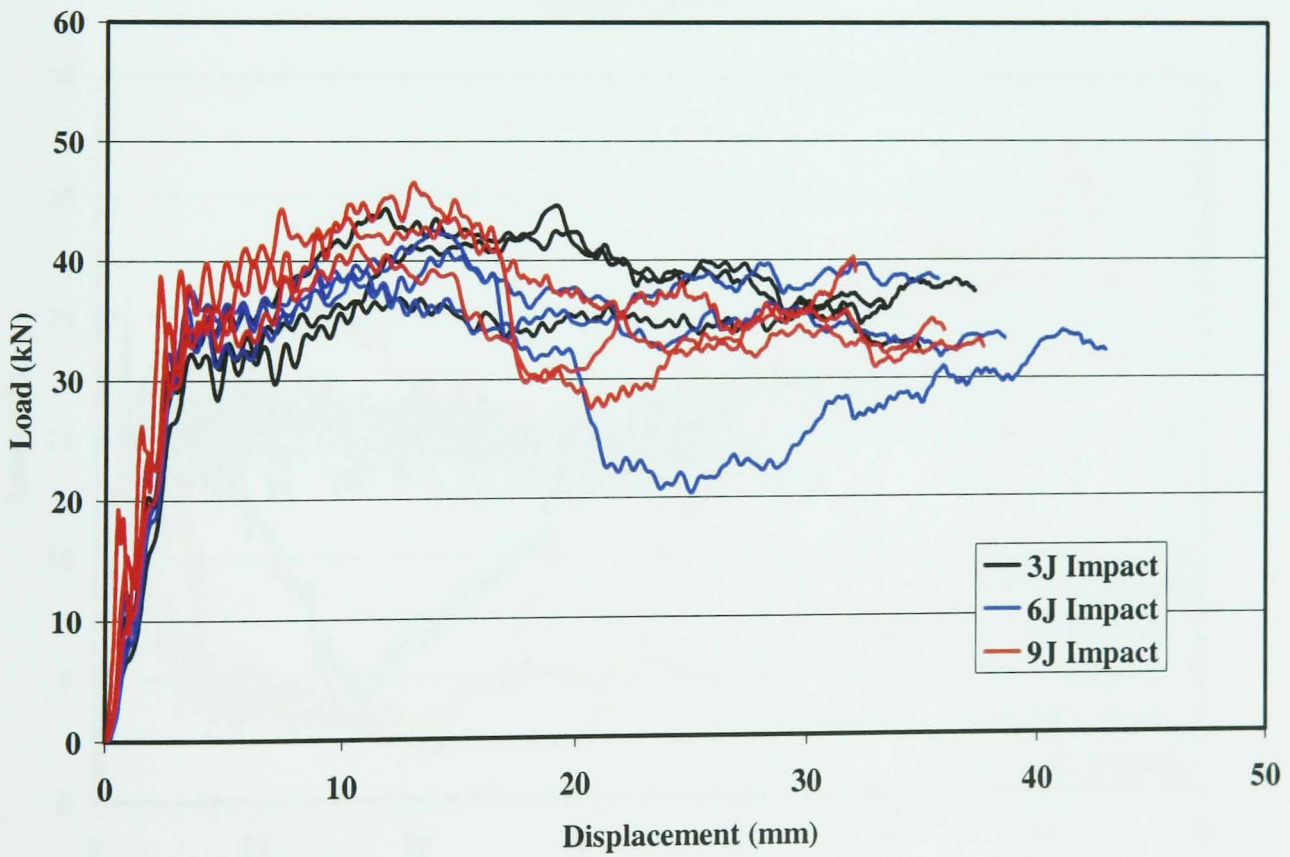


Figure 46: Dynamic Results for Square Tubes (t=4mm) with Impact Damage on the Face

Square on Corner (t=2mm)

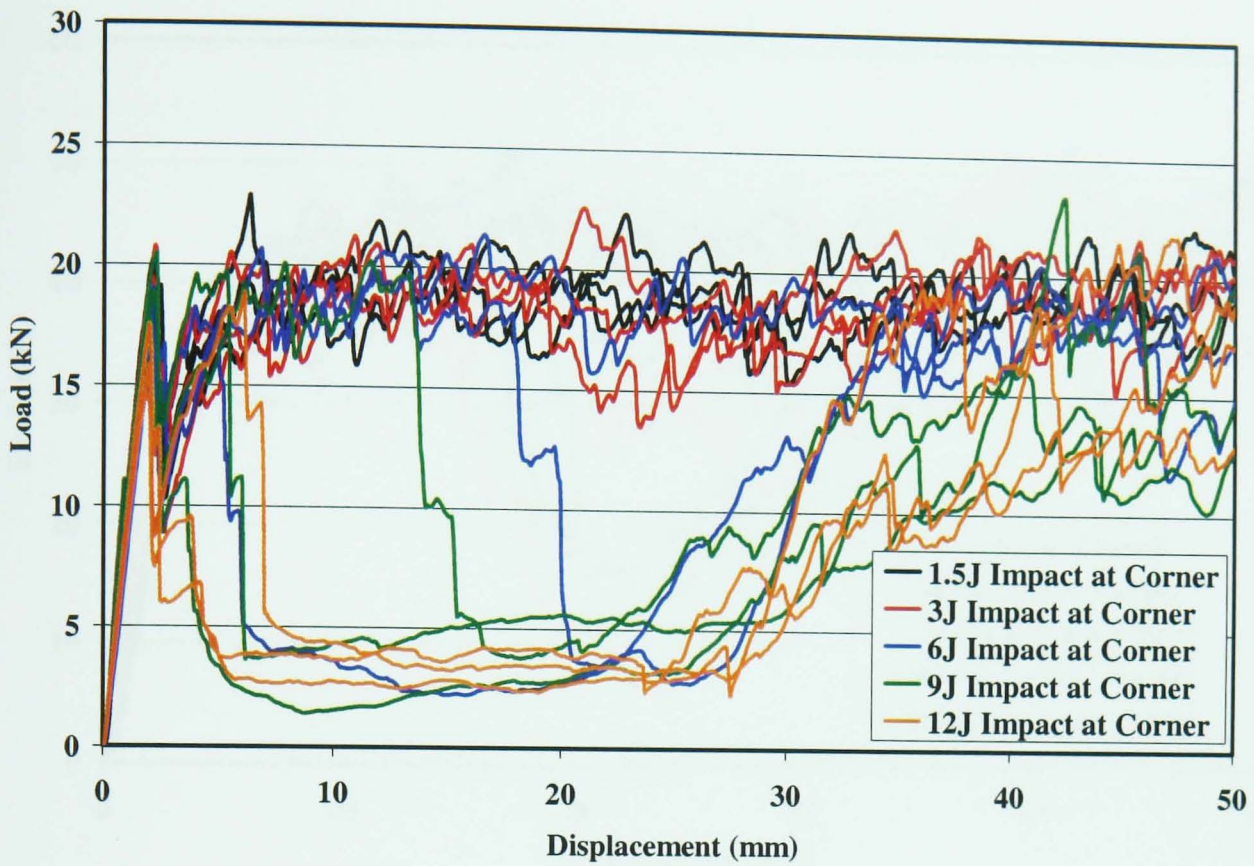


Figure 47: Quasi-Static Results for Square Tubes (t=2mm) with Impact Damage at the Corner

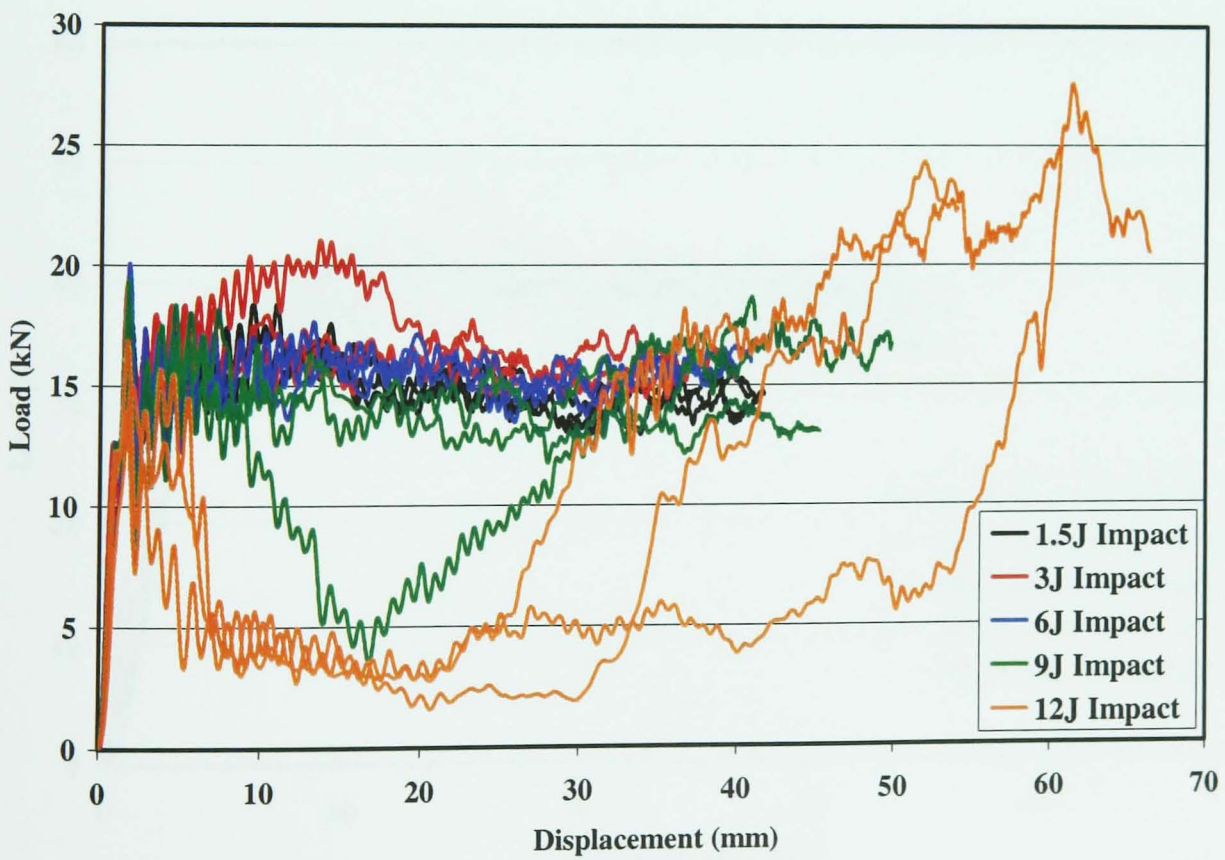


Figure 48: Dynamic Results for Square Tubes (t=2mm) with Impact Damage at the Corner

Square on Corner (t=4mm)

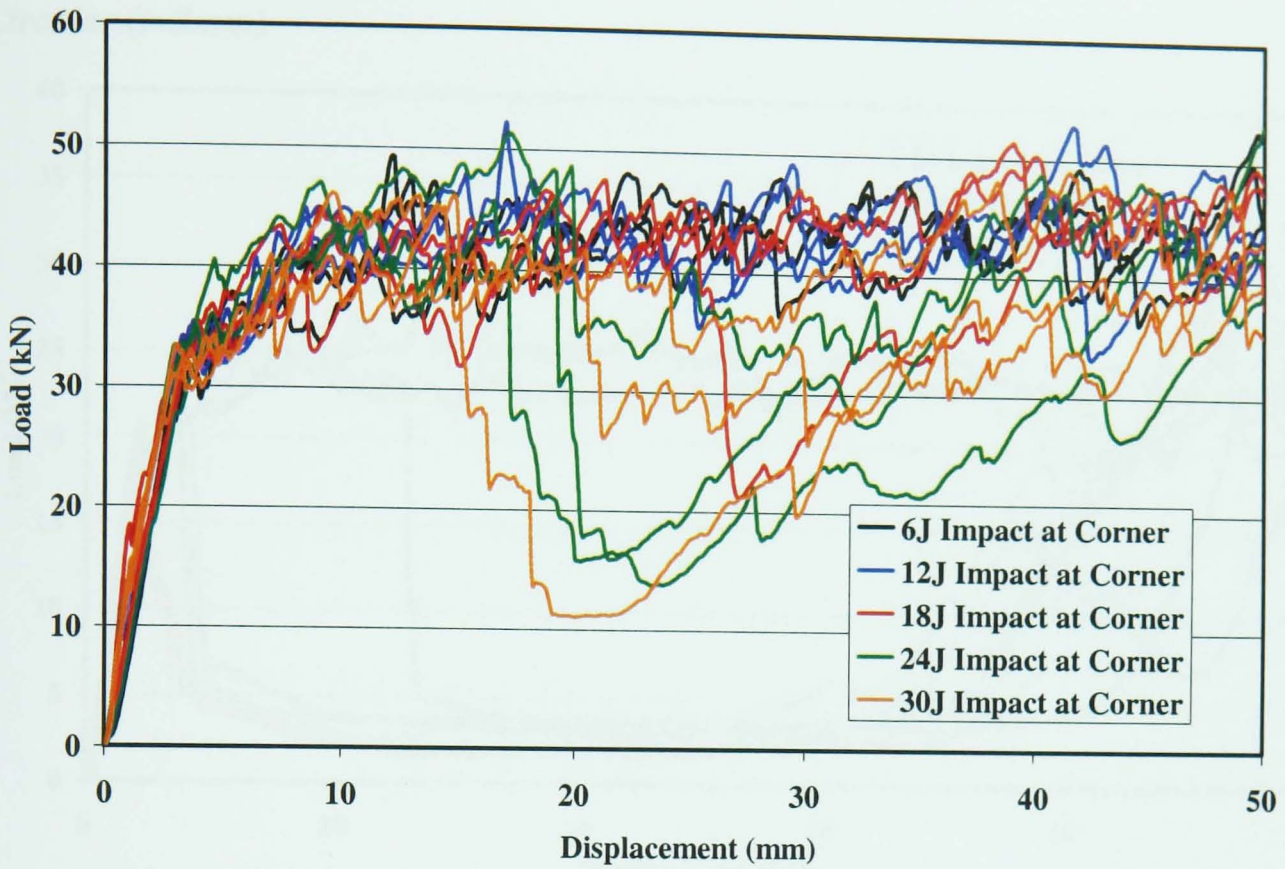


Figure 49: Quasi-Static Results for Square Tubes (t=4mm) with Impact Damage at the Corner

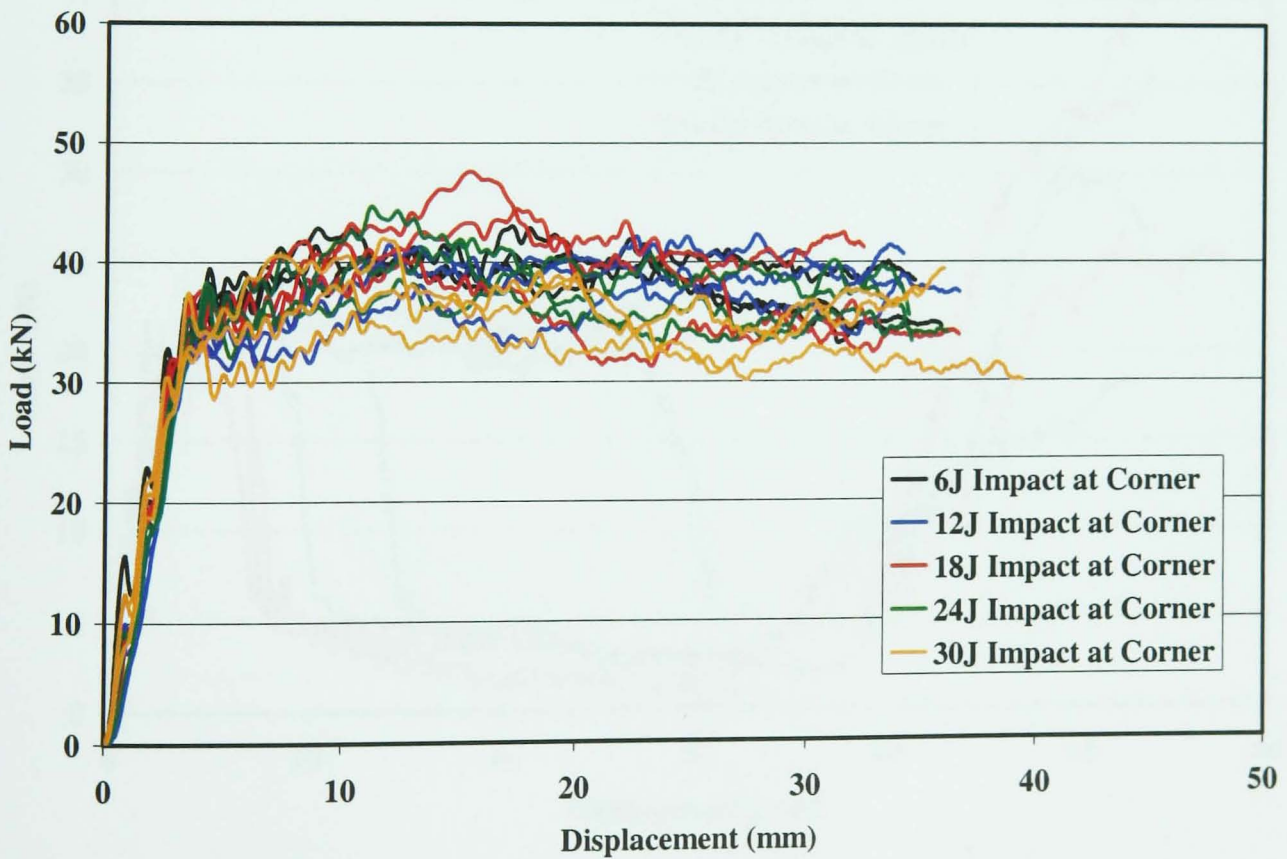


Figure 50: Dynamic Results for Square Tubes (t=4mm) with Impact Damage at the Corner

9.4.2 Damage Position – Axially

Circular ($t=2mm$)

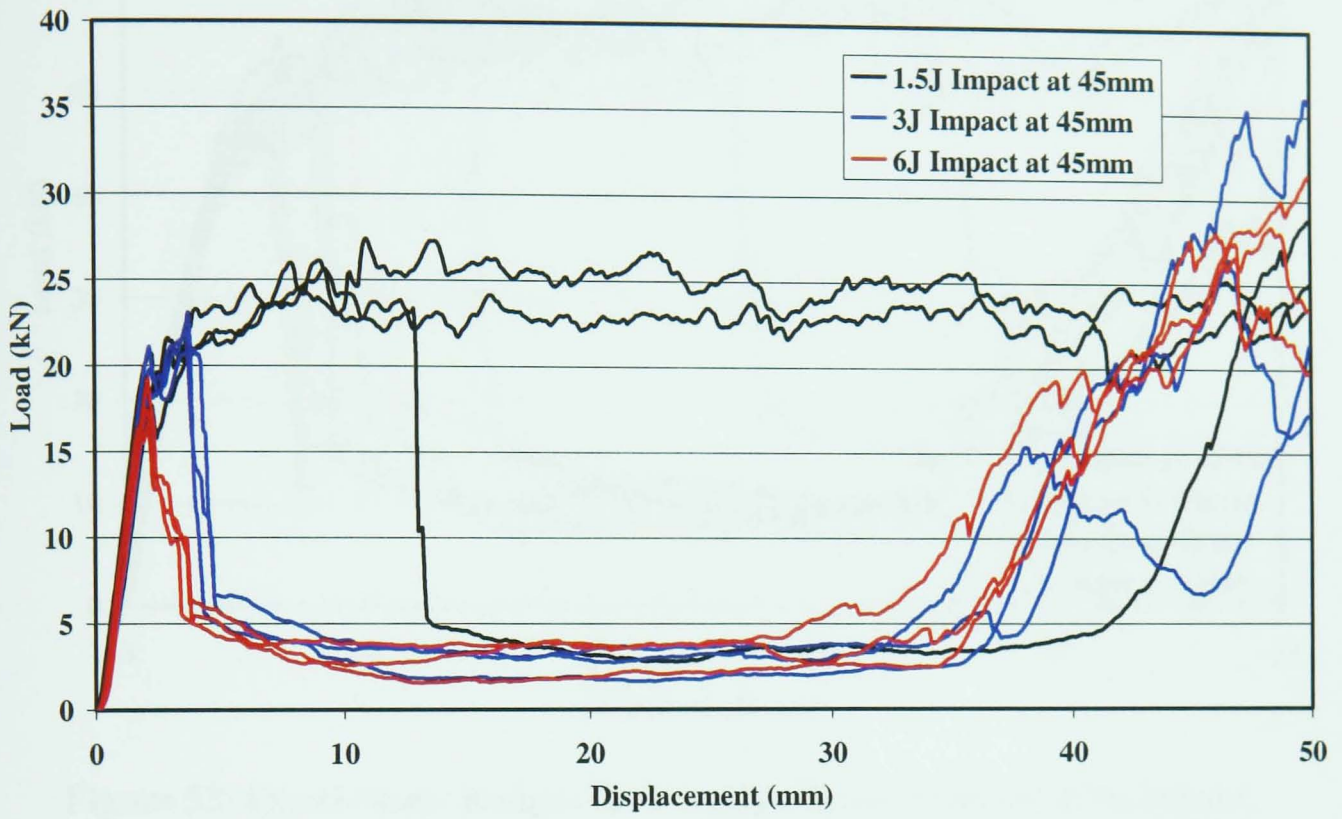


Figure 51: Quasi-Static Results for Circular Tubes ($t=2mm$) with Impact Damage at 45mm

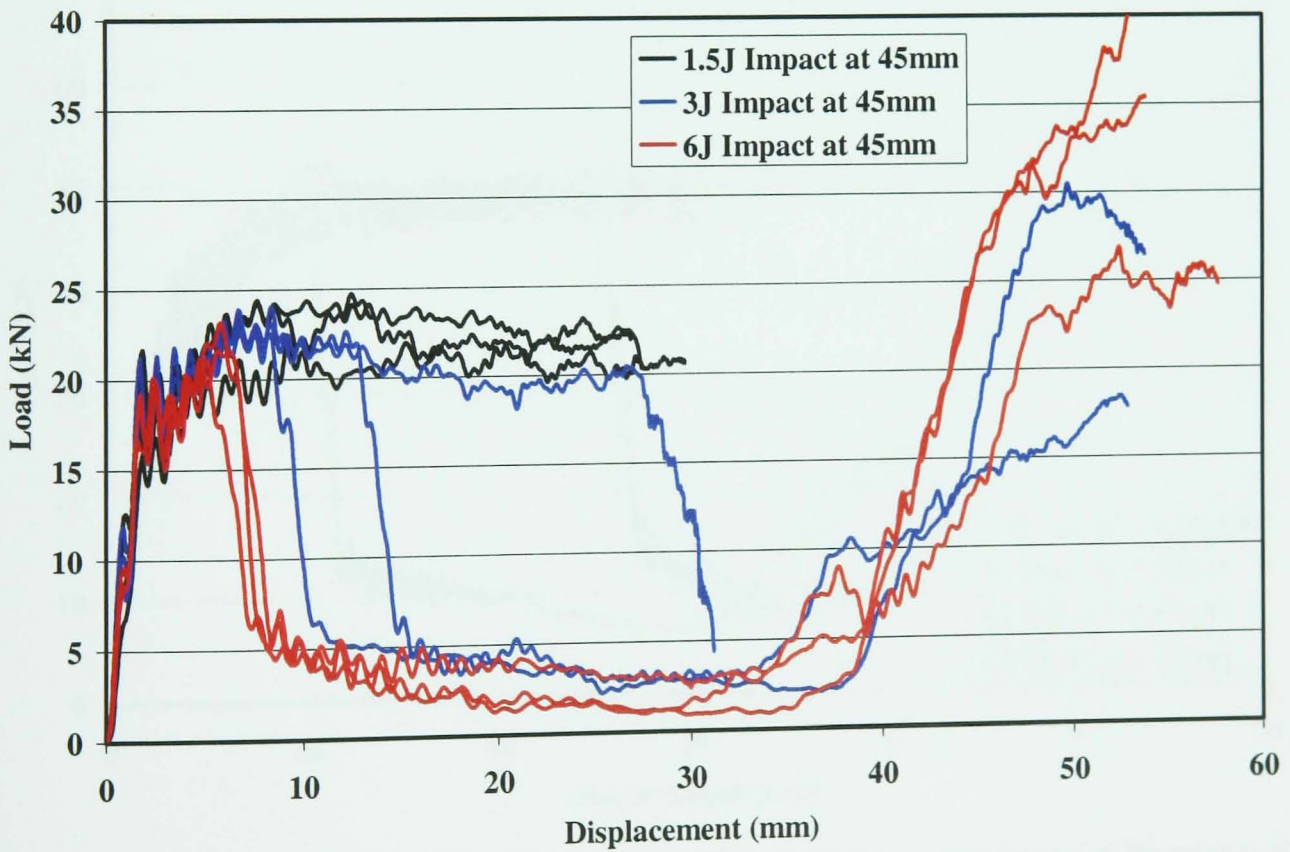


Figure 52: Dynamic Results for Circular Tubes ($t=4mm$) with Impact Damage at 45mm

Circular ($t=4\text{mm}$)

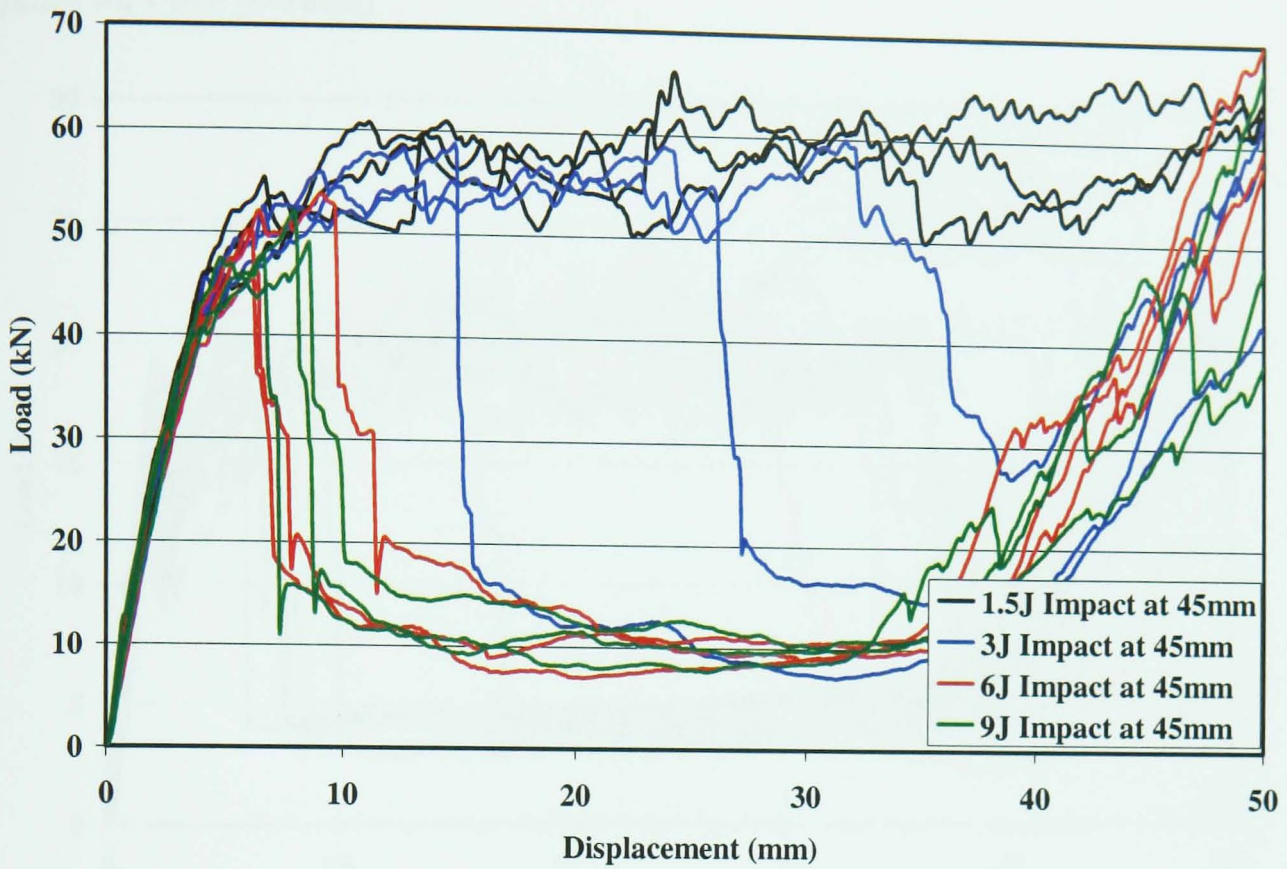


Figure 53: Quasi-Static Results for Circular Tubes ($t=4\text{mm}$) with Impact Damage at 45mm

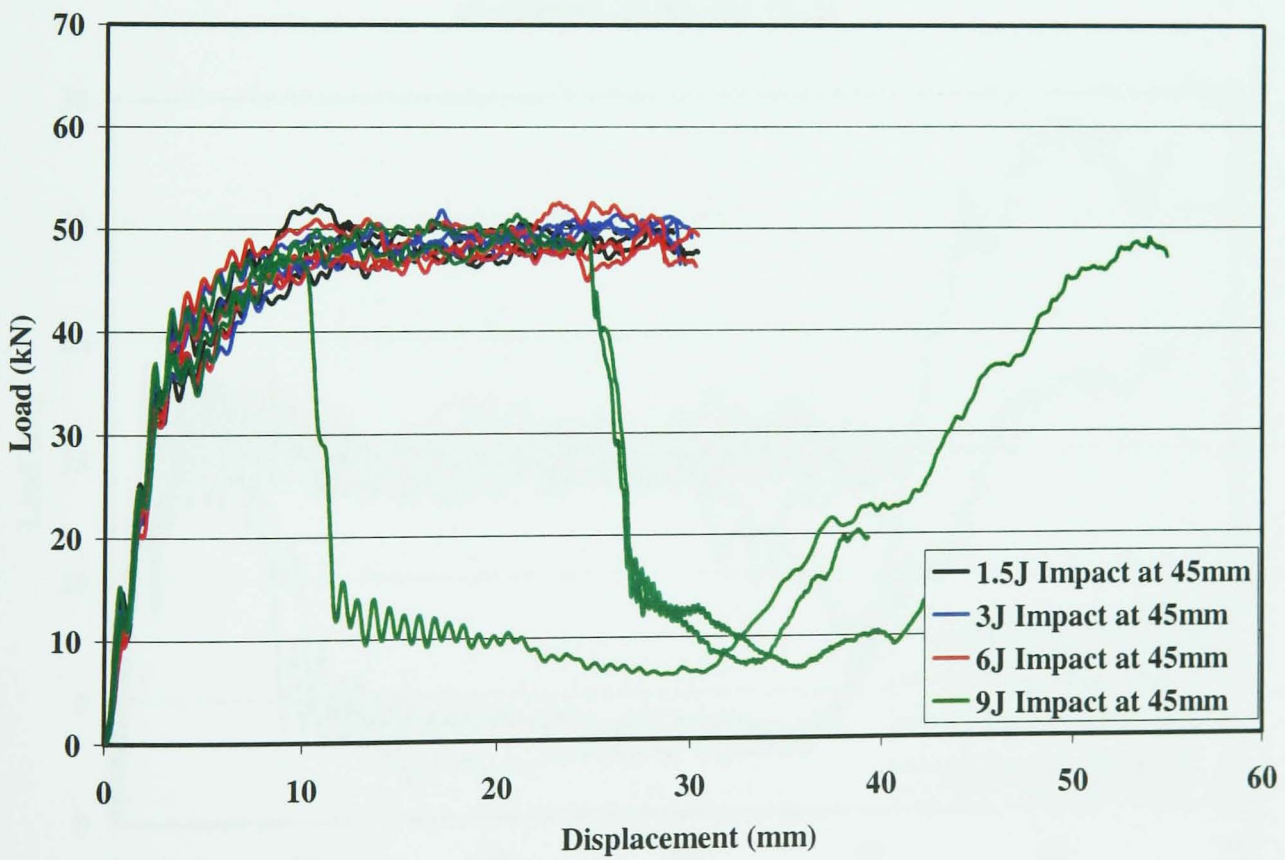


Figure 54: Dynamic Results for Circular Tubes ($t=4\text{mm}$) with Impact Damage at 45mm

Square on Face (t=2mm)

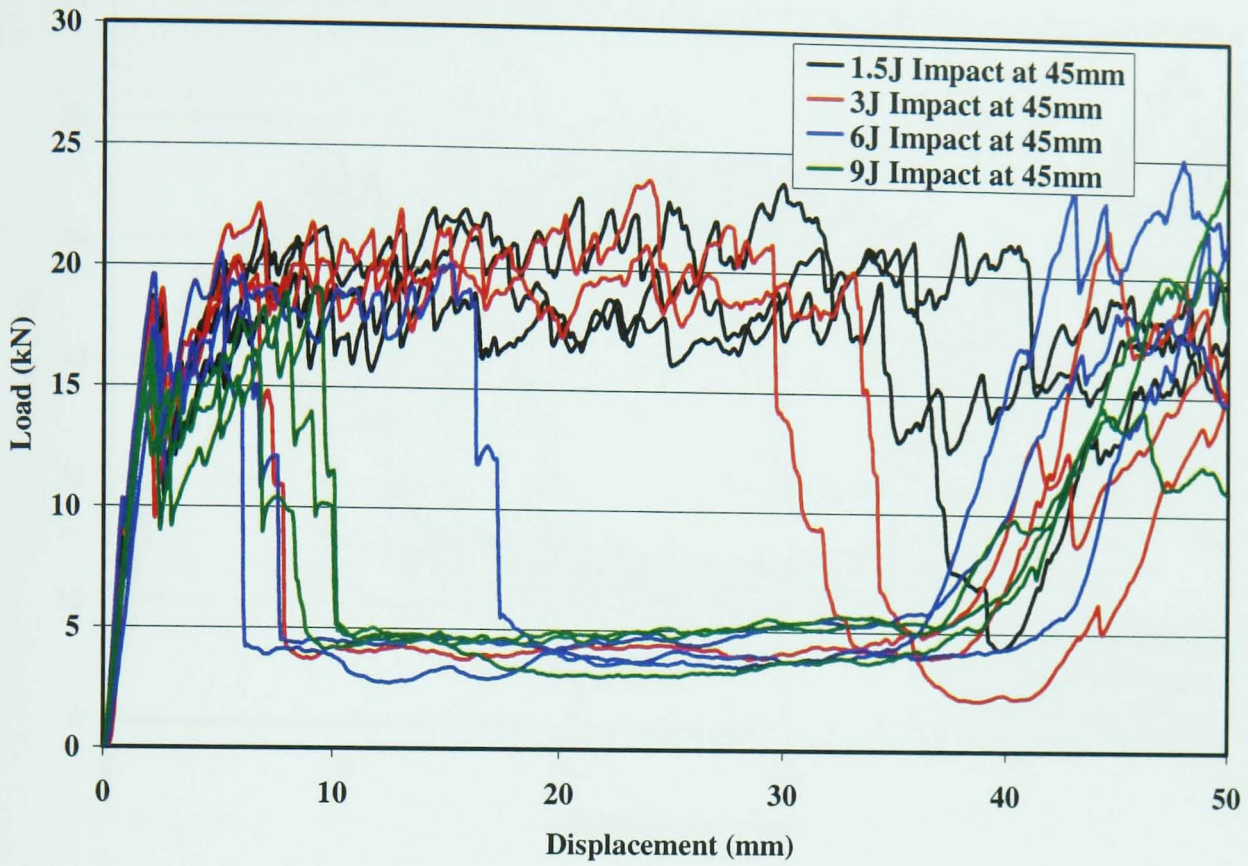


Figure 55: Quasi-Static Results for Square Tubes (t=2mm) with Impact Damage at 45mm along the Face

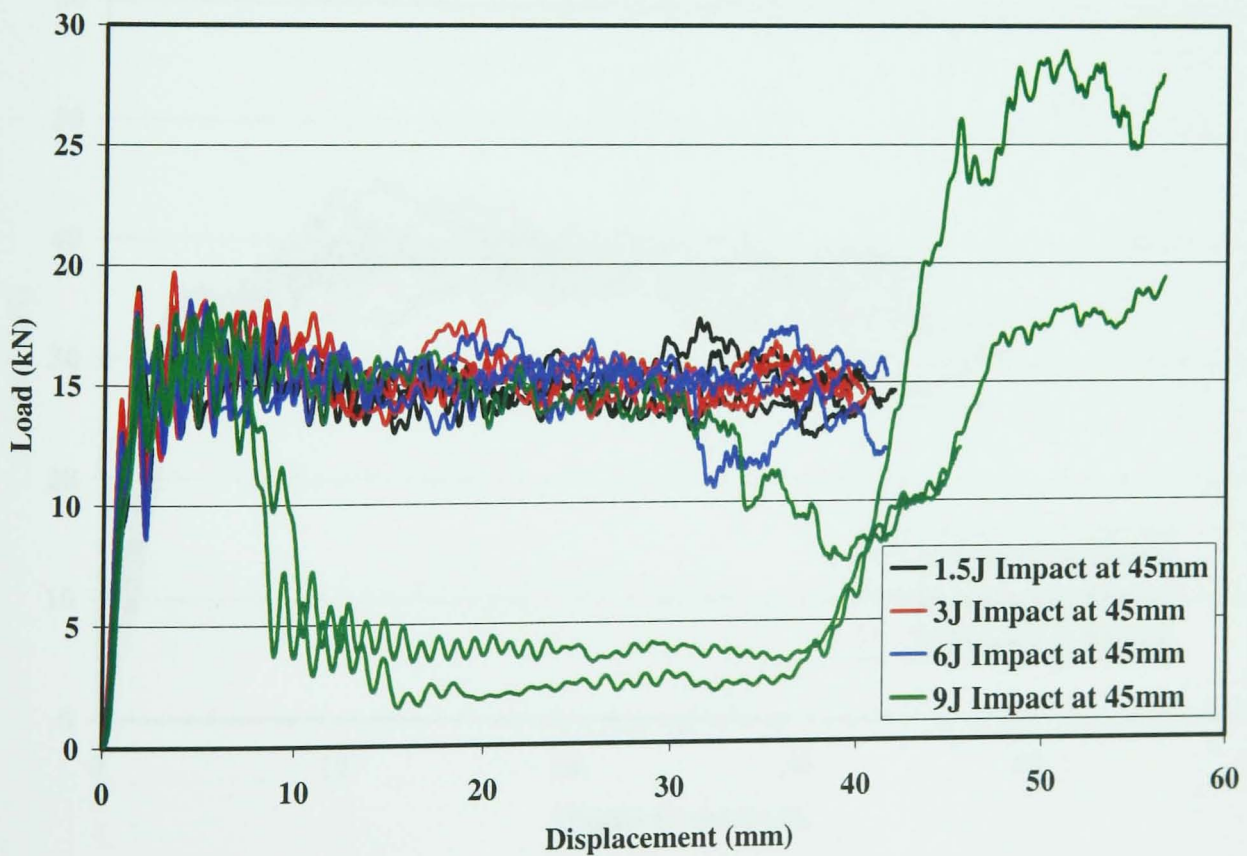


Figure 56: Dynamic Results for Square Tubes (t=2mm) with Impact Damage at 45mm along the Face

Square on Face (t=4mm)

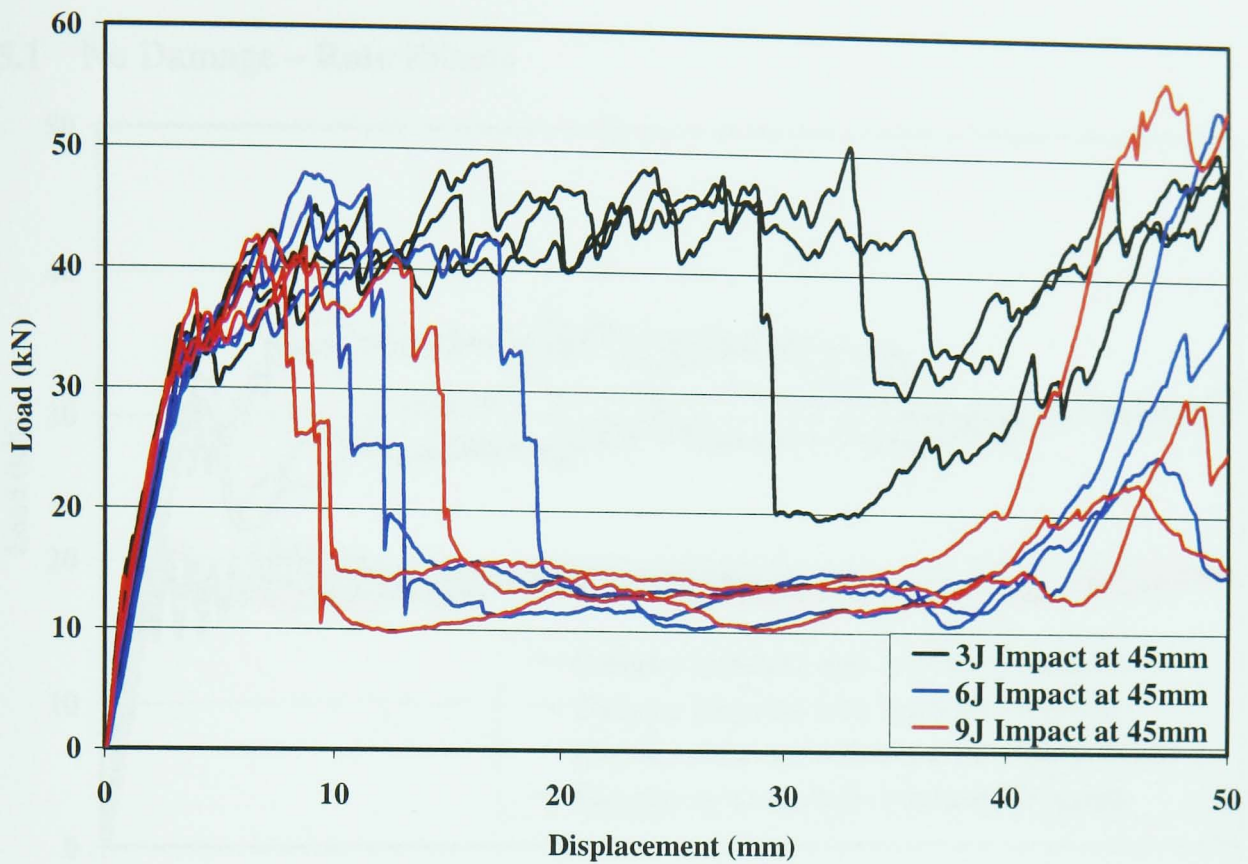


Figure 57: Quasi-Static Results for Square Tubes (t=4mm) with Impact Damage at 45mm along the Face

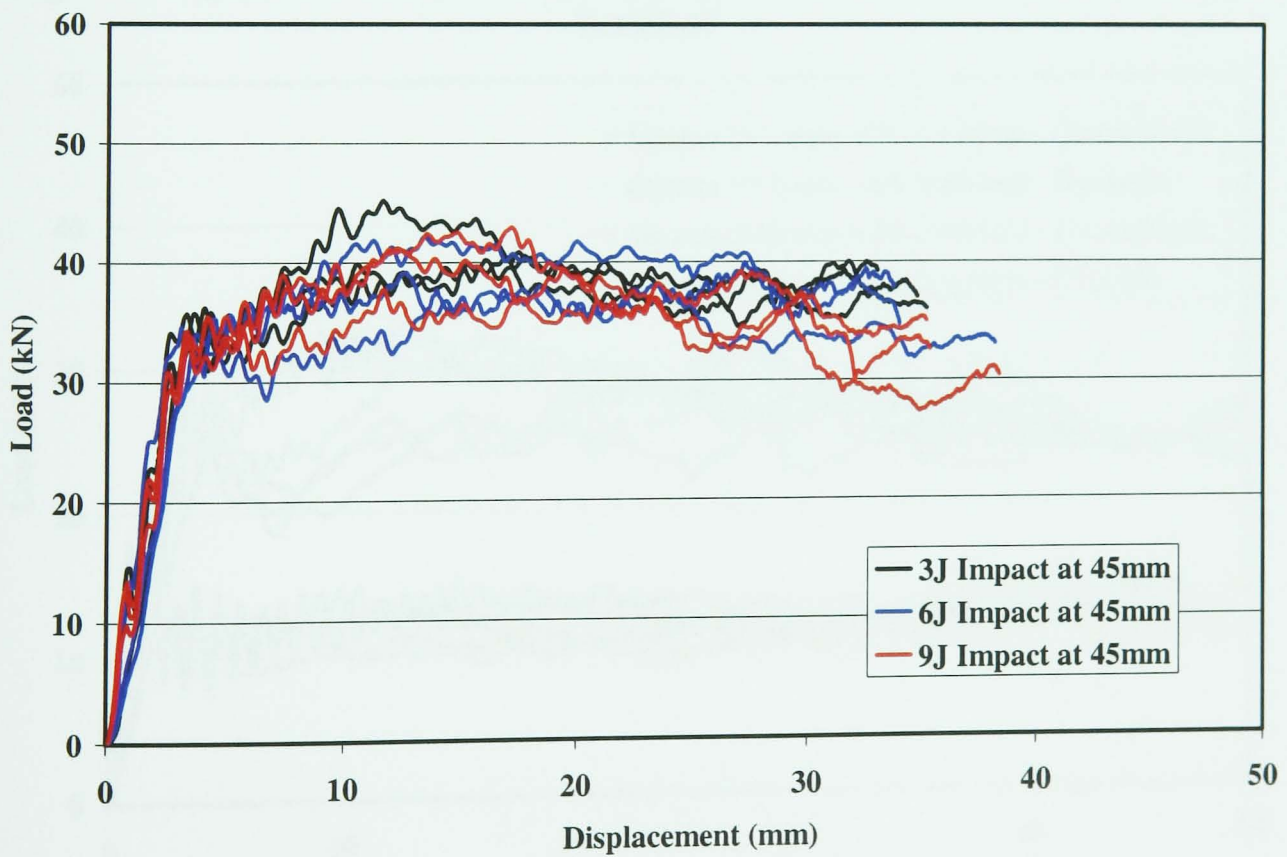


Figure 58: Dynamic Results for Square Tubes (t=4mm) with Impact Damage at 45mm along the Face

9.5 Interleaf

9.5.1 No Damage – Rate Effects

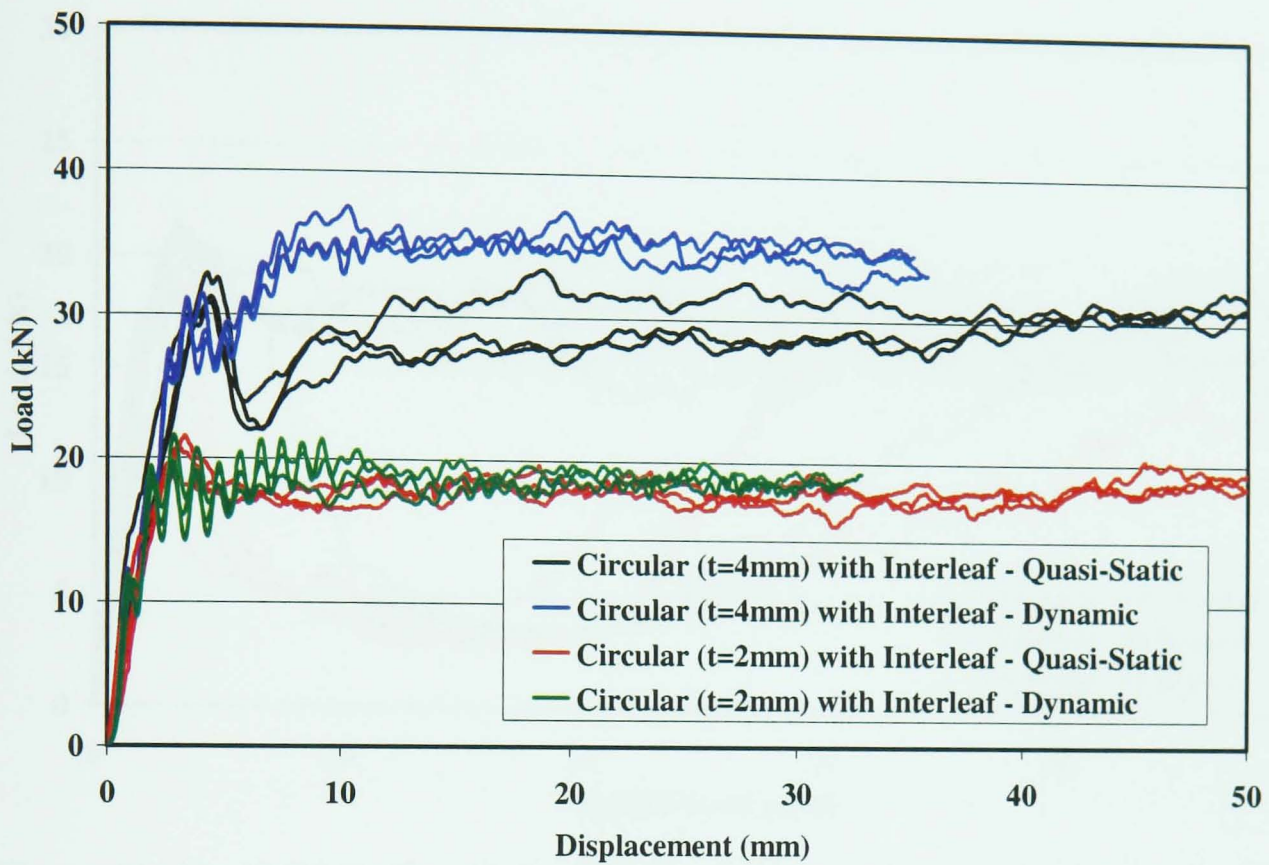


Figure 59: Quasi-Statically and Dynamically Results for Circular Tubes with Interleaf

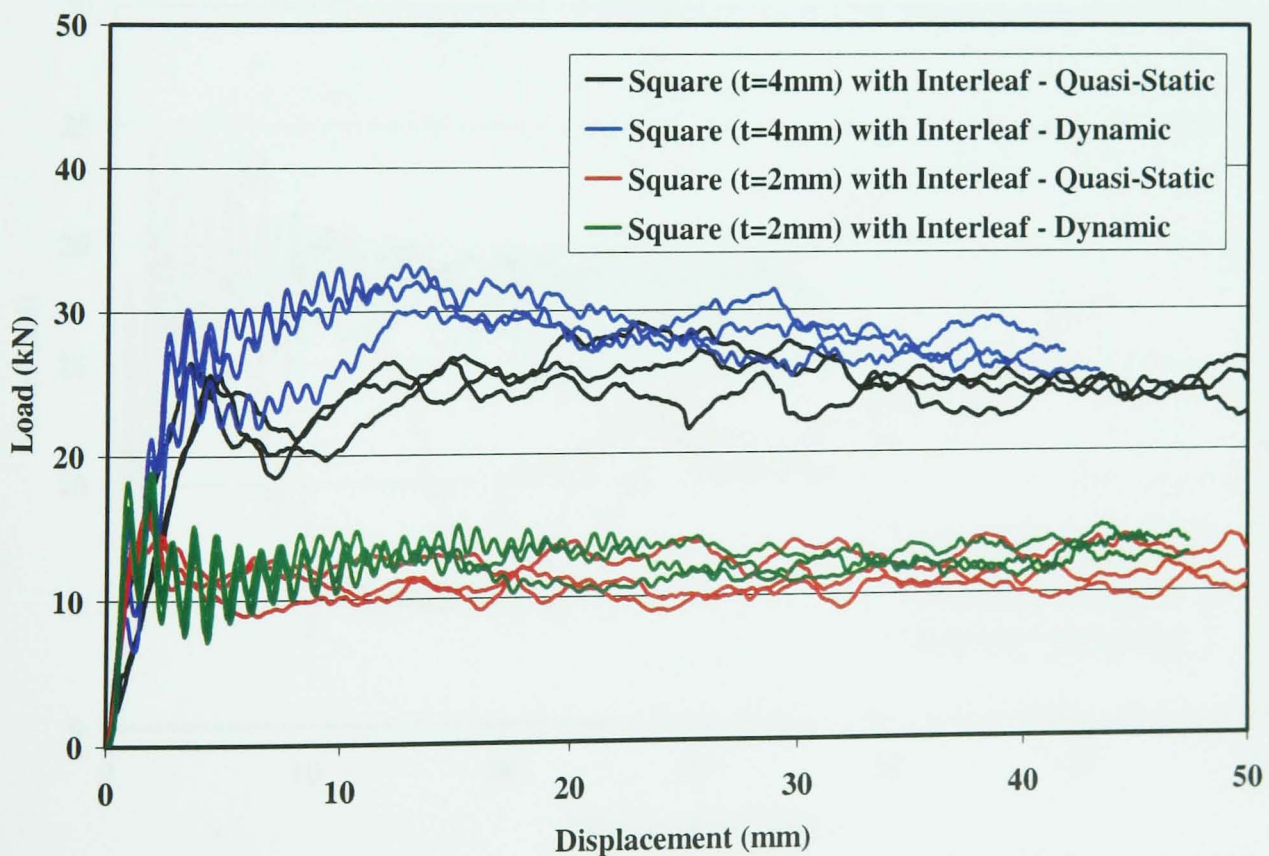


Figure 60: Quasi-Statically and Dynamically Results for Square Tubes with Interleaf

9.5.2 Damage Levels

Circular (t=2mm)

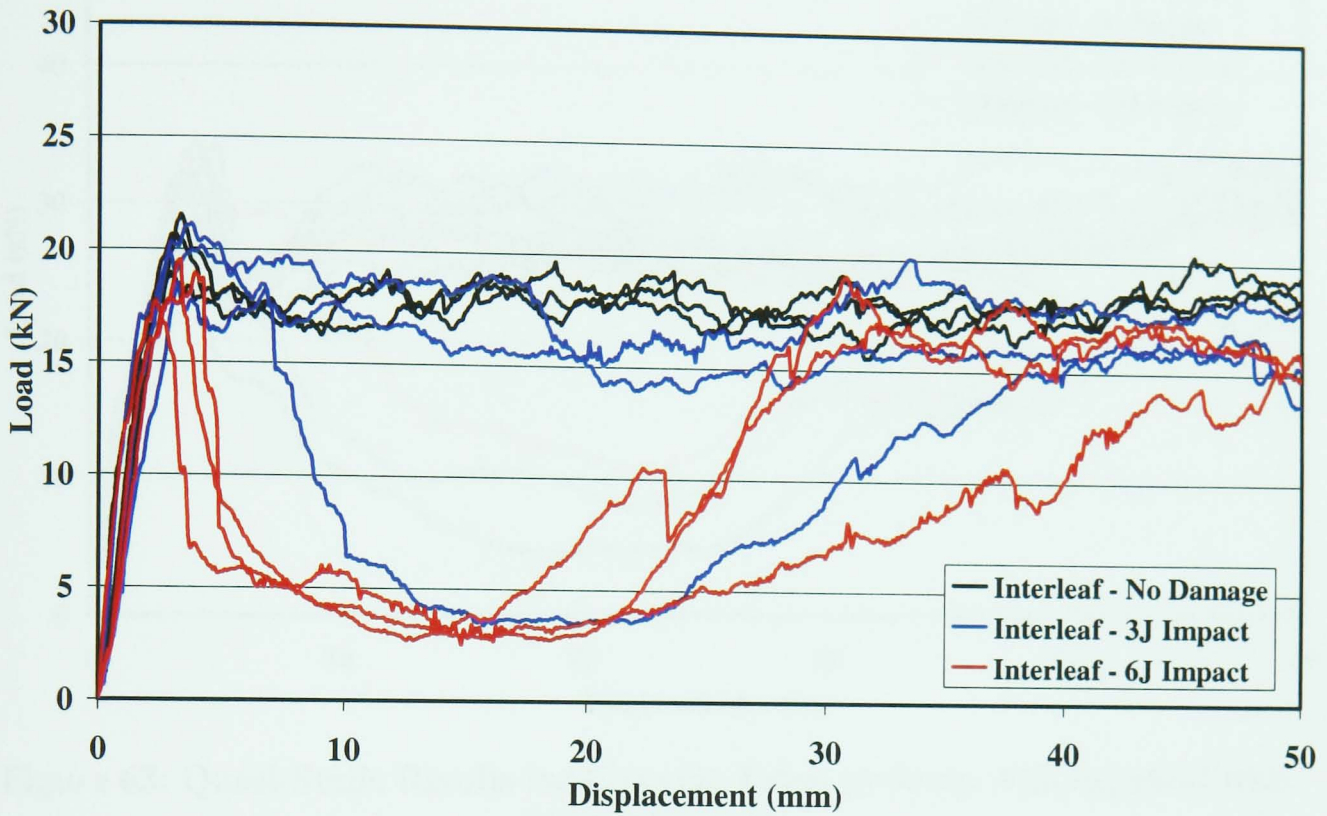


Figure 61: Quasi-Static Results for Circular Tubes (t=2mm) with Interleaf with Impact Damage

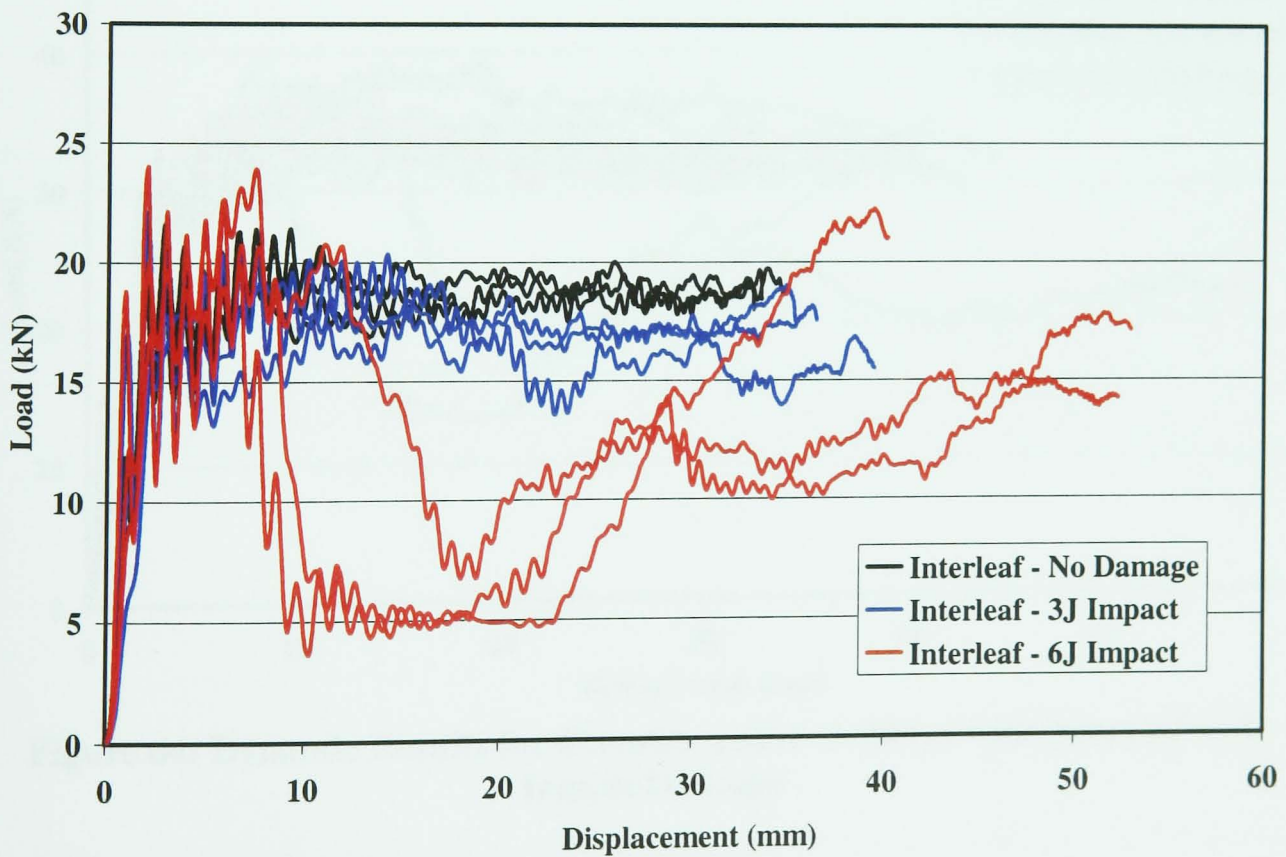


Figure 62: Dynamic Results for Circular Tubes (t=2mm) with Interleaf with Impact Damage

Circular ($t=4\text{mm}$)

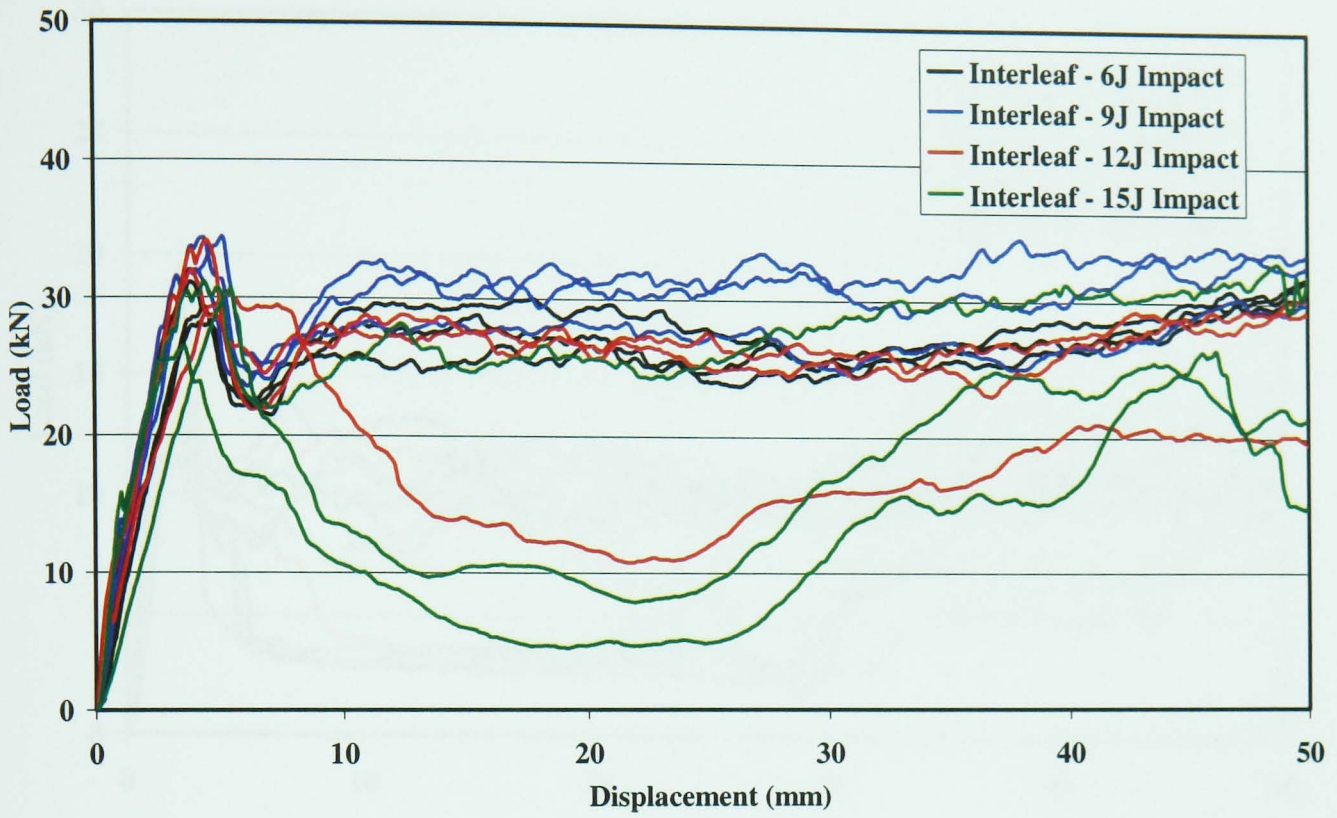


Figure 63: Quasi-Static Results for Circular Tubes ($t=4\text{mm}$) with Interleaf with Impact Damage

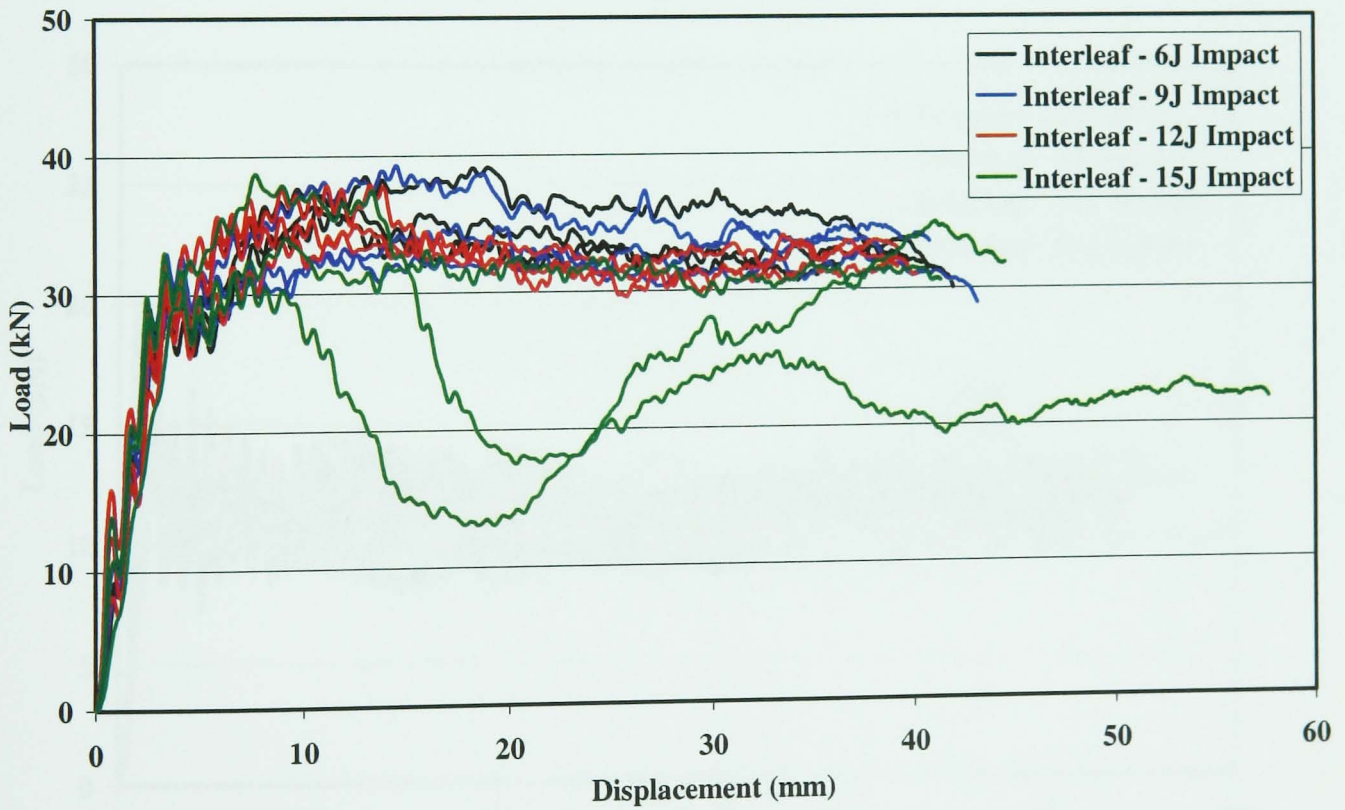


Figure 64: Dynamic Results for Circular Tubes ($t=4\text{mm}$) with Interleaf with Impact Damage

Square on Face (t=2mm)

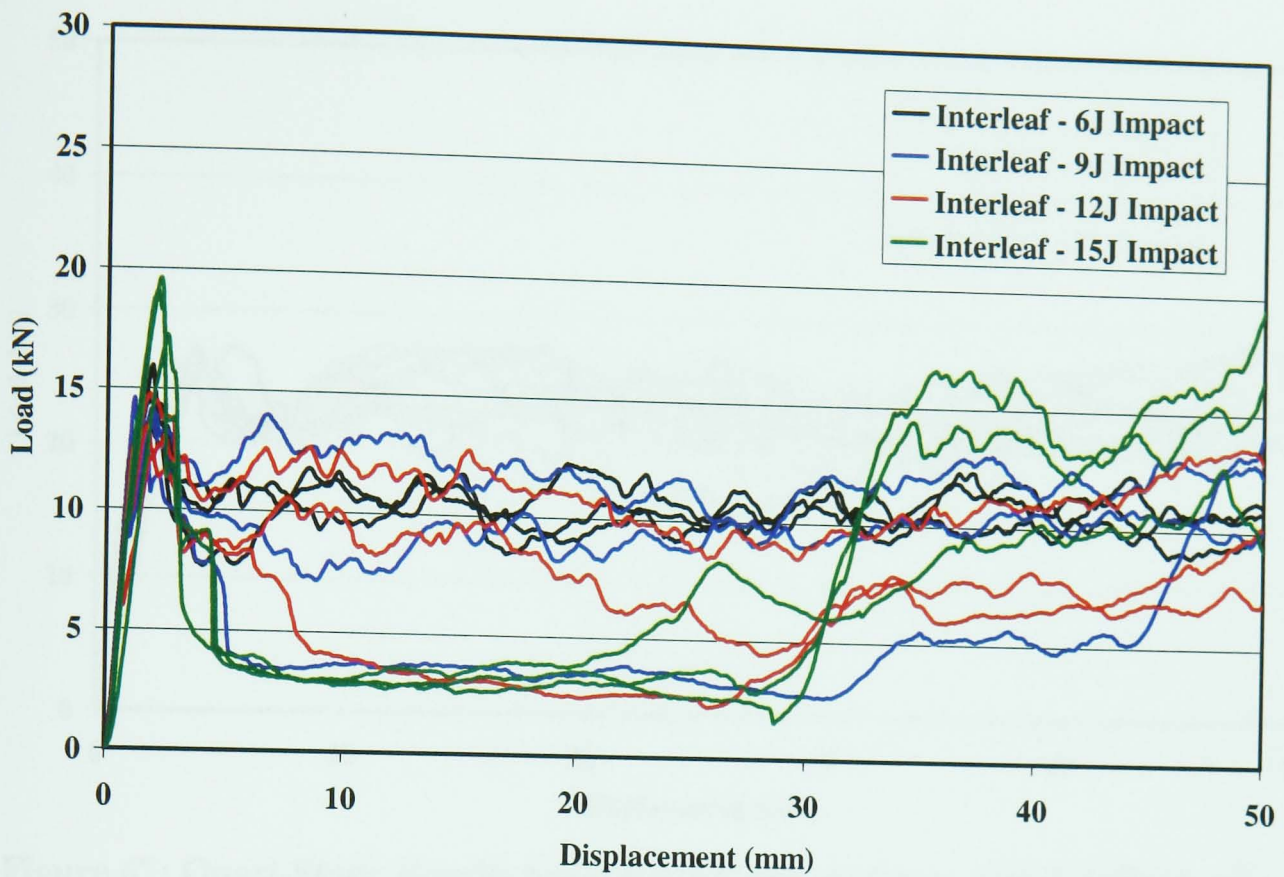


Figure 65: Quasi-Static Results for Square Tubes (t=2mm) with Interleaf with Impact Damage on the Face

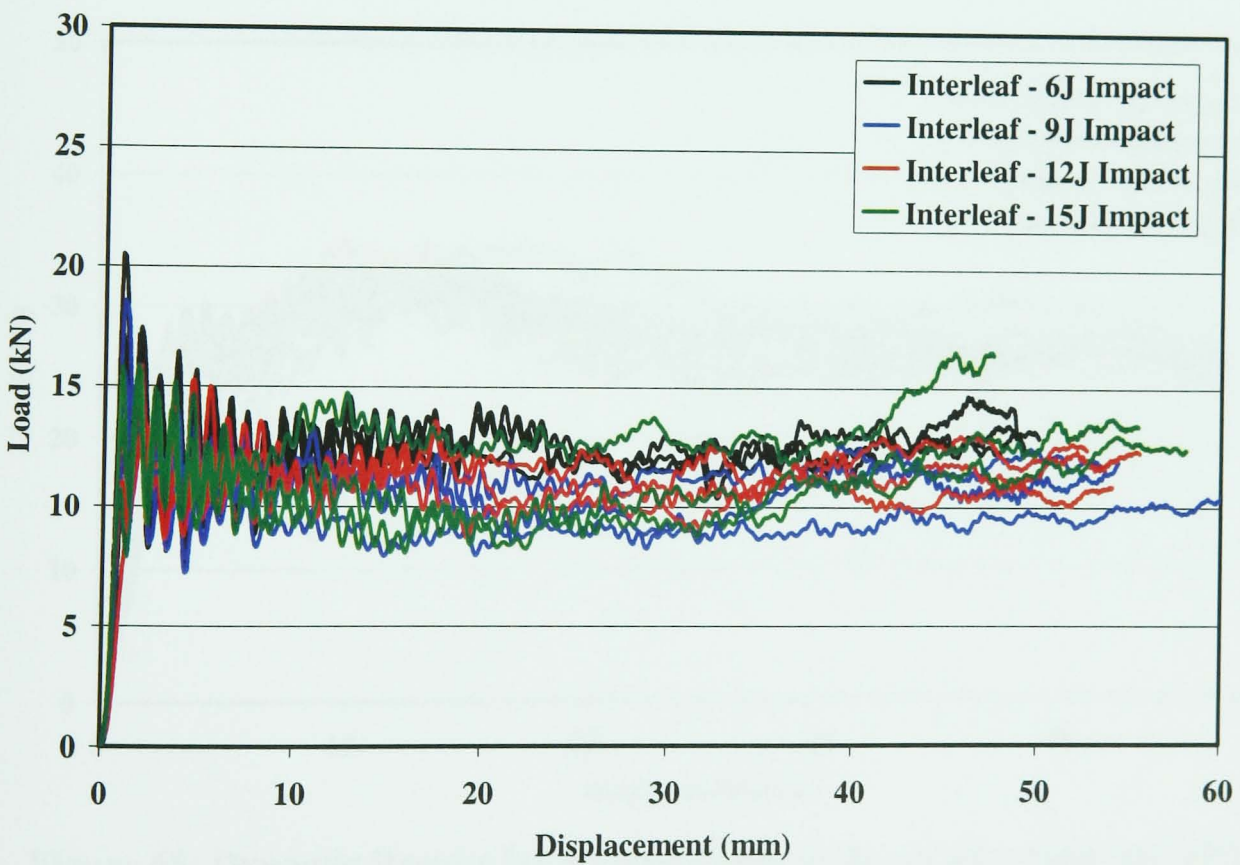


Figure 66: Dynamic Results for Square Tubes (t=2mm) with Interleaf with Impact Damage on the Face

Square on Face (t=4mm)

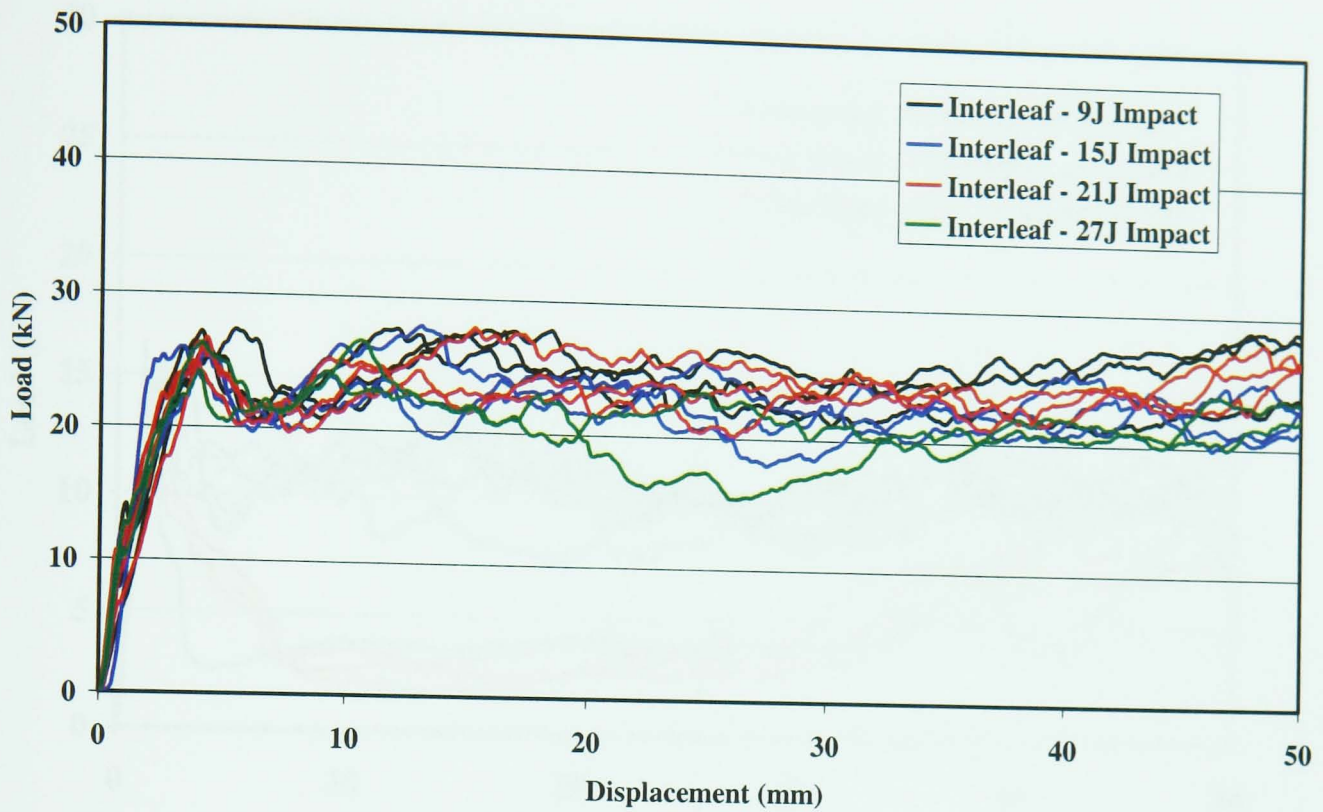


Figure 67: Quasi-Static Results for Square Tubes (t=4mm) with Interleaf with Impact Damage on the Face

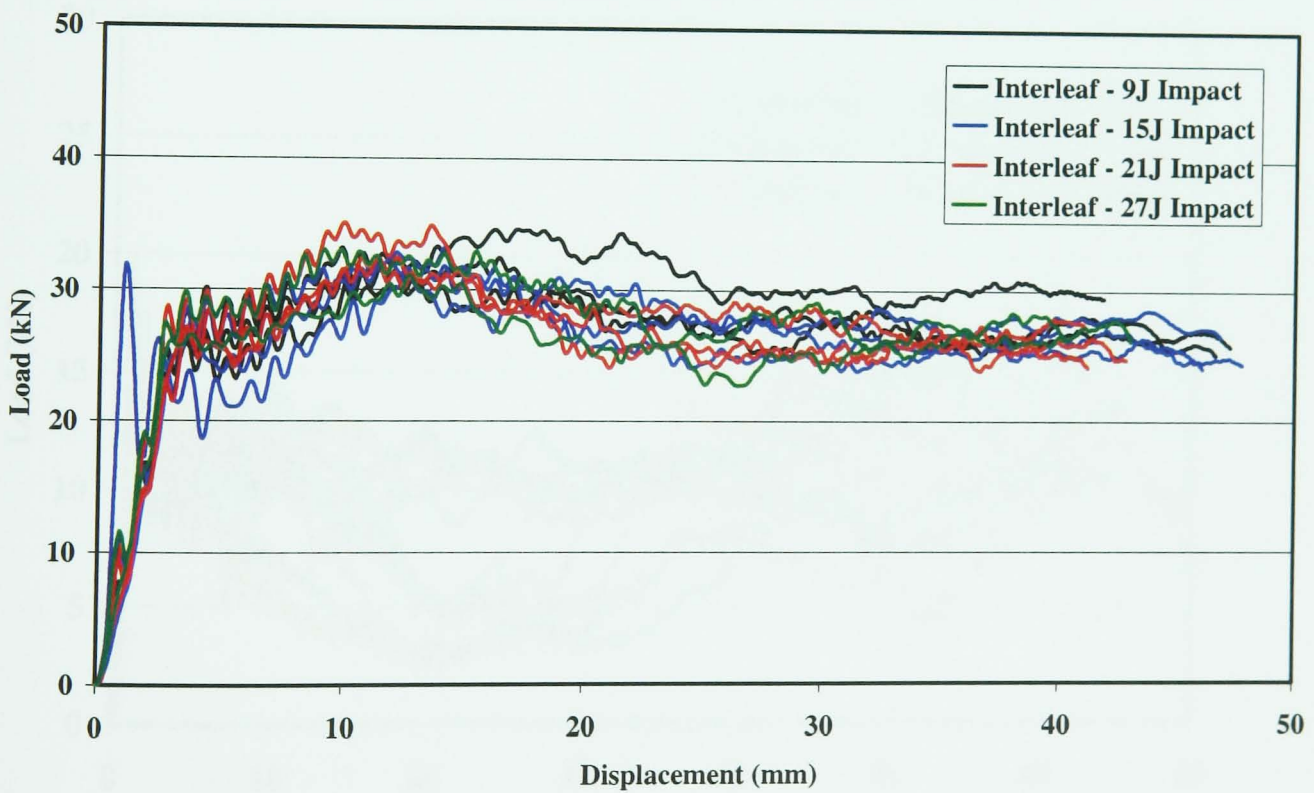


Figure 68: Dynamic Results for Square Tubes (t=4mm) with Interleaf with Impact Damage on the Face

Square on Corner (t=2mm)

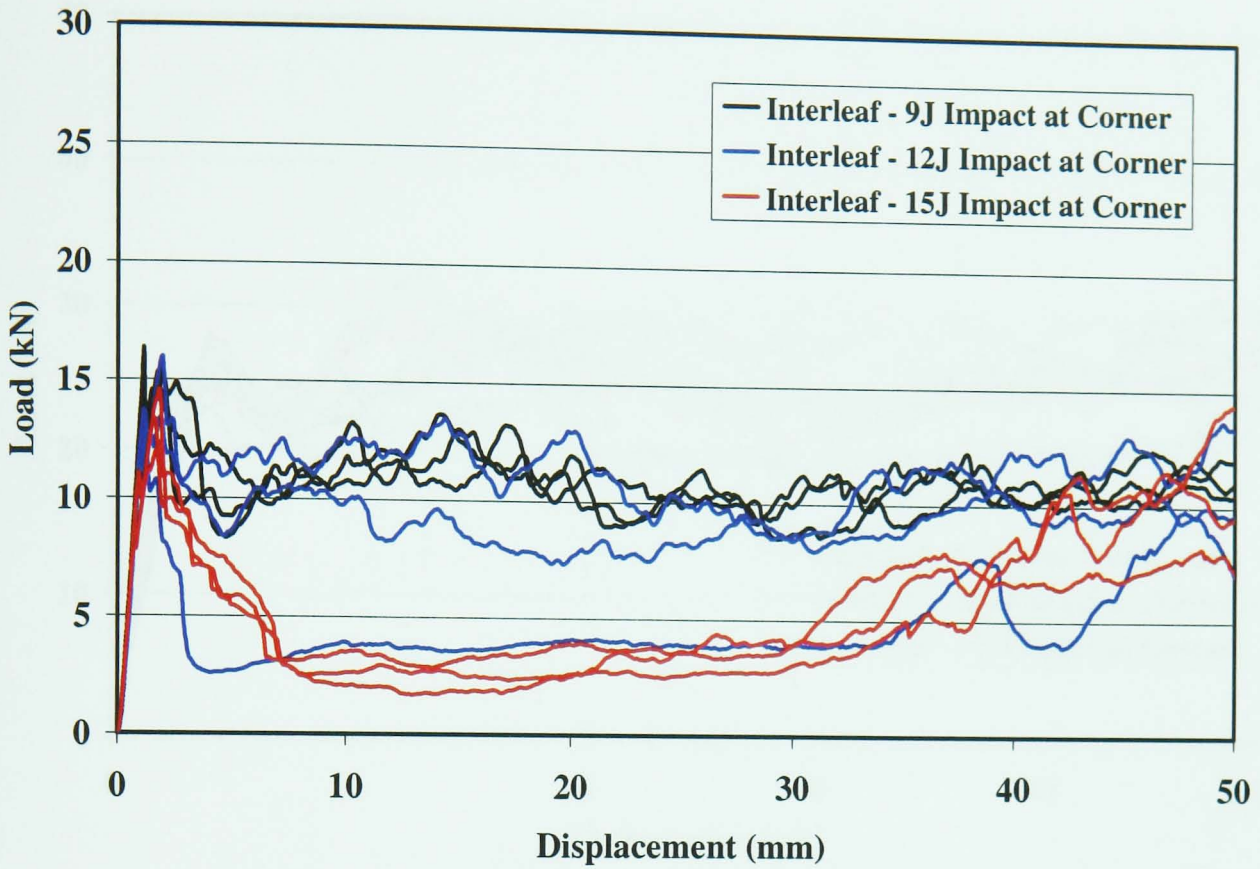


Figure 69: Quasi-Static Results for Square Tubes (t=2mm) with Interleaf with Impact Damage at the Corner

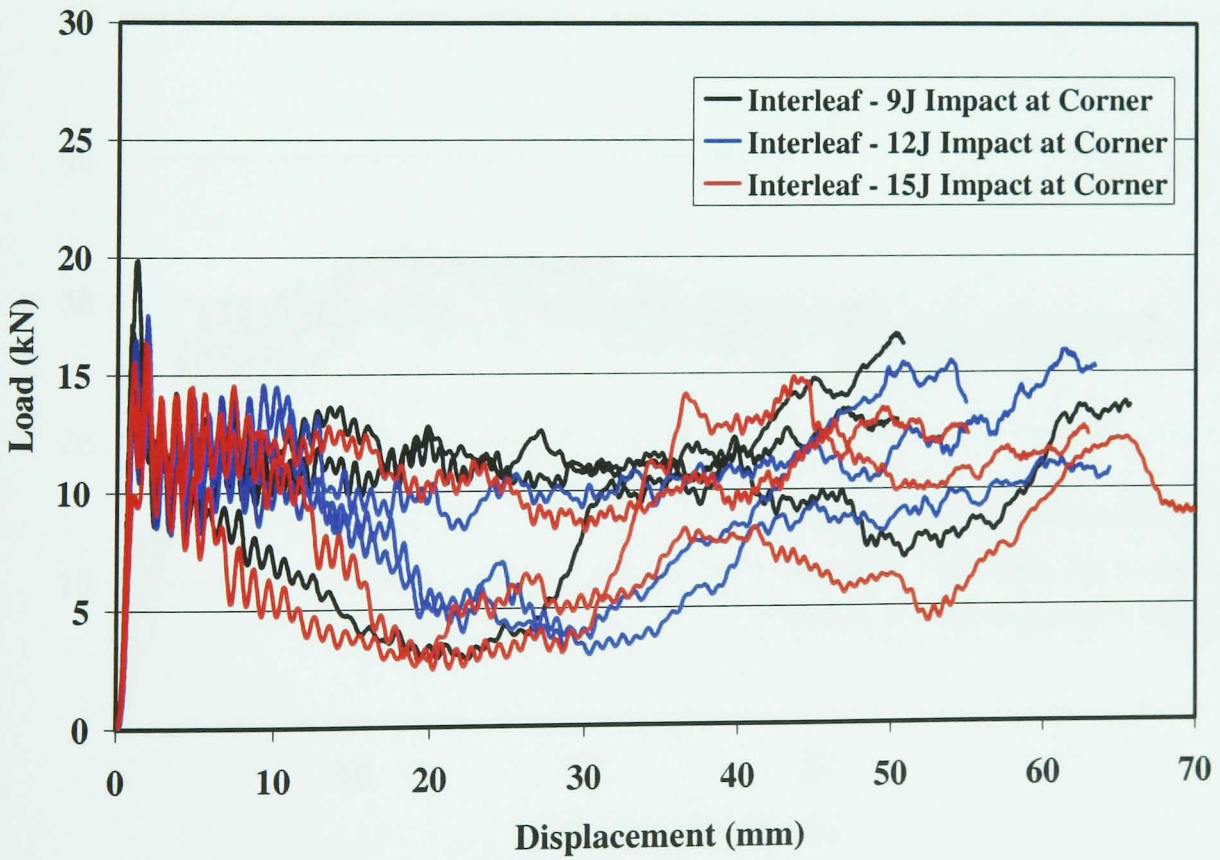


Figure 70: Dynamic Results for Square Tubes (t=2mm) with Interleaf with Impact Damage at the Corner

Square on Corner (t=4mm)

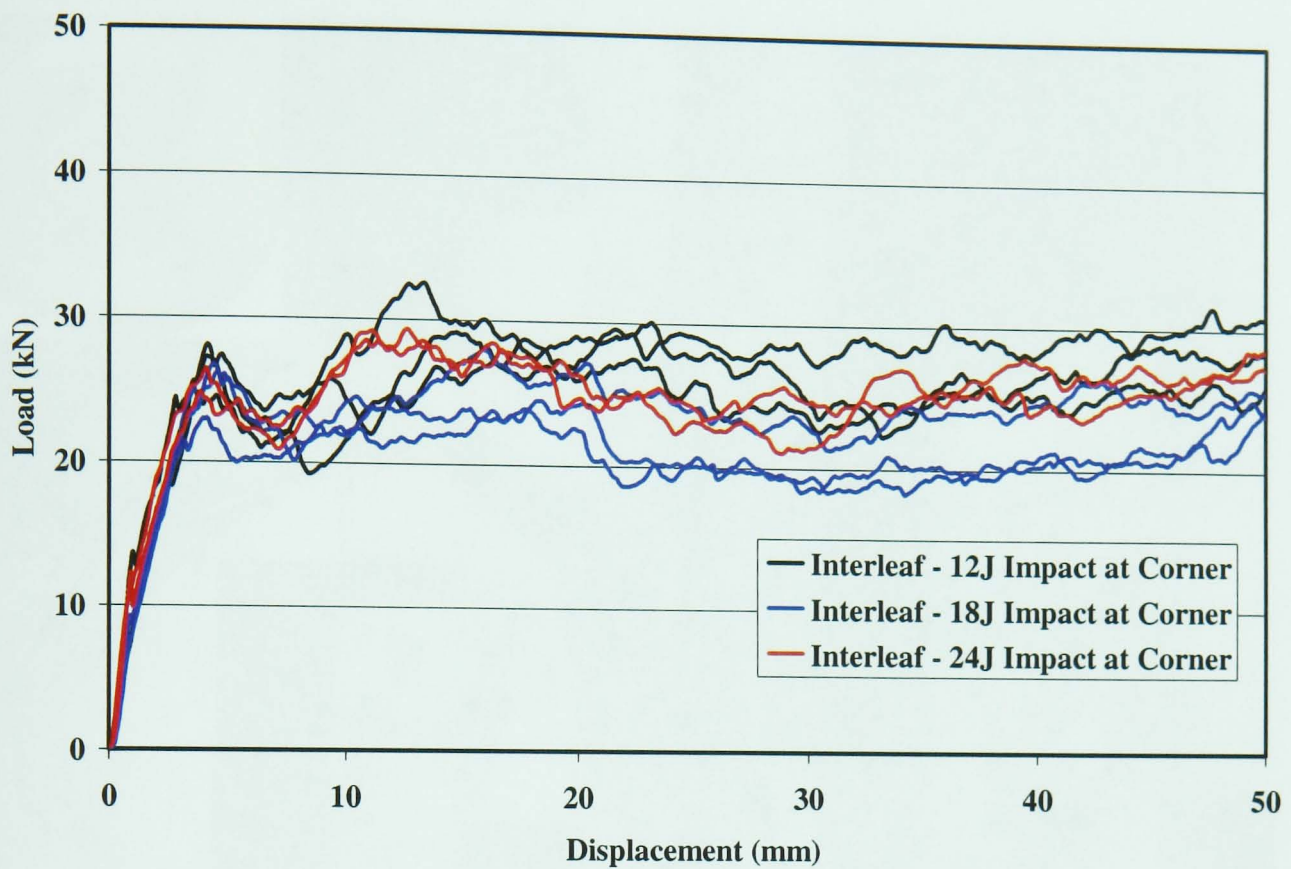


Figure 71: Quasi-Static Results for Square Tubes (t=4mm) with Interleaf with Impact Damage at the Corner

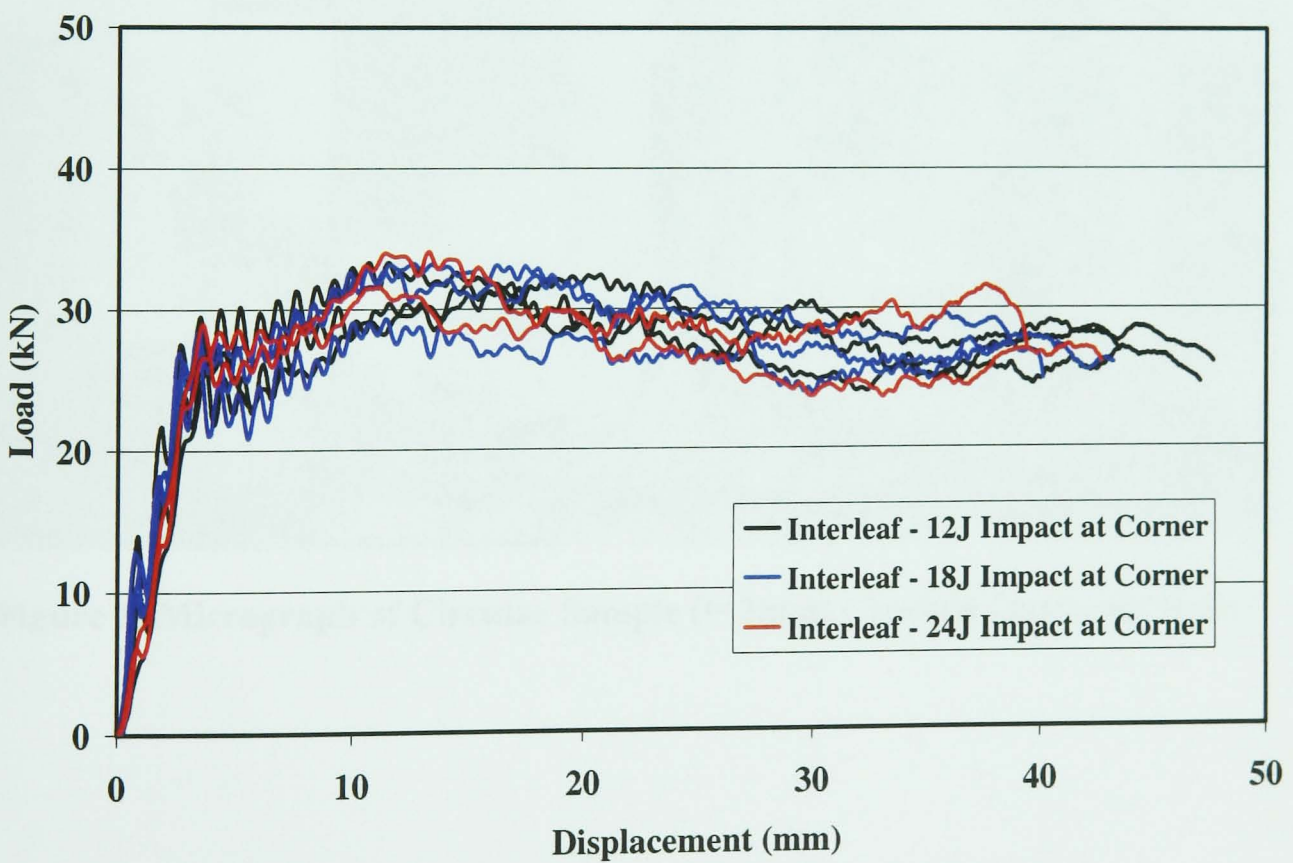


Figure 72: Dynamic Results for Square Tubes (t=4mm) with Interleaf with Impact Damage at the Corner

10 Appendix 2 - Micrographs



Figure 1: Micrograph of Circular Sample (t=2mm) Crushed Quasi-Statically



Figure 2: Crush Zone Morphology of Circular Sample ($t=2\text{mm}$) Crushed Quasi-Statically

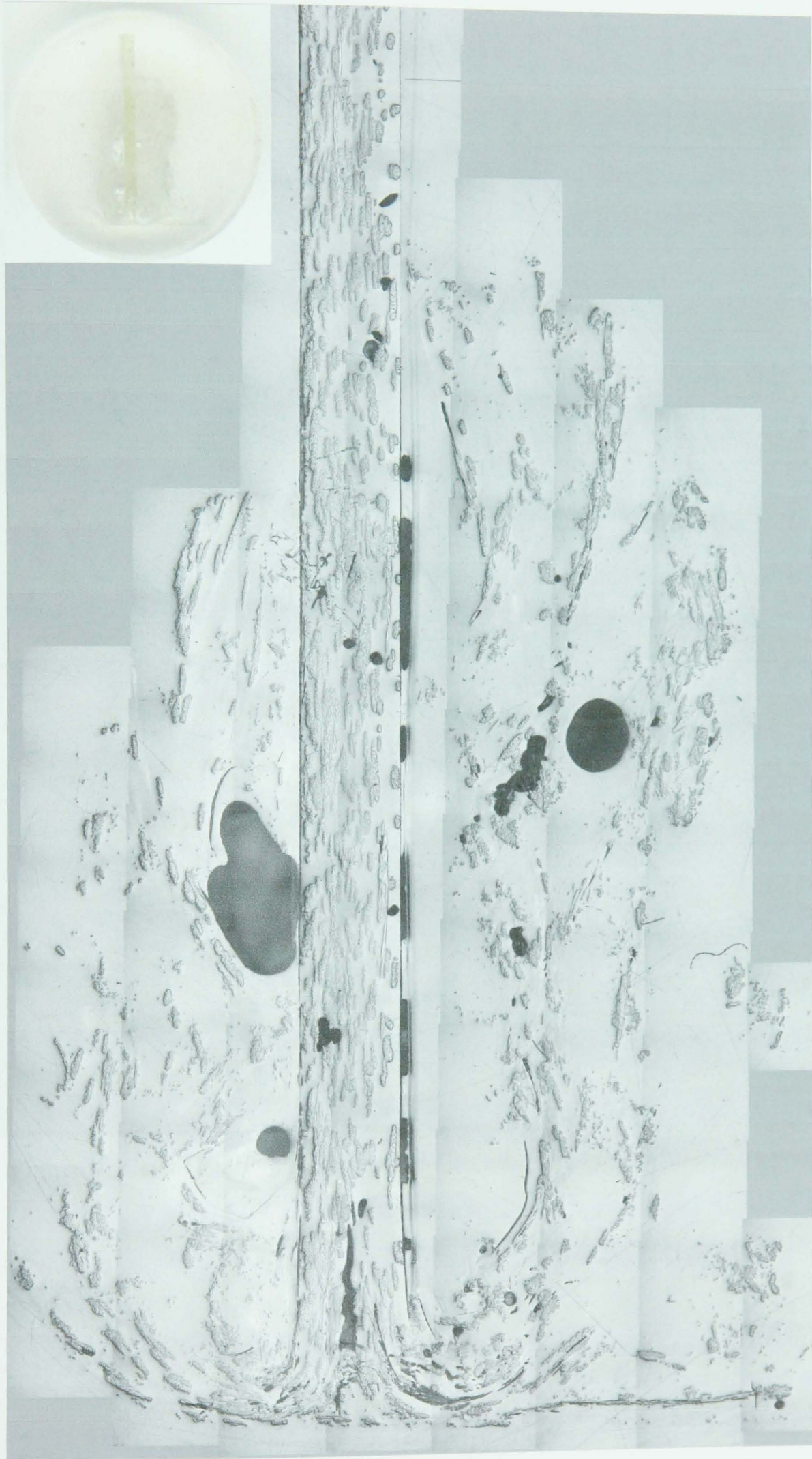


Figure 3: Micrograph of Circular Sample ($t=2\text{mm}$) Crushed Dynamically

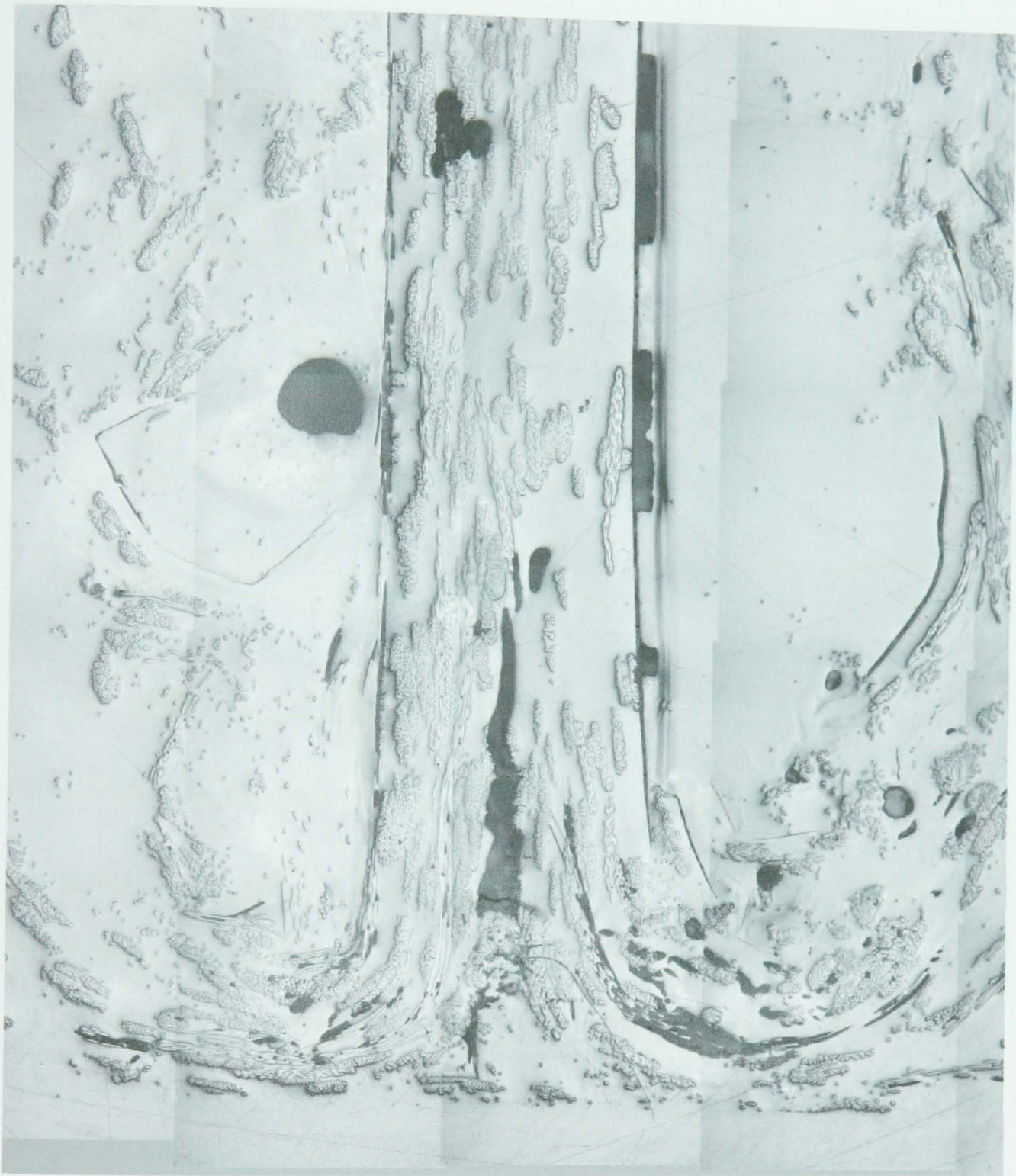


Figure 4: Crush Zone Morphology of Circular Sample (t=2mm) Crushed Dynamically

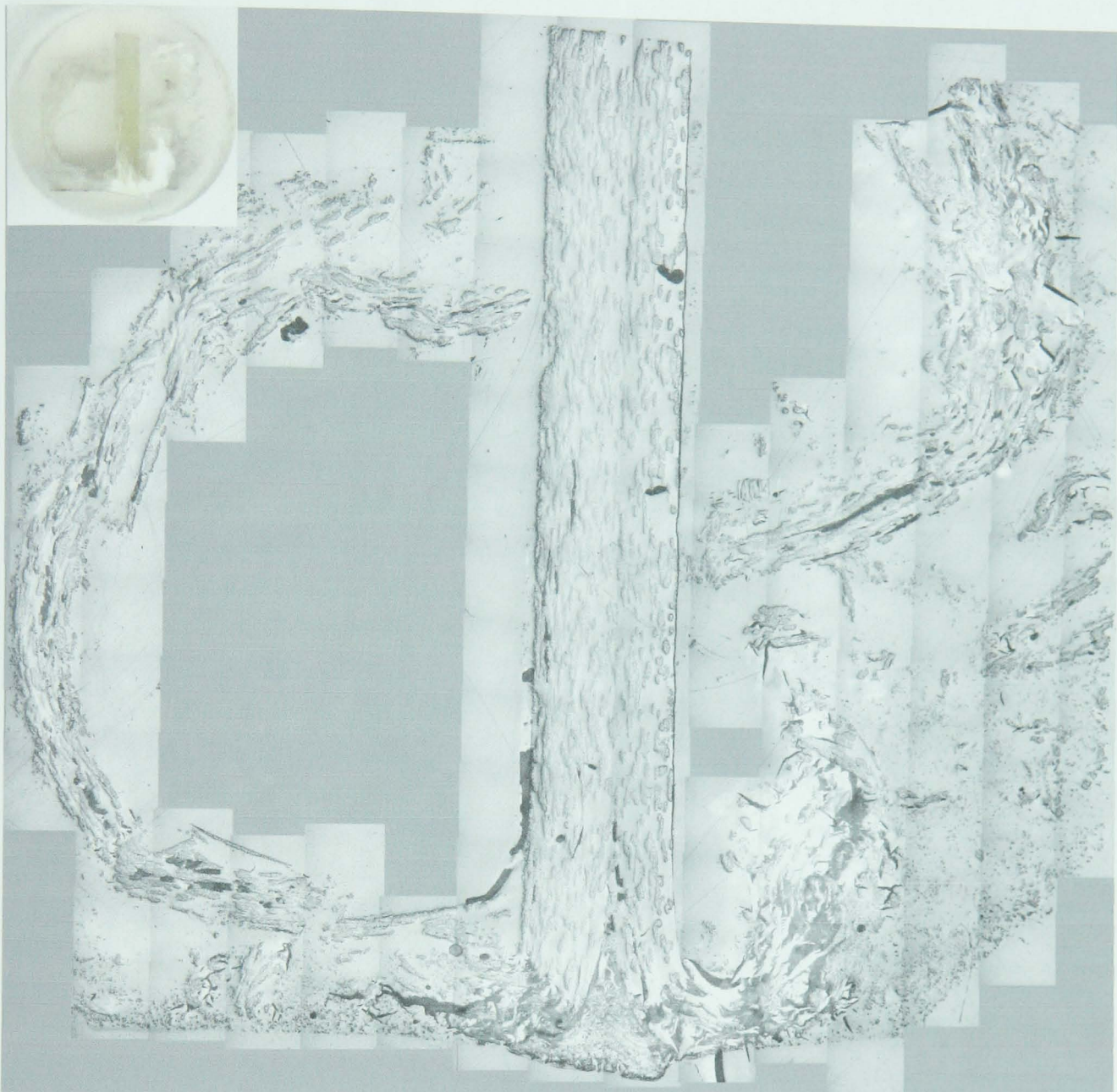


Figure 5: Micrograph of Circular Sample ($t=4\text{mm}$) Crushed Quasi-Statically



Figure 6: Crush Zone Morphology of Circular Sample ($t=4\text{mm}$) Crushed Quasi-Statically

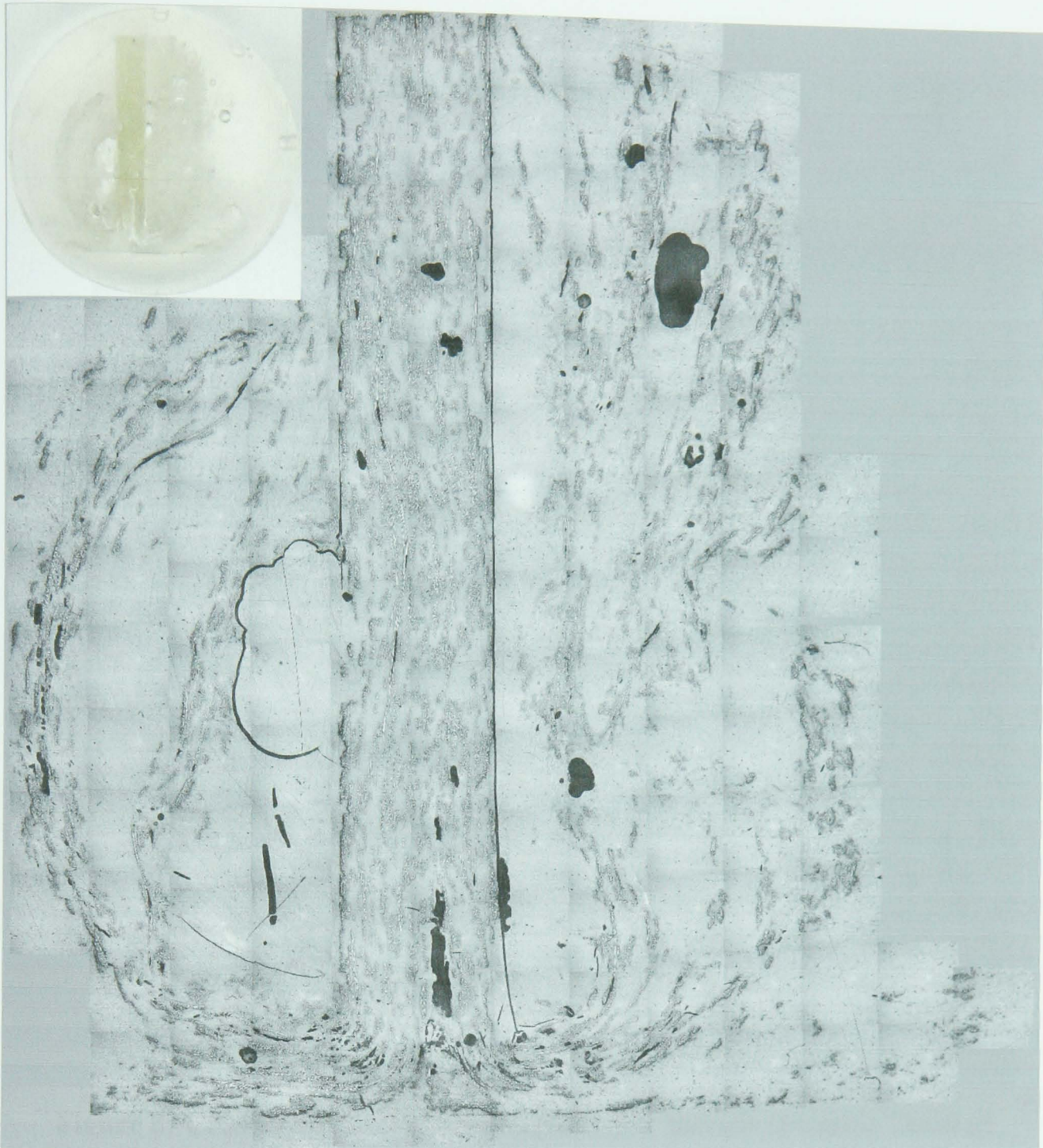


Figure 7: Micrograph of Circular Sample (t=4mm) Crushed Dynamically



Figure 8: Crush Zone Morphology of Circular Sample (t=4mm) Crushed Dynamically

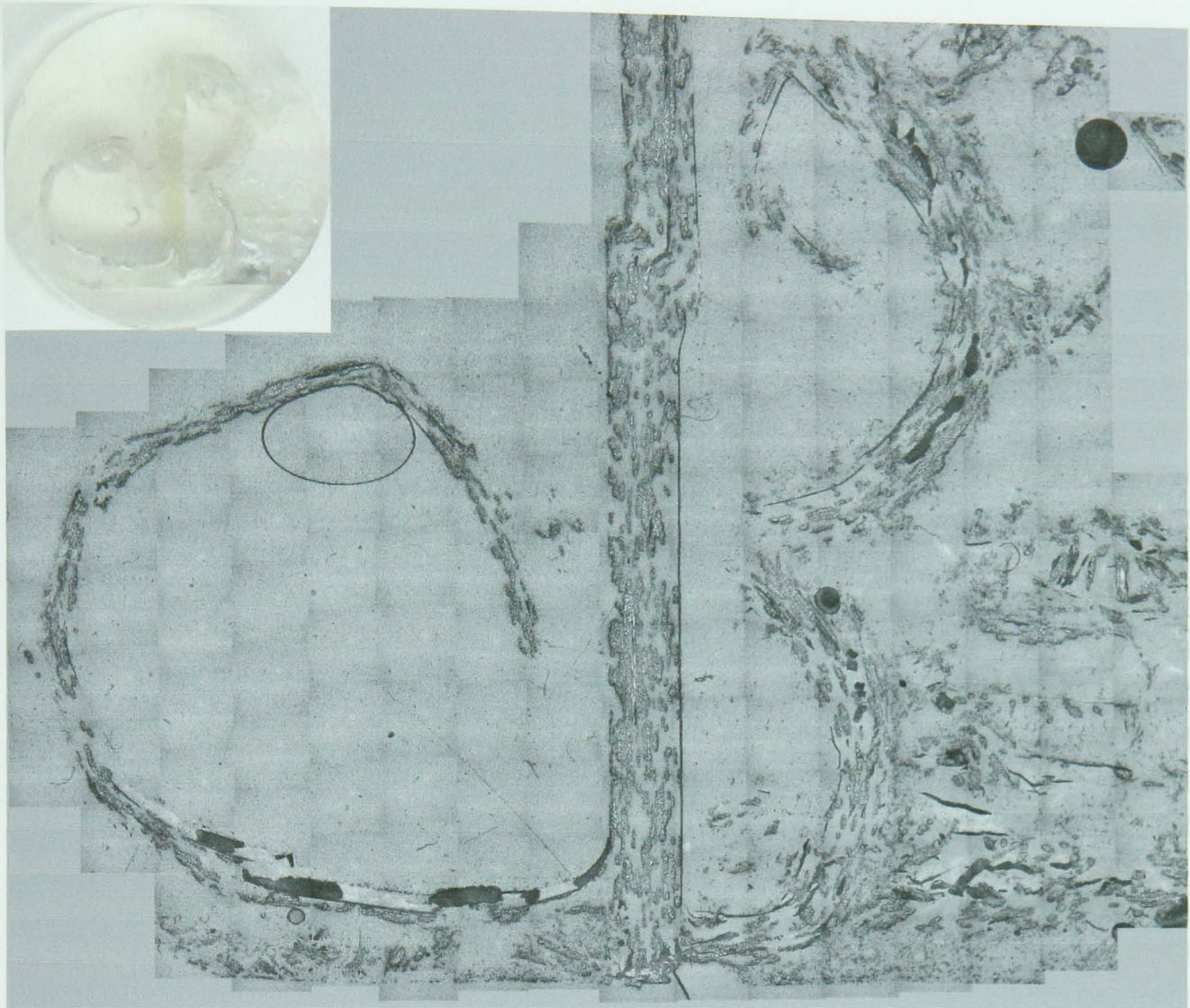


Figure 9: Micrograph of Square Sample (t=2mm) Crushed Quasi-Statically



Figure 10: Crush Zone Morphology of Square Sample ($t=2\text{mm}$) Crushed Quasi-Statically

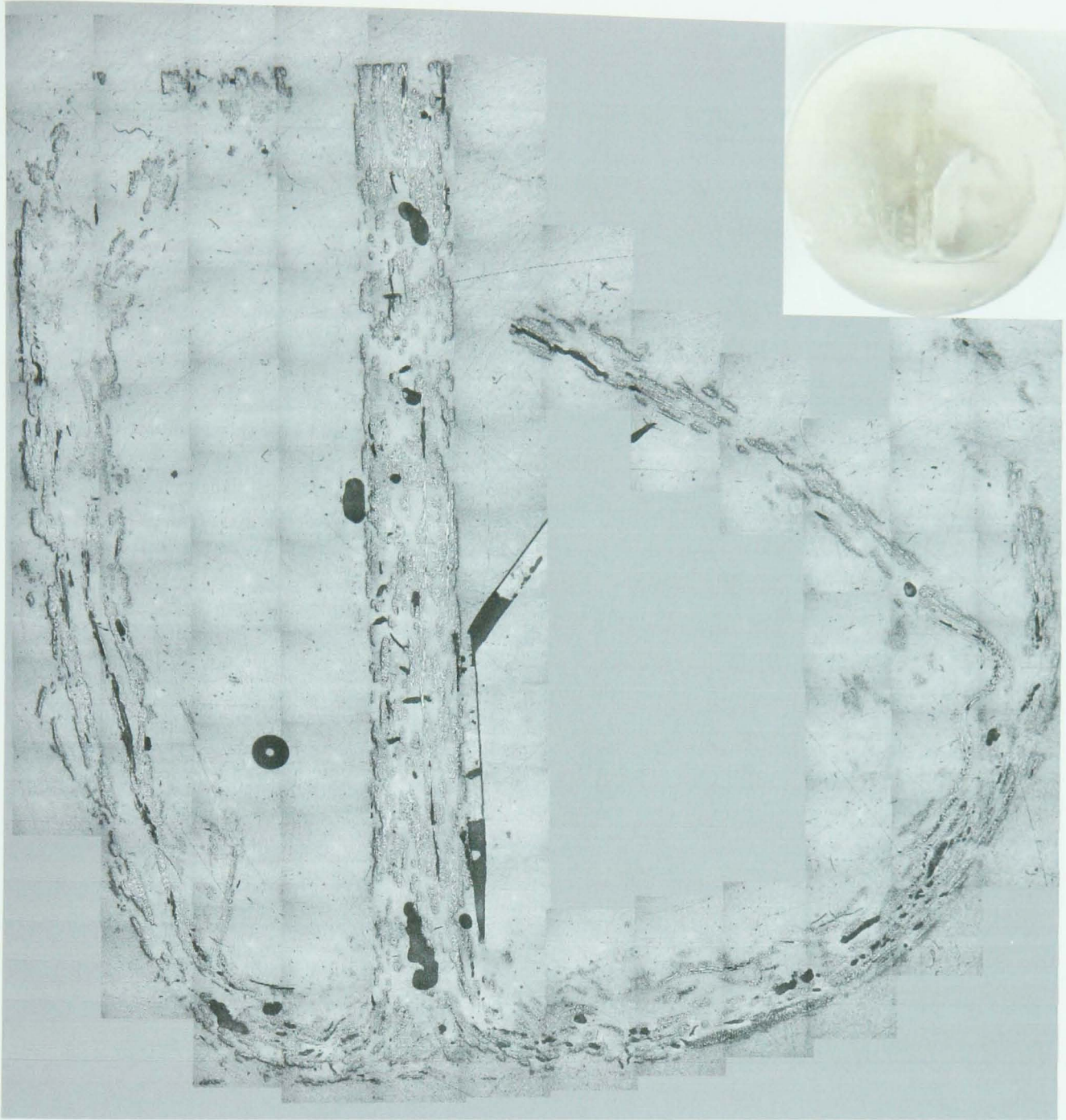


Figure 11: Micrograph of Square Sample ($t=2\text{mm}$) Crushed Dynamically



Figure 12: Crush Zone Morphology of Square Sample ($t=2\text{mm}$) Crushed Dynamically

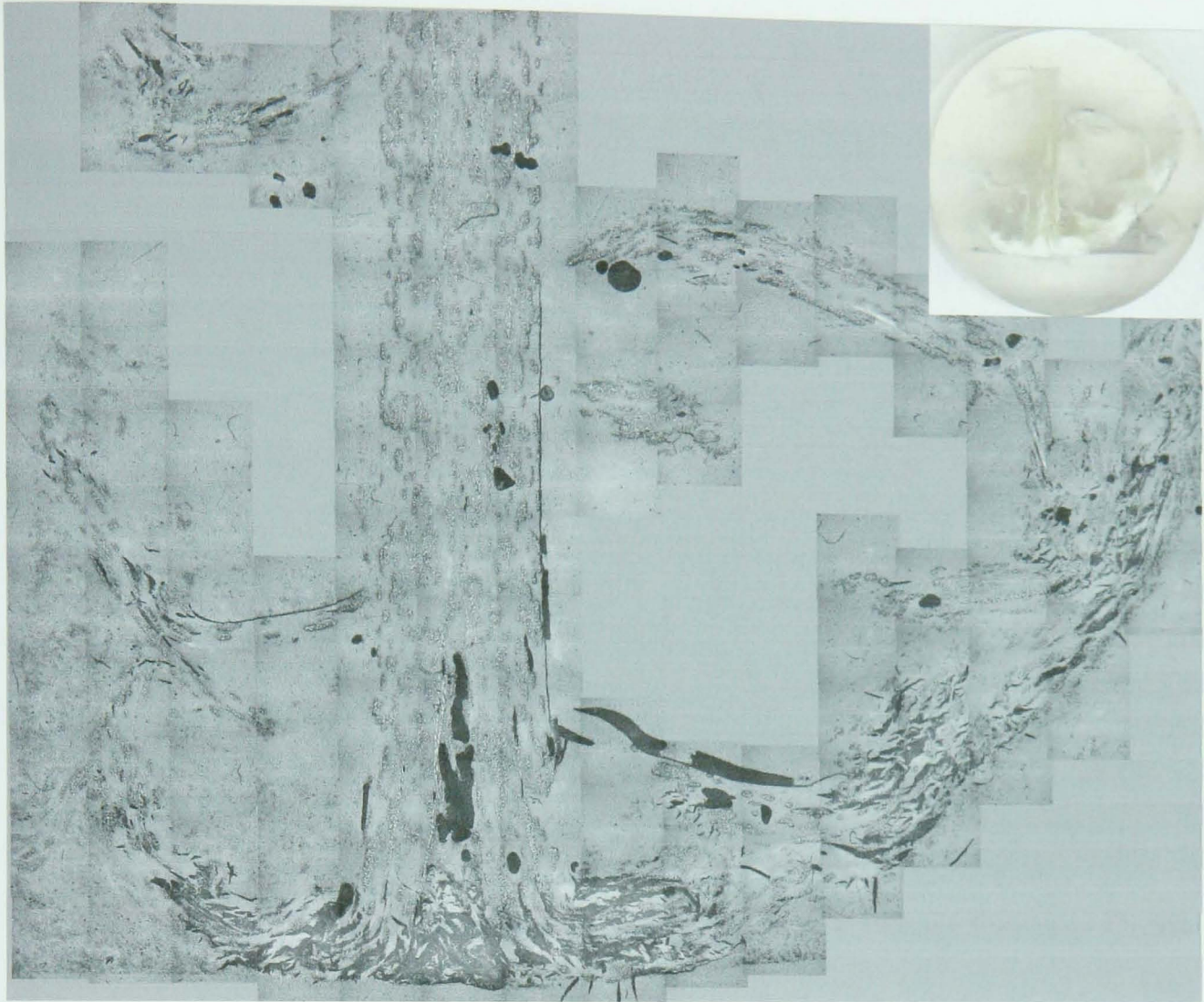


Figure 13: Micrograph of Square Sample (t=4mm) Crushed Quasi-Statically



Figure 14: Crush Zone Morphology of Square Sample ($t=4\text{mm}$) Crushed Quasi-Statically

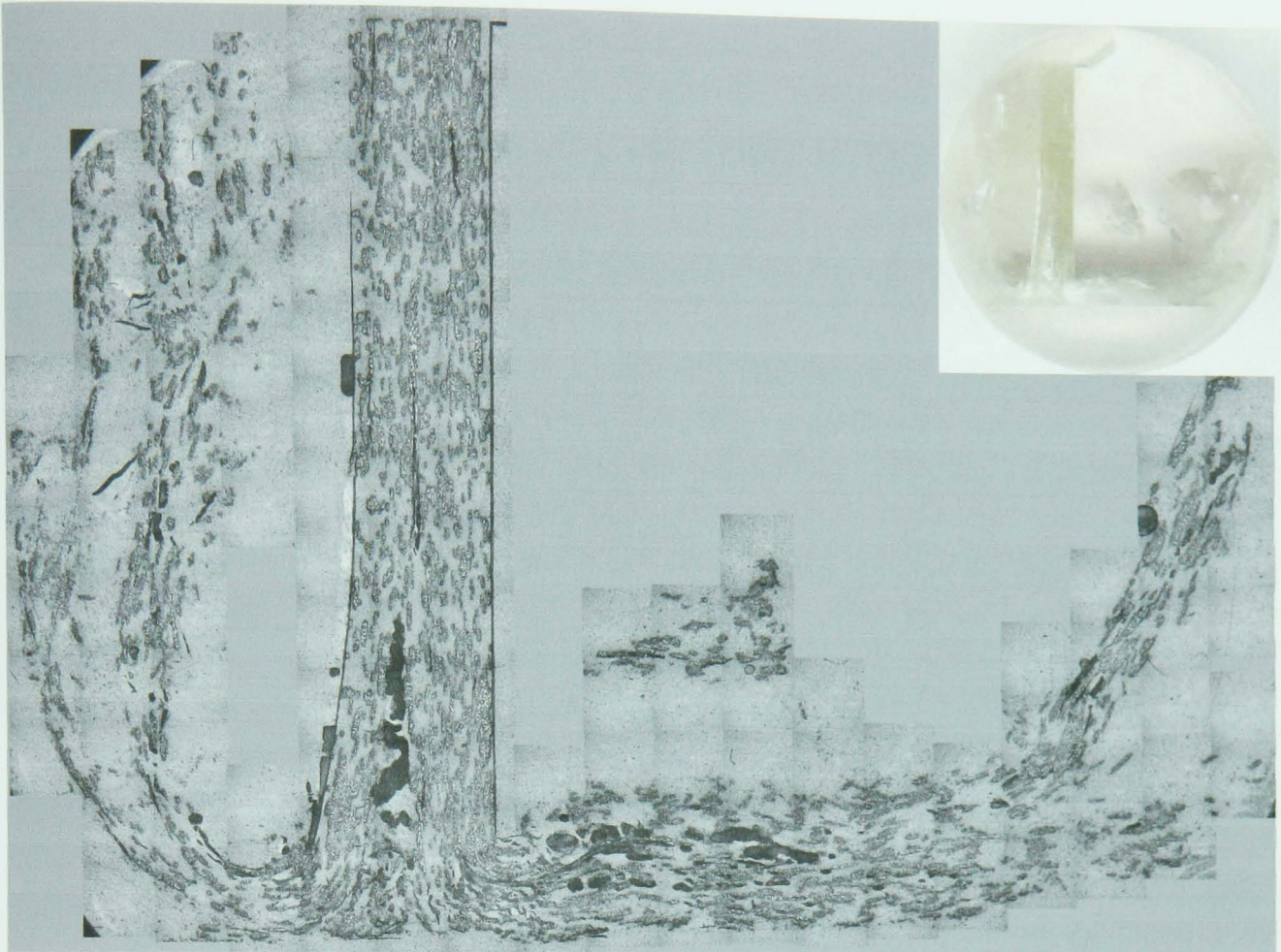


Figure 15: Micrograph of Square Sample (t=4mm) Crushed Dynamically

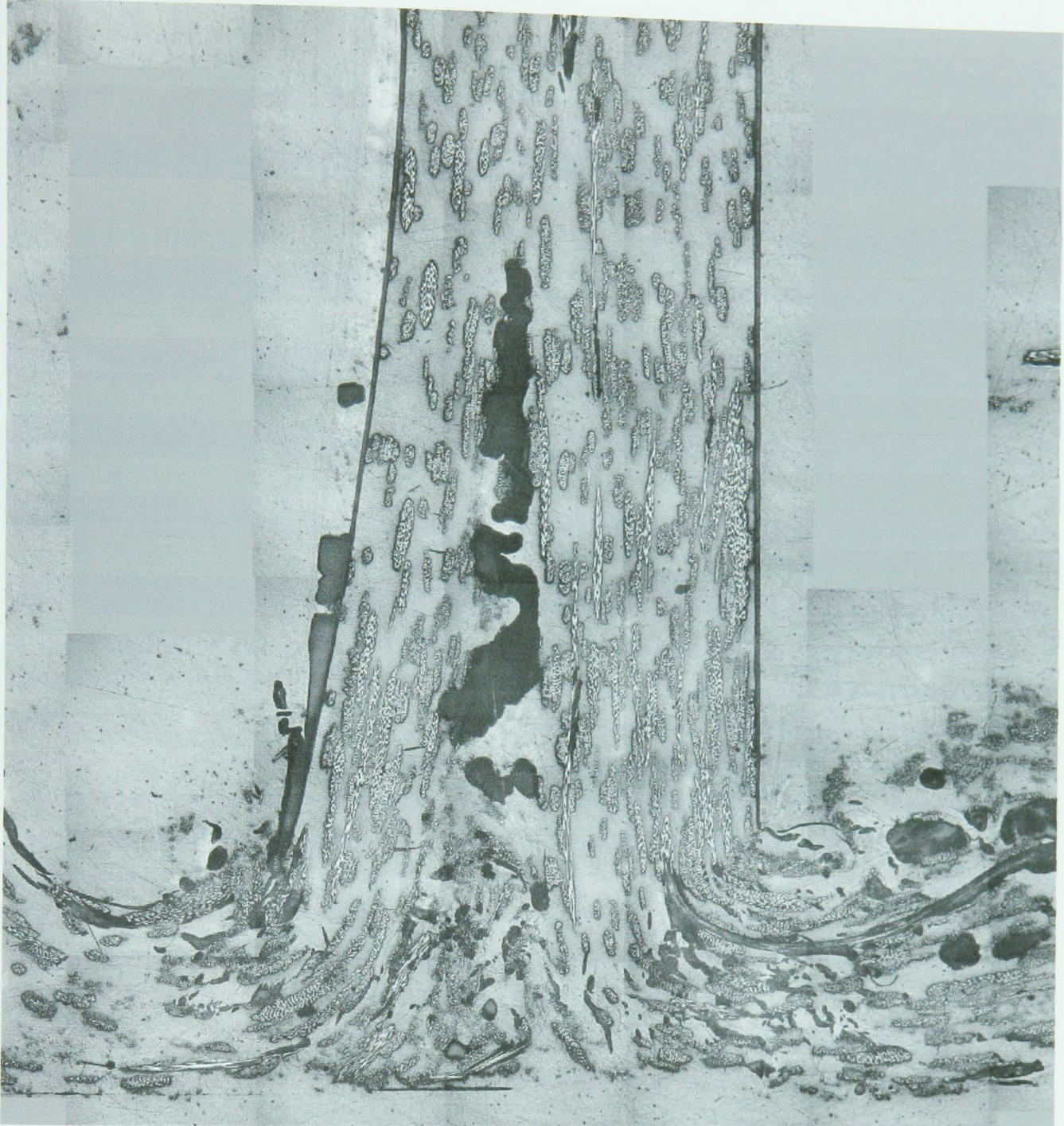


Figure 16: Crush Zone Morphology of Square Sample (t=4mm) Crushed Dynamically

10.1 Micrographs – Samples with Interleaf

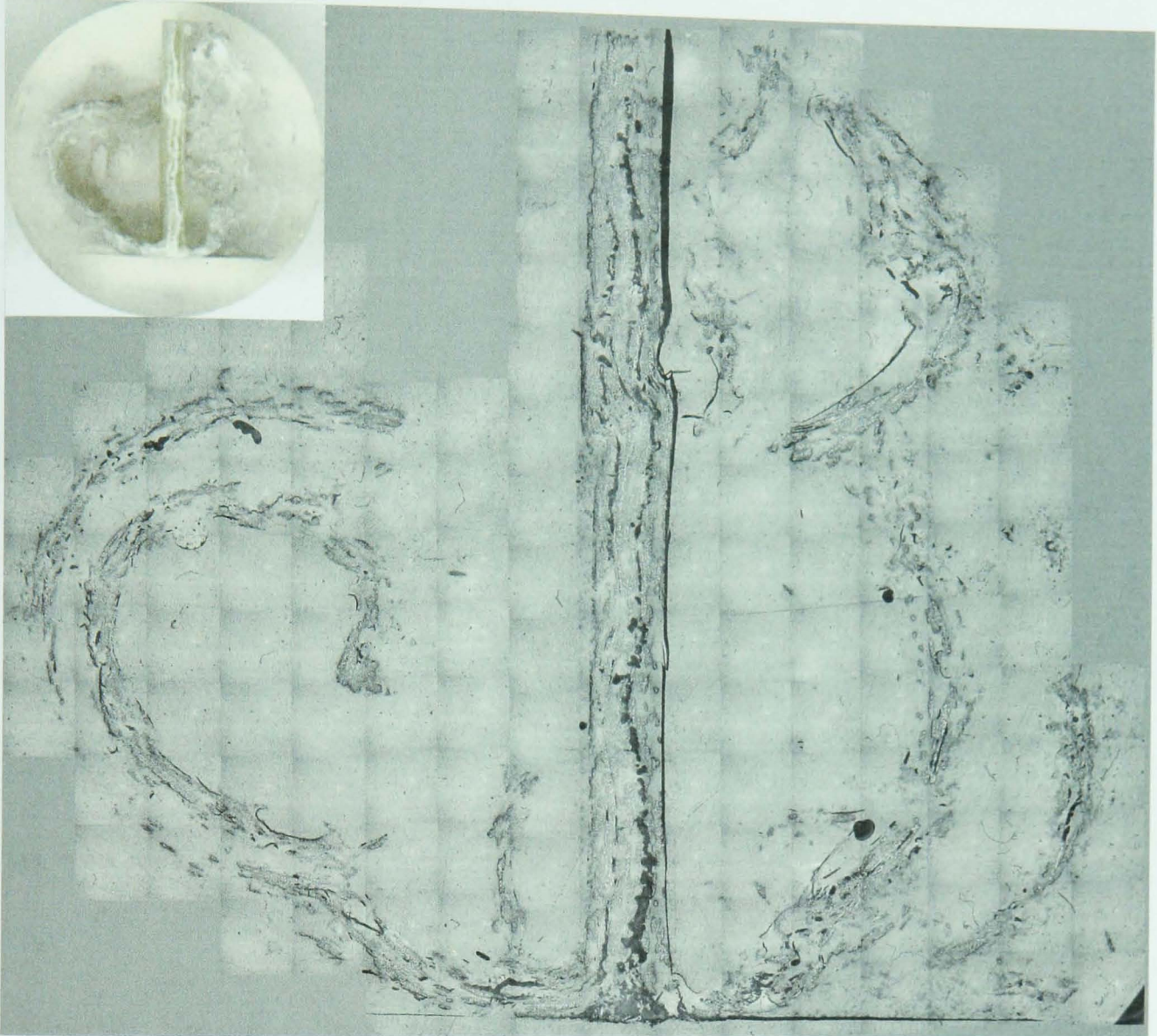


Figure 1: Micrograph of Circular Sample ($t=2\text{mm}$) with Interleaf Crushed Quasi-Statically

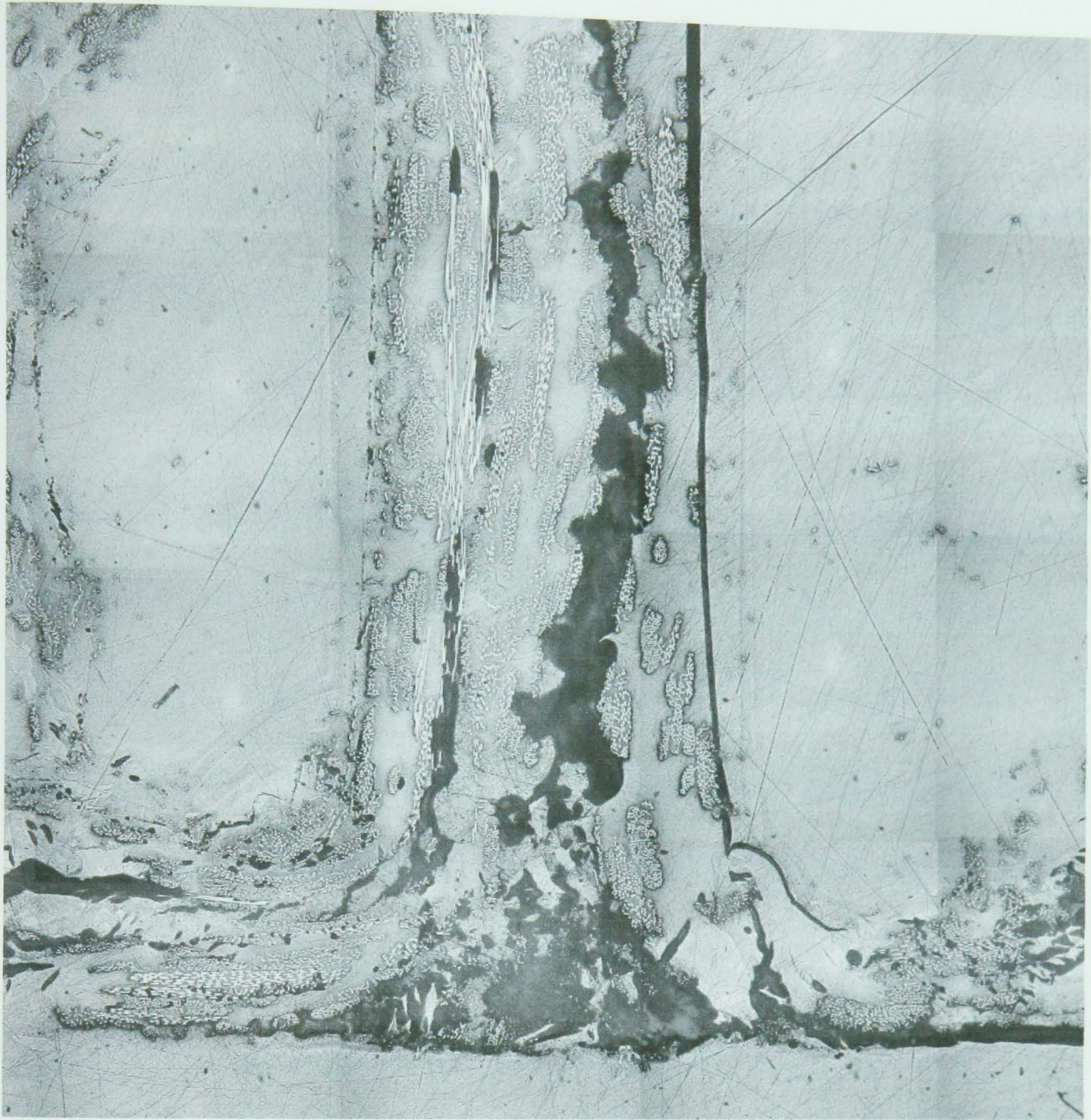


Figure 2: Crush Zone Morphology of Circular Sample ($t=2\text{mm}$) with Interleaf Crushed Quasi-Statically

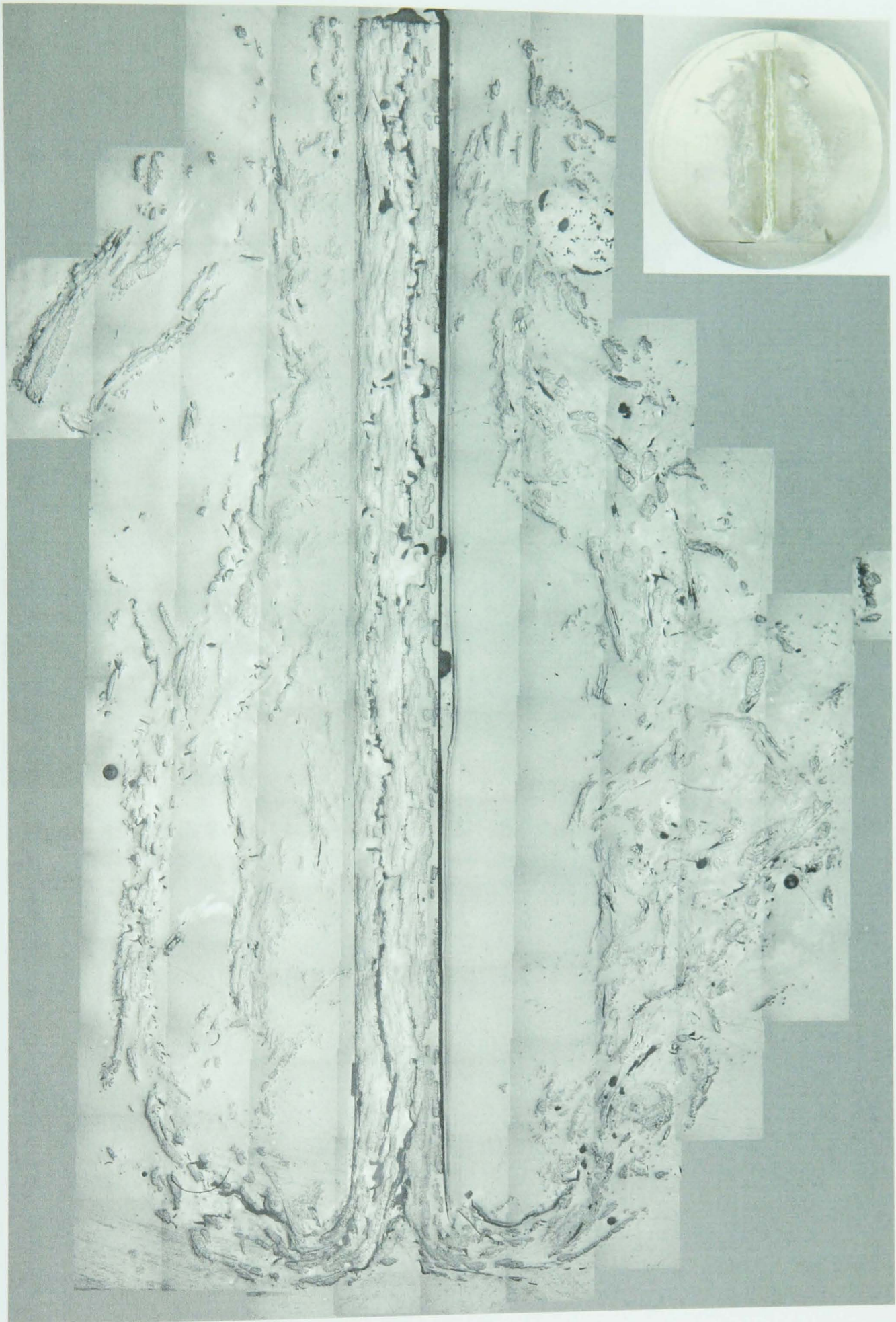


Figure 3: Micrograph of Circular Sample ($t=2\text{mm}$) with Interleaf Crushed Dynamically

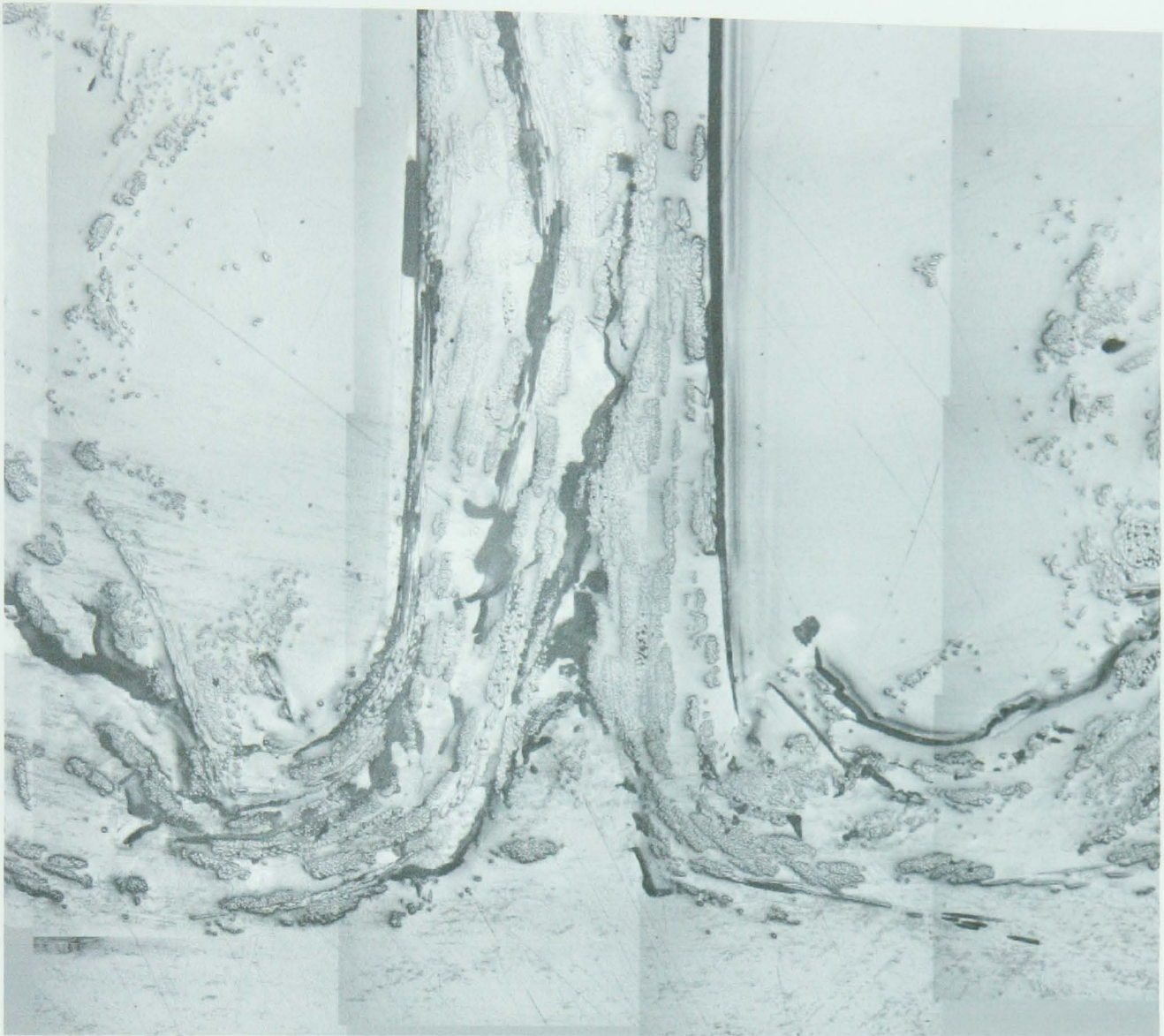


Figure 4: Crush Zone Morphology of Circular Sample (t=2mm) with Interleaf Crushed Dynamically

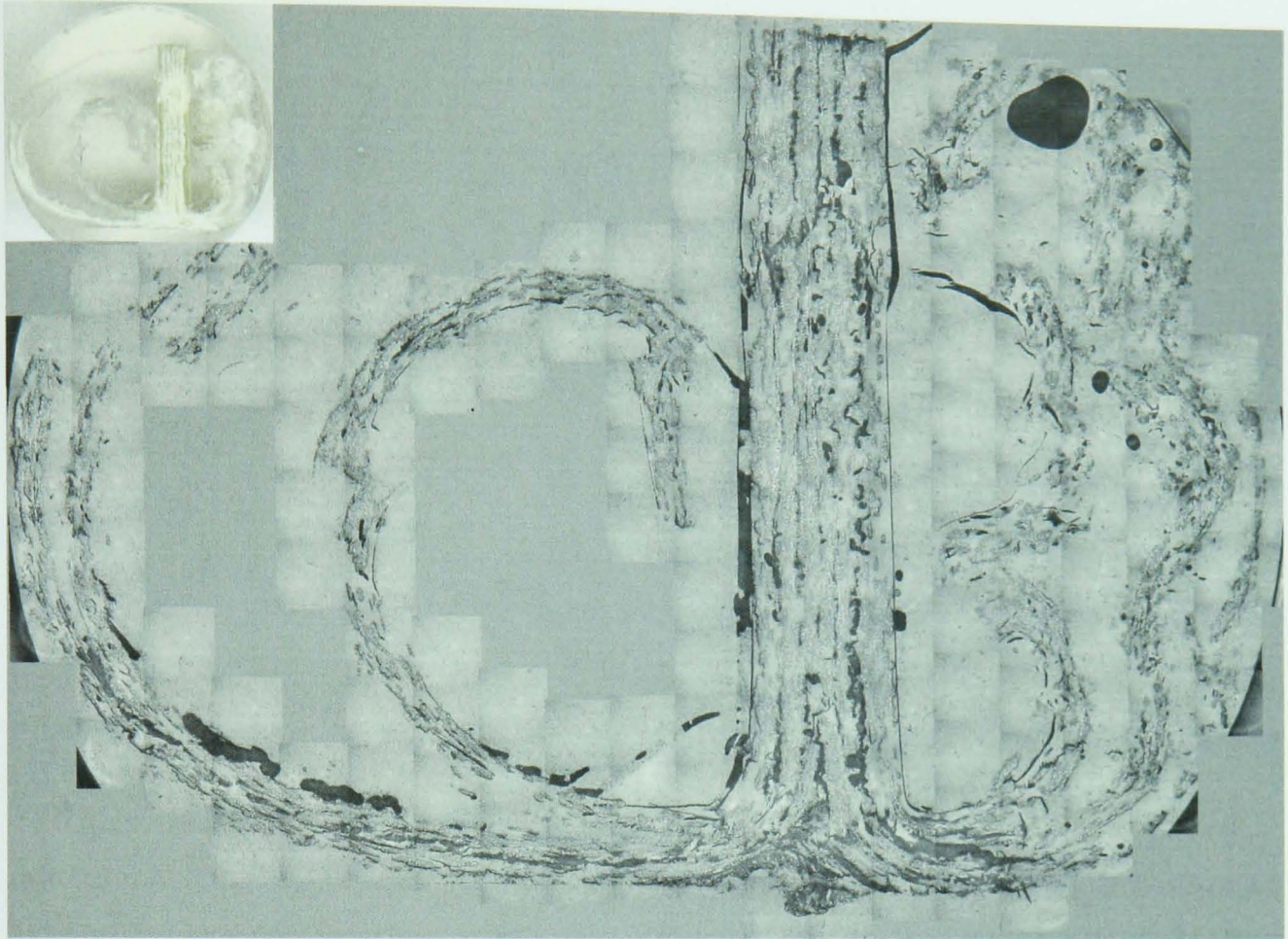


Figure 5: Micrograph of Circular Sample (t=4mm) with Interleaf Crushed Quasi-Statically

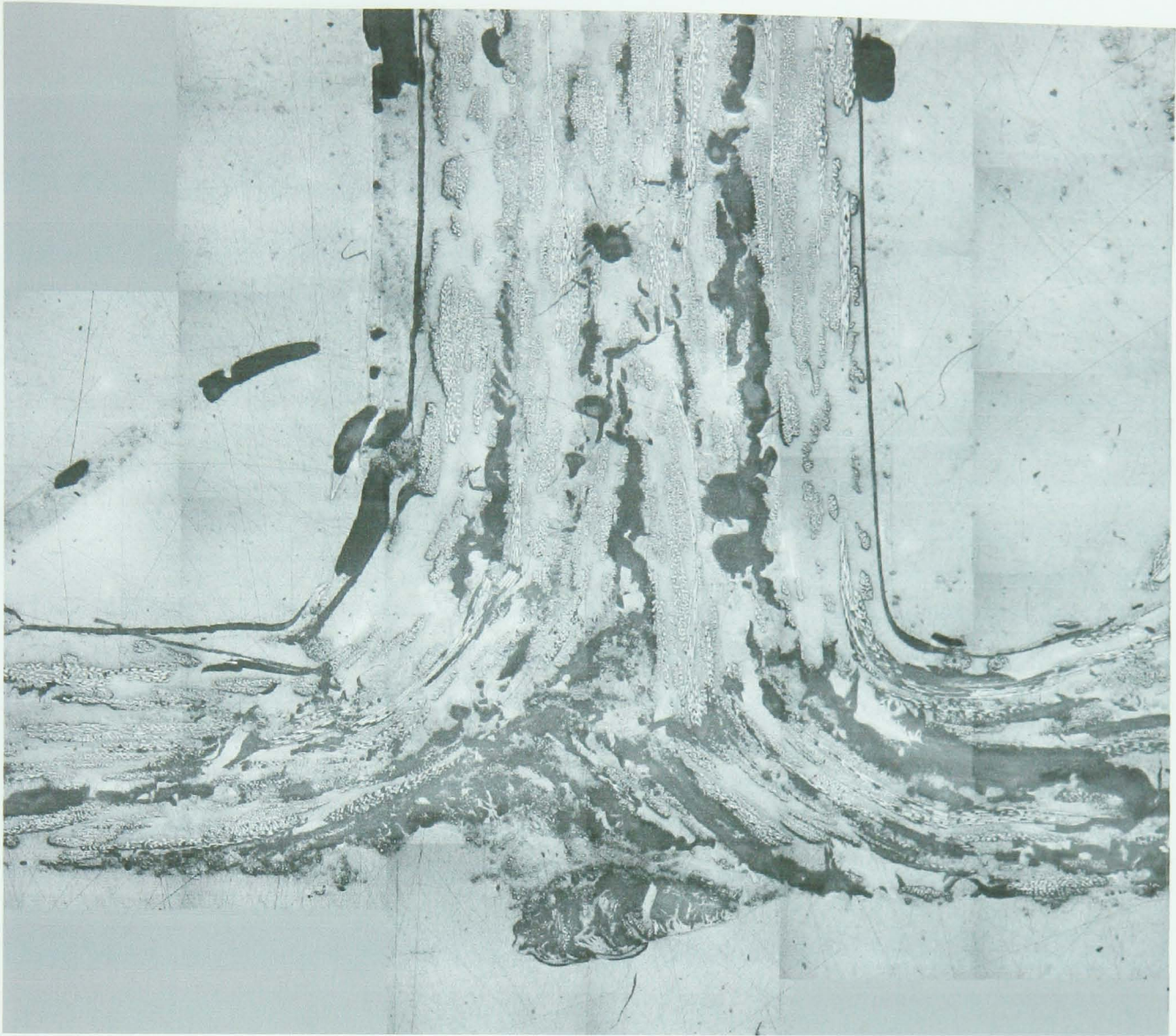


Figure 6: Crush Zone Morphology of Circular Sample ($t=4\text{mm}$) with Interleaf Crushed Quasi-Statically

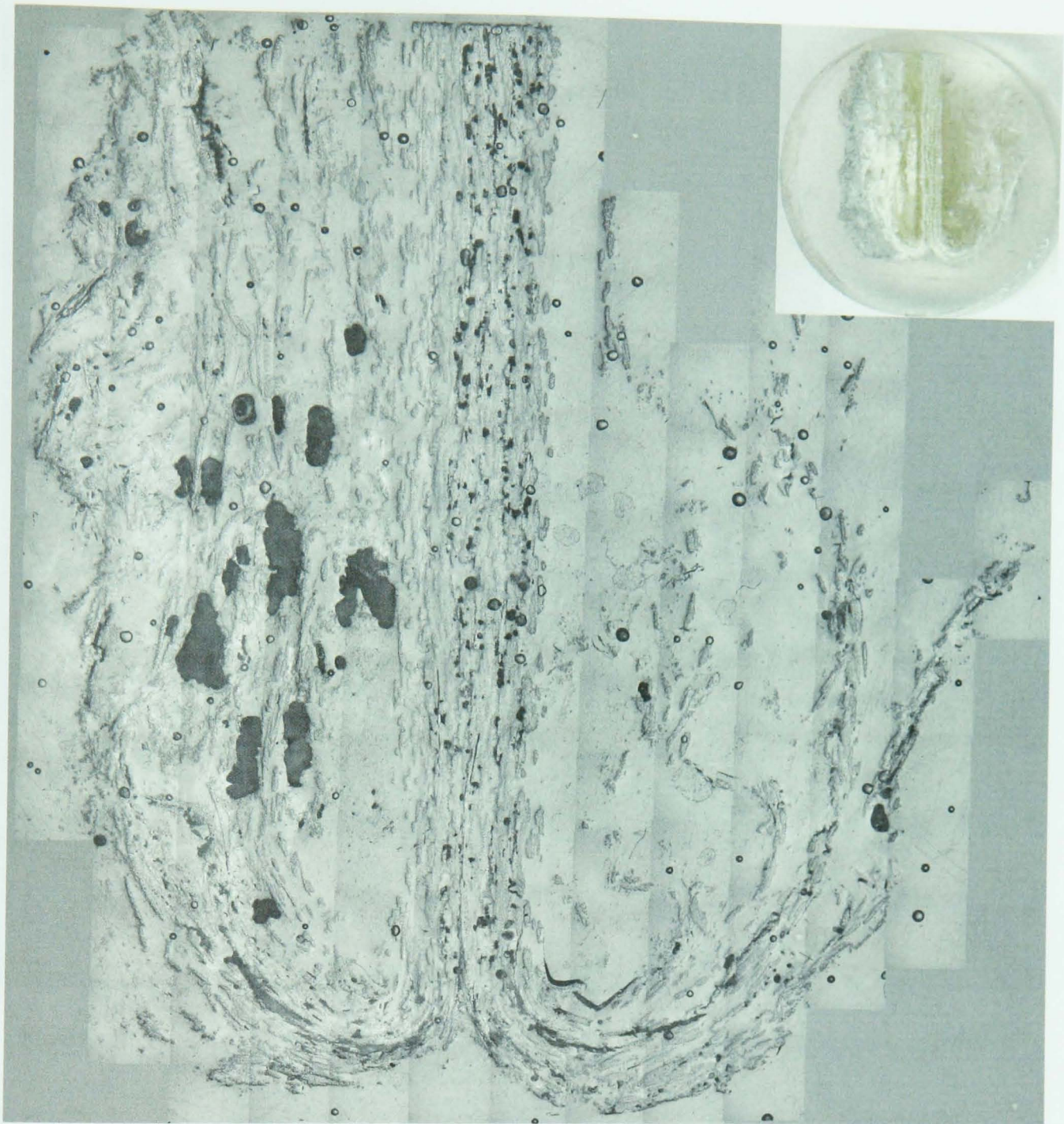


Figure 7: Micrograph of Circular Sample ($t=4\text{mm}$) with Interleaf Crushed Dynamically

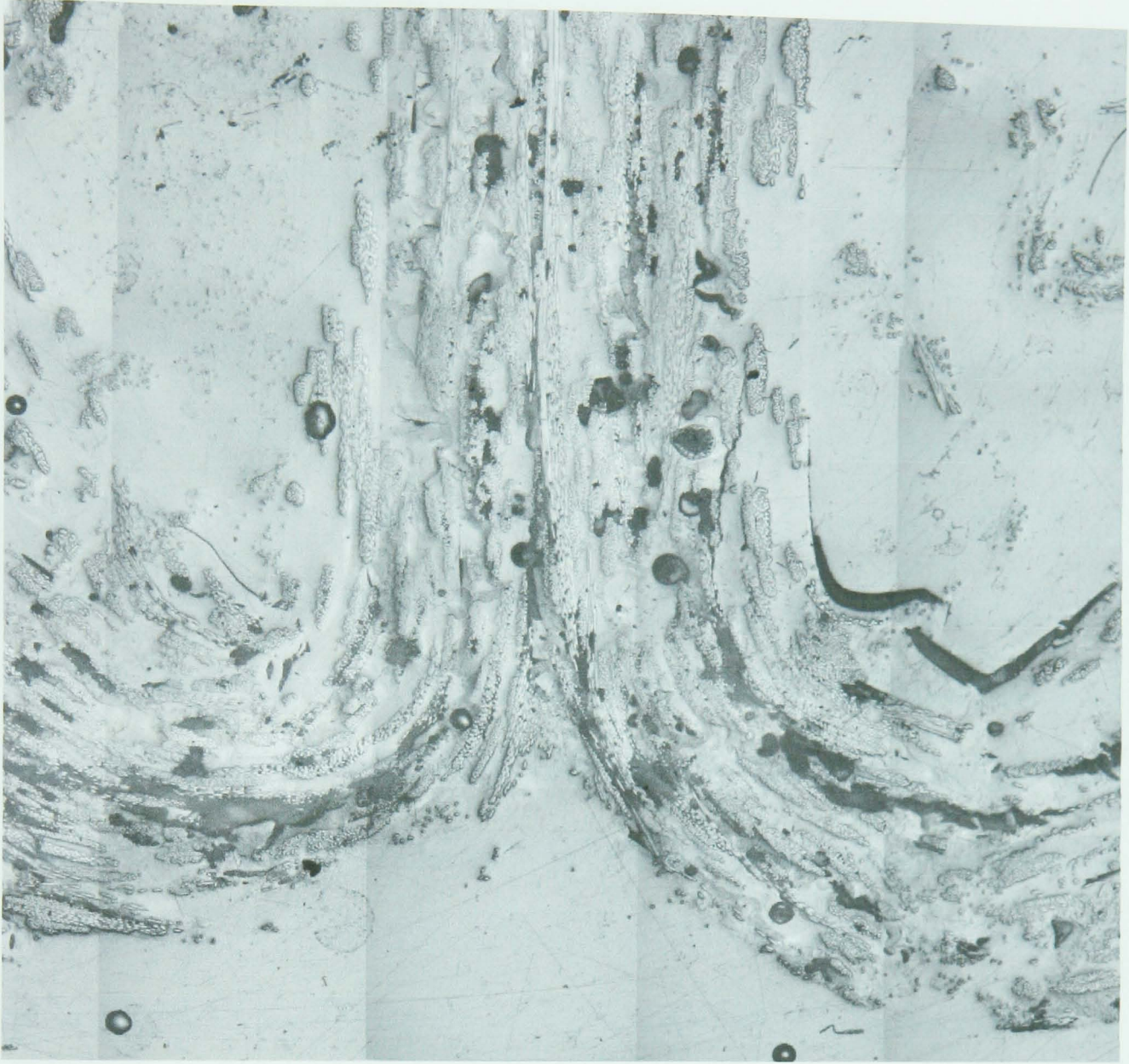


Figure 8: Crush Zone Morphology of Circular Sample (t=4mm) with Interleaf Crushed Dynamically

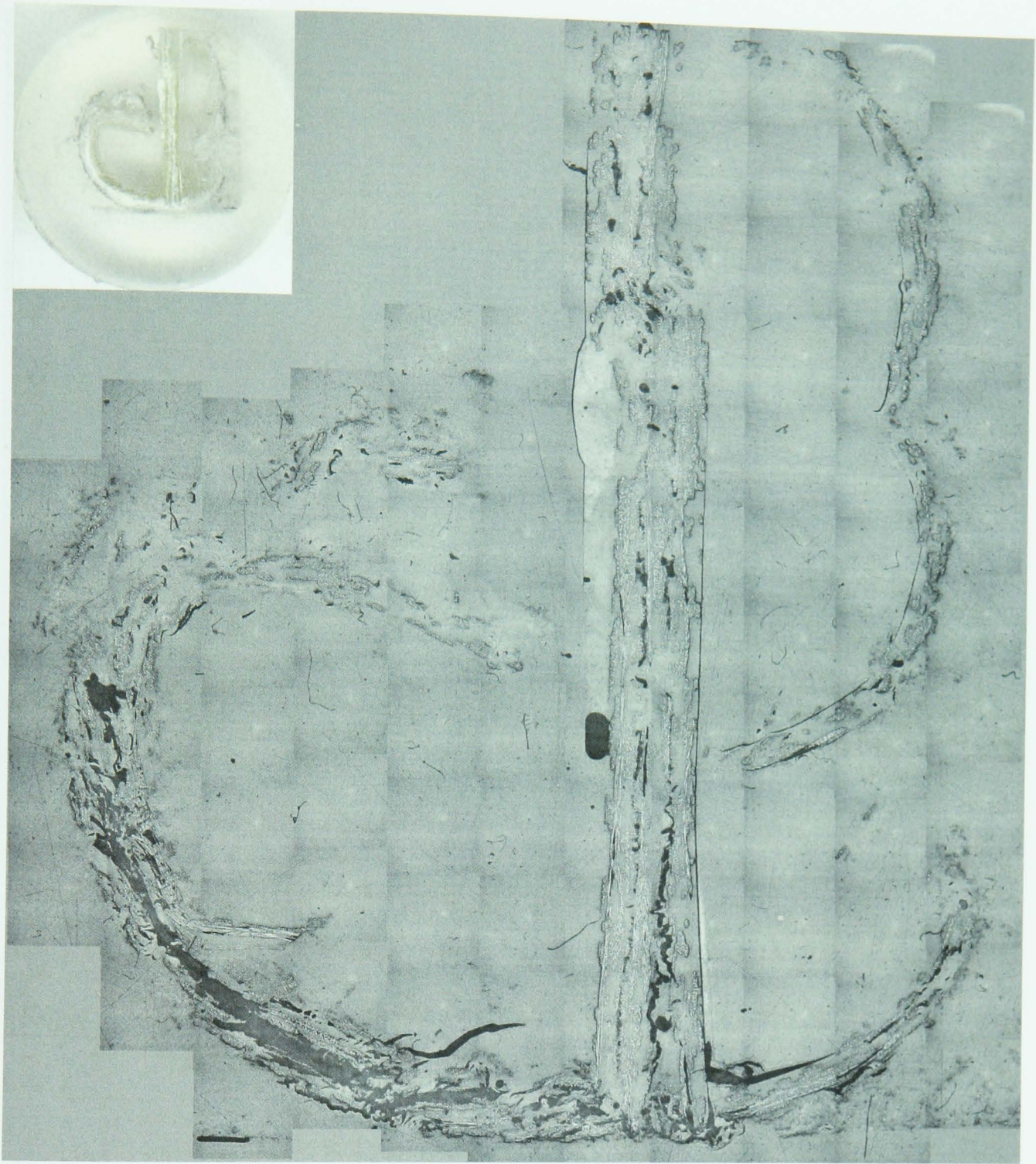


Figure 9: Micrograph of Square Sample ($t=2\text{mm}$) with Interleaf Crushed Quasi-Staticly

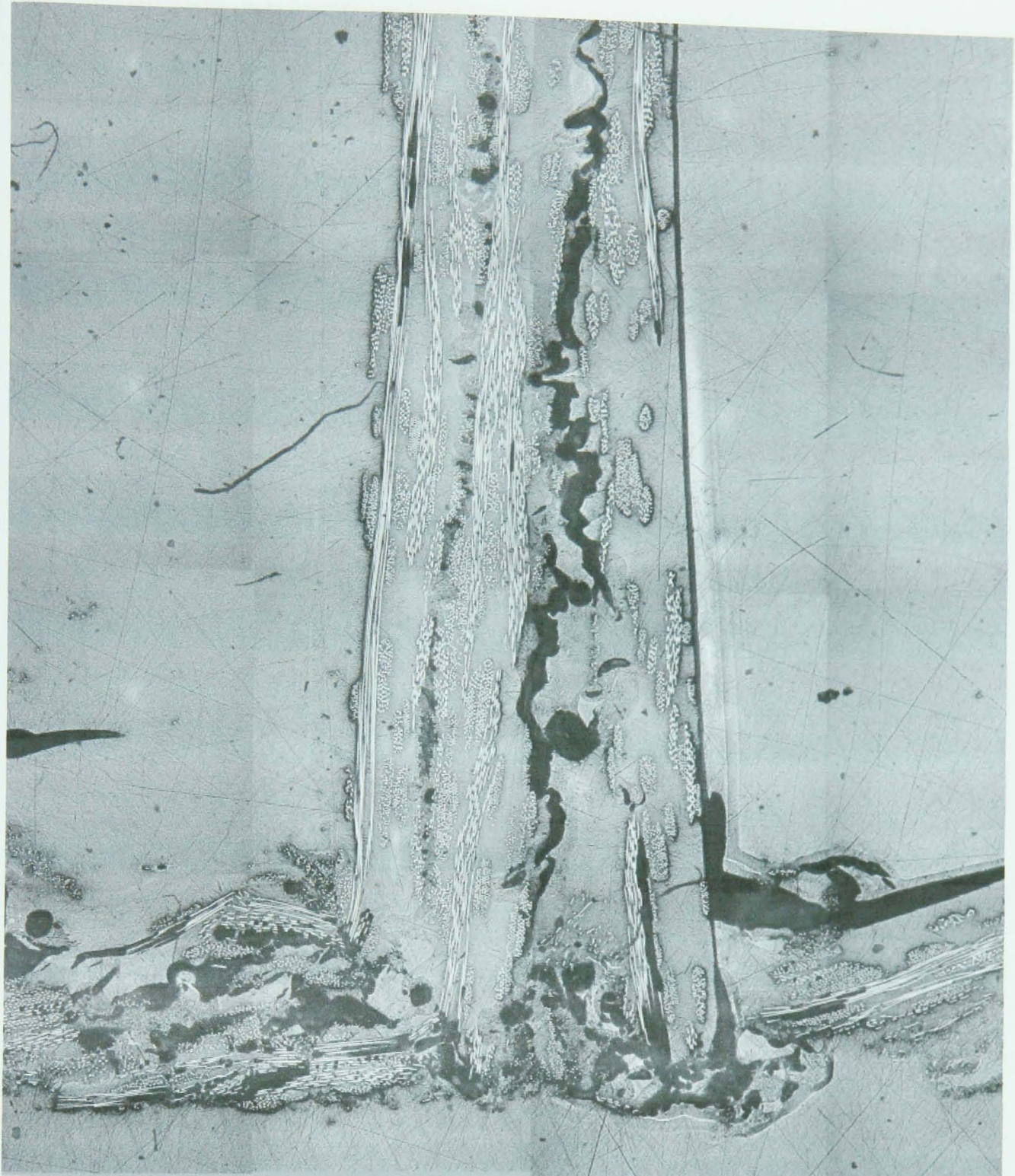


Figure 10: Crush Zone Morphology of Square Sample ($t=2\text{mm}$) with Interleaf Crushed Quasi-Statically

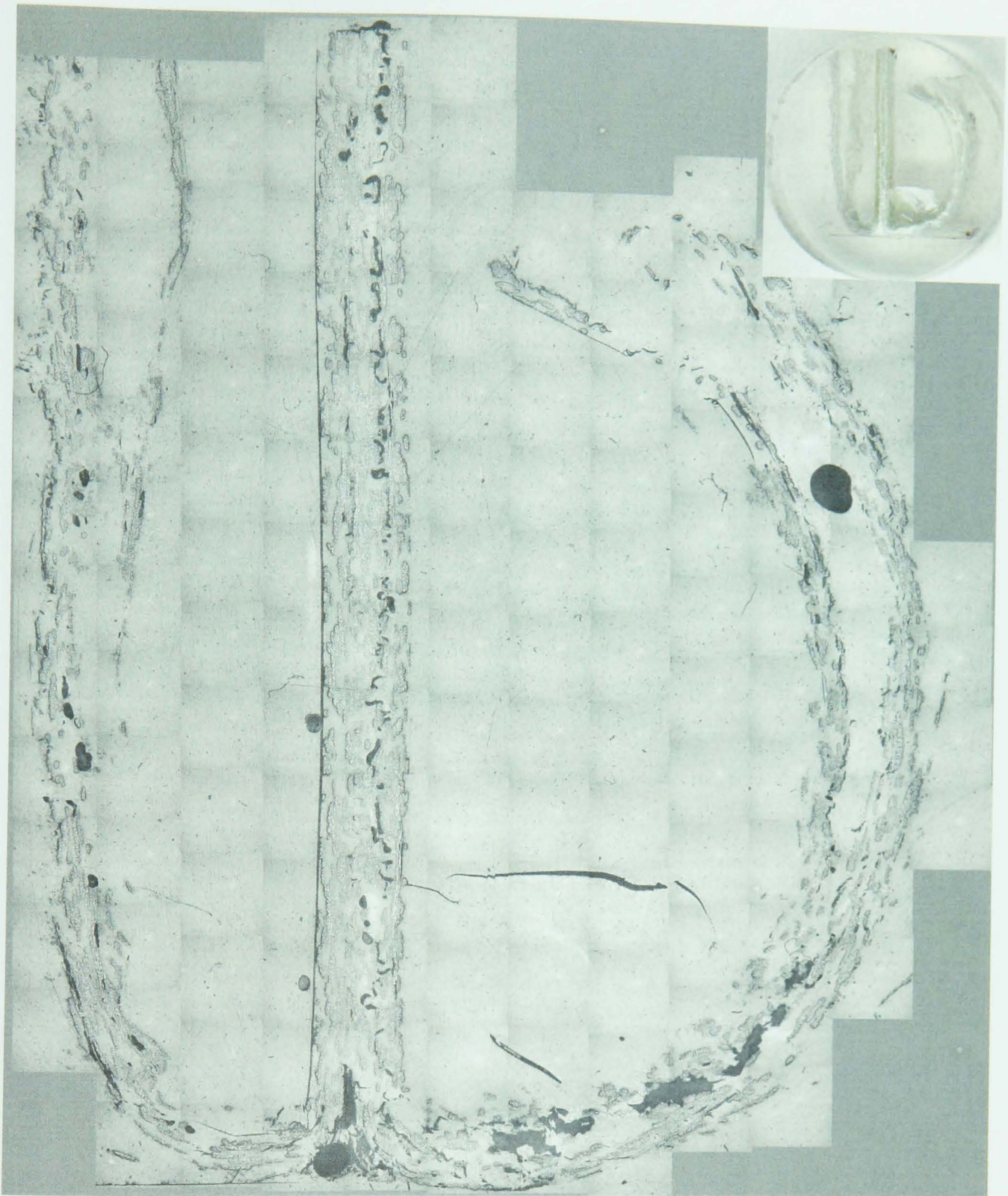


Figure 11: Micrograph of Square Sample ($t=2\text{mm}$) with Interleaf Crushed Dynamically



Figure 12: Crush Zone Morphology of Square Sample ($t=2\text{mm}$) with Interleaf Crushed Dynamically

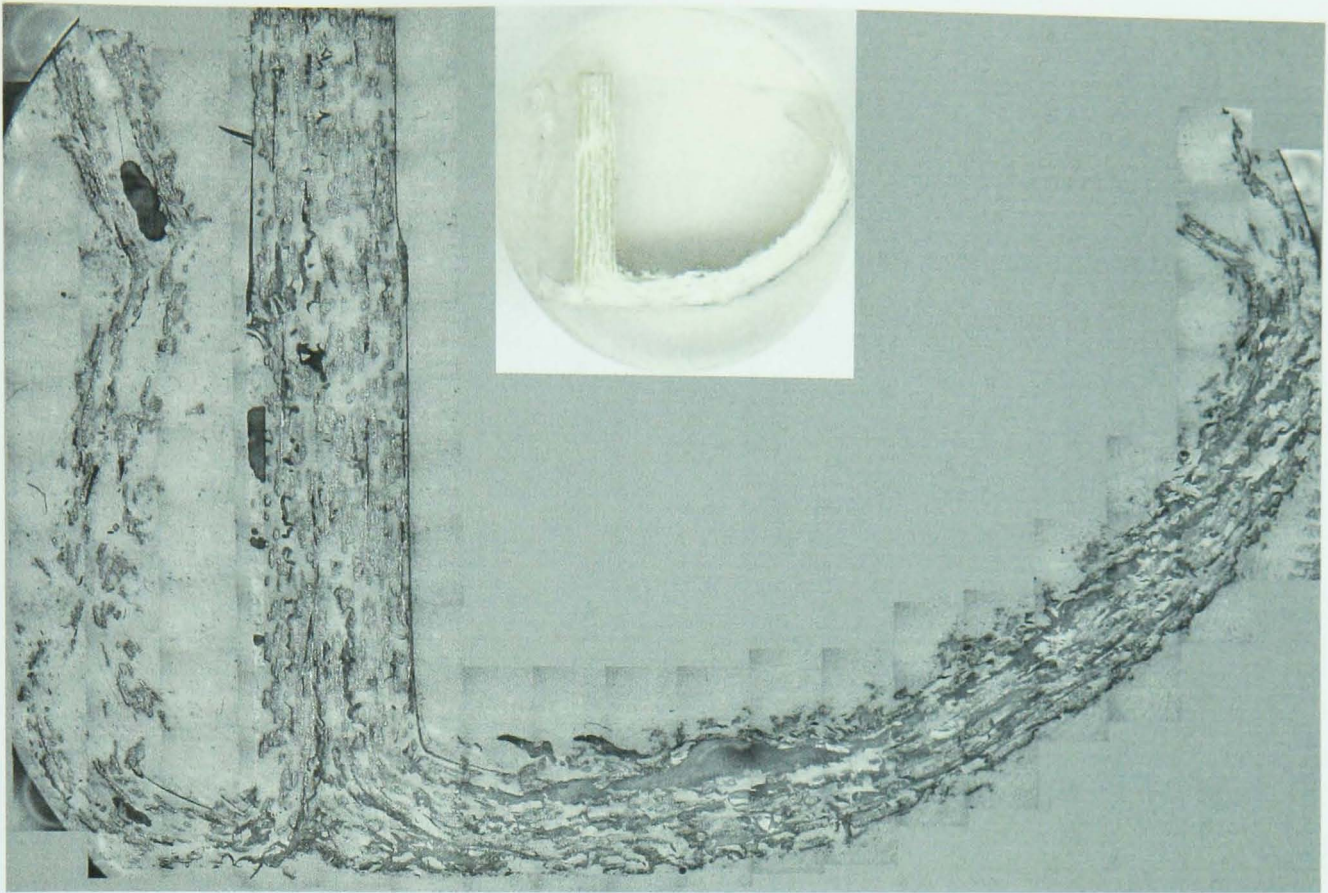


Figure 13: Micrograph of Square Sample ($t=4\text{mm}$) with Interleaf Crushed Quasi-Statically



Figure 14: Crush Zone Morphology of Square Sample ($t=4\text{mm}$) with Interleaf Crushed Quasi-Statically

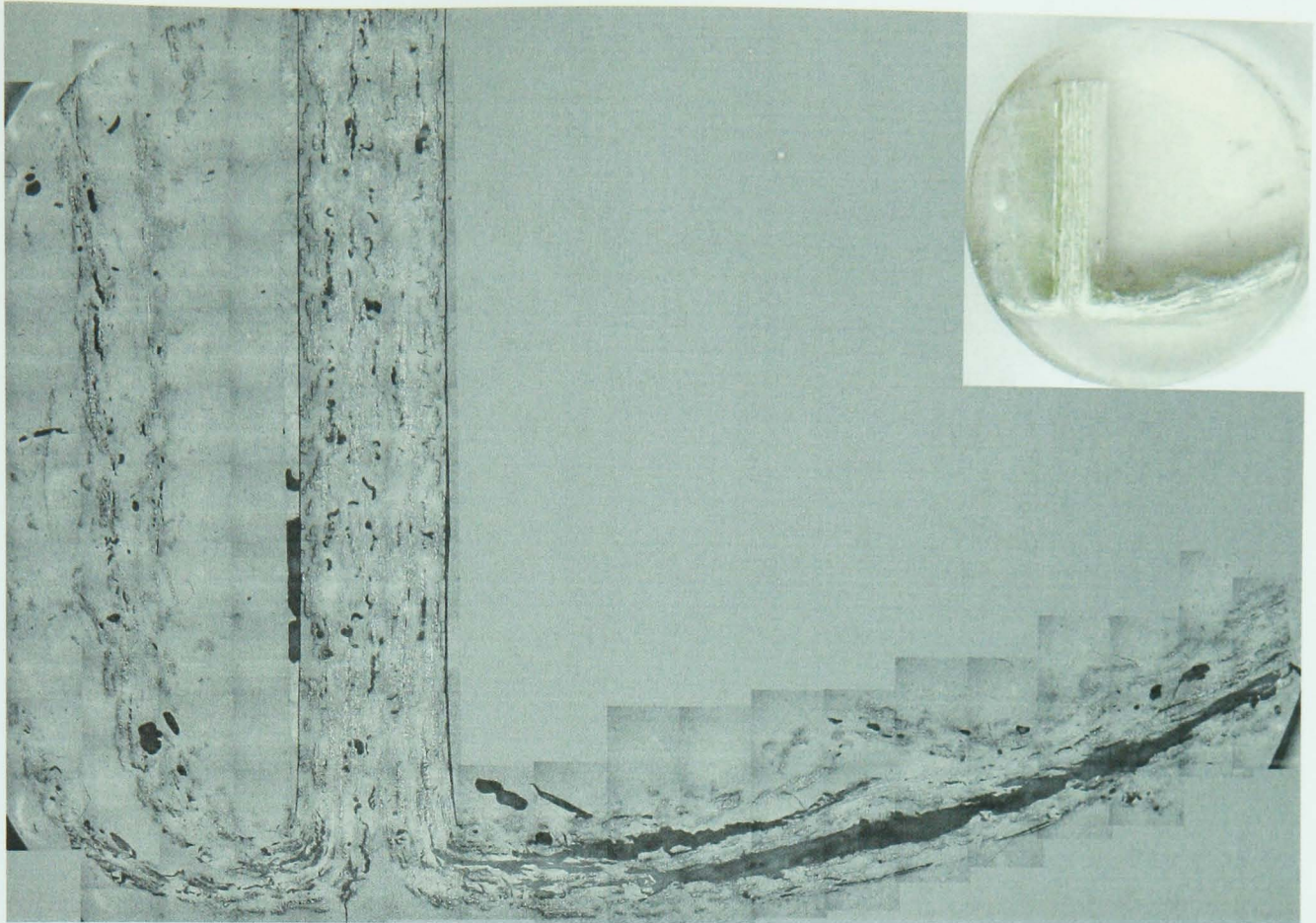


Figure 15: Micrograph of Square Sample (t=4mm) with Interleaf Crushed Dynamically



Figure 16: Crush Zone Morphology of Square Sample (t=4mm) with Interleaf Crushed Dynamically